Efficiënte methoden voor de geautomatiseerde omzetting
van windturbinebladontwerpen naar eindige-elementenmodellen
met schaal- en continuümelementen

Efficient Methods for Automated Conversion
of Wind Turbine Blade Designs into High-Fidelity Finite Element Models
with Shell and Solid Elements

Mathijs Peeters

Promotoren: prof. dr. ir. W. Van Paepegem, prof. dr. ir. J. Degroote
Proefschrift ingediend tot het behalen van de graad van
Doctor in de ingenieurswetenschappen: werktuigkunde-elektrotechniek

UNIVERSITEIT
GENT

Vakgroep Materialen, Textiel en Chemische Proceskunde
Voorzitter: prof. dr. P. Kiekens
Faculteit Ingenieurswetenschappen en Architectuur
Academiejaar 2018 - 2019

ISBN 978-94-6355-165-6
NUR 978
Wettelijk depot: D/2018/10.500/83

Promotor

Prof. dr. ir. W. Van Paepegem
Ghent University
Faculty of engineering
Department of Materials, Textiles and Chemical Engineering

Co-promotor

Prof. dr. ir. J. Degroote
Ghent University
Faculty of engineering
Department of Flow, Heat and Combustion Mechanics

Examination Committee

Prof. P. Kiekens (Chair)	Ghent University, Belgium
Prof. W. Van Paepegem	Ghent University, Belgium
Prof. J. Degroote	Ghent University, Belgium
Prof. F. Gilabert	Ghent University, Belgium
Prof. L. Vandevelde	Ghent University, Belgium
Prof. D. Van Hemelrijck	Vrije Universiteit Brussel, Belgium
Prof. H. Bersee	Delft University of Technology, The Netherlands SE Blades Technology B.V.
dr. P. Greaves	Offshore Renewable Energy Catapult, UK

Research Institute

Ghent University Department of Materials, Textiles and Chemical Engineering Mechanics of Materials and Structures
Tech Lane Ghent Science Park – Campus A
Technologiepark-Zwijnaarde 903
9052 Zwijnaarde
Belgium

Mathijs.Peeters@UGent.be
MathijsPeeters@telenet.be

This research is funded by VLAIO (Flemish Government Agency for Innovation and Entrepeneurship) under the SBO project "OptiWind: Serviceability optimisation of the next generation offshore wind turbines" (project No. 120029) and "FWO-project G030414N-Fluid-structure interaction simulations of wind turbines with composite blades".

Acknowledgements

Doing a PhD study has turned out to far from straightforward. When I try to explain to others why, I like to compare it to wandering around in a desert, under a scorching sun, looking for water. Typically, you set out in a certain direction where you think you may have spotted something, an idea, of which you hope it's an oasis. Since it appears within reach, you devote a lot of time and energy going in that direction. However, things always turn out to be further than you imagined and unexpected obstacles appear on your path. You often reach a dead end and have to back track to take a very different route to get to your goal. Worse still, more often than you would expect, you find yourself travelling for months, only to discover that the oasis you were hoping for turns out to be a fata morgana. The trouble is then to keep moving. To shake it off, let go and move on. In such times, having the support of the people around me has been beyond valuable. Simply put, without them, this book would not exist. Having made it out of that desert, I would like to express my sincere gratitude to the many people who were there for me and helped me.

Firstly, I would like to express my sincere gratitude to my promotors. I would like to thank prof. Wim Van Paepegem for the opportunity to work with him and for his unwavering support and optimism. Wim, you have a rare gift to make people look on the bright side of things. Every single meeting we had together left me feeling positive and hopeful about the future. Thank you for the vast amounts of time and energy. In addition, I would also like to thank prof. Joris Degroote for his advice and support.

Secondly, I would also like to express my deepest, most profound gratitude towards my family and close friends. They were there for me during difficult times. Looking back, I remember several points at which my morale dropped below the greatest debts I had ever experienced before. You pulled me through and kept me going.

I would also like to thank all the colleagues for the great atmosphere, the awesome mood and the positive vibes. An important part were the people I shared an office with. Frederik, out of all the people I know, you are the easiest to get along with. You are cheerful and have an incredible work ethic. Working in the same office really helped to try to do the same. Hethog, thank you for bringing club mate into my life. As you know, Albert Einstein once said: "There are only two ways to live your life. One is as though nothing is a miracle. The other is as though everything is a miracle." Thank you for showing me what the latter option looks like. Lasers! Piew piew !

Next, I would also like to thank Siebe for regularly bringing me to reality and creating a sense of urgency. You are one of the people who contributed to improving my lifestyle. Similarly, I would like to thank Gabriele. You are a very positive person, who gets things done and is fearless when it comes to making drastic changes in your life, which is something I`ve come to admire. Ruben, I

keep being impressed by your ability to make decisions. To my friends prof. Kersemans and Erik, I would like to say I really enjoy the boardgames and will try to keep joining for those. To Joren, I really like your idea of a life full of travel. I'm also very grateful for the huge doses of positivity brought by other colleagues such as Dung, Ruben Geerinck, Joachim, Sam, Pascal, Luc and Ives. Not to forget the many other colleagues that made life at the department good.

And Joanna, you are pure happy optimism, like the cookie eating unicorns you so admire. Never change ! I am truly very grateful for your support.

Further, I would like to express my gratitude to Gilberto Santo and prof. Joris Degroote of the fluid mechanics department for the collaboration and fruitful discussions we had together.

Furthermore, I would also like to thank the companies I had the honor to collaborate with. Specifically, I would like to thank Geert Nouwen from PowerComposites for his help and express my gratitude towards the people working at CTC Engineering. They really helped to steer the PhD in the right direction and greatly increased the relevance of the work. Further, I would like to thank Ivo Van Mechelen from logistics+ for his support. I would also like to express my gratitude towards the people at XANT and Bekaert for the collaboration. Specifically, I would like to thank Simon Reijniers for performing the HAWC2 simulations that allowed validation of the newly implemented coupling. Furthermore, even though I turned out not feasible within this study, I would like to thank the people at Suzlon blades for their willingness to collaborate.

In addition, I would like to thank the people from LM wind power, GL and Abaqus for the fruitful conference calls we had. These filled me with enthusiasm and motivation.

I would also like to thank the thesis students, Stijn Ketele, Aeneas Baert and Wouter Nyckees, which I supervised, for their efforts and perseverance. Finally, I would also like to acknowledge VLAIO for funding the projects I worked on.

In short, to everyone who had a positive impact, thank you !

About the author

Mathijs Peeters was born on December 1st 1989 in Jette, Belgium. His interest in engineering was sparked at the age of 4 when visiting the bottling plant of Codorniu in Spain. During his studies in science and mathematics his enthusiasm for engineering grew and he also became passionate about rowing. He was part of the Belgian national team in 2007 and participated twice at Henley Royal Regatta in the UK. He decided to pursue his passion for engineering at the Faculty of Engineering & Architecture of Ghent University.

After graduating as an electromechanical engineer, he continued his studies in the field of wind energy in the form of a PhD. The results of this effort are presented in this dissertation. During this research, the author gained extensive knowledge and experience in the field of wind energy, engineering and life in general.

During his doctoral studies, the author contributed to several scientific publications and participated in multiple international conferences within his field of study. An overview of the publications is given further on in this manuscript.

List of Publications

Publications in peer reviewed international journals (A1)

1. G. Santo, **M. Peeters**, W. Van Paepegem, and J. Degroote, "Dynamic load and stress analysis of a large Horizontal Axis Wind Turbine using full scale fluid-structure interaction simulation," Renewable Energy, Under review.
2. **M. Peeters**, G. Santo, J. Degroote, and W. Van Paepegem, "High-fidelity finite element models of composite wind turbine blades with shell and solid elements," Compos. Struct., May 2018.
3. **M. Peeters**, G. Santo, J. Degroote, and W. Van Paepegem, "Comparison of Shell and Solid Finite Element Models for the Static Certification Tests of a 43 m Wind Turbine Blade," Energies, vol. 11, no. 6, p. 1346, May 2018.
4. **M. Peeters**, G. Santo, J. Degroote, and W. Van Paepegem, "The concept of segmented wind turbine blades : a review," ENERGIES, vol. 10, no. 8, 2017.
5. B. Lemmens, H. Springer, **M. Peeters**, I. De Graeve, J. De Strycker, D. Raabe, K. Verbeken, "Deformation induced degradation of hot-dip aluminized steel," Mater. Sci. Eng. -Struct. Mater. Prop. Microstruct. Process., vol. 710, pp. 385–391, Jan. 2018.

Publications in ISI proceedings (P1)

1. G. Santo, **M. Peeters**, W. Van Paepegem, and J. Degroote, "Transient modelling of the rotor-tower interaction of wind turbines using fluid-structure interaction simulations," In 7th International Conference on Coupled Probems in Science and Engineering, 2017.
2. G. Santo, **M. Peeters**, W. Van Paepegem, and J. Degroote, "The effect of gravity in transient fluid-structure interaction simulations of a large wind turbine with composite blades," In 8th International Conference on Textile Composites and Inflatable Structures, 2017.

Publications in international conference proceedings (C1)

1. G. Santo, **M. Peeters**, W. V. Paepegem, and J. Degroote, "Analysis of the aerodynamic loads on a wind turbine in off-design conditions," p. 12.
2. G. Santo, **M. Peeters**, W. V. Paepegem, and J. Degroote, "Transient aeroelastic simulations of wind turbines with composite blades.," p. 4.

3. **M. Peeters** and W. Van Paepegem, "Development of automated finite element models for large wind turbine blades," in CompTest 2013, 2013, pp. 167–168

Publications in international conference proceedings (C3)

1. **M. Peeters** and W. Van Paepegem. 2013. "Development of Automated Finite Element Models for Large Wind Turbine Blades." In CompTest, Abstracts, ed. OT Thompson, Bent F Sorensen, and Christian Berggreen, 167–168. Aalborg, Denmark: Dept of Mechanical and Manufacturing Engineering, Aalborg University, Denmark.
2. **M. Peeters** and W. Van Paepegem. 2015. "Fluid-structure Interaction of a Wind Turbine Blade Employing a Refined Finite Element Model Coupled with a Blade-element Momentum Method." In Windfarms, Book of Abstracts, ed. Johan Meyers, Charles Meneveau, and Ben Hobbs, 72–72.
3. G. Santo, **M. Peeters**, W. Van Paepegem, and J. Degroote. 2016. "Transient Modelling of the Fluid-structure Interaction of Wind Turbines with Composite Blades." In 7th European Congress on Computational Methods in Applied Sciences and Engineering, 1. Crete Island, Greece.
4. G. Santo, **M. Peeters**, W. Van Paepegem, and J. Degroote. 2017. "Comparison Between a Chimera Technique and Sliding Interfaces for Fluid-structure Interaction Simulations of Wind Turbines." In Wind Energy Science Conference.
5. **M. Peeters** and W. Van Paepegem, "Finite element modeling of wind turbine blades.," in *SIMULIA Benelux User's Meeting*, 2014.

List of Acronyms

A

ABL - atmospheric boundary layer

AEP – annual energy production

AoA – angle of attack

B

BECAS - "Beam cross section analysis software"

BEM – blade element momentum

BMT- blade modelling tool

BPE – beam property extraction

BSDS – blade system design studies

C

CAD – computer aided design

CAE – computed aided engineering

CFD – computational fluid dynamics

CFRP - Carbon fiber reinforced polymers

COE – cost of energy

COG - center of gravity

CPU - central processing unit

CSM - computational structural model

D

DMO – discrete material optimization

DNS - direct numerical simulation

DOWEC - Dutch offshore wind energy converter

DTU - Technical University of Denmark

E

EU – European Union

F

FCR – fixed charge rate

FE- finite element

FEA – finite element analysis

FF – fiber failure

FML – fiber metal laminate

FSI – fluid-structure-interaction

G

GA – genetic algorithm

GFRP – glass fiber reinforced polymer

GHG – Greenhouse gas

GLA – geometrically linear analysis

GNA – geometrically non-linear analysis

GUI – graphical user interface

H

HAWT – Horizontal axis wind turbine

I

ICC – initial capital cost

IEC - International Electrotechnical Commission

IFF – inter fiber failure

L

LAB – laboratory

LCOE – levelized cost of energy

LE – leading edge

LES - large eddy simulation

LLC – land lease cost

LRC – levelized replacement cost

M

MPC – multi-point-constraint

MPC – multi-point-constraint

N

NASA - National Aeronautics and Space Administration

NuMAD – Numerical Manufacturing and Design tool

O

O&M – operations and maintenance

OML – outer mold layer

OSOW - oversized and overweight

P

PCHIP- piecewise cubic hermite interpolating polynomial

PI – performance index

PS – pressure side

PSO – particle swarm optimization

PVC – Polyvinyl chloride

R

RANS - Reynolds-averaged Navier-Stokes

RWT - reference wind turbine

S

SF – safety factor

SIMP – Solid Isotropic Material with Penalization

SS – suction side

STAR – sweep-twist adaptive rotor blade

T

TE – trailing edge

TFI – transfinite interpolation

TSR – tip speed ratio

U

UD – unidirectional

UMAT – user material

USA – United States of America

V

VARTM – vacuum assisted resin transfer molding

VAWT- vertical axis wind turbines

Nederlandse Samenvatting -Dutch summary-

In het licht van een veranderend klimaat in geopolitieke instabiliteit, hebben vele naties zich geëngageerd om de productie van broeikasgassen te verminderen en in te zetten op hernieuwbare energiebronnen waaronder windenergie. Gedurende de afgelopen decennia is de ontwikkeling van windturbines drastisch vooruit gegaan. Een typische rotor diameter is gegroeid van 40 m in het begin van de jaren 90 tot soms wel 180 m de dag van vandaag om de kostprijs van de geproduceerde energie te verminderen. Hoewel het voor de turbine beschikbare vermogen toeneemt met het kwadraat van zijn straal, neemt zijn massa toe met een grotere exponent. Dit betekent dat de opschaling niet onbeperkt kan voortgaan. Daarenboven komt tevens het feit dat de schaalvergroting leidt tot uitdagingen m.b.t. de productie, manipulatie en het transport van de bladen. Bovendien is de prevalentie van schadegevallen eerder hoog ondanks de hoge veiligheidsfactoren die typisch gebruikt worden. De oorzaak ligt grotendeels bij de gebruikte productiemethodes, waarbij de kosten sterk onder druk staan. Dit resulteert echter in een vermindering in betrouwbaarheid van de turbines. De weg vooruit is bij gevolg het verbeteren van de technologie om lichtere en meer performante bladen toe te laten die voor betere betrouwbaarheid zorgen.

Om dit te realiseren, zijn de methodes die in de wind industrie gebruikt worden gestaag aan het evolueren. Blad productie verandert en wordt meer modulair. Verschillende onderdelen worden als pre-fabricaten gemaakt. Gesegmenteerde torens en mallen vonden hun introductie en verschillende methodes produceren zelfs bladen bestaande uit verscheidene segmenten die pas geassembleerd worden na het transport naar de site van de turbine. De stand van de technologie van dergelijke “gesegmenteerde” bladen werd binnen dit werk onderzocht.

Voorts kunnen precieze modelleringstechnieken helpen om het gedrag van de structuur te begrijpen en verbeteren. Ze laten toe om materiaal efficiënter te gebruiken en ontwerpvariaties te onderzoeken zonder dat de productie van dure prototypes noodzakelijk is.

Hoewel huidige modelleringsmethodes eerder goede resultaten opleveren hebben ze ook beperkingen. In het bijzonder bestaan de gebruikte modellen vaak uit schaal elementen gepositioneerd op het buitenoppervlak van het blad. Hoewel computationeel efficiënt ontbreekt hierbij het binnenoppervlak. Ondanks de aanbeveling van verscheidene auteurs om geavanceerdere modellen te gebruiken, komen deze zelden aan bod in de industrie doordat ze een heel stuk moeilijker te bekomen zijn.

Hoewel verscheidene applicaties bestaan die eindige elementen modellen van windturbine bladen produceren, zijn de meeste beperkt tot conventionele schaal modellen. Voorts zijn de meeste specifiek gemaakt voor een type model en steunen ze op een bestaand commercieel stuk software zoals een eindige elementen preprocessor. De mogelijkheden van bestaande oplossingen zijn vaak beperkt en het uitbreiden ervan geen optie.

Wegens deze redenen werden binnen dit werk meerdere aanpakken voor het maken van gedetailleerde eindige elementen modellen met een hoge waarheidsgetrouwheid onderzocht. Dit resulteerde in verschillende software oplossingen. Een eerste aanpak automatiseert de Abaqus/CAE preprocessor om schaal modellen te genereren. Hoewel succesvol is de bruikbaarheid beperkt door praktische problemen zoals de grootte van bestanden, snelheid en sporadische problemen die manuele tussenkomst vergen. Deze uitdagingen werden aangepakt door een op zichzelf staande oplossing te creëren die blad modellen aanmaakt als een reeks sneden. Dit laat de vlotte creatie van accurate schaal modellen toe. Hoewel geprobeerd werd om de aanpak uit te breiden om de productie van geavanceerdere continuüm modellen toe te laten, veroorzaken talrijke uitdagingen beperkingen.

Deze uitdagingen werden aangepakt in een finale, blok aanpak, waarbij het blad wordt beschouwd als bestaande uit een verzameling parametrische blokken. Dit laat een verdeel-en-heers strategie toe die geïmplementeerd werd als een op zichzelf staande software oplossing.

Deze oplossing slaagt erin om de buitenvorm van elk blad te berekenen, vertrekkend van genormaliseerde vleugelprofielen en een beschrijving van de planvorm van het blad. Tussen de vleugelstations in wordt de vorm van het blad bepaald door dikte interpolatie waarvoor verschillende functies beschikbaar zijn. De software is in staat om het blad oppervlak op te delen op een zeer intuïtieve en precieze manier, gebruik makende van keyline functies. Dit laat accurate positionering toe van lagen en onderdelen. Voorts berekent de software hierbij de topologie van het blad, waaraan de composiet stapeling en blokken kunnen worden toegewezen. Daarbij wordt de stapeling gedefinieerd op basis van de keylines, zodat deze ongewijzigd blijft als additionele partities worden toegevoegd.

Dankzij de blok aanpak kan de software dienen als een platform voor de creatie van gedetailleerde eindige elementen blad modellen met een hoge waarheidsgetrouwheid. Binnen een enkele procedure kunnen zowel modellen op basis van shell elementen (met het element op de midden, boven of onder positie) solid elementen, continuüm schaal elementen of combinaties daarvan aangemaakt worden. Voorts zijn er meer opties beschikbaar dan louter op basis van het type element. Het gebruik van continuüm elementen is bijvoorbeeld mogelijk met behulp van blokken die het laminaat als een enkele cel voorstellen of via een andere familie van blokken die het laminaat met drie cellen doorheen de dikte voorstellen. Gebruik van gepaste blokken laat toe om de lijmverbindingen, flenzen en webs op een geometrisch correcte manier voor te stellen.

Voorts bevat de software nieuw ontwikkelde modules die het rekenrooster aanmaken. Zowel lineaire als kwadratische schaal en continuüm elementen en verschillende element types zijn beschikbaar.

Verder is de oplossing ook in staat om juiste lokale materiaal oriëntaties te berekenen, welke gevarieerd kunnen worden voor elke component van een blok. Deze worden berekend voor elk afzonderlijk element en toegevoegd met behulp van een distributie. Dit is bijzonder belangrijk daar vaak gebruik wordt gemaakt van materialen met anisotrope eigenschappen waarbij de stijfheid snel verandert met de oriëntatie. Op deze manier laat de software toe om modellen te maken die goed overeen komen met de realiteit. In tegenstelling tot vele aanpakken worden de lijmverbindingen die niet zelden aanleiding geven tot problemen gemodelleerd op hun geometrisch correcte positie. Een verval in het aantal lagen en dikteveranderingen kunnen op een goede manier worden voorgesteld. De software is daardoor ook geschikt om het effect van productie fouten te onderzoeken daar deze vlot kunnen worden toegevoegd en gelokaliseerde buiging mee in beschouwing kan worden genomen.

In de loop van dit werk werden verschillende blad ontwerpen succesvol gemodelleerd, waaronder een referentie blad dat in de academische wereld gebruikt wordt en drie verschillende commerciële bladen met lengtes van 10 m, 43 m en 49 m. De modellen werden gevalideerd op basis van hun vorm, massa verdeling, de massa van de constituenten en eigenfrequenties en vervolgens gebruikt in geavanceerdere onderzoeken.

Een eerste dergelijk onderzoek was aero-elastische analyse, welke typisch gedaan wordt met behulp van simulaties die steunen op blad element momentum (BEM) theorie langs de aerodynamische zijde en balk elementen langs de structurele zijde. Dergelijke modellen zijn niet in staat om het geavanceerde structurele gedrag te vatten. Complexe stromingseffecten worden artificieel toegevoegd. Om onderzoek van het aero-elastische gedrag met geavanceerdere modellen toe te laten op een kost efficiënte manier werd een nieuwe koppeling ontwikkeld tussen HAWC2aero en de Abaqus eindige elementen software. Deze werd ingezet om het gedrag van het 10 m blad te berekenen onder een reeks stabiele wind snelheden. Verder droeg het werk toe aan een samenwerking met de vakgroep Mechanica van Stroming, Warmte en Verbranding van Universiteit Gent waarbij meer gedetailleerde fluidum-structuur-interacties (FSI) werden uitgevoerd. Deze maakten gebruik van gedetailleerde modellen van het 49 m blad samen met verfijnde computationeel dynamische stromingsmodellen. Dit onthulde het belang van FSI effecten en de invloed van verschillende factoren zoals de atmosferische grenslaag en zwaartekracht op het resultaat.

Een tweede onderzoekspiste concentreerde zich op de modellering van statische proeven. Als deel van de certificering van een nieuw bladontwerp, waarbij de veiligheid van het ontwerp wordt geverifieerd door een derde partij, worden bladen typisch statisch getest onder extreme belastingen. Dit wordt gedaan door het blad op een proefstand te monteren en zadels op het oppervlak aan te brengen langs waar belasting wordt geïntroduceerd. In dit werk werden dergelijke testen voor een 43 m blad bestudeerd. Aangezien de testen onder gecontroleerde omstandigheden worden uitgevoerd, is het mogelijk om instrumentatie te voorzien, wat toelaat om de modellen van het blad te valideren. De experimentele testen werden numeriek gerepliceerd met modellen bekomen via de nieuw ontwikkelde software bestaande uit schaal en continuüm elementen. De

resulterende buigende momenten aan de bladvoet, verplaatsingen en rekken uit de simulaties werden vergeleken met experimentele waarden, welke goed overeen bleken te komen.

In het finale hoofdstuk van dit werk worden de verwezenlijkingen en conclusies in detail besproken.

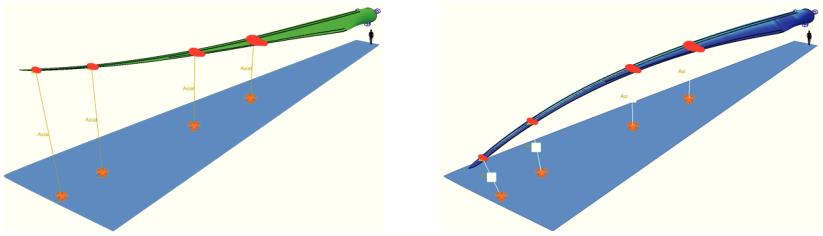

(a) (b)

Figure 1: Numerieke reconstructie van de statische certificeringstesten van het 43 m blad beschouwd in deze studie. Het getoonde belastinggeval is in de negatieve vlaksgewijze richting. (a) De onvervormde configuratie. (b) De vervormde configuratie onder maximale belasting.

English summary

In the face of a changing climate and geopolitical uncertainty, many nations are putting effort into the reduction of greenhouse gas emissions and the development of renewable energy sources such as wind power. Over the past decades, wind turbines designs have drastically developed as common rotor diameters have increased from 40 m in the early 90's to 180 m recently to reduce the cost of energy. However, while the rotor power increases with the square of its radius, the mass rises more rapidly, meaning that there are limits to this upscaling. Furthermore, the increase in dimensions leads to challenges in manufacturing, handling, transportation and installation which all need to be addressed. In addition, the prevalence of damages is rather high despite the use of typically high safety factors. While this is largely due to the production quality that results from strict cost constraints, the reliability of the turbines suffers. The way forward is therefore to improve the technology, allowing lighter blades, with a better performance, that are more reliable to be produced.

For this purpose, the methods used in the wind industry are evolving. Blade manufacturing processes are becoming more modular as several subcomponents are often pre-fabricated. Likewise, segmented towers and molds have been introduced. Several approaches even produce the blade in multiple segments that are only assembled together after transport to the site of the turbine. Within this work the state-of-the-art of these so-called "segmented" blades has been investigated.

In addition, accurate modelling techniques can help to understand and improve the behavior of the structures. They help to use material more efficiently and allow design variations to be investigated without producing costly prototypes.

While current modelling techniques provide fairly good results, these have limitations. In particular, they typically consist of shell elements positioned on the outer surface. While computationally efficient, an inside surface is missing. Despite various authors advocating the use of more advanced models, these are rarely used in industry as they are vastly more difficult to obtain.

Even though several tools exist that create finite element (FE) models of blades, most create conventional shell models. Furthermore, many are dedicated to one specific type of model and rely on other commercial tools such as FE pre-processor packages. The capabilities of existing tools are often limited to a specific type of output and extending these is generally not an option.

For these reasons, within this work, several different approaches for the creation of detailed, high fidelity FE models have been investigated. This resulted in several tools. A first approach automates the Abaqus/CAE pre-processor to create shell models. While effective, practical hurdles such as file sizes, performance and a frequent need for manual intervention exist. These were countered by creating a stand-alone tool that generates blade models as a sequence of slices. This allows the rapid creation of accurate shell models. While an attempt was made to extend

this approach to produce more advanced continuum models, various challenges with the creation of solid models limit its capabilities.

These challenges were tackled in a final, block based approach, in which the blade is considered as a collection of pre-defined parametric blocks. This enables a divide-and-conquer strategy, implemented as an object-oriented, stand-alone software tool.

This tool is able to calculate the outer shape of any blade starting from normalized airfoil files and a planform description. The shape of the blade in between airfoil stations is calculated using thickness interpolation for which several interpolation functions are possible. The tool is able to partition the surface of the blade in a very straightforward and accurate fashion using keyline functions that can be based on specific locations on the blade, on references or on other keyline functions. This allows very accurate positioning of plies and features. Furthermore, the software calculates a topology for the structure, onto which the composite layup and blocks can be assigned. The layup is assigned using the keylines, so that it remains unaltered if more partitions are introduced.

Thanks to the block approach, the tool can serve as a platform for creating detailed high-fidelity FE models for wind turbine blades. Within a single procedure, the creation of models with shell elements (with or without material offsets), solid elements, continuum shell element or combinations of those can be produced. Furthermore, more possibilities exist than simply types of elements. For example, for the use of solid elements, some blocks represent the laminate in a single cell, whereas another family of blocks represents the laminate using three cells in the thickness direction. Using the right type of blocks allows the adhesive, flanges and webs to be represented in a way that is geometrically correct. Further, the software contains newly developed modules that handle meshing. Both linear and second order shell and continuum elements can be produced and various element types such as regular solids, layered solids and continuum shell elements are available.

Furthermore, the software is also able to calculate accurate local material orientations which can be varied for each of the individual components of each block. These are calculated on an element-by-element basis and added to the models using a distribution. This is particularly important as anisotropic materials with a high stiffness are often used for which the stiffness rapidly changes with its orientation. Furthermore, the software enables the creation of models that align closely with reality. Unlike in many approaches, the adhesive bonds which are typically a source of concern in the blade design are modelled at their geometrically correct location. Ply drop-offs and thickness changes can also be included in an accurate fashion. The software is also useful for the study of manufacturing flaws, as these can easily be added with the used approach while localized bending can be considered.

During this work, several blade designs were successfully modelled including a reference design used in academia and three different commercial designs with lengths of 10 m, 43 m and 49 m. The models were validated using their shape, total mass, mass distribution and center of gravity, the mass of the constitutive

materials and the eigenfrequencies of the structure and subsequently used for more advanced investigations.

One such investigation was aero-elastic analysis which, typically, is done using coupled simulations that rely on blade element momentum (BEM) theory on the aerodynamic side and beam models on the structural side. These models do not capture the more complex structural behavior and complex flow effects are added artificially. To allow cost-effective investigation of the aero-elastic behavior with more advanced structural models, a new coupling was developed combining HAWC2aero with the Abaqus FE solver. This was used to investigate the behavior of the 10 m blade for a series of steady-state wind conditions. In addition, the work contributed to a collaboration with the department of Flow, Heat and Combustion Mechanics of Ghent University in which more detailed fluid-structure interaction (FSI) simulations were conducted. These used detailed models of the 49 m blade together with refined computational fluid dynamics (CFD) models. This revealed the importance of FSI effects and the influence of several factors such as the atmospheric boundary layer and gravity on the solution.

A second investigation focused on the modelling of static blade tests. As part of the certification process in which the soundness of a design is verified by a third party, new blade designs are typically tested under extreme static loads. This is done by mounting the structure on a test stand and placing fixtures on the surface which are used to apply loads. In this work the static tests for a commercial 43 m blade are investigated. Since the tests are conducted under controlled conditions, various instruments were installed, providing an opportunity to validate the blade models. The tests were numerically replicated using models produced using the developed software, consisting of shell and solid elements. The resulting root bending moments, displacements and strains were compared to the experimentally obtained values, revealing a good match between the models and reality.

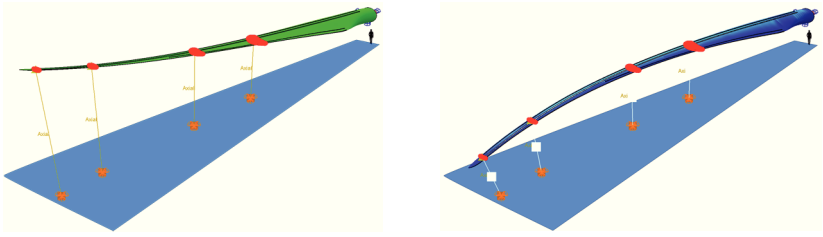

(a) (b)

Figure 2: Numerical reconstruction of the static certification tests of the 43 m blade considered in this study showing the negative flatwise load case. (a) Un-deformed configuration. (b) Deformed configuration under maximum load.

In the final chapter of this work, an overview of the most important achievements and conclusions is repeated.

Table of Contents

1 Introduction

"There's one issue that will define the contours of this century more dramatically than any other, and that is the urgent threat of a changing climate *"- Barack Obama, Former President of the United States of America*

Chapter summary: In this chapter, the topic of this PhD dissertation is introduced. The need for alternative energy sources is discussed, focusing on the share that comes from wind. Subsequently, typical horizontal axis wind turbines (HAWT) are described and the state-of-the art of modern blade designs is explained in a nutshell. Furthermore, the need for advanced modelling of the structural blade behavior is motivated and the SBO project OptiWind is introduced. In addition, the outline of this dissertation is explained.

1.1 Motivation for the development of wind energy

In the face of climate change and geopolitical instability, there is value in energy from alternative domestic resources which can be obtained without the emission of greenhouse gasses (GHG) [1]. These resources include wind energy, solar power, cogeneration, biomass and others. Since wind energy does not cost fuel, its cost is unaffected by fuel prices and no direct CO_2 emissions are caused.

There is scientific consensus that climate change is occurring and that humans are the cause [2]. The effects of global warming are becoming apparent and appear to align with predicted changes. Species are found to be moving in territory towards the poles and glaciers worldwide are retreating [3], [4]. Moreover, global warming has been found to result in increased CO_2 emissions coming from the oceans [5]. Therefore, there is an urgent need to drastically reduce GHG emissions in order to limit the global temperature increase to 2 °C [6]. For this reason, many countries have set goals to produce more energy from alternative resources and reduce GHG emissions. At the Paris climate conference in December 2015, 195 countries adopted a global climate deal aimed at limiting global warming to below 2 °C [7]. The current target set by the European Union (EU) is to reduce the total CO_2 emissions with 20 % by the year 2020 [8]. This target will most likely be achieved [9]. In addition, in 2014, a new target was set, aiming to have at least 27 % renewable energy consumption (both electricity and other forms) at European level by 2030. At least 46 % of the electricity production would come from renewable energy [10]. Nearly half (21 % of the 46 %) of this energy production would come from wind. To make this possible, the cumulative power capacity from wind in the EU has been increasing rapidly over the last decade. This can be seen in Figure 3, along with the fact that wind became the second largest capacity in 2016 [11]. In a similar fashion, the United States of America (USA), set a goal to have 20 % of the domestic electricity supply generated using wind energy by 2030 [5].

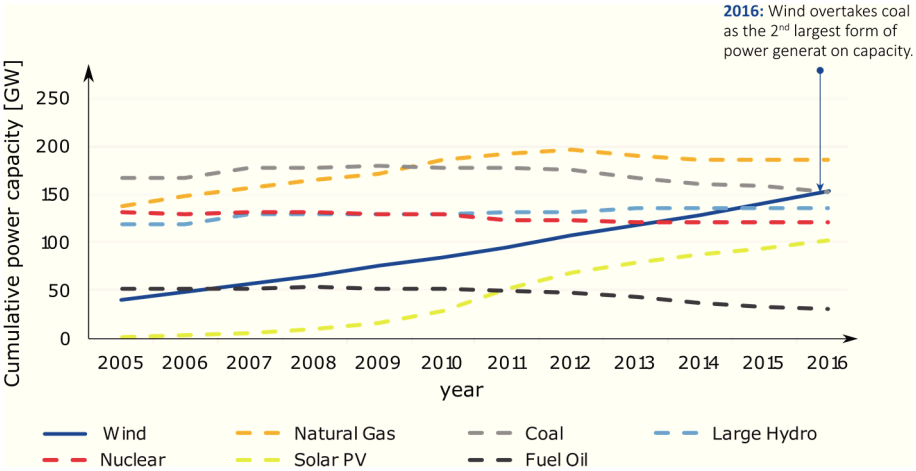

Figure 3: Historic overview of the cumulative installed power for different energy sources in the EU, showing the rapid increase in wind energy capacity. Since 2016 wind is the second largest capacity. Reproduced from Ref. [11].

1.2 Wind energy: economics

The wind energy industry is driven by economic incentive. In practice, wind turbines are designed with the goal of minimizing the cost per kilowatt-hour (kWh) of electricity generated. This is commonly referred to as the cost of energy (COE). This value can be calculated as the total costs of the turbine divided by the total energy captured over its lifetime (seen in equation (1)) [12].

$$COE = \frac{total\ costs\ of\ the\ turbine}{total\ energy\ captured} \tag{1}$$

The cost of energy (COE) can be modelled as shown in equation (2) [13]. It depends on the fixed charge rate (FCR), the initial capital cost (ICC), the net annual energy production of the turbine (AEP_{net}), the land lease cost (LLC), operations and maintenance (O&M) cost and the levelized replacement cost (LRC).

$$COE = \frac{FCR.ICC}{AEP_{NET}} + LLC + \frac{O\&M + LRC}{AEP_{net}} \tag{2}$$

To allow comparison between various turbines, the costs that are incurred over different points in time are "levelized" over the economic lifetime of the turbine. The result is the levelized cost of energy (LCOE) [8]. Minimizing the LCOE is the

primary goal pursued by the wind energy industry. It is the primary explanation for the current-state-of-the-art of wind turbines and the trends that occur in their development. Table 1 provides an overview of the LCOE, ICC and O&M of recent wind turbines. It shows that the costs for offshore wind are still much higher than those for onshore wind installations.

Table 1: An overview of the LCOE, the ICC and O&M costs for different categories of wind turbines. Reproduced from [14]. Small wind turbines are defined as having a rated power below 100 kW.

Typical cost [USD/kWh]	Onshore Wind	Offshore wind	Small wind
LCOE	0.06-0.12	0.10-0.21	0.15-0.35
ICC: installed cost	1280-2290	2700-5070	3100-4400
O&M cost	0.005-0.025	0.027-0.054	0.01-0.05

In Table 2 the LCOE of different energy sources in the UK can be seen. It shows that the current LCOE of wind energy is getting close to that of other sources. However, direct comparison of the LCOE from different energy sources should be taken with a grain of salt as energy from different sources does not necessarily have the same value. This is due to spatial and temporal differences. Wind energy has the advantage that it does not require fuel and is therefore completely unaffected by fluctuating fuel prices. However, on the other hand, wind energy has the drawback that energy production cannot be controlled in time. This way, a lot of energy may be produced at a time when the demand for electricity is low, resulting in energy of a relatively low value. For this reason, wind energy should only be a portion of the energy mix. To take spatial and temporal effects into account and allow direct comparison, the system value (SV) can be used [15].

Table 2: A direct comparison between the levelized cost of energy (LCOE) of all primary energy sources in the United Kingdom (UK) anno 2013. This comparison should be taken with a grain of salt as the LCOE does not account for temporal and spatial differences between the different sources. Based on data from Ref. [16].

Energy source	Nuclear	Coal	Gas	Photovoltaics	Onshore wind	Offshore wind
LCOE [€/MWh]	79	63	60	145	81	140

1.3 Wind turbines

There are different wind turbine designs in use today. They range from very small domestic turbines to extremely large multi-MW machines. For efficiency, modern designs make use of lift rather than drag to turn the flow of air into mechanical energy. A flow of air passes over an airfoil shape, resulting in a pressure difference which accumulates to a lifting force, resulting in rotation of the rotor. This can be seen in Figure 4. Wind turbines are divided in two main categories: those with a rotor turning around an axis parallel to the wind direction: horizontal axis wind turbines (HAWT) and those with a rotor turning about an axis perpendicular to the wind direction: vertical axis wind turbines (VAWT). Today, most modern, large wind turbines are HAWT designs. For this reason, the scope of this work is limited to that category of turbines.

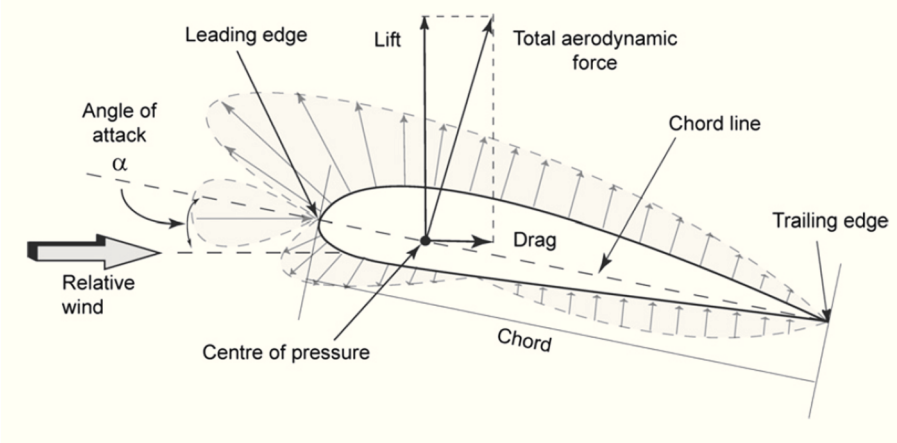

Figure 4: Overview of basic airfoil concepts. Wind passes over an airfoil, that is positioned at an angle of attack to the relative wind velocity, creating a pressure distribution over the surface that accumulates to lift and drag forces. Reproduced from Ref. [17].

In Figure 5 a typical modern HAWT is shown. It consists of a rotor, consisting of individual blades connected to a hub. Modern blades are made of composite materials, bolted to a metal or glass fiber reinforced polymer (GFRP) hub [18]. The rotor is connected to a nacelle which houses the transmission and generator. The transmission serves to increase the rotational speed that is fed to the generator. Alternatively, a so-called "direct drive" system can be used, in which case, no transmission system is required. The original rotation speed of the rotor is then fed to a heavier, more expensive generator with more poles. Such a generator typically has a larger diameter. This approach is often preferred because of lower number of moving components resulting in superior reliability and higher

efficiency. Modern direct drive generators use permanent magnets, which has helped to reduce the cost of these components [19].

The nacelle rests on top of a tower. These are mostly made of rolled steel or concrete. The tower is typically the biggest component to be transported. Therefore, to simplify transportation, various segmented tower designs have been developed [20]-[22]. On land, the tower is typically installed on a steel-reinforced concrete foundation. Offshore, different types of foundations are used [23].

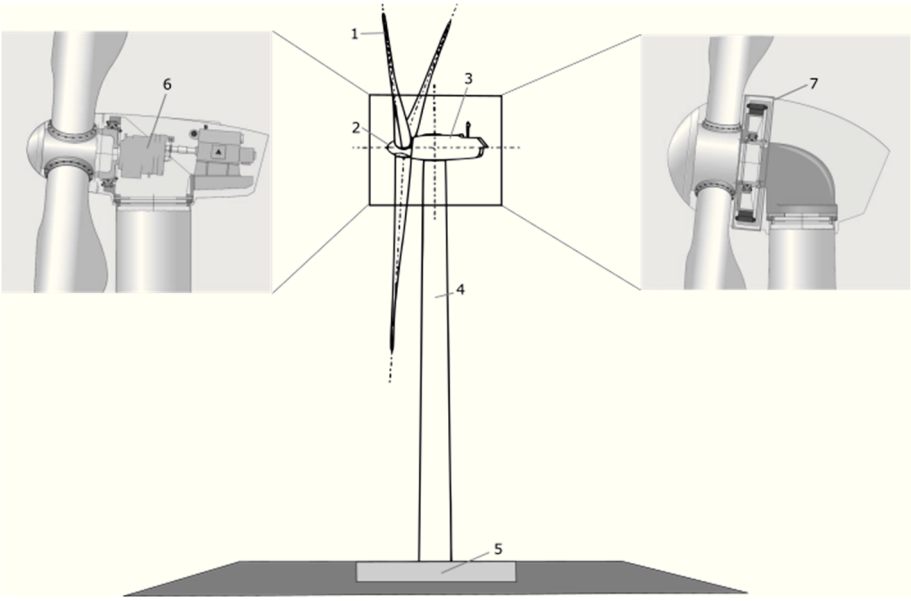

Figure 5: Schematic view of a typical horizontal axis wind turbine (HAWT). (left) A configuration with a gearbox. (right) A configuration with a direct drive system. (1) blades. (2) hub. (3) nacelle. (4) tower. (5) foundation. (6) transmission. (7) direct drive multi-pole generator.

1.4 Wind turbine blades

1.4.1 Minimizing the cost of Energy: rotor aerodynamics

An obvious approach to minimize the COE is to maximize the energy production of the turbine. This can be achieved by optimizing the aerodynamic shape of the rotor. The shape of a blade is typically defined by a series of airfoils positioned at different positions along the span. Chord length, twist and offset distributions are applied to the airfoils to obtain the so-called "planform" of the blade. An example of such a blade planform can be seen in Figure 6. While several methods exist to optimize the planform, Betz optimization, shown in equation (3), is the

simplest [24]. It can be used to calculate the optimal chord and twist distribution to maximize the annual energy production (AEP).

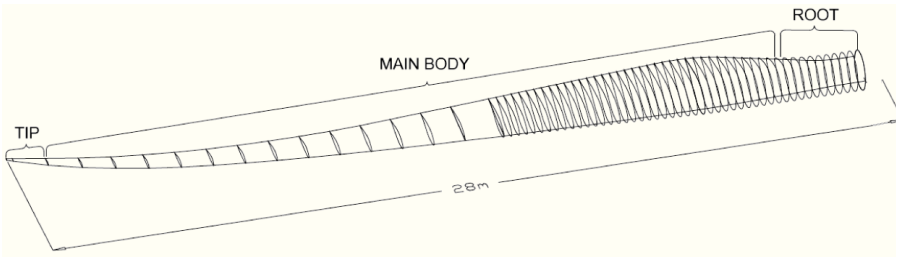

Figure 6: Example of a wind turbine blade planform. It consists of a distribution of airfoils and their chord length, twist and offset. The blade can be divided in the root region, where the blade is connected to the hub, a transition region, where the transition is made from a circular cross-section to an airfoil shape, the main body, where the shape varies only gradual and the tip which is typically designed to limit tip losses and noise production. Reproduced from [25].

$$C_{opt} = \frac{2\pi r}{r}\frac{8}{9C_L}\frac{V_W}{\lambda V_r} \tag{3}$$

With:

$C_{opt} = optimum\ blade\ chord\ length\ [m]$
$r = local\ blade\ length\ [m]$
$C_L = lift\ coefficient$
$V_r = \sqrt{V_w^2 + U^2} = local\ effective\ flow\ velocity\ \left[\frac{m}{s}\right]$
$V_w = design\ wind\ speed\ \left[\frac{m}{s}\right]$
$\mathrm{U} = local\ peripheral\ speed\ \left[\frac{m}{s}\right]$
$\lambda = \frac{\Omega r}{V_w} = local\ tip\ speed\ ratio\ [-]$
$\Omega = rotational\ velocity\ \left[\frac{rad}{s}\right]$

Due to the rotation of the blade, the local peripheral speed increases along the span of the blade. This results in a change in orientation and magnitude of the local effective flow, as seen in Figure 7. The result is a variation in chord length and twist along the span.

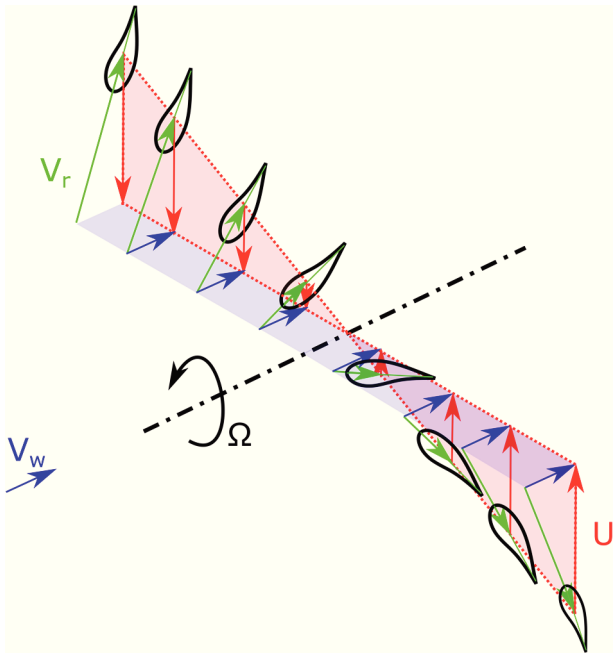

Figure 7: A schematic drawing of a two-bladed wind turbine rotor showing several stations with their local peripheral speed U (red), the design wind speed V_w (blue) and the local effective flow V_r (green). Due to the rotation of the rotor, the effective wind speed changes in magnitude and orientation along the span, resulting in a twisted blade.

1.4.2 Minimizing the cost of Energy: structural aspects

To minimize the COE, the structural design of the blades should also be considered. This is needed to minimize the ICC of the blade. The rotor experiences a complex combination of loads. As shown in Figure 8, these consist of both steady and unsteady loads, caused by aerodynamic effects, gravity and inertial forces.

Blades are designed to withstand these loads for a design life of typically 20 years. During this time, an enormous number of loading cycles take place and situations with exceptionally strong winds are likely to occur. The number of expected rotations is in the order of 10^8 to 10^9 [26]. For this reason, the blades are designed sufficiently strong and structurally stable that they are able to survive the strongest loads that are expected, known as the extreme loads, without sustaining damage. This means that the stresses and strains in the materials should remain within the allowable spectrum. Furthermore, the structure may not buckle and sufficient clearance should remain between the blade tips and the tower under these loads. In order to survive the intended lifetime, the blades should be able to resist the fatigue loads and resonance should be avoided. This last requirement is

typically achieved by creating a blade with a high specific stiffness, of which the first eigenfrequency is above excitation frequencies such as the first tower passing frequency [27].

While initially, the aerodynamic and structural aspects of a blade were considered separately, there is a strong link between both [28]. Especially regarding the shape of the rotor, both aspects have counteracting interests. The aerodynamic aspects give preference to thin airfoils with low drag coefficients, while structural aspects prefer airfoils with a high relative thickness. As the blades can be considered cantilevered beams, a cross-section with a higher thickness will result in a better shape factor and higher second moment of area. Tradeoffs between both aspects are made. In modern blades, the structural side governs the design of the root and transition regions, while further outboard aerodynamic aspects are dominant [24]. For this reason, modern blades often make use of a large root diameter and so called "flatback" airfoils in the root region [29]–[31]. Figure 9 shows both a design that is focused on aerodynamics and a design that considers both aerodynamics and structural aspects by using a large root diameter and flatback airfoils.

Further, the shape of the blade has also been used to reduce the strictness of structural requirements. This is done by creating a pre-coned or pre-curved planform shape which shifts the blade tip away from the tower and makes the tower clearance requirement less strict as can be seen in Figure 10 [32]. This requirement can be the strictest for certain blades. It has even been suggested to locally reduce the tower diameter to increase the inherent tip clearance [33].

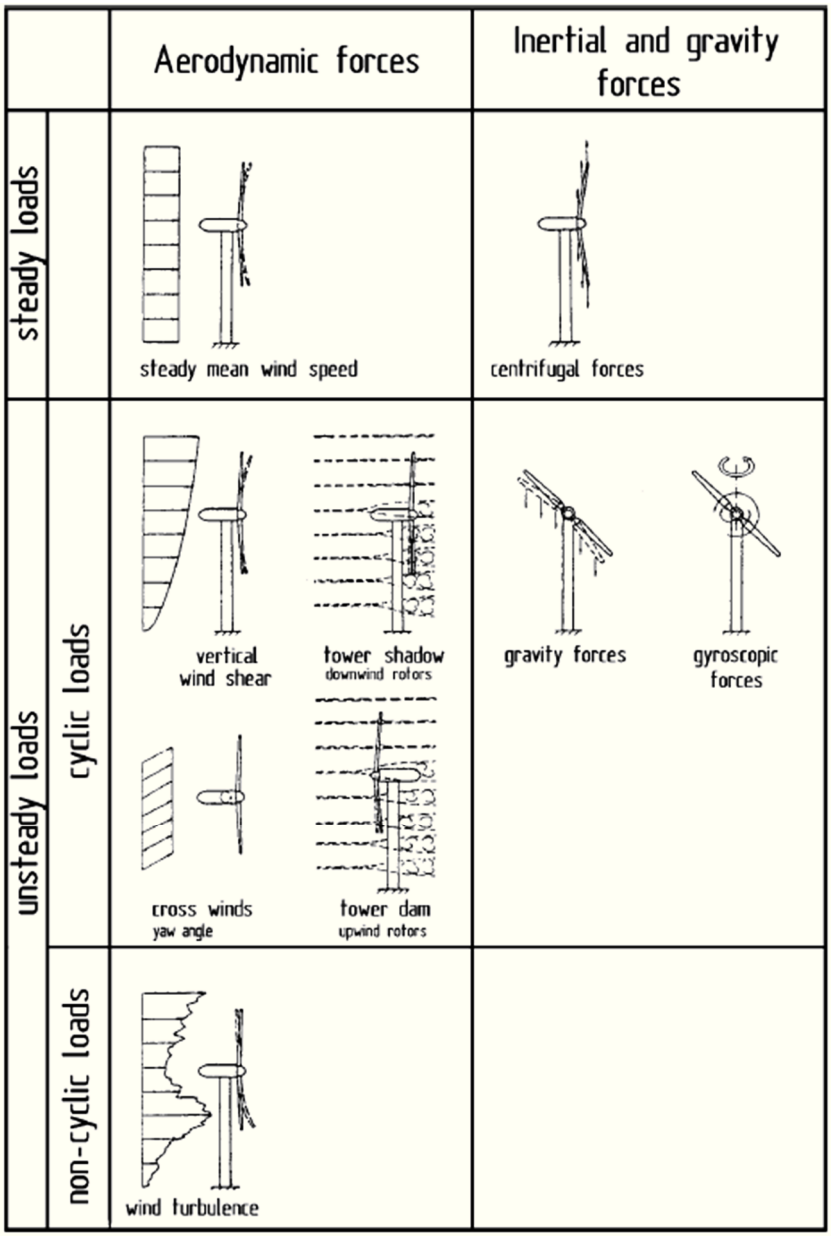

Figure 8: Overview of the loads experienced by the blades. Steady and unsteady loads result from aerodynamic, inertial and gravitational forces. Reproduced from Ref. [34].

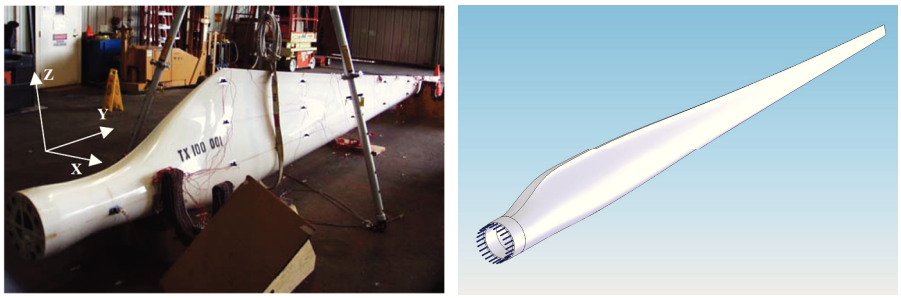

(a) (b)

Figure 9: Comparison between a design where aerodynamic aspects and structural aspects were considered separately and a design where the tradeoff between both aspects is considered. (a) The TX-100 blade with a small root diameter and conventional airfoils. The blade planform design is focused on aerodynamic performance. Reproduced from Ref. [35]. (b) The "Blade Systems Design Studies" (BSDS) blade with a large root diameter and flatback airfoils. The blade planform combined aerodynamic and structural aspects. Reproduced from Ref. [36].

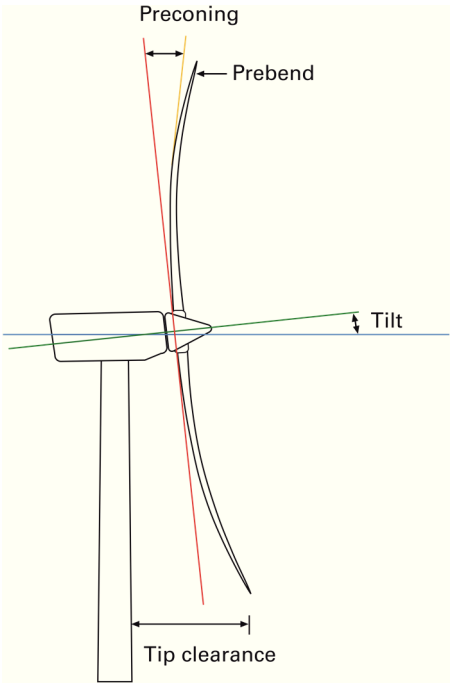

Figure 10: A wind turbine with a pre-coned and a pre-curved or "pre-bent" blade. By altering the shape in this way, the requirement to provide sufficient tower clearance under extreme loads becomes less strict. Reproduced from Ref. [37].

1.4.3 Material selection for wind turbine blades

1.4.3.1 Motivation for the use of composite materials

Older blade designs such as the NASA Mod designs were constructed from steel and aluminum, whereas modern rotor blades are made from composite materials. This evolution can be understood by using Ashby's material selection method [26], [38]. A conventional HAWT blade can be considered to be a cantilevered beam loaded in bending. At the root connection, displacement and rotations are constrained, while aerodynamic and gravitational loads are applied over its full length. The purpose is to find the lowest mass for a given stiffness. Considering the mass of the beam as:

$$m = AL\rho \tag{4}$$

with length L and density ρ

And the stiffness as:

$$S = \frac{F}{\delta} = \frac{CEI}{L^3} \tag{5}$$

with:

F: force
δ: compliance
C: $constant$
E: $Younghs\ modulus$
I: $second\ moment\ of\ area\ of\ the\ section$

Together with the shape factor:

$$\varphi_B^e = \frac{I}{I_0} = \frac{12I}{A^2} \tag{6}$$

with:
I_0: *second moment of area of a reference cross section (solid square)*
This gives:

$$m = \left(\frac{12S}{C}\right)^{1/2} L^{\frac{5}{2}} \left[\frac{\rho}{(\varphi_B^e E)^{1/2}}\right] \tag{7}$$

$$PI = \frac{\sqrt{E}}{\rho} \tag{8}$$

Equation (7) can be considered to contain a factor that solely depends on material properties. Considering that we want to minimize the mass for a given stiffness, we can derive a performance index (PI) for each material for this specific

application as $PI = \frac{\sqrt{E}}{\rho}$. In Figure 11 a plot of these values is shown for different materials with logarithmic scales. The PI can be added to this plot as a straight line. Materials with a higher Young's modulus for a given density have a higher PI and are more desirable. Furthermore, we should include an absolute minimum stiffness requirement, considering that the tower clearance should be respected. From the resulting diagram we can see that composite materials reach a very high PI. For this reason, modern wind turbine blades are manufactured from composite materials such as glass fiber reinforced polymers (GFRP) and carbon fiber reinforced polymers (CFRP). An additional reason is their high fatigue resistance. While ceramics also reach very high PI values, they should be excluded for their low fracture toughness.

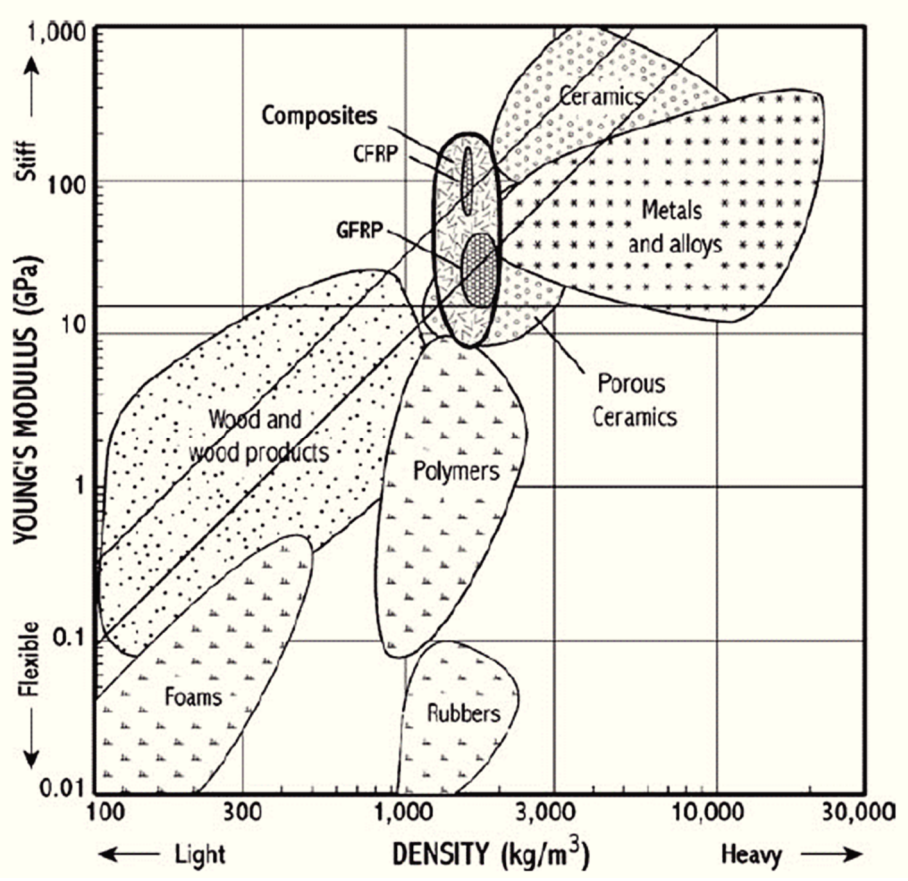

Figure 11: Diagram showing the stiffness and density of candidate materials for building wind turbine blades. For a beam loaded in bending, the performance index (PI) can be calculated as $PI = \sqrt{E}/\rho$. This can be represented by lines in the diagram. Two lines are

shown: one for PI=0.003 (lower line) and one for PI=0.006 (upper line). Furthermore, a minimum absolute stiffness of 15 GPa is imposed, which is shown as a horizontal line in the diagram. The plot shows that composite materials are excellent candidates. Reproduced from Ref. [26].

1.4.3.2 *Motivation for the use of sandwich materials*

Initial composite blades used a simple skin to carry the loads, that was made entirely out of GFRP laminate. However, since blades are large hollow structures, this makes buckling the most critical requirement. This means that the material thickness needs to be much greater than would suffice for the strength and stiffness requirements, resulting in a heavy blade. To reduce the total mass, sandwich structures were introduced. These use a core material to space the laminate skins on the top and bottom sides. Similar to an I-profile loaded in bending, the top and bottom flanges are loaded in tension and compression, while the core is mainly loaded in shear [37]. This allows for a big increase in bending stiffness and thus buckling resistance without adding much weight [39].

1.4.4 Wind turbine blade structural layout

Different structural layouts are used in modern wind turbine blades. Essentially, blades contain (i) a structural beam, known as the "spar", which is the main structural component and (ii) aerodynamic shells which form the outer shape of the blade. The spar consists of flanges, also known as "girders" or "spar caps" and connecting pieces known as "shear webs". As shown in Figure 12, some manufacturers produce this beam as one component, to which subsequently the aerodynamic shells are added using adhesive. This is known as the "stressed spar" approach. The alternative approach is known as the "stressed skin" approach and consists of producing the aerodynamic shells with the flanges of the spar structure embedded. The shear webs are then added as separate components. The main structural difference between both approaches is in the location of the adhesive bonds.

To provide a high specific bending stiffness, the spar consists of flanges or girders made primarily from UD fibers oriented in the longitudinal direction of the beam. The flanges are connected by shear webs, which typically consist of a sandwich structure with ±45 ° layers to transfer shear between the flanges. Meanwhile, the aerodynamic skin is typically made from a sandwich structure with ±45 ° layers in the skins.

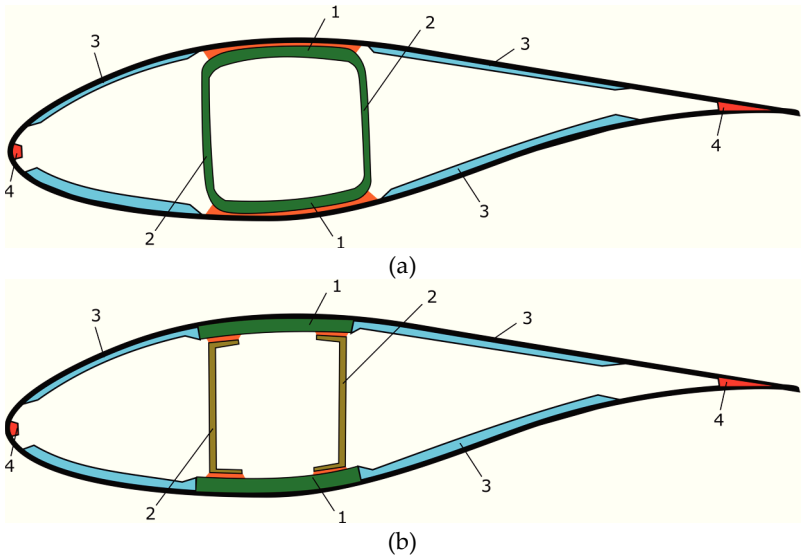

Figure 12: Schematic view of different structural layouts of wind turbine blades. (a) stressed spar approach. The main structural spar is manufactured as a single component onto which the aerodynamic shells are added using adhesive bonds. (b) Stressed skin approach. The flanges (girders or spar caps) of the spar are embedded in the aerodynamic skins. Adhesive bonds are used to connect the shear webs to the flanges. Numbers: 1: flange, 2: shear web, 3: sandwich skin, 4: adhesive joint.

1.5 Wind turbine blade manufacturing

1.5.1 State-of-the-art

While wind turbine blades were initially constructed using methods derived from aerospace, most modern wind turbine blades are built using methods derived from composite ship building [34], [40]. This is motivated by a strong drive to produce the blades at low costs [28]. Different stages in the production process used at PowerComposites Limburg[1] can be seen in Figure 13. Large clamshell molds are used to manufacture separate pressure (PS) and suction sides (SS) and up to three shear webs, which are later joined together using thick adhesive bonds [41]. The main components are produced using processes such as bladder molding, wet-layup or vacuum assisted resin transfer molding (VARTM) [42]–[44]. Alternatively, some manufacturers use an approach that allows blades to be produced with a single infusion step [43], [44]. This has the advantage that the structural adhesive bonds can be avoided. Typically, the blades are created by

[1] PowerComposites Limburg was a manufacturer of wind turbine rotor blades. The company was closed in 2012.

manual placement of the dry fabric material in the mold after which the material is infused and cured.

Figure 13: Pictures of the wind turbine blade manufacturing process at PowerComposites Limburg. (a) Manual positioning of glass fiber mats in the mold for producing the spar cap of a blade. (b) Manual placement of PVC core material in the mold. (c) Installation of a shear web. (d) Closing of the clamshell molds. (e) Manual over-lamination of the adhesive joints in the root region. (f) Grinding of the edges of the wet layup to obtain a smooth leading edge (LE).

1.6 Future trends

1.6.1 Upscaling

Over the past decades wind turbines have been developing rapidly. Most notably, the size of the rotor diameter and the corresponding power output has been increasing steadily from rotor diameters of 30 m and a rated power of about 100 kW up to diameters of 180 m, with rated powers as high as 9.5 MW [34], [45]. This up-scaling trend is still ongoing, especially offshore. Recently, blade designs of over 100 m in length have been announced [46]. The EU project "Upwind" even suggested that 20 MW turbines are feasible. Figure 14 illustrates the dimensions of such a hypothetical turbine. The motivation for this upscaling is an expected reduced cost of energy (COE) for larger rotors because of increased economics of scale [47]. As shown in equation (9), the power of the rotor increases with the square of the rotor radius.

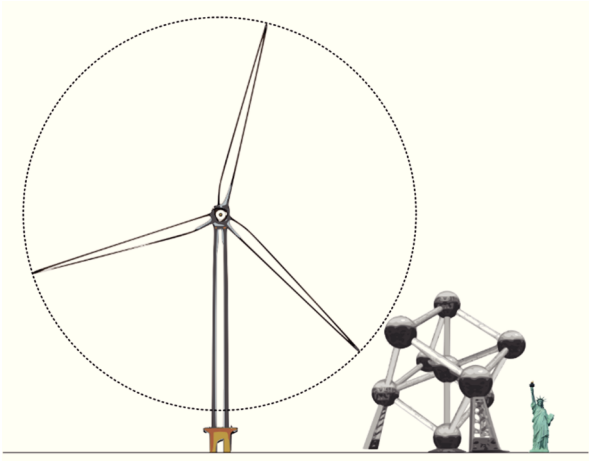

Figure 14: Height comparison between a hypothetical 20 MW wind turbine, the atomium monument in Brussels (Belgium) and the statue of liberty monument in New York city (USA). The statue of liberty is 46 m tall and the atomium 102 m while the dimensions of the wind turbine are based on those reported for the hypothetical 20 MW turbine in the UpWind project [48].

$$P = C_{PR}\frac{\rho}{2}v_W^3 A = C_{PR}\frac{\rho}{2}v_W^3 \pi r^2 \quad (9)$$

with:

$P = rotor\ power\ [W]$
$C_{PR} = power\ coefficient\ of\ the\ rotor\ [-]$
$\rho = air\ density\ \left[\frac{kg}{m^3}\right]$
$A = swept\ area\ of\ the\ rotor\ [m^2]$
$v_w =$ wind velocity $\left[\frac{\mathrm{m}}{\mathrm{s}}\right]$
$r = rotor\ radius\ [m]$

However, this up-scaling leads to issues which can cause a steep increase in costs related to the production and handling of blades, to the extent that further up-scaling may no longer be beneficial. As shown in Figure 15, the blade mass scales more rapidly than the power of the turbine. With larger blades, production tolerances increase resulting in thickness variations of the adhesive bonds. This adds weight and causes stress concentrations [49]. Heating and temperature control become more difficult while very thick laminates give exothermic reactions which can cause damage [50]. At the same time defects become more severe and prevalent in larger volumes resulting in a lower strength than assumed from coupon data [51]. These lower the load-carrying capacity of the structure and may require scrapping the part, which is more expensive for a larger blade [52], [53]. Therefore, optimal rotor sizes exist for on- and offshore wind turbines. These optima can be increased by technical improvements [54].

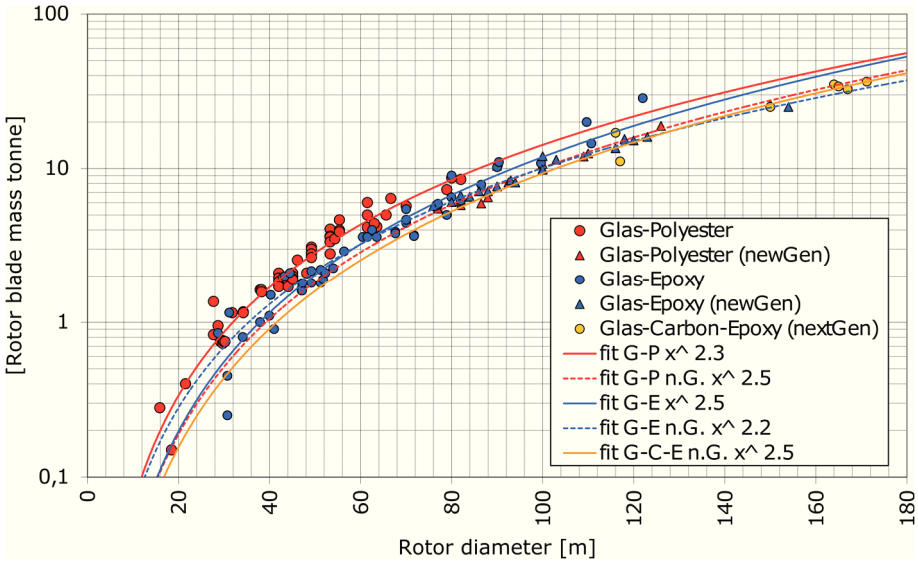

Figure 15: Overview of rotor blade mass as function of size for different blades made of different materials. Different scaling exponents can be observed for blades using different materials. These are higher than 2, meaning that the blade mass increases more rapidly than the power of the turbine. Reproduced from Ref. [55].

1.6.2 Advancements in manufacturing

Modifications to the conventional production process have been suggested to counter the issues with manufacturing large blades. Some examples are shown in Figure 16. Typically, these modifications allow the structure to be produced in separate components, allowing better quality of the individual pieces. Frequently, a separately cured spar structure is used [51]. To avoid thick laminates, the girders can even be divided in several parts that are glued on top of each other [56]. Similarly, the root region, where very thick laminates are common, is often created as a pre-fabricated part or constructed using pre-fabricated modules [50]. Furthermore, automation of these processes is under development [57], [58]. Sometimes, large parts of the blades are produced separately and joined together using adhesive bonds before transport [59]. This approach can be taken one step further, by producing so-called “segmented”, “split” or “modular” blades. These are produced as several separate components, that are assembled together after transport to the turbine site [60].

1.6.3 Advancements in structural layout and materials

The structural design of wind turbine blades is still evolving. Various changes to the typical layout and materials have been suggested. Changes that have been

considered include the use of core material in the spar caps [61], [62], the use of ribs and bulkheads [61], replacing the sandwich structure with a space-frame structure [63], [64] and the use of other materials such as carbon fiber in the spar caps [62], [65], [66] and layups with fibers angled at different orientations in the skin [67].

Furthermore, methods have been proposed to improve the quality of the adhesive joints. These include reducing the notch effect by producing a bond with a better shape [68], [69] and using vacuum infusion to prevent voids [70], [71].

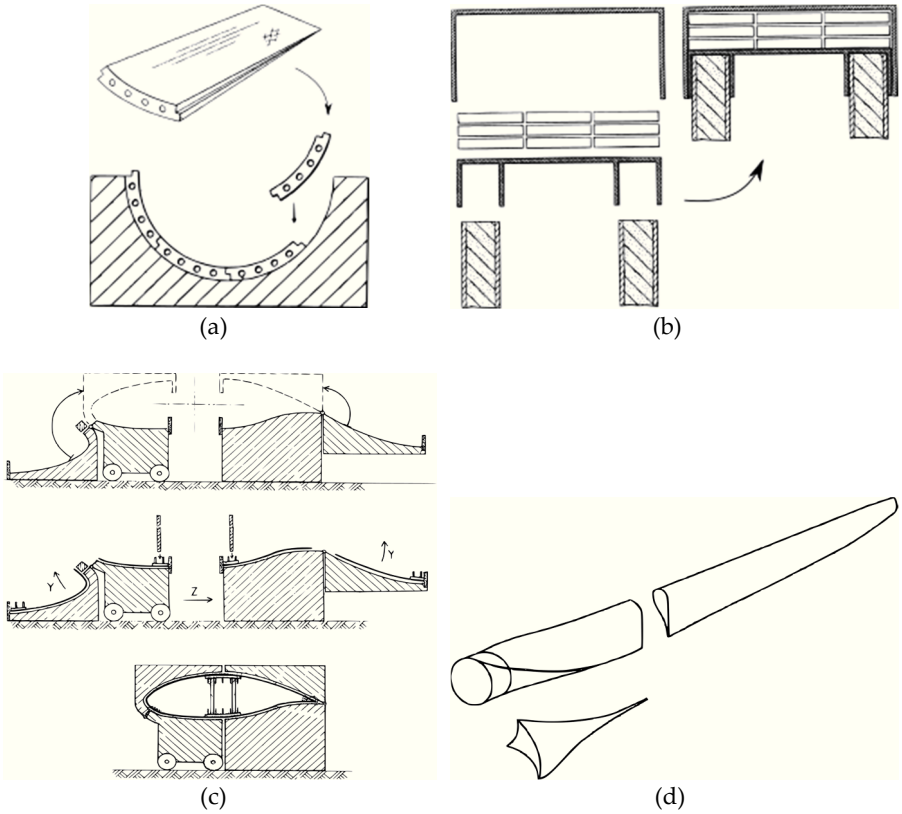

Figure 16: Suggested improvements in the manufacturing process. (a) Blade root joint consisting of pre-fabricated segments as suggested in Ref. [50]. (b) Blade spar structure with a girder assembled from adhesively joining several pultruded planks as suggested in Ref. [56]. (c) Manufacturing method for blades which uses several separated molds, allowing good access to each part as suggested in Ref. [72]. (d) Example of a segmented blade design, suggested in Ref. [73].

1.7 The need for accurate modelling of the blades

One aspect which has a strong influence on the COE is the reliability of the turbine. If energy production is halted due to a fault in a certain component, this naturally affects the AEP. Figure 17 shows which components cause reliability problems. The rotor is an area where improvements in reliability are desirable. Despite high safety factors, failure rates are relatively high [73], [74].

In the past, blades could only be developed by creating actual prototypes and experimentally testing them. This is costly and slow. An alternative is provided by using a modelling approach, which allows the cost-effective investigation of many design variations [76].

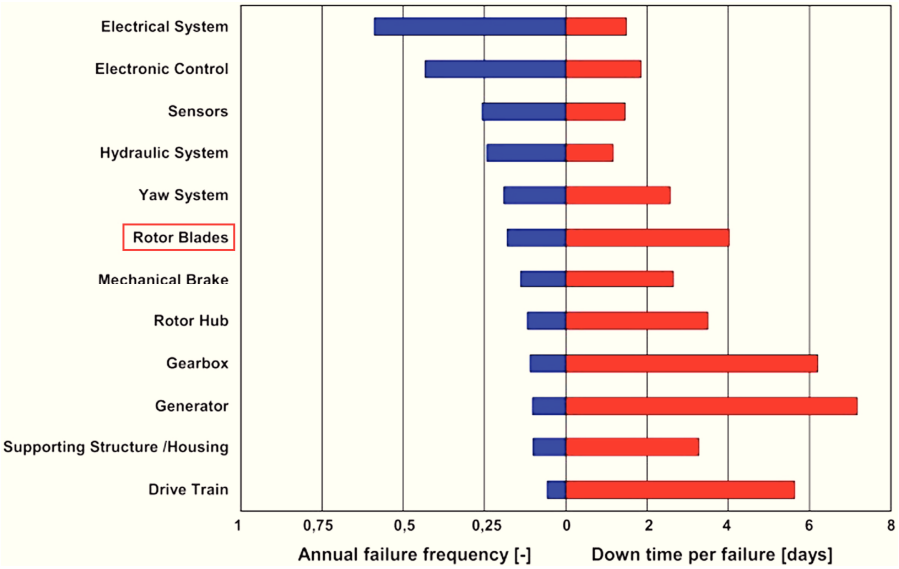

Figure 17: Failure rate and turbine downtime for different components of the wind turbine, based on historical data for a large number of turbines. This indicates the need to improve the reliability of the blades. Reproduced from Ref. [77].

1.8 The OptiWind project

This PhD-thesis was conducted as part of the SBO project OptiWind (Serviceability Optimization of the Next Generation Offshore Wind Turbines) [78]. The project focusses on research and developments benefitting the next generation of offshore wind energy installations. Six consortium partners were involved and a variety of wind turbine subassemblies were included in the seven different work packages. An overview of the work packages can be seen in

Figure 18. The work presented in this dissertation was conducted under work package 4 (WP4): "Blades". Within the work package, the finite element modelling of blades and the investigation of the concept of segmented blades were the key tasks. In addition, the presented work contributed to the FWO project "Fluid-structure interaction simulations of wind turbines with composite blades" in which the coupled interaction of blades and the surrounding airflow are numerically investigated.

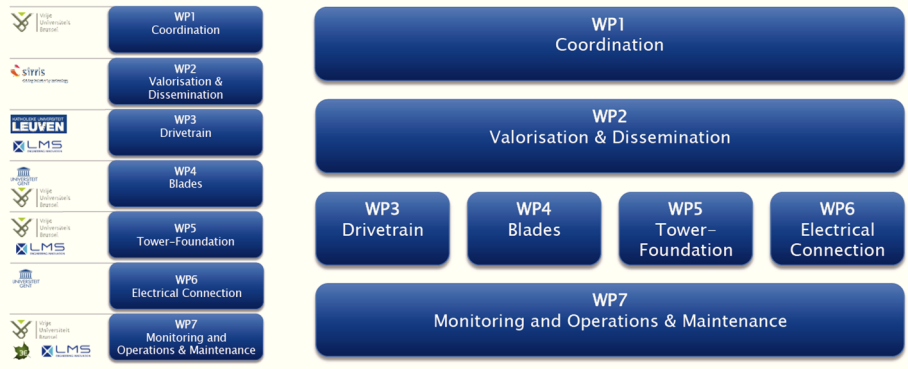

Figure 18: Overview of the work packages and the assigned project partners within the SBO project "OptiWind- Serviceability Optimization of the Next Generation Offshore Wind Turbines". This work was performed under WP4: Blades. Reproduced from Ref. [78].

1.9 Innovative aspects of this work

- Development of novel tools for the finite element (FE) modelling of blades: More advanced FE models are needed for the detailed investigation of blades. Most blade models consist purely of shell elements positioned on the outside of the blades. While these models suffice for some calculations, limitations exist. For this reason, more advanced models, using continuum elements or combinations of shell and solid elements have been suggested. However, few existing tools are capable of creating such models. Within this work, several different approaches have been investigated and software tools developed for the creation of detailed FE models. The final result is an object-oriented stand-alone tool that divides the complex task of modelling a blade in a series of far simpler tasks. This is achieved by using a new approach, which considers the blade as a collection of pre-defined parametric blocks. This allows a wide variety of types of models to be created and can serve as a platform that is flexible and can easily be extended.

Furthermore, the tool handles the processes of creating the blade geometry, the calculation of all required partitions, the creation of the FE mesh and calculation of accurate local material orientations on an element-by-element basis.

- Development of an approach for cost-effective aero-elastic calculations of blades using a detailed FE model: Aero-elastic calculations are typically conducted using beam models on the structural side. However, these do not provide the same level of detail as more advanced shell or solid models. To allow a computationally cost-effective fluid structure interaction (FSI) to be investigated, a new coupling was created between an aerodynamics code that relies on blade element momentum (BEM) theory (HAWC2aero) and the FE solver (Abaqus). Furthermore, a commercial 49 m blade was modelled. In a collaboration with the department of flow, heat and combustion mechanics of Ghent University, the aero-elastic behavior of that blade was investigated using a detailed CFD-FEM approach.
- Investigation of the static certification tests using advanced FE models: Certification of a new blade design typically requires the static testing of a full-scale prototype. Such tests were conducted for the 43 m long blade considered in this study. During the tests, loads, displacements and strains were recorded. In this work, the tests are numerically replicated using both conventional shell and advanced solid models. The resulting root bending moments, displacements and strains are extracted and compared to the experimental values, validating the simulations and approach. Furthermore, the influence of choices in the modelling approach were investigated.
- Segmented blades: The drive to reduce the LCOE from wind has resulted in an upscaling of the blade dimensions. Therefore, issues have risen regarding the manufacturing, handling and transportation, installation and maintenance of blades. These problems are severe and have resulted in the search for alternative approaches, such as the development of so-called “segmented” blades consisting of multiple components. In this work a thorough investigation into the existing segmented blade concepts was conducted, revealing that most blade manufacturers have filed patents claiming approaches to build split blades. This indicates a strong industrial interest, which so far has gone largely unnoticed in academia.

1.10 Structure of this manuscript

Chapter 2 provides an overview of the state-of-the-art regarding the use of finite element (FE) modelling of wind turbine blades. The use of FE

analyses for blades is motivated and the types of analyses and models used in industry and academia are discussed.

Chapter 3 discusses tools for the creation of blade FE models. Firstly, the need for tools is explained and an overview of existing tools is provided. Subsequently, the novel tools developed within this work are described. Several approaches have been used, ranging from the automation of a commercial pre-processor to the development of stand-alone tools for the creation of shell models using a slice based approach and the creation of shell and solid models using a block based approach. This last approach is discussed in detail as it is the final result of the experience gained using the earlier approaches.

In Chapter 4 the creation of models for several blades is discussed. First, the differences between academic reference blades and detailed commercial blades are discussed. Subsequently, the considered blades are introduced and the validity of the produced models is verified in terms of shape, mass and eigenfrequencies. This is also used to point out the importance of correct material orientations.

In Chapter 5 the coupled interaction between blades and the surrounding flow is considered. This interaction presents a fluid-structure-interaction that is typically solved in aero-elastic blade simulations using beam models and blade element momentum (BEM) theory. To allow more detail to be considered at the structural level, a new coupling was developed between HAWC2aero and Abaqus. The behavior of a 10 m blade incorporating planform sweep was investigated under various steady wind conditions. In addition, the result of detailed FSI investigations using strongly coupled computational fluid dynamics (CFD) and FE models resulting from a collaboration with the department of flow, heat and combustion mechanics of Ghent University are briefly discussed.

Chapter 6 presents the numerical investigation of the static certification testing of a 43 m wind turbine blade. The blade was tested under extreme static loads at a certified test center. Various instrumentation was used to record the behavior of the blade. The loads, displacements and strains were recorded. The tests were numerically replicated using both shell and detailed solid models. Data were extracted from the simulations and compared to the experimental values. Furthermore, influences of the analysis approach on the result are investigated.

In Chapter 7 an overview of the conclusions of the performed work is provided and an outlook towards future research is given.

Appendix A presents a detailed overview of the state-of-the-art segmented blades. While initially the research project envisioned investigating joint connections for split blades, priority was given to the development and validation of accurate simulations of single segment blades.

1.11 Bibliography

[1] "Scientific consensus: Earth's climate is warming," *Climate Change: Vital Signs of the Planet*. [Online]. Available: https://climate.nasa.gov/scientific-consensus. [Accessed: 01-Nov-2017].

[2] J. Cook *et al.*, "Consensus on consensus: a synthesis of consensus estimates on human-caused global warming," *Environ. Res. Lett.*, vol. 11, no. 4, p. 048002, 2016.

[3] C. Parmesan and G. Yohe, "A globally coherent fingerprint of climate change impacts across natural systems," *Nature*, vol. 421, no. 6918, pp. 37–42, Jan. 2003.

[4] W. Cramer *et al.*, *Detection and Attribution of Observed Impacts*, vol. 18. Cambridge: Cambridge University Press, 2014.

[5] P. M. Cox, R. A. Betts, C. D. Jones, S. A. Spall, and I. J. Totterdell, "Acceleration of global warming due to carbon-cycle feedbacks in a coupled climate model," *Nature*, vol. 408, no. 6809, pp. 184–187, Nov. 2000.

[6] M. Meinshausen *et al.*, "Greenhouse-gas emission targets for limiting global warming to 2 °C," *Nature*, vol. 458, no. 7242, pp. 1158–1162, Apr. 2009.

[7] Anonymous, "Paris Agreement," *Climate Action - European Commission*, 23-Nov-2016. [Online]. Available: https://ec.europa.eu/clima/policies/international/negotiations/paris_en. [Accessed: 09-Jan-2018].

[8] The European parliament and the council of the European uniton, *Directive 2009/28/EC on the promotion of the use of energy from renewable sources*. 2009.

[9] European commission, "Report from the comission to the European parliament, the council, the European economic and social committee and the committee of the regions - Renewable Energy Progress Report," Brussels, COM(2017) 57 final, 2017.

[10] G. Corbetta, A. Ho, I. Pineda, and K. Ruby, "Wind energy scenarios for 2030," European Wind Energy Association, Aug. 2015.

[11] I. Pineda and P. Tardieu, "Wind in power - 2016 European statistics," WindEurope, Feb. 2017.

[12] S. Tegen, E. Lantz, M. Hand, B. Maples, A. Smith, and P. Schwabe, "2011 Cost of Wind Energy Review," National Renewable Energy Laboratory, NREL/TP-5000-56266, Mar. 2013.

[13] L. J. Fingersh, M. M. Hand, and A. S. Laxson, "Wind turbine design cost and scaling model," National Renewable Energy Laboratory, NREL/TP-500-40566, Dec. 2006.

[14] P. Lako and M. Koyama, "Wind Power - Technology Brief," International Renewable Energy Agency, Mar. 2016.

[15] S. Mueller *et al.*, "Next Generation Wind and Solar Power - From cost to value," International Energy Agency, 2016.
[16] Siemens AG, "What is the real cost of offshore wind? - A macro-economic viewpoint." 2014.
[17] C. Monroy Aceves, M. P. F. Sutcliffe, M. F. Ashby, A. A. Skordos, and C. Rodríguez Román, "Design methodology for composite structures: A small low air-speed wind turbine blade case study," *Mater. Des. 1980-2015*, vol. 36, pp. 296–305, Apr. 2012.
[18] H. Heerkes and R. Scherer, "Wind Turbine Rotor, and Hub and Extender Therefor," WO0142647 (A2), 14-Jun-2001.
[19] L. Morris, "Direct Drive vs. Gearbox: Progress on Both Fronts," *Power Engineering*, 2011. [Online]. Available: http://www.power-eng.com/articles/print/volume-115/issue-3/features/direct-drive-vs-gearbox-progress-on-both-fronts.html. [Accessed: 17-Mar-2017].
[20] J. Lockwood and W. Lockwood, "Precast Concrete Post Tensioned Segmented Wind Turbine Tower," WO2014021927 (A3), 30-May-2014.
[21] A. Cortina-Cordero, J. P. Cortina-Ortega, and J. P. Cortina-Cordero, "Segmented Concrete Tower for Wind Power Generators and Method of Erecting Thereof," EP2215320 (B1) Abstract of corresponding document: WO2009056969 (A2), 22-Jun-2016.
[22] A. Cortina-Cordero, J. P. Cortina-Ortega, and J. P. Cortina-Cordero, "Segmented Concrete Tower for Wind Power Generators and Method of Erection Thereof," WO2009056969 (A3), 22-Oct-2009.
[23] C. Golightly, "Offshore Wind Foundations Brussels 8th November 2017," Nov-2017.
[24] P. J. Schubel and R. J. Crossley, "Wind Turbine Blade Design," *Energies*, vol. 5, no. 12, pp. 3425–3449, Sep. 2012.
[25] T. Ashwill and G. Kanaby, "Sweep-twist adaptive blade," *EWEC 2007*, 2007.
[26] P. Brøndsted, H. Lilholt, and A. Lystrup, "Composite materials for wind power turbine blades," *Annu. Rev. Mater. Res.*, vol. 35, no. 1, pp. 505–538, Aug. 2005.
[27] C. Berggreen, K. Branner, J. F. Jensen, and J. P. Schultz, "Application and Analysis of Sandwich Elements in the Primary Structure of Large Wind Turbine Blades," *J. Sandw. Struct. Mater.*, vol. 9, no. 6, pp. 525–552, Nov. 2007.
[28] M. Froese, "The manufacturing evolution of wind-turbine blades," *Windpower Engineering & Development*. [Online]. Available: http://www.windpowerengineering.com/featured/business-news-projects/manufacturing-evolution-wind-turbine-blades/. [Accessed: 14-Apr-2017].

[29] F. Grasso, "Development of thick airfoils for wind turbines," *J. Aircr.*, vol. 50, no. 3, pp. 975–981, 2013.
[30] K. J. Jackson, M. D. Zuteck, C. P. van Dam, K. J. Standish, and D. Berry, "Innovative design approaches for large wind turbine blades," *Wind Energy*, vol. 8, no. 2, pp. 141–171, Apr. 2005.
[31] J. A. Paquette and P. S. Veers, "Increased strength in wind turbine blades through innovative structural design," in *Proceedings, European Wind Energy Conference*, 2007.
[32] S. Andersen, H. Albertsen, and P. Grabau, "Windmill Rotor and Wind Blades Therefor," WO9914490 (A1), 25-Mar-1999.
[33] J. J. NIES and T. H. MALIK, "WIND TURBINE, TOWER AND METHOD FOR FABRICATING THE SAME," US7997876, 2011.
[34] E. Hau, *Wind Turbines*. Berlin, Heidelberg: Springer Berlin Heidelberg, 2013.
[35] S. Reese, D. T. Griffith, M. Casias, T. W. Simmermacher, and G. A. Smith, "Modal testing of the TX-100 wind turbine blade.," SAND2005-6454, 920816, May 2006.
[36] D. S. Berry and D. E. Berg, "Blade system design studies phase II: final project report," SAND2008-4648, 2008.
[37] Gurit, "Wind Energy Handbook," 2016. [Online]. Available: http://www.gurit.com/wind-energy-handbook.aspx. [Accessed: 02-Sep-2016].
[38] M. F. Ashby, *Materials selection in mechanical design*, 3rd ed. Amsterdam ; Boston: Butterworth-Heinemann, 2005.
[39] O. T. Thomsen, "Sandwich Materials for Wind Turbine Blades -- Present and Future," *J. Sandw. Struct. Mater.*, vol. 11, no. 1, pp. 7–26, Jan. 2009.
[40] S. C. Nolet, "Composite Wind Blade Engineering and Manufacturing," presented at the Independent Activities Period Mini-Course, 2011.
[41] W. Tong, Ed., *Wind power generation and wind turbine design*. Southampton ; Boston: WIT Press, 2010.
[42] P. S. Veers *et al.*, "Trends in the design, manufacture and evaluation of wind turbine blades," *Wind Energy*, vol. 6, no. 3, pp. 245–259, 2003.
[43] H. Stiesdal, P. B. Enevoldsen, K. Johansen, J. J. O. Kristensen, M. Noertem, and M. Winther-Jensen, "Method for manufacturing windmill blades," EP1310351 (A1), 19-Apr-2006.
[44] H. Stiesdal, "Method for manufacturing a wind turbine rotor blade and wind turbine rotor blade," EP2377674 (A1), 19-Oct-2011.
[45] S. Campbell, "10 big wind turbines | Windpower Monthly," *Windpower Monthly*, 05-Jul-2017. [Online]. Available: http://www.windpowermonthly.com/10-biggest-turbines. [Accessed: 14-Jul-2017].

[46] "GE unveils Haliade-X: The world's largest offshore wind turbine, powered by 107-meter LM blades." [Online]. Available: https://www.lmwindpower.com/en/stories-and-press/stories/news-from-lm-places/ge-announces-haliade-x-the-worlds-largest-offshore-wind-turbine. [Accessed: 06-Mar-2018].

[47] M. Caduff, M. A. J. Huijbregts, H.-J. Althaus, A. Koehler, and S. Hellweg, "Wind Power Electricity: The Bigger the Turbine, The Greener the Electricity?," *Environ. Sci. Technol.*, vol. 46, no. 9, pp. 4725–4733, May 2012.

[48] "UpWind: Design limits and solutions for very large wind turbines," Mar. 2011.

[49] M. D. Banea and L. F. M. da Silva, "Adhesively bonded joints in composite materials: an overview," *Proc. Inst. Mech. Eng. Part J. Mater. Des. Appl.*, vol. 223, no. 1, pp. 1–18, Jan. 2009.

[50] P. Hayden and P. Broome, "A Method of Making a Root End Joint of a Wind Turbine Blade and a Root Segment for Such a Joint," WO2013061016 (A1), 02-May-2013.

[51] D. A. Griffin, "Blade system design studies volume I: Composite technologies for large wind turbine blades," Sandia National Laboratories, SAND2002-1879, Jul. 2002.

[52] H. S. Toft, K. Branner, P. Berring, and J. D. Sørensen, "Defect distribution and reliability assessment of wind turbine blades," *Eng. Struct.*, vol. 33, no. 1, pp. 171–180, Jan. 2011.

[53] D. S. Cairns, T. Riddle, and J. Nelson, "Wind turbine composite blade manufacturing: the need for understanding defect origins, prevalence, implications and reliability," SAND2011-1094, Feb. 2011.

[54] G. Sieros, P. Chaviaropoulos, J. D. Sørensen, B. H. Bulder, and P. Jamieson, "Upscaling wind turbines: theoretical and practical aspects and their impact on the cost of energy: Upscaling wind turbines: theoretical and practical aspects," *Wind Energy*, vol. 15, no. 1, pp. 3–17, Jan. 2012.

[55] A. Krimmer, "Experience with design and production of large-scale rotor blades," presented at the 3rd International Conference Advances in Rotor Blades for Wind Turbines, Bremen, Feb-2014.

[56] P. T. Hayden and H. Behmer, "A Modular Structural Composite Beam," WO2011135306 (A1), 03-Nov-2011.

[57] T. Hart and J. C. Serrano, "Recovery Act: Wind Blade Manufacturing Innovation," DE-EE0001372, Dec. 2011.

[58] G. Mironov, "A Wind Turbine Blade Automated Production System," WO2011035539 (A1), 31-Mar-2011.

[59] M. Kontis and J. Kulenkampff, "Rotor Blade of a Wind Power Plant, Method of Fabricating a Rotor Blade and a Pair of Belts for a Rotor Blade," US9011103 (B2), 21-Apr-2015.

[60] A. G. Dutton, C. Kildegaard, C. Kensche, F. Hahn, D. R. V. van Delft, and G. D. de Winkel, "Design, structural testing, and cost effectiveness of sectional wind turbine blades," Aug. 1997.
[61] F. M. Jensen, H. Stang, and K. Branner, *Ultimate strength of a large windturbine blade*. 2009.
[62] M. Rosemeier and M. Bätge, "A concept study of a carbon spar cap design for a 80m wind turbine blade," *J. Phys. Conf. Ser.*, vol. 524, p. 012039, Jun. 2014.
[63] K. K. Wetzel, "Modular Blade Design & Manufacturing," presented at the Wind Turbine Blade Workshop 2014, 2014.
[64] M. L. Baker and C. P. Arendt, "Lightweight composite truss wind turbine blade," US7517198, Apr-2009.
[65] P. A. Joosse, D. R. V. van Delft, C. Kensche, D. Soendergaard, R. M. van den Berg, and F. Hagg, "Cost Effective Large Blade Components by Using Carbon Fibers," *J. Sol. Energy Eng.*, vol. 124, no. 4, p. 412, 2002.
[66] P. Grabau and L. Andersen, "Wind Turbine Blade with Carbon Fibre Tip," WO03078833 (A1), 25-Sep-2003.
[67] S. K. Ha, K. Hayat, and L. Xu, "Effect of shallow-angled skins on the structural performance of the large-scale wind turbine blade," *Renew. Energy*, vol. 71, pp. 100–112, Nov. 2014.
[68] L. Nielsen, "Notch-Reduced Composite Joint," WO2012004383 (A3), 29-Nov-2012.
[69] A. Yarbrough, "Wind Turbine Blade Shear Web with Spring Flanges," US8262362 (B2), 11-Sep-2012.
[70] B. S. Van, W. Bakhuis, and A. Billen, "Bond Line Forming Method," US7824592 (B2), 02-Nov-2010.
[71] R. Windbichler and M. Korjahn, "Leading Edge Finish by Means of a Vacuum Infusion Process," WO2015014724 (A1), 05-Feb-2015.
[72] J. Kulenkampff and B. Faulkner, "Method and Production of a Rotor Blade for Wind Energy Plant," US2011100533 (A1), 05-May-2011.
[73] R. Rohden, "Rotor Blade for a Wind Energy Installation," WO2007131937 (A1), 22-Nov-2007.
[74] S. Campbell, "Annual blade failures estimated at around 3,800," *wind power monthly*, 14-May-2015. [Online]. Available: https://www.windpowermonthly.com/article/1347145. [Accessed: 28-Dec-2017].
[75] N. Sharpley, "GCube says blade damage and gearbox failure top chart for most common US wind energy claims," *Windpower Engineering & Development*. [Online]. Available: https://www.windpowerengineering.com/business-news-projects/gcube-

says-blade-damage-and-gearbox-failure-top-chart-for-most-common-us-wind-energy-claims/. [Accessed: 20-Mar-2018].

[76] F. M. Jensen, B. G. Falzon, J. Ankersen, and H. Stang, "Structural testing and numerical simulation of a 34m composite wind turbine blade," *Compos. Struct.*, vol. 76, no. 1–2, pp. 52–61, Oct. 2006.

[77] B. Hahn, M. Durstewitz, and K. Rohrig, "Reliability of wind turbines: Experiences of 15 years with 1,500 WTs," *Fraunhofer IWES*, Jan. 2006.

[78] P. Guillaume *et al.*, "SBO Project Proposal - Serviceability Optimisation of the Next Generation Offshore Wind Turbines (OptiWind)." Jan-2012.

2 Finite element modelling of wind turbine blades: state-of-the-art

"If I have seen further than others, it is by standing on the shoulders of giants"

– *Isaac Newton*

Chapter summary: In this chapter, the available literature regarding the finite element modelling of wind turbine blades is reviewed. Reasons for using this approach are discussed, along with the various types of models that have been presented in literature and different types of analyses and their purpose.

2.1 Motivation for wind turbine blade finite element modelling

Wind turbine blade designs have been increasing in size during the last decades. They are complex structures, both in terms of shape and layup of composite materials. Furthermore, the rotor is at the beginning of the energy conversion chain. Therefore, the blades are at the beginning of a cost cascade system. For example, reducing the blade mass allows for cost savings in many other turbine components such as the bearings, generator, tower and foundation [1]. Meanwhile, the aerodynamic performance directly contributes to the overall cost of energy (COE) of the turbine. As a result, there is great value in optimizing blade designs. Nevertheless, current wind turbine blades are often designed with relatively high safety factors (SF). However, the numbers of repairs and early replacements are much higher than the SF would imply [2], [3]. According to Ref. [4] blades and rotors result in approximately 12 % of a wind turbine down time. In 2008 a survey from Sandia National Laboratories in the USA found that about 7 % of all blades from five wind farms had to be replaced. Even though the majority of issues are related to the manufacturing processes [4], [5], one could argue that this also indicates a gap in understanding of the structure's behavior. This gap should be closed by means of detailed structural analysis.

Furthermore, wind turbine blades have typically been optimized by simplified analytical methods and experimental tests [6]. Such simplified analytical models are not able to account for all the details present in blades. Similarly, analytical models fail to accurately predict the non-linear behavior that is present. This behavior is present even at moderate deformations [1]. In addition, experimental tests are very expensive and allow only idealized loads to be considered.

Alternatively, detailed analysis is possible by means of detailed finite element (FE) simulations. FE analysis allows large amounts of complexity to be considered simultaneously. This includes the full complexity of the shape, layup and boundary conditions. Furthermore, FE analysis allows non-linear effects to be considered. It provides a much more economical alternative to building and testing blades for each concept [7]. Furthermore, once the finite element model has been built, various complex load cases representing actual operating conditions can be analyzed.

In industry FE modelling is typically used to verify the stiffness, strength and stability of the design. The analyses allow a full strain field to be calculated, showing strain hotspots and allowing the calculation of fatigue behavior. Design codes such as GL2010 [8] and IEC-64100 [9] state the requirement to use FE modelling in order to verify the strength and stability of the structure.

2.2 Wind turbine blade FE models

In Figure 19, a schematic breakdown of the FE modelling of wind turbine blades is presented. Any FE model consists of a mesh to which material sections are assigned. These consist of a single material or a stack of materials as well as a local material orientation definition. The mesh is positioned in space and one or more calculation steps are assigned for which boundary conditions and loads are defined. The resulting finite element analysis (FEA) is performed by running the simulation using a solver on a computer system. The resulting data are typically stored in a database. Depending on the type of analysis, the data can contain stress and strain values in the integration points of the elements and displacements values at the nodes or eigenvalues and eigenvectors.

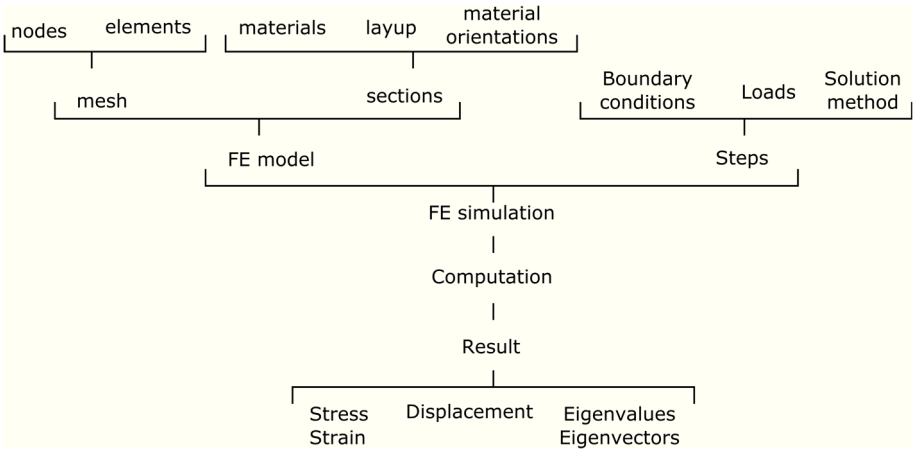

Figure 19: A schematic breakdown of FE modelling of wind turbine blades. In the presented tree structure, items ranked lower are dependent on the items ranked above.

2.2.1 Blade FE meshes

The FE model depends on the mesh in multiple ways. It provides an approximation of the geometry of the actual structure. In addition, the level of refinement of the mesh affects the complexity of the problem that can accurately be represented. Further, the level of refinement of the mesh also affects the computation effort required to obtain results. For this reason, mesh refinement analyses are used to determine a sufficient level of mesh density. In literature, it is reported that in general the displacements require a less refined mesh to converge than strain values. Refinement criteria are sometimes used. For example in GL2010, a refinement criterion is defined that considers convergence if doubling the number of elements affects values less than 5 % [8]. Furthermore, at the level of the mesh, different types of models can be produced, depending on

the types of elements that are employed. These elements hold inherent assumptions.

2.2.1.1 *Wind turbine blade beam representations*

To calculate the loads on the blades during operation, aero-elastic calculations are conducted. These are used to analyze how the turbine behaves over a time series. Due to the huge number of time steps required for the total transient load analysis, beam models are required to make the calculations feasible. These are suited since they accurately describe the overall stiffness of the blade [10].

Beam models are calculated using one of the following approaches: (i) directly from the section representation using an analytical approach, (ii) by extracting the properties from 3D FE models or (iii) by means of a 2D FE model of the cross-section.

The first approach is the most straight forward and fastest. It is typically used in the first preliminary design. The second approach is commonly known as the "beam property extraction" (BPE) method and was first presented in [11]. The BPE method, shown in Figure 20, works by applying six tip loads and extracting the resulting displacements at several sections along the span. The motivation for this approach is that it allows 3D effects such as the warping of the cross-sections to be accounted for in the beam properties.

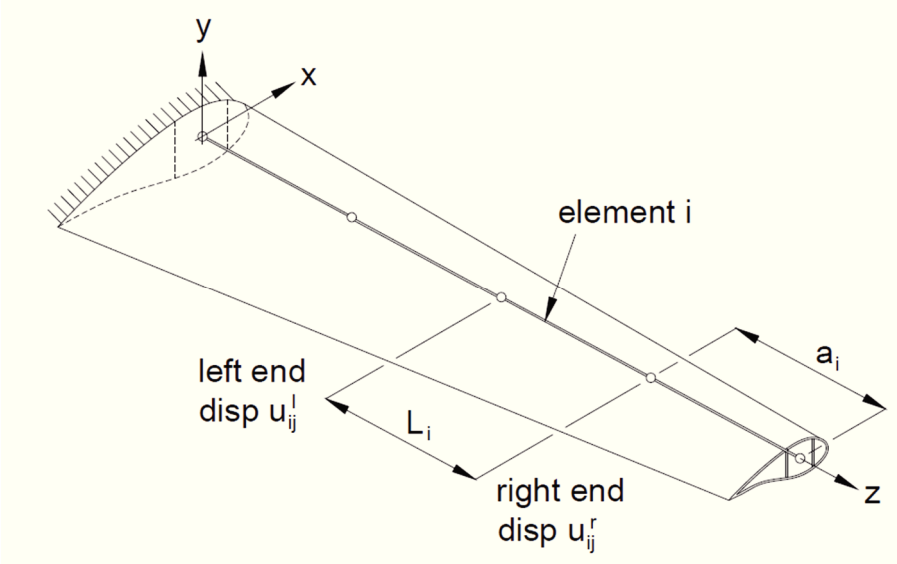

Figure 20: Schematic view of the beam property extraction method. Reproduced from Ref. [11].

In the third approach, beam properties can be calculated by means of 2D FE models for the blade sections. Such an approach is implemented in the "BEam Cross section Analysis Software" (BECAS) tool [12]. This tool was developed at DTU as MATLAB code and allows for fully populated stiffness matrices to be obtained. These are particularly suited for blades incorporating pre-curving or material couplings. Input files can be generated from either airfoils (via Airfoil2BECAS [13]) or from a python script that accepts an OML shell model in the form of an ABAQUS input file (shellexpander [14]). In addition, a version using layered solid elements also exits. An example of a meshed 2D cross-section with resulting points of interest calculated by BECAS can be seen in Figure 21. The BPE method and BECAS were compared in the master thesis of Aeneas Baert [15], which was conducted under the supervision of the author. It was concluded that more accurate results can be obtained with BECAS for asymmetric cross-sections.

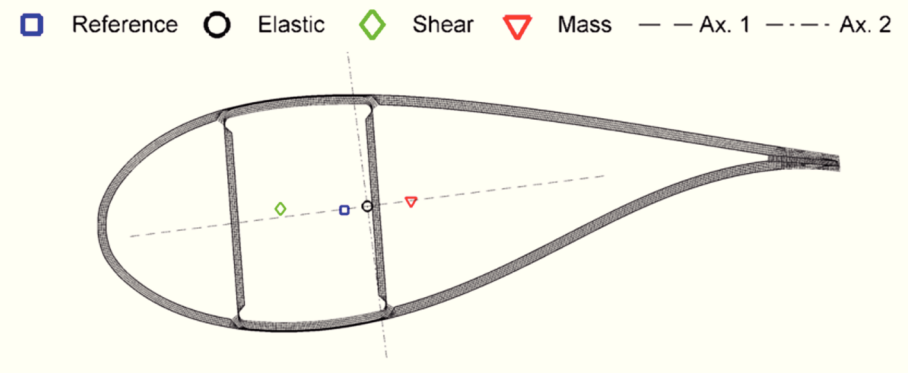

Figure 21: Plot of the mesh and calculated positions of interest of a blade cross-section using the BEam Cross-section Analysis (BECAS) Software tool developed at DTU. The properties of an anisotropic beam are calculated using 2D FEM. Reproduced from Ref. [16].

Of course, differences in accuracy exist between the different levels of modelling detail. In Bottasso et al. [17] both beam, shell and solid FE models were used to represent a wind turbine blade. Differences between the different models were observed. Specifically, the stress concentrations at the beginning and end of the spar caps or at regions with rapidly changing geometry in the span-wise direction cannot be modelled correctly by beam models. The transition zone was found to be complex, rapidly changing and poorly captured by the beam model.

2.2.1.2 *Models using shell elements positioned on the outer mold layer surface*

In industry, typical FE models of complete wind turbine blades use shell elements at the outer mold layer (OML). Such a model can be seen in Figure 22, while a comparable cross-section of an actual blade can be seen in Figure 23. The OML surface is known from the aerodynamic shape of the blade and is independent of the layup. A CAD representation of this surface is typically already present. This modelling approach mimics the manufacturing process in the sense that the elements are placed at the mold surface and material is placed inwards from that surface. OML shell models are generally accepted to be quite accurate for predicting strains and displacements of blades loaded in bending as well as for predicting their flat and edge-wise eigenfrequencies.

However, OML shell models contain several challenges. First, such models do not contain an inside surface. Consequently, the modelling of interior features such as the adhesive bonds or shear webs lacks in accuracy. In practice, the shear webs and adhesive bonds are therefore typically attached to the outside surface, which does not align with reality. This is a practical issue for all the adhesive bonds including those at the LE, TE and at the webs or spar (depending on whether a stressed shell or stressed spar approach is used).

One approach to deal better with the lack of inside surface was suggested in Branner et al. [18]. There, an attempt was made to compensate the geometric inaccuracy of the adhesive connecting a spar structure to the aerodynamic shells. This can be seen in Figure 24. The dimensions of the adhesive bonds were increased from their physical location up to the OML surface. The stiffness of the adhesive material was subsequently scaled to obtain the same section stiffness as in a physically correct representation. While this does result in an acceptable behavior, the section varies along the span of the blade. If this technique would be applied to a full-scale blade model, several "virtual" materials would have to be created.

Further, Zhang et al [19] compared different modelling methods for the TE of a blade for linear buckling analysis. These included adding beam elements representing the TE adhesive that connect the node on the PS with those opposite on the SS and simple joining of TE nodes. While it was clear that further research was needed, it was concluded that a simple merging of nodes of the PS and SS at the TE (which is common practice [20]) does not result in good predictions.

An alternative approach was suggested in Haselbach et al. [21], where the adhesive at the trailing edge was modelled with solid elements that had correct dimensions and was attached to the laminate of a conventional OML shell model using a series of distributing couplings. Nevertheless, there is a scientific

consensus that including the trailing edge adhesive is important to calculate the buckling reserve of the trailing edge panels.

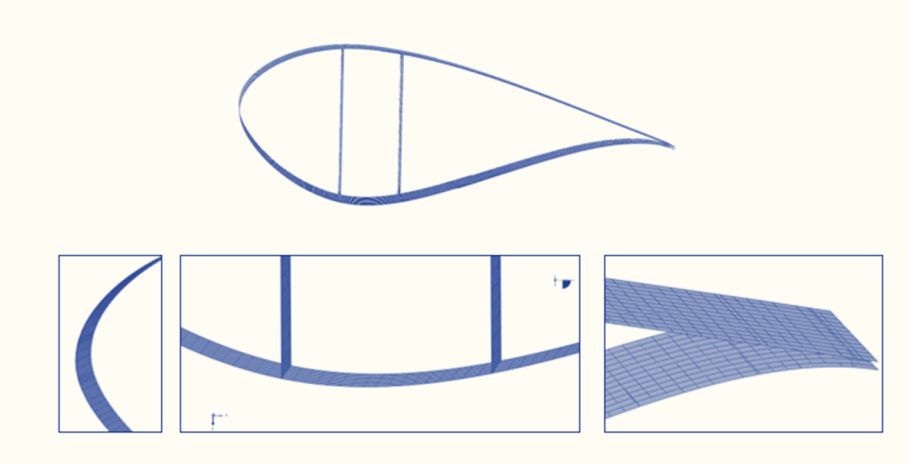

Figure 22: A typical outer mold layer (OML) shell model, which is used in industry. The elements are positioned on the outer surface and the material is offset inwards. No internal surface is present. Therefore, correctly incorporating internal features such as adhesive joints or shear webs is a challenge.

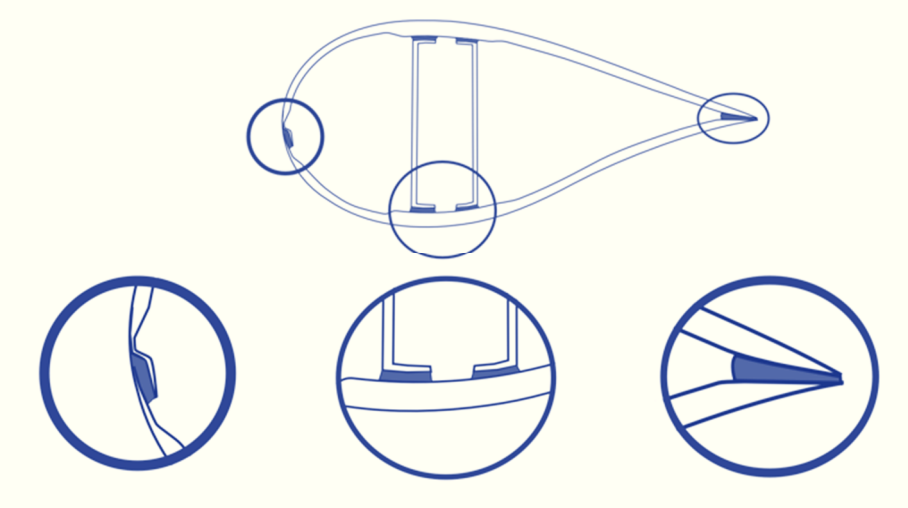

Figure 23: Schematic drawing of a cross-section of an actual wind turbine blade with a stressed shell layout (the girders are included in the PS and SS aerodynamic shell parts). Adhesive joints are used to connect the different components.

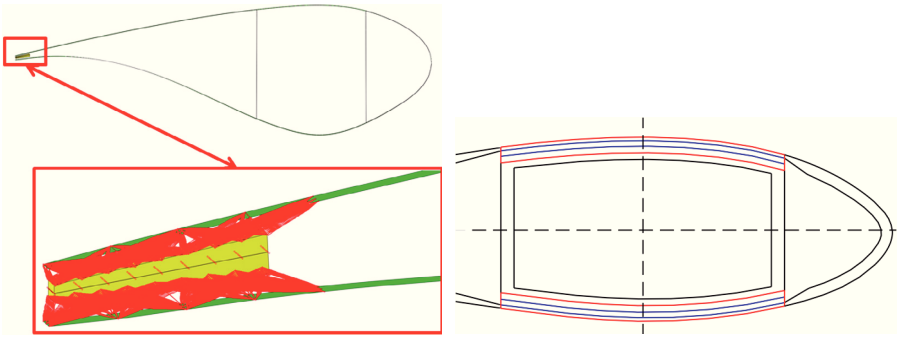

(a) (b)

Figure 24: Method for including the adhesive bonds in an OML shell model. (a) TE model suggested by Haselbach [21]. The adhesive bond is modelled with solid elements at their physical position. The bond is connected to the OML surface by means of multi-point-constraints. (b) Schematic view of a cross-section of the model considered in Branner et al. [18]. The adhesive bond between the stressed spar and the aerodynamic shell is increased in thickness to allow attaching the bond to the OML surface. The material properties of the adhesive are scaled to obtain a resulting section stiffness that matches the theoretical value. The real bond is show in blue while the modified bond is shown in red.

An additional challenge was brought up by Laird et al. [11], [22] who discovered that shell elements with material offsets produced poor results when predicting torsion. This was found to be particularly relevant for high material thickness-to-curvature ratios. This can be seen in Figure 25.

In Ref. [23] an attempt was made to avoid this issue by scaling the thickness and stiffness of the laminate. The torsional behavior is particularly important for blade designs that undergo torsional deformation such as blades with a swept planform [24], [25] or bend-twist coupling [26]. Such behavior is used as a passive way to alleviate loads. Furthermore, for larger blades the torsional eigenfrequency becomes lower and may couple with other modes. This may result in stability issues.

Alternative FEM approaches have been suggested for wind turbine blades. An overview of the possibilities is presented in Table 3. These include the use of shell elements at mid-thickness, solid elements or hybrid approaches where the skins of the sandwich structures are modelled with shell elements while the core material and adhesive bonds are modelled with solid elements. The disadvantages of these approaches are mainly that the models are much harder to obtain, since they require surfaces which are dependent on the layup to be defined [27]. However, these models are well suited for capturing inter-laminar stresses, which is interesting for example for delamination and de-bonding analysis [17].

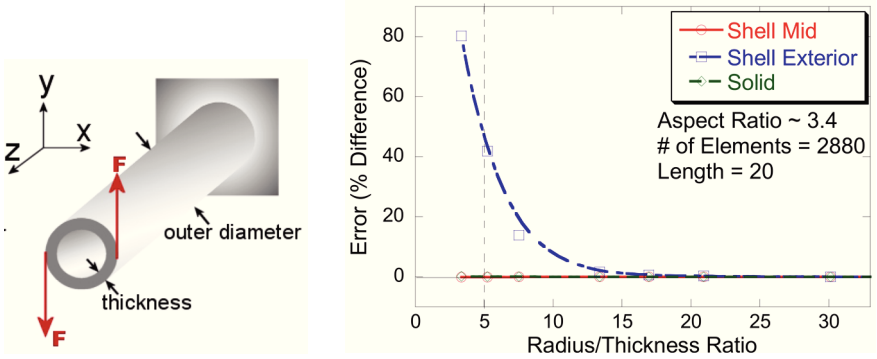

(a) (b)

Figure 25: Erroneous results for an OML shell model of a cylinder loaded in torsion reported in Ref. [22]. Different thickness-to-radius ratios are compared. (a) Set-up overview. (b) Error difference for different radius-to-thickness ratio's.

In Ref. [33] the torsional behavior of a swept wind turbine blade was investigated using a model consisting mainly of solid elements. Likewise, Refs. [18], [26], [34] used models obtained using different shell, solid and hybrid strategies to investigate the torsional behavior of a blade section with additional off-axis fibers and compared the results. The OML shell model produced poor torsional results while the solid and hybrid strategies were found to work best.

In addition, various authors have also used continuum models in regions requiring more detail. For example, in Ref. [6] the behavior of a 34 m blade under extreme loads was investigated. A shell model with elements on the OML was used, while a sub-model using both shell and solid elements was used. In Wetzel [32] a solid model of a 44 m blade was used to compare the damage tolerance of stressed spar and stressed shell blade designs. Damage introduced in the adhesive bonds would either result in a redistribution of stress or in "unzipping" of the adhesive bond resulting in blade collapse. It was found that stressed spar designs are more tolerant to damage in the adhesive. In Chen et al. [35] a model of the blade root and transition region consisting of a single layer of layered solid elements was used to investigate damage progression under ultimate load.

In Ref. [36] a 34 m wind turbine blade was modelled using second order layered solid elements. The blade was loaded in every direction up to the point of failure. In Refs. [21], [37] a model consisting of shell elements for the laminate and solid elements for the adhesive at the trailing edge joint was used to predict the behavior of a blade under ultimate leading edge to trailing edge load.

Table 3: An overview of the different approaches that have been used to model wind turbine blades. Models using shell elements on the OML surface are most common. However, models using shell elements at the mid-thickness surface, models using solid elements and hybrid configurations such as those using solid elements for the core material with shell elements on the top and bottom surfaces have been investigated.

	Approach	References
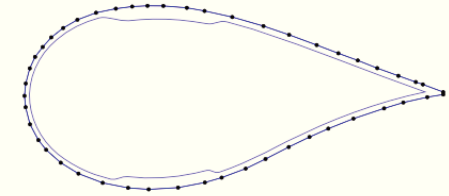	OML shell	Berring et al. [18], Kim et al. [28], Lee et al. [29], Yang et al. [30], Richards et al. [31]
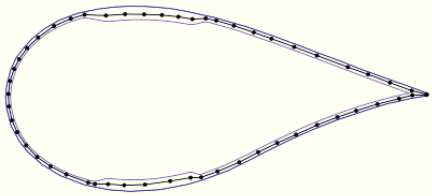	Mid-thickness shell	Bottasso et al. [17], Berring et al. [18]
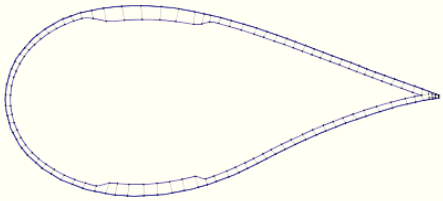	Solid	Berring et al. [18], Wetzel [32] Bottasso et al [17]
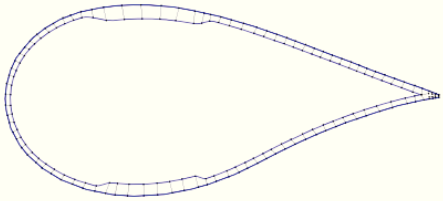	hybrid	Berring et al. [18]

2.2.1.3 *Considerations regarding the finite elements used*

While in the previous section different types of models were discussed, this does not fully define the mesh. Within each element class, different elements are still available. Most FE solvers contain a large library of element types.

For beams loaded in bending so-called "shear locking" effects can occur. An example of this effect can be seen in Figure 26 where the results of cantilevered beams loaded in bending with different thickness-to-length ratios are compared to the analytical solutions. The result of the thick beam agrees with the analytical solution, while that of the thin beam differs. The reason is that the element interpolation functions give rise to large, unphysical shear strains in bent elements. This issue would however disappear with a much more refined mesh. Alternatively, the issue can be avoided by using more advanced elements such as second order elements or elements using incompatible modes [38], [39].

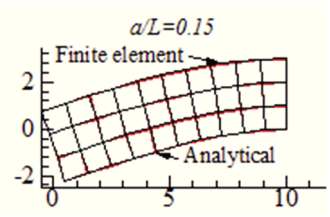

(a)

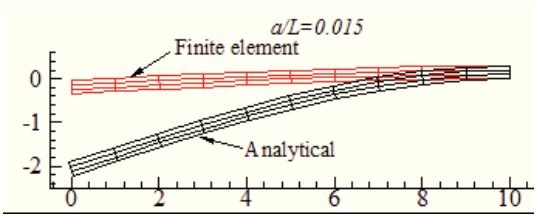

(b)

Figure 26: An example of shear locking effects. A cantilever beam with height 2a, length L and width b is considered. On the left-hand side of the beam, a force P is applied, while on the right-hand side the beam is clamped. The result of an FE analysis with linear elements is compared to the analytical solution for both a thick and a thin beam. (a) Result for a/L=0.15. (b) Result for a/L=0.015. Reproduced from Ref. [38].

Another aspect to consider is how well the element allows the modelling of transverse shear deformation. For shell elements, different approximating theories exist in this regard. In its most simple form, the Kirchoff-Love hypothesis is used, which assumes that the transverse displacement field is linear in the z-direction and the transverse shear strain is zero [40]. More accurately, the Mindlin-Reissner plate theory assumes that there is a linear variation of displacement across the plate thickness, but that this thickness does not change during deformation [41]. This can schematically be seen in Figure 27. Higher order shear theories exist, which try to remedy the issue of non-zero stress at the free top and bottom faces [41]. For a sandwich structure, the transverse shear

deformation can be significant and general-purpose shell elements or a stack of continuum (shell) elements should be used [39].

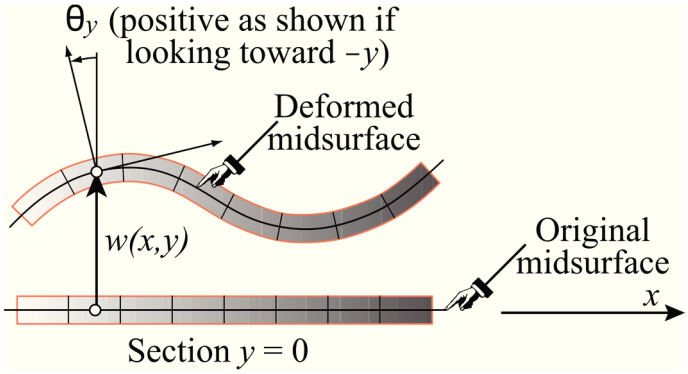

(a)

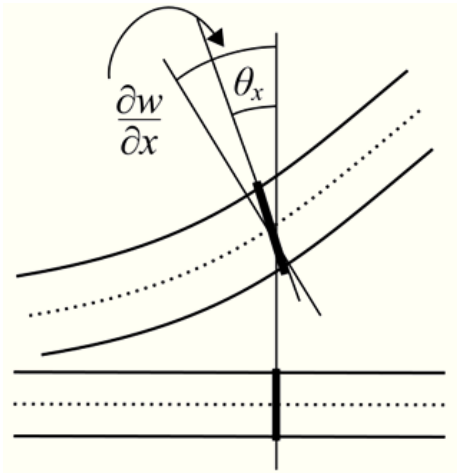

(b)

Figure 27: transverse shear/ warping. (a) The Kirchoff-Love hypothesis. The transverse displacement field is assumed to be linear in the z-direction and the transverse shear strain is zero. Reproduced from Ref. [40] (b) The Mindlin-Reissner theory. A linear variation of displacement across the thickness is assumed, but the plate thickness does not change. Reproduced from Ref. [39].

In Wetzel et al. [42] the need to use "thick" shell elements, able to account for transverse shear deformation, is underlined. When modelled correctly, the transverse shear stiffness of the considered materials has a significant effect on the buckling resistance of the structure. Similarly, in the master dissertation of Stijn Ketele [43], which was conducted under the supervision of the author, the

transverse shear stress was investigated for a beam in bending meshed with solid elements. A beam consisting of a stack of three plies in the thickness was analyzed using second order layered solid elements. It was found that the resulting displacements were accurate, but that the predicted transverse shear stress only approximated the analytical solution coarsely when a single element was used in the thickness direction. The results became more precise as the number of elements in the thickness direction was increased.

2.2.2 Material sections and orientations

Typical blade FE models incorporate simple linear elastic material models. A single value is assigned for the stiffness of the material. In reality, the material properties tend to vary even within a single blade structure. In practice it is assumed that the fiber volume fraction is uniform. This is generally not the case. Furthermore, it is typically assumed that the structure is produced perfectly, without flaws. However, it is commonly known that in reality, the blades are riddled with defects [44]. These include voids, wrinkles (fiber waviness), delamination and dry spots [45], [46]. In addition, abstraction is made of several effects such as for example the transition between layers. Pieces of core material that are positioned adjacent to each other in the mold will in practice often have a resin rich zone between them, which could be a point where damage initiates.

In Leong et al. [47] the effect of wrinkling defects is investigated both experimentally and numerically at the level of samples containing intentionally added wrinkles. It was found that failure of the specimens occurred in three modes: (i) face sheet-core debonding, (ii) layer-wise delamination of the face sheet, (iii) total specimen failure. It was found that the Northwestern University failure criterion was effective at predicting the second failure mode.

Typically, material properties are assumed to be linear elastic. This is largely accurate for typical glass fiber reinforced polymer (GFRP) and carbon fiber reinforced polymer (CFRP) laminates used in wind turbine blades for limited strain levels. However, this is not the case once degradation due to damage occurs. Furthermore, ±45 laminates show strongly non-linear behavior when loaded in shear [48]. In Hua et al. [49] a simplified prismatic blade model is used to investigate the adhesive joint between the shear webs and spar caps as presented in Figure 28. The plasticity of the adhesive is included and found to have a significant effect in the stress distribution. Furthermore, the effect of an imperfection in the adhesive is considered. A void in the joint is found to result in earlier crack initiation and reduced joint strength.

For the verification of the strength of a wind turbine blade structure, laminate failure criteria are typically used. These allow the calculation of failure indices such as those in the fiber direction resulting in fiber failure (FF) and between the

different fibers, inter fiber failure (IFF). In current blade design, IFF is one of the more strict constraints [28]. For wind turbine blades common failure criteria are those of Tsai-Wu and Puck [50], [51]. The latter is used in the GL2010 design guidelines [8]. An alternative failure criterion is suggested in Rajadurai et al. [52]. For a detailed discussion on different laminate failure criteria, the interested reader is referred to Ref. [53].

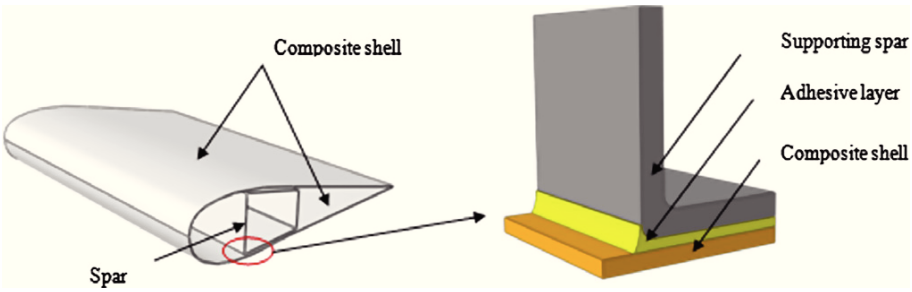

Figure 28: The prismatic model used in Hua et al. [49] to investigate influences on the adhesive bonds. It is found that including plasticity for the adhesive affects the stress distribution and that voids result in a weaker joint.

In addition to material properties, local material orientations are particularly relevant for composite materials with anisotropic properties. Van Buren et al. [7] investigated the level of detail required to model a wind turbine blade. This was done by creating a base model and several models that were successively deteriorated. This was done using the Numerical Manufacturing and Design (NuMAD) tool [54]. Eigenfrequencies, deflections and stresses at the blade root were compared. From the results, it can be concluded that deviations from the baseline model are severe once the correct material orientations are removed, which was the first deterioration in a series of stages.

In practice, material orientations are often coarsely approximated. However, special purpose software such as Composites Modeler for Abaqus/CAE [55], exists to calculate material orientations after draping of a fiber mat onto a mold.

2.2.3 Boundary and loading conditions

For modelling and testing purposes, a worst-case scenario is extracted. The assumption is that if the structure can withstand this combination of loads, it is able to withstand any combination it can be expected to encounter. However, this is not necessarily true. For example, in Ref. [56] the buckling reserves were calculated for every single load case considered in the design and compared to the buckling reserve calculated for the extreme loads extracted from these load cases. It was found that the conventional approach was non-conservative. Lower reserves were found for a specific load case than for the envelope of all load cases

(the extreme loads). It was concluded that the reason for this is that not necessarily the highest total loads, but rather combinations of loads are critical.

Loads are typically calculated in different levels of detail. For actual blades attached to a turbine that is producing power, the loads are a combination of an aerodynamic pressure distribution over the surface, gravitational, inertial and gyroscopic loads. To calculate these loads, either very computationally expensive methods are used such as Computational Fluid Dynamics (CFD). However, the airflow creates load which deforms the structure, thereby altering the flow. This results in a coupled problem known as fluid-structure-interaction (FSI).

In Uchida et al. [57] the critical wind loads experienced by a turbine during the passage of a typhoon were calculated using detailed CFD modelling of the surrounding terrain. The resulting loads were applied to a FE model the blades. Analysis predicted high stresses in the area where damage occurred (near the LE). A reinforced blade model was then created which did not show this weakness.

In practice, much cheaper methods are used. Frequently, these consist of calculating a time series of loads applied to models containing beam elements. In this way, an explicit approach is used to account for the different aerodynamic, gravitational and inertial forces. The result however, consists of concentrated moments and forces that are applied to the nodes of the beam model. An example of a beam model used for a full turbine is shown in Figure 29.

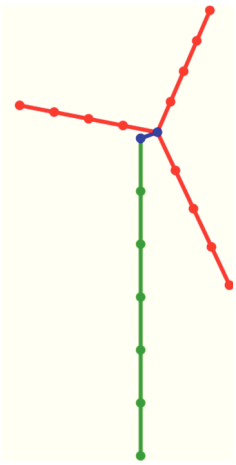

Figure 29: Beam model representation of a wind turbine as used in a typical aero-elastic calculation. Reproduced from Ref. [58].

To apply these loads to a more advanced 3D FE model, several methods have been proposed. An overview of these methods is provided in Figure 30. In Berg et al. [59] a procedure for mapping loads from an aero-elastic simulation to a 3D FE

model for the purpose of performing buckling analysis is presented. When mapping the loads from a point to a circumference, the equations are essentially underdefined. For this reason, the assumption is added that the forces in chord-wise direction do not produce any torsional moment on the blades. It was concluded that using a geometrically linear buckling analysis good results can be achieved using the mapping method. However, influence of the mesh density at the trailing edge was observed and the mapping was found to be more useful for non-linear buckling analysis. Furthermore, this method was included in NuMAD and used in Ref. [31].

In Tang et al. [60] concentrated forces are spread over the airfoil shape using a triangular (bilinear) pressure distribution. Similarly, a triangular distribution was applied in Ref. [61]. The position of the maximum pressure was varied along the chord ranging from 0 % chord to 45 % chord. The position of the pressure peak had only minor influence on the resulting strains.

Further, in many studies, loads are applied by means of constraints, connecting a center node to a section of the blade. These constraints can be multi-point-constraints (MPC), kinematic coupling constraints [62] or distributing constraints (equivalent to the use of RBE3 elements used in MSC NASTRAN [63] as for example used in Ref. [17]) [64], [65]. Alternatively, the loads can be applied along the central nodes of the spar caps. This approach was used in Ref. [24].

Further, a pressure distribution can be used to calculate how the loads obtained from BEM theory should be spread over the model. This is typically done by means of a panel code which calculates a pressure distribution over a 2D airfoil for a given angle of attack (AoA) and wind speed. This mapping is subsequently interpolated and mapped onto the 3D FE mesh. For example, in Chen et al. [66] this was done using the panel code RFOIL (a modified version of XFOIL) while in Ref. [67] a similar approach was used combining Aerodyn [68] with the panel code XFOIL [69]. In addition, in Rafiee et al. [70] an in-house BEM code was coupled to an ANSYS model. In the same fashion, in Grujicic et al. [71], [72] loads are applied to a blade shell model by calculating the pressure distribution at 10 span-wise positions and interpolating along the span. Furthermore, in Lee et al. [73] an iteration loop was created between a BEM code, XFOIL and a FE model to obtain a full fluid-structure-interaction (FSI) simulation.

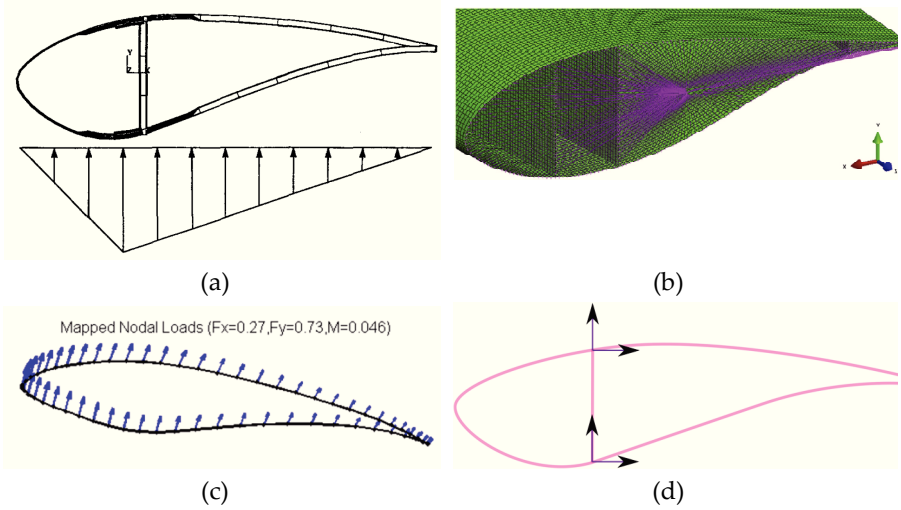

Figure 30: load introduction methods. (a) Bi-linear load distribution. Reproduced from Ref. [61]. (b) Distributing coupling load introduction. Reproduced from Ref. [62]. (c) Pressure mapping method proposed by Berg et al. [59]. (d) Load applied to the spar cap nodes.

2.2.4 FE solving

The results that are obtained from FE analysis are of course dependent on the underlying constitutive models. The behavior of structures has been the subject of study over many decades. While it is true that the scientific model is incomplete, the underlying mathematical models have been validated extensively. FE modelling is in general considered to be a correct and reliable practice, especially for the case where speeds are very limited. However, it is worth noting that results can depend on solver settings. Specifically, multiple authors have reported the need for the consideration of non-linear effects. Jensen investigated the Brazier [74] effect in wind turbine blades [1], [6], [75]. It was concluded that severe non-linear effects occur when blades are loaded in bending. The displacement of the spar caps that is predicted using a geometrically linear simulation was found to be in the opposite sense from the displacement that was measured and calculated using a geometrically non-linear model [8].

Similarly, in McKittrick et al. [61] the design of a 7.5 m blade is verified. The results from geometrically linear buckling analyses (eigenvalue analyses) are compared to non-linear buckling analyses. It is concluded that linear analyses can yield non-conservative values. For this reason, design standards allow a lower safety factor if the buckling predictions are conducted in a non-linear fashion.

Further, Rosemeier et al. [76] compared the strength predictions obtained with geometrically linear analysis (GLA) with those resulting from a geometrically

non-linear analysis (GNA) and found that the linear analysis was lacking. Both the critical areas and failure mechanism were not correctly predicted. The results from the non-linear analysis were confirmed by an experimental test.

2.3 FE modelling applications

The previous section discussed and classified different blade FE models. However, FE modelling can be applied for several different purposes, which are discussed in this section. An overview of the different applications of FE modelling of blade is presented in Figure 31.

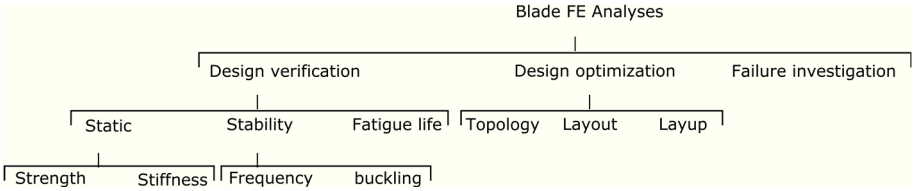

Figure 31: Schematic overview of the applications of FE modelling of wind turbine blades.

2.3.1 Blade design verification

HAWT blade designs should fulfill a series of structural requirements to ensure that the turbine can operate normally. Such requirements are for example discussed in Berggreen et al. [77]. An overview of the requirements can be seen in Figure 32 and summarized as follows:

- Strength: under the extreme loads the blades should remain undamaged.
- Stiffness: under the extreme loads, a minimum clearance between the blade tips and the tower should exist.
- Structural stability:
    - Static stability: The structure may not buckle under extreme loads.
    - Dynamic stability: Resonance of the structure should be avoided. Typically, this means that the first eigenfrequency of the blade should be higher than the tower passing frequency.
- Fatigue: Under the expected loads, the fatigue life of the structure should be sufficient.

One application of the FE modelling of blades is the verification of the design in terms of stress hot-spots and tower clearance. For example in Kim et al. [28] the design of a multi-MW blade was verified. Strain hot-spots were found at the transition between different core-thicknesses and at the start of the shear webs. Likewise, in Lanting [78] the stiffness and strength of different layups for a

1.2 MW blade are verified. Stress levels are found to be below the maximum allowable values including safety factors.

Another aspect of the structural requirements of wind turbine blades is their structural stability. On one hand this means that under extreme loads, the structure will not buckle. This has been subject to numerical investigation in various studies. While methods exist to predict the buckling resistance based on a 2D blade section, such approaches are often non-conservative. To be more accurate, 3D FE models are used. In this sense, either a geometrically linear analysis is used, solving an eigenvalue problem, or a non-linear buckling approach is used.

On the other hand, the dynamic stability of the structure is also investigated. This is often done in the aero-elastic model, where aero-elastic instabilities, such as flutter should be discovered. In addition, blades are also designed so that the first eigenfrequency would be above the first tower passing frequency. The reason for this can be seen in the Campbell plot provided in Figure 33.

Further, in Larsen et al. [81] damage was introduced in a full-scale blade and it was investigated if this could be observed in the modal behavior of the structure. While it was found that there is little shift in eigenfrequencies, the associated mode shapes do change.

To verify that a blade satisfies the fatigue life requirements, experimental tests are typically performed on the final blade. However, numerical approaches exist to verify this requirement ahead of producing a costly prototype blade. In Kong et al. [80] the fatigue life of a composite blade is assessed using a numerical approach. The procedure for evaluating it relies on calculating the load spectrum, grouping and arranging the cycles and using S-N curve data to calculate the allowable fatigue strengths. A shell FE model was then used to verify that the stresses remained in the allowable range for the calculated loads. Similarly, in Hu et al. [67] a method for predicting a blade's fatigue life is presented. The calculated loads are applied to a FE model of the blade as a distributed pressure, obtained using section-wise distributions calculated using the potential flow model XFOIL. Further, in Dutton et al. [82] the fatigue behavior of a part of a reference blade is investigated by means of a parametric blade model.

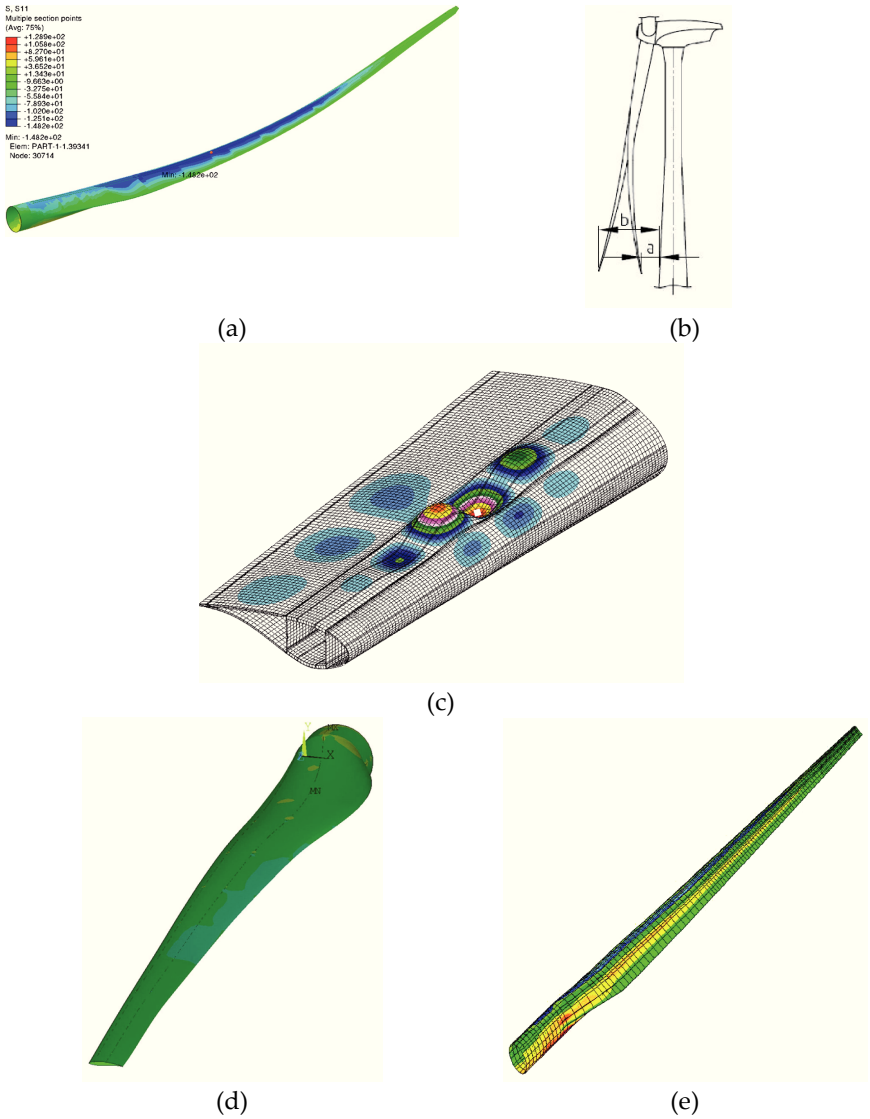

Figure 32: blade structural requirements: (a) Strength requirement: the stresses and strains should not exceed critical values under extreme load to ensure damage will not occur. Stress distribution as calculated in Ref.[30] . (b) Stiffness requirement: tower clearance under extreme load. Reproduced from Ref. [79]. (c) Static stability: the structure should not buckle under extreme load. Buckling mode for the blade of the DTU10MW reference turbine. Reproduced from Ref. [76] . (d) Dynamic stability: the structure's eigenfrequency should be higher than the first tower passing frequency at nominal rotational speed. First eigenmode calculated in Ref. [64]. (e) The fatigue life of the structure should allow the turbine to operate for its full design life. Resulting strain distribution from a fatigue load calculation. Reproduced from Ref. [80].

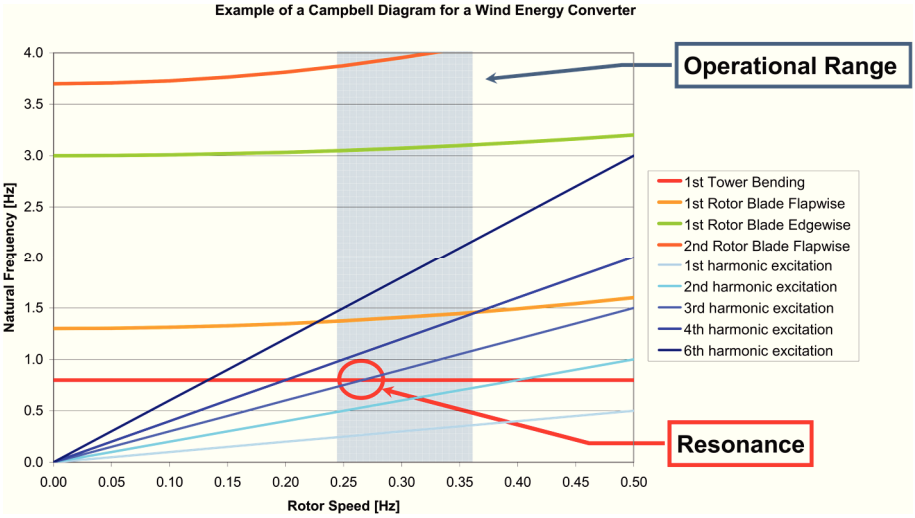

Figure 33: Example of a Campbell plot, giving a typical overview of the blade's eigenfrequencies and important excitation frequencies for different rotational speeds. The eigenfrequencies of the blade increase with rotational speed of the rotor due to centrifugal stiffening. Reproduced from Ref. [79].

Furthermore, in Ref. [83] a composite blade root is investigated. The root consists of an aluminum part glued into a composite part. Damage is initiated at the interface under an extreme gust load case resulting in a load of ten times normal fatigue load values. After this event it is found that damage grows during normal operation. It is concluded that this method can predict the life reduction caused by various loadings and overloading. In Lee et al. [29] the fatigue behavior of the T-bolt root joint of a wind turbine blade was investigated. Even though the blade was designed to withstand fatigue loads, the root joint failed during testing. It was hypothesized that this was due to an assumption that is commonly used in the root joint design process, which suggests that the root region can be considered to act as a simple cylinder onto which axial and bending loads are imposed. A small model consisting of half a bolt connection was used to assess which loads had to be applied to obtain the same strains in the bolts as measured during the test. It was found that these loads differ significantly from those calculated in the design process. This led to opening of the joint and loss of contact between the opposite surfaces. This resulted in crack initiation and progression.

2.3.2 Reliability analysis

One of the main goals of blade modelling is to decrease the prevalence and severity of blade failures. One aspect that must be accounted for is the variability that exists at different levels. The reliability of a blade is for example assessed by means of Monte Carlo simulations using stochastic distributions. For example, in

Ref. [84] such an approach was used to assess the reliability of adhesively bonded scarf joints. The same procedure was applied to stepped joint in Ref. [85]. In both cases it was found that the used failure criterion has a strong influence on the reliability values. In addition, in Ref. [86] a method for calculating the reliability of a blade, developed within the UpWind project, is presented.

2.3.3 Blade design optimization

2.3.3.1 Topology optimization

Various authors have used topology optimization routines on wind turbine blades. In such an approach, the locations where the material is most useful are found. An extensive overview of topology optimization techniques can be found in Cazacu et al. [87].

For wind turbine blades specifically, Wang et al. [88] consider the similarity between leaves of trees and the structural layout of a wind turbine blade. In leaves a main vein is present which is considered similar to the spar of a wind turbine blade and the skins corresponds to the lateral veins of the leaf. The Solid Isotropic Material with Penalization (SIMP) method is first applied to a leaf with the target function set to the minimum weighted compliance and the constraint function the volume fraction which was set to 0.3. The results show the appearance of veins as present in real leaves. Next the SIMP method was applied with the same settings to a reference wind turbine blade for a 1.5 MW turbine. The wind loading at 50 m/s wind speed and gravitational loads were applied.

Similarly, Joncas [89], [90] used SIMP topology optimization (Altair OptiStruct [91]) to investigate the internal structure of a HAWT blade. The motivation was that the study investigated the potential use of thermoplastic composites. First the method was used to optimize a root and transition region of the blade for flap-wise and edge-wise loads. In a second stage the method was applied to a half blade. Loads were applied to a single node that was connected to the tip portion of the model using rigid elements. The results show the appearance of the spar caps and shear connections between the caps, as can be seen in Figure 34. In addition, the results show the appearance of ribs, which are typically not used in today's blade designs.

Buckney et al. [92], [93] used SIMP topology optimization on a 45 m blade of which the shape was based on an industrial design. A total of seven load cases was considered with the objective function to minimize the maximum compliance for all load cases. Additionally, a constraint limiting the tip rotation to 2 ° was imposed. Different materials were considered, but this did not alter the optimal topology. The results showed a change in topology along the span of the blade, with asymmetric spar caps, as presented in Figure 35.

However, the limitations of this approach are severe. Firstly, the SIMP topology optimization method assumes properties for a single, isotropic linear elastic material, while blades are manufactured using anisotropic materials. In this sense, the optimization can also not make use of sandwich structures, which explains the appearance of ribs. Secondly, the SIMP optimization method solves an eigenvalue problem, thereby assuming geometric linearity, which, as discussed earlier, is not sufficient to capture the structural behavior of a wind turbine blade structure. Furthermore, regarding the twist deformation of a blade, it should be noted that when solid elements are used only displacement degrees of freedom are available. This is not sufficient to predict the twist deformation using a geometrically linear problem. Additionally, this approach does not account for other requirements such as structural stability. Moreover, the mentioned studies did not consider manufacturing concerns of the structure during the topology optimization.

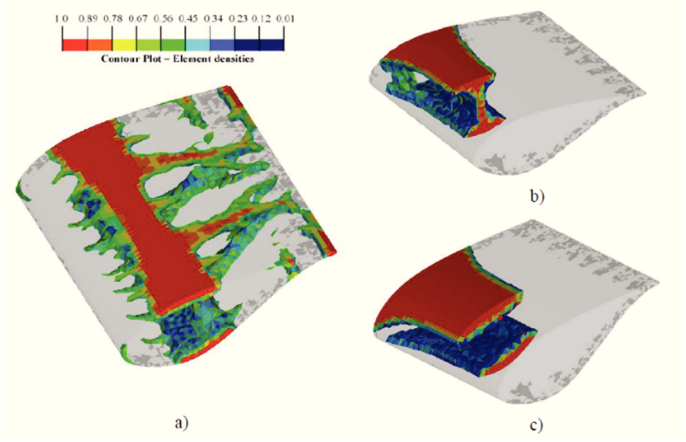

(a)

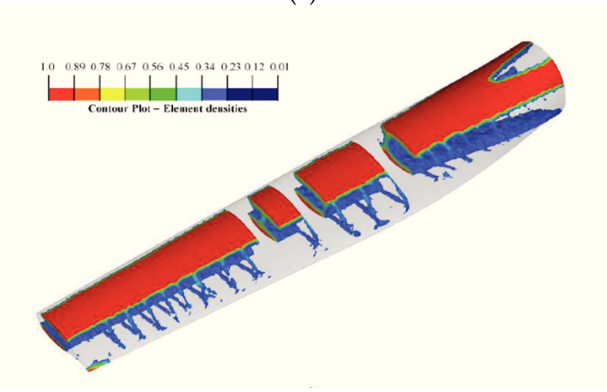

(b)

Figure 34: Contour plots showing the material densities as a result of SIMP topology optimizations of wind turbine blades under combined loading. resulting material densities

presented in Ref. [89]. The results clearly show the appearance of a spar structure, along with shear webs to connect them and ribs towards the TE. (a) Result of combined flap and edge-wise loading applied to a small blade portion. (b) Result of combined flap and edge-wise loading applied to the inboard half of a blade.

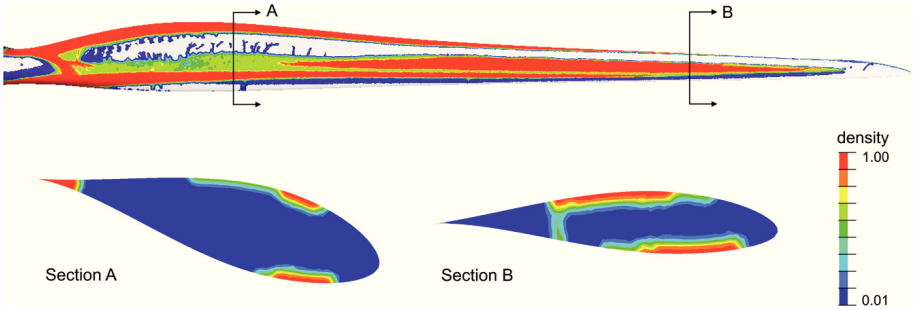

Figure 35: Contour plots showing the material densities as a result of SIMP topology optimizations of wind turbine blades under combined loading. Reproduced from Ref. [92].

2.3.3.2 *Layout optimization*

Aside from optimizing a complete free-form structural layout, different pre-defined structural topologies can be optimized and compared. This was for example done in Barnes et al. [94], where different structural configurations are modelled and compared. Five different parametric models were created and optimized. Similarly, in Buckney et al. [93] the results of a topology optimization are used to suggest structural configurations which are then optimized. The study concluded that the transition in cross-section along the span of the blade results in a structural configuration that transitions in layout along the span. Further, in Capuzzi et al. [95] the layout for a swept wind turbine blade is optimized. This is done by optimizing the shape and positioning of the spar. In Rosemeier et al. [65] a comparison was made between a conventional continuous spar cap and a split spar cap design, focusing on obtaining better buckling resistance. This is shown in Figure 36.

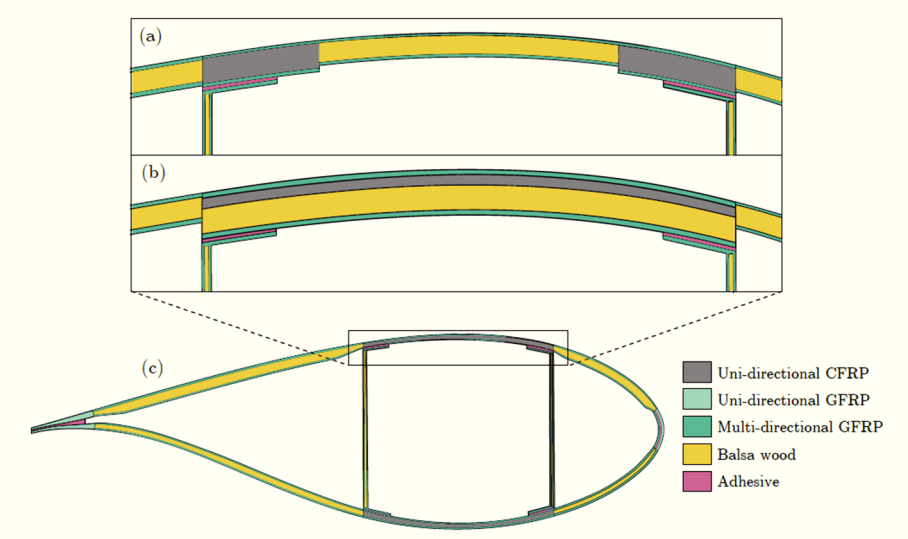

Figure 36: The different structural configurations considered in Rosemeier et al. [65] with the aim of investigating the buckling resistance. (a) Split spar cap configuration. (b) Continuous spar cap configuration. (c) Baseline configuration.

2.3.3.3 *Layup optimization*

Various studies have investigated the optimization of the composite layup. This is done by combining well known optimization techniques with FEM. However, running a full 3D FE analysis is computationally expensive. Therefore, brute-force approaches are not feasible. Instead, most applied techniques use heuristic methods such as genetic algorithms (GA). In addition, the models are often rather simple, the considered load cases limited and the geometrically linear analyses (GLA) are used. Typically, the blade model is already constructed and meshed, leaving only the assigned material sections to be varied between models. For example, Liao et al. [96] used a particle swarm optimization (PSO) algorithm combined with FEA to optimize the layout of a commercial 1.5 MW blade. This paper considers the optimization strategy of minimizing the blade mass. A multi-criteria constrained optimization design is carried out under ultimate (extreme) flap-wise load conditions. Further in Cox et al. [97] a blade for a hypothetical 10 MW turbine was designed. After meeting the initial design constraints (tip deflection, buckling resistance and allowable strains under the extreme loads), the layup was optimized to reduce weight. Similarly, Jureczko et al. [98] created a multi-criteria optimization tool for wind turbine blades. An aerodynamic shape can be created and structural aspects are considered by optimizing with a built-in genetic algorithm.

Differently, in Lund et al. [99] an optimization approach called the discrete material optimization method (DMO) is presented. Given a shape and layup thickness, it uses an approach similar to multiphase topology optimization to compute a material stiffness as a weighted sum of candidate materials. This method is then applied to the layup for a wind turbine blade spar structure.

In general, optimization of the full blade layup using FE modelling is computationally very costly. For these reasons, the majority of research articles simplify the calculations to some extent. Often geometrically linear calculations are used and only a very small number of load cases (sometimes just one) are considered. Alternatively, the FE analyses are only used after obtaining a preliminary design and computationally cheaper methods are used for the first design iterations. For example, in Bottasso et al. [17] a multilevel optimization method is proposed, where in a first tier, simple 2D models are used, followed by a second tier of 3D shell or solid models. The loop is closed by feeding the results of the latter models back to the first tier.

2.3.4 Blade structural failure behavior and the influence of defects and damage

As mentioned earlier, actual wind turbine blades are rarely perfect. Instead, they are prone to various defects. In Haselbach et al. [62] the effect of delamination in the spar cap on the local buckling behavior was investigated. This was done on a section of the DTU10MW reference turbine blade. Delamination close to the surface was found to be critical since these were found to grow even under normal operation conditions, while delamination closer to the middle were found not to have a significant effect under normal conditions. In addition, Leong et al. [47] numerically and experimentally investigated the effect of fiber waviness on the structural behavior of a laminate.

In Shah et al. [100] a global shell model was created of a commercial blade. In a first tier, the model was used to model the static blade tests. In subsequent tiers, structurally sensitive zones were investigated by means of sub-models. First, a shell sub-model of a blade section is used, followed by a solid sub-model of the section, followed by more local solid sub-models, eventually including cohesive elements. However, several aspects are not fully considered. Firstly, the mesh of the global model is converged with respect to the blade root reaction moment. This value can be expected to converge for a much coarser mesh than the strain distribution in the laminate. Secondly, since the nodal displacement sub-modelling technique is used, boundary effects exist near the sub-modelling boundary conditions. Since the sub-models only consist of a 2 mm long section, these effects are present in the full model. In addition, the results are validated by comparing the longitudinal strain in the global model and sub-models to the value measured in the experiments. By imposing the displacements (using the nodal

displacement sub-modelling technique) on a blade section that is only 2 mm long, the longitudinal strain is essentially imposed.

Further, Ji et al. [101] applied a sub-modelling approach to investigate de-bonding of the shear web at the root end as shown in Figure 37. A shell global model was loaded with the extreme loads. From the obtained result, boundary conditions were applied to a model representing a small portion of the shear web and blade laminate with a cohesive zone model at the interface of the adhesive. Damage occurred at the interface at limited load levels. However, only a very small region was included in the sub-model, while some additional distance may be required to account for boundary effects. Furthermore, the shear web was modelled as being straight, without any cutout at the root end. Such a cutout is typically used to avoid creating a high stress concentration at the root end of the shear web. This can explain why damage was found to occur even at low load levels.

To strengthen blades, the ultimate limit state and failure behavior of blade is investigated in various studies. This is of great interest to the industry since it allows identification and quantification of failure mechanisms. Several studies have been conducted in which a full-scale blade is experimentally tested until failure. This failure behavior is then investigated and an attempt is made to reconstruct the failure event numerically. For example in Jensen et al. [6] a 34 m blade was tested to failure in a full scale flat-wise test. A global OML shell model and a solid sub-model of a 13 m long section were used to investigate the mechanism behind the failure. It was concluded that the de-bonding of the outer skin was the initial failure mechanism, followed by delamination buckling leading to the collapse of the structure. Further, in Yang et al. [30] a full-scale 40 m blade is statically loaded in the flat-wise direction up till failure. This was found to occur at 160 % of the extreme design load. A videometric technique was used during the experiments and the blade failure was investigated using an OML shell model. It was concluded that the de-bonding of the adhesive shells from the adhesive bonds was the initial failure mechanism.

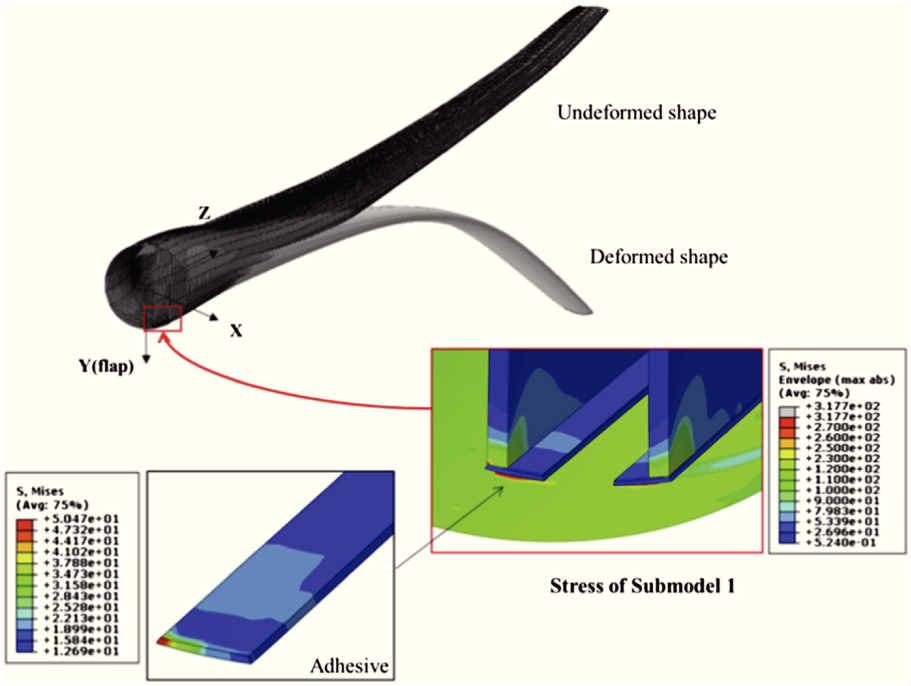

Figure 37: Overview of the global OML shell and local solid sub-model used in Ji et al. [101] to investigate the de-bonding of the shear-web joint at the root end. However, the shear web is modelled without the cut-out that is typically present to reduce the stress concentration at this position.

Furthermore, in Chen et al. [35] a 52.3 m blade was tested under static loads up to failure. FE analyses including progressive failure methods were used to reproduce the failure numerically as shown in Figure 38.

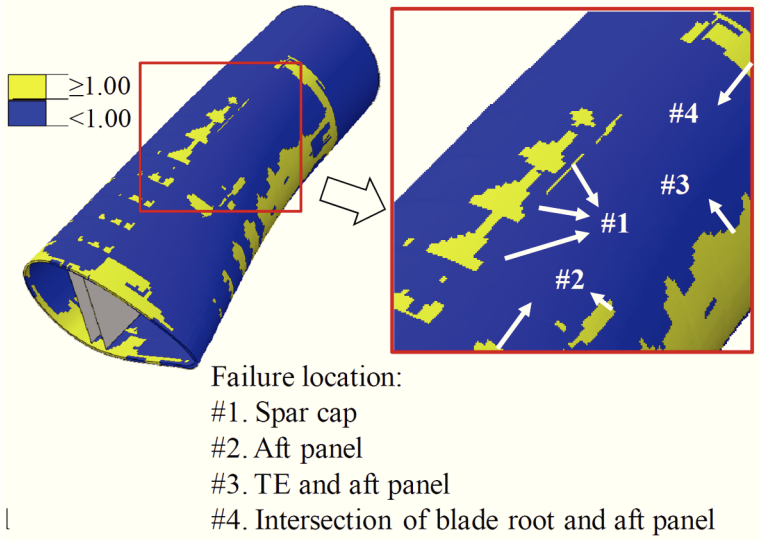

Figure 38: Finite element model of a blade loaded up till failure. Progressive damage modelling is applied to a solid model of the blade root transition region. Local failure is indicated by the failure index (yellow where failure has occurred). Reproduced from Ref. [35].

2.4 Conclusions

A significant amount of literature is available regarding the FE modelling of wind turbine blades. This is because FE analyses of blades are common in industry and academia. FE modelling allows for high accuracy by including complex 3D geometry, materials, loads and boundary conditions. Once a model has been created, various load cases can be investigated. In industry the method is used to verify the final blade design with high precision. This is often also required for the type certification of the blade design. In academia, the FE method is used for research purposes, leading to an improved understanding of the structural behavior of the blades.

Over the last decades the importance of FE analyses of blades has been increasing, as blade dimensions have increased and simplifications, such as linear assumptions are no longer valid. In this respect, research indicates the need to account for non-linearities. Several authors advocate the use of non-linear geometry to account for higher order effects such as the ovalization of the blade cross-section, non-linear material models which incorporate damage and non-linear boundary conditions which mimic the structural tests more accurately. In addition, while smaller blade designs were very stiff in torsion, in longer blades the torsional behavior is very significant. Furthermore, despite the high safety

factors commonly used in blade designs, repairs and replacements are frequently needed. This indicates a need for a better understanding of the structural behavior. In addition, the value of optimizing the structure keeps rising as the dimensions grow. There are many authors presenting optimizations, regarding the topology, structural layout and composite layup, using the FE method. However, these rarely contain the analysis of a detailed, geometrically non-linear, full-scale blade FE model, for a variety of load cases. This is due to the very high computation cost of such an endeavor. A better approach, that few authors have presented is to use such analyses as only part of an optimization cycle.

For aero-elastic load calculations, the blades are typically represented by equivalent beam models. However, these beam models are insufficient in regions with rapid changes such as the transition region. Therefore, the wind turbine blade FE models that are used in industry and academia mostly consist of shell elements positioned on the OML. While these are the easiest to obtain, several authors have warned of inaccurate behavior when loaded in torsion. Other modelling approaches are more difficult to obtain, but have been investigated. These include models with shell elements at mid-thickness, layered solid elements and combinations of shell and solid elements.

For these reasons, investigation of the differences between conventional shell modelling and more advanced methods and by extension making more advanced models easier to obtain are opportunities, which are explored in the current research.

2.5 Bibliography

[1] F. M. Jensen, H. Stang, and K. Branner, *Ultimate strength of a large windturbine blade*. 2009.

[2] S. Campbell, "Annual blade failures estimated at around 3,800," *wind power monthly*, 14-May-2015. [Online]. Available: https://www.windpowermonthly.com/article/1347145. [Accessed: 28-Dec-2017].

[3] "Blade failure and load monitoring," Sep-2008. [Online]. Available: https://www.windpowermonthly.com/article/953663/blade-failure-load-monitoring. [Accessed: 28-Dec-2017].

[4] D. S. Cairns, T. Riddle, and J. Nelson, "Wind turbine composite blade manufacturing: the need for understanding defect origins, prevalence, implications and reliability," SAND2011-1094, Feb. 2011.

[5] D. Nielow, "Prüfstand für die Evaluation der Betriebsfestigkeit von Rotorblattschalensegmenten, presented at 'Rotorblätter von Windenergieanlagen - Wind turbine rotor blades 6th Technical Conference', 2-3 july, Essen," presented at the Rotorblätter von Windenergieanlagen Wind turbine rotor blades 6th Technical Conference, Essen, 02-Jul-2014.

[6] F. M. Jensen, B. G. Falzon, J. Ankersen, and H. Stang, "Structural testing and numerical simulation of a 34m composite wind turbine blade," *Compos. Struct.*, vol. 76, no. 1–2, pp. 52–61, Oct. 2006.

[7] K. L. Van Buren and S. Atamturktur, "Model Form Error of Alternate Modeling Strategies: Shell Type Wind Turbine Blades," in *Rotating Machinery, Structural Health Monitoring, Shock and Vibration, Volume 5*, T. Proulx, Ed. New York, NY: Springer New York, 2011, pp. 53–64.

[8] "Guideline for the Certification of Wind Turbines, GL-IV-1," Germanischer Lloyd, Hamburg, GL-IV-1, Jul. 2010.

[9] International Electrotechnical Commission, "Wind turbines- Part 1: Design requirements," in *IEC 61400-1*, Third Edition., 2005.

[10] T. J. Larsen, J. P. A. A. Blasques, A. M. Hansen, and P. Berring, "WP8 Detailed Blade Modelling Implemented in Aero-Elastic load simulation. In Torsional Stiffening of Wind Turbine Blades – Mitigating leading edge damages: EUDP project 64013-0115 – Final report (pp. 80-106). Bladena.," 2016.

[11] D. J. Malcolm and D. L. Laird, "Extraction of equivalent beam properties from blade models," *Wind Energy*, vol. 10, no. 2, pp. 135–157, Mar. 2007.

[12] "BECAS," *http://www.becas.dtu.dk*. [Online]. Available: http://www.becas.dtu.dk/. [Accessed: 05-Apr-2018].

[13] R. D. Bitsche, "Airfoil2BECAS: A preprocessor for the cross-section analysis software BECAS," p. 3.

[14] R. D. Bitsche, "Shellexpander: A preprocessor for the cross-section analysis software BECAS," p. 6.
[15] A. Baert, "Investigation into extraction methods of equivalent beam properties from full 3D finite element models for wind turbine blades," Universiteit Gent, 2014.
[16] K. Branner *et al.*, "Anisotropic beam model for analysis and design of passive controlled wind turbine blades," DTU Wind Energy, 2012.
[17] C. L. Bottasso, F. Campagnolo, A. Croce, S. Dilli, F. Gualdoni, and M. B. Nielsen, "Structural optimization of wind turbine rotor blades by multilevel sectional/multibody/3D-FEM analysis," *Multibody Syst. Dyn.*, vol. 32, no. 1, pp. 87–116, 2014.
[18] K. Branner, P. Berring, C. Berggreen, and H. W. Knudsen, "Torsional performance of wind turbine blades–Part II: Numerical validation," in *16th International Conference on Composite Materials*, 2007, pp. 8–13.
[19] J. D. Zhang and Y. Xu, "Numerical analysis of linear buckling of wind turbine blade with different trailing bonding models," *IOP Conf. Ser. Mater. Sci. Eng.*, vol. 52, no. 5, p. 052003, Dec. 2013.
[20] J. Locke and V. Ulyses, "Design studies for twist-coupled wind turbine blades." Jun-2004.
[21] P. U. Haselbach, "An advanced structural trailing edge modelling method for wind turbine blades," *Compos. Struct.*, vol. 180, no. Supplement C, pp. 521–530, Nov. 2017.
[22] D. Laird, F. Montoya, and D. Malcolm, "Finite Element Modeling - old," 2005.
[23] D. T. Griffith and T. D. Ashwill, "The Sandia 100-meter all-glass baseline wind turbine blade: SNL100-00," SAND2011-3779, 2011.
[24] T. Ashwill, "Sweep-Twist Adaptive Rotor Blade: Final Project Report," Sandia National Laboratories, SAND2009-8037, Jan. 2010.
[25] M. Zuteck, "Adaptive blade concept assessment: curved planform induced twist investigation," Sandia National Laboratories, SAND2002-2996, Oct. 2002.
[26] V. Fedorov, C. Berggreen, S. Krenk, and K. Branner, "Bend-Twist Coupling Effects in Wind Turbine Blades," DTU Wind Energy, Denmark, 2012.
[27] P. R. Greaves, "Fatigue analysis and testing of wind turbine blades," Durham University, 2013.
[28] S.-H. Kim, H.-J. Bang, H.-K. Shin, and M.-S. Jang, "Composite Structural Analysis of Flat-Back Shaped Blade for Multi-MW Class Wind Turbine," *Appl. Compos. Mater.*, vol. 21, no. 3, pp. 525–539, Jun. 2014.
[29] H. G. Lee, M. G. Kang, and J. Park, "Fatigue failure of a composite wind turbine blade at its root end," *Compos. Struct.*, vol. 133, pp. 878–885, Dec. 2015.

[30] J. Yang *et al.*, "Structural investigation of composite wind turbine blade considering structural collapse in full-scale static tests," *Compos. Struct.*, vol. 97, pp. 15–29, Mar. 2013.

[31] P. W. Richards, D. T. Griffith, and D. H. Hodges, "High-fidelity Modeling of Local Effects of Damage for Derated Offshore Wind Turbines," *J. Phys. Conf. Ser.*, vol. 524, p. 012036, Jun. 2014.

[32] K. K. Wetzel, "Defect- old," presented at the 50th AIAA/ASME/ASCE/AHS/ASC Structures, Structural Dynamics, and Materials Conference, Palm Springs, California, 2009.

[33] D. M. Hoyt, "Rapid FEA of Wind Turbine Blades - Summary of NSE Composites' structural analysis capabilities for blades," May-2008.

[34] P. Berring, K. Branner, C. Berggreen, and H. W. Knudsen, "Torsional performance of wind turbine blades-Part 1: Experimental investigation," in *16th International Conference on Composite Materials*, 2007, vol. 43.

[35] X. Chen, W. Zhao, X. Zhao, and J. Xu, "Failure Test and Finite Element Simulation of a Large Wind Turbine Composite Blade under Static Loading," *Energies*, vol. 7, no. 4, pp. 2274–2297, Apr. 2014.

[36] K. Branner, P. Berring, and P. U. Haselbach, "Subcomponent testing of trailing edge panels in wind turbine blades," in *Proceedings of 17th European Conference on Composite Materials*, 2016.

[37] P. U. Haselbach and K. Branner, "Effect of trailing edge damage on full-scale wind turbine blade failure," in *20th International Conference on Composite Materials*, 2015.

[38] A. F. Bower, *Applied Mechanics of Solids*, 1 edition. Boca Raton: CRC Press, 2009.

[39] *Abaqus 6.14 Online Documentation, Dassault Systèmes*. 2014.

[40] "Advanced Finite Element Methods (ASEN 6367) - Spring 2017," Department of Aerospace Engineering Sciences University of Colorado at Boulder.

[41] C. Steele and C. D. Balch, *Introduction to the Theory of Plates*. Stanford University.

[42] K. Wetzel, "Necessity for using nonlinear structural analysis in designing blades." .

[43] S. Ketele, W. Van Paepegem, and M. Peeters, "Detailed modeling of connections in large composite wind turbine blades," Ghent University, 2013.

[44] H. S. Toft, K. Branner, P. Berring, and J. D. Sørensen, "Defect distribution and reliability assessment of wind turbine blades," *Eng. Struct.*, vol. 33, no. 1, pp. 171–180, Jan. 2011.

[45] K. K. Wetzel, "Defect-Tolerant Structural Design of Wind Turbine Blades," in *50th AIAA/ASME/ASCE/AHS/ASC Structures, Structural Dynamics, and*

Materials Conference, 0 vols., American Institute of Aeronautics and Astronautics, 2009.

[46] J. F. Jensen, J. P. Schultz, C. Berggreen, and K. Branner, "Application of Load Carrying Sandwich Elements in Large Wind Turbine Blades," in *Sandwich Structures 7: Advancing with Sandwich Structures and Materials: Proceedings of the 7th International Conference on Sandwich Structures, Aalborg University, Aalborg, Denmark, 29–31 August 2005*, O. T. Thomsen, E. Bozhevolnaya, and A. Lyckegaard, Eds. Dordrecht: Springer Netherlands, 2005, pp. 947–956.

[47] M. Leong, L. C. T. Overgaard, O. T. Thomsen, E. Lund, and I. M. Daniel, "Investigation of failure mechanisms in GFRP sandwich structures with face sheet wrinkle defects used for wind turbine blades," *Compos. Struct.*, vol. 94, no. 2, pp. 768–778, Jan. 2012.

[48] W. Van Paepegem, I. De Baere, and J. Degrieck, "Modelling the nonlinear shear stress–strain response of glass fibre-reinforced composites. Part II: Model development and finite element simulations," *Compos. Sci. Technol.*, vol. 66, pp. 1465–1478, Aug. 2006.

[49] Y. Hua, A. R. M. Kasavajhala, and L. Gu, "Elastic–plastic analysis and strength evaluation of adhesive joints in wind turbine blades," *Compos. Part B Eng.*, vol. 44, no. 1, pp. 650–656, Jan. 2013.

[50] A. Puck and H. Schurmann, "Failure analysis of FRP laminates by means of physically based phenomenological models.," *Compos Sci Technol.*, no. 58, pp. 1045–1067, 1998.

[51] C.-S. Lee, J.-H. Kim, S. Kim, D.-M. Ryu, and J.-M. Lee, "Initial and progressive failure analyses for composite laminates using Puck failure criterion and damage-coupled finite element method," *Compos. Struct.*, vol. 121, pp. 406–419, Mar. 2015.

[52] J. S. Rajadurai, T. Christopher, G. Thanigaiyarasu, and B. N. Rao, "Finite element analysis with an improved failure criterion for composite wind turbine blades," *Forsch. Im Ingenieurwesen*, vol. 72, no. 4, pp. 193–207, Dec. 2008.

[53] R. Talreja, "Assessment of the fundamentals of failure theories for composite materials," *Compos. Sci. Technol.*, vol. 105, pp. 190–201, Dec. 2014.

[54] J. Berg and B. Resor, "Numerical manufacturing and design tool (NuMAD V2. 0) for wind turbine blades: User's guide," *Sandia Natl. Lab. Albuq. NM Tech. Rep. No SAND2012-728*, 2012.

[55] "Composites Modeler | ABAQUS CAE - Dassault Systèmes®." [Online]. Available: https://www.3ds.com/products-services/simulia/products/abaqus/add-ons/composites-modeler-for-abaquscae/. [Accessed: 02-May-2018].

[56] A. Gagel, "Blade design beyond requirements of certifying agencies - Advances in static structural analyses," presented at the 3rd International IQPC Conference, Bremen, Feb-2014.

[57] T. Uchida, T. Maruyama, H. Ishikawa, M. Zako, and A. Deguchi, "Investigation of the Causes of Wind Turbine Blade Damage at Shiratakiyama Wind Farm in Japan– A Computer Simulation Based Approach–," *Rep. Res. Inst. Appl. Mech.*, no. 141, pp. 13–25, 2011.

[58] R. D. Bitsche, "BECAS - an open-source cross section analysis tool," presented at the EWEA 2012 conference, Copenhagen, 16-Apr-2012.

[59] J. Berg, J. Paquette, and B. Resor, "Mapping of 1D beam loads to the 3D wind blade for buckling analysis," in *52nd AIAA/ASME/ASCE/AHS/ASC Structures, Structural Dynamics and Materials Conference 19th AIAA/ASME/AHS Adaptive Structures Conference 13t*, 2011, p. 1880.

[60] X. Tang, R. Peng, and X. Liu, "Design and Finite Element Analysis of Mixed Aerofoil Wind Turbine Blades," 2011.

[61] L. R. McKittrick, D. S. Cairns, J. Mandell, D. C. Combs, D. A. Rabern, and R. D. Van Luchene, "Analysis of a composite blade design for the aoc 15/50 wind turbine using a finite element model," Sandia National Laboratories, SAND2001-1441, May 2001.

[62] P. U. Haselbach, R. D. Bitsche, and K. Branner, "The effect of delaminations on local buckling in wind turbine blades," *Renew. Energy*, vol. 85, pp. 295–305, Jan. 2016.

[63] MSC, "Nastran," 2017. [Online]. Available: http://www.mscsoftware.com/product/msc-nastran. [Accessed: 04-Apr-2017].

[64] K.-N. Chen and P.-Y. Chen, "Structural Optimization of 3 MW Wind Turbine Blades Using a Two-Step Procedure," *Int. J. Simul. Multidiscip. Des. Optim.*, vol. 4, no. 3–4, pp. 159–165, Jul. 2010.

[65] M. Rosemeier and M. Bätge, "A concept study of a carbon spar cap design for a 80m wind turbine blade," *J. Phys. Conf. Ser.*, vol. 524, p. 012039, Jun. 2014.

[66] J. Chen, Q. Wang, W. Z. Shen, X. Pang, S. Li, and X. Guo, "Structural optimization study of composite wind turbine blade," *Mater. Des.*, vol. 46, pp. 247–255, Apr. 2013.

[67] W. Hu, K. K. Choi, O. Zhupanska, and J. H. J. Buchholz, "Integrating variable wind load, aerodynamic, and structural analyses towards accurate fatigue life prediction in composite wind turbine blades," *Struct. Multidiscip. Optim.*, vol. 53, no. 3, pp. 375–394, Mar. 2016.

[68] "AeroDyn | NWTC Information Portal." [Online]. Available: https://nwtc.nrel.gov/AeroDyn. [Accessed: 20-Apr-2018].

[69] M. Drela and H. Youngren, "Xfoil: Subsonic Airfoil Development System." [Online]. Available: http://web.mit.edu/drela/Public/web/xfoil/. [Accessed: 19-Apr-2018].

[70] R. Rafiee, M. Tahani, and M. Moradi, "Simulation of aeroelastic behavior in a composite wind turbine blade," *J. Wind Eng. Ind. Aerodyn.*, vol. 151, pp. 60–69, Apr. 2016.

[71] M. Grujicic, G. Arakere, B. Pandurangan, V. Sellappan, A. Vallejo, and M. Ozen, "Multidisciplinary Design Optimization for Glass-Fiber Epoxy-Matrix Composite 5 MW Horizontal-Axis Wind-Turbine Blades," *J. Mater. Eng. Perform.*, vol. 19, no. 8, pp. 1116–1127, 2009.

[72] M. Grujicic, G. Arakere, E. Subramanian, V. Sellappan, A. Vallejo, and M. Ozen, "Structural-Response Analysis, Fatigue-Life Prediction, and Material Selection for 1 MW Horizontal-Axis Wind-Turbine Blades," *J. Mater. Eng. Perform.*, vol. 19, no. 6, pp. 790–801, Aug. 2010.

[73] Y.-J. Lee, Y.-T. Jhan, and C.-H. Chung, "Fluid–structure interaction of FRP wind turbine blades under aerodynamic effect," *Compos. Part B Eng.*, vol. 43, no. 5, pp. 2180–2191, Jul. 2012.

[74] L. G. Brazier, "On the Flexure of Thin Cylindrical Shells and Other 'Thin' Sections," *Proc. R. Soc. Math. Phys. Eng. Sci.*, vol. 116, no. 773, pp. 104–114, Sep. 1927.

[75] F. M. Jensen, P. M. Weaver, L. S. Cecchini, H. Stang, and R. F. Nielsen, "The Brazier effect in wind turbine blades and its influence on design: Brazier effect in wind turbine blades," *Wind Energy*, vol. 15, no. 2, pp. 319–333, Mar. 2012.

[76] M. Rosemeier, P. Berring, and K. Branner, "Non-linear ultimate strength and stability limit state analysis of a wind turbine blade: Non-linear ultimate strength and stability limit state analysis of a wind turbine blade," *Wind Energy*, vol. 19, no. 5, pp. 825–846, May 2016.

[77] C. Berggreen, K. Branner, J. F. Jensen, and J. P. Schultz, "Application and Analysis of Sandwich Elements in the Primary Structure of Large Wind Turbine Blades," *J. Sandw. Struct. Mater.*, vol. 9, no. 6, pp. 525–552, Nov. 2007.

[78] Z. Lanting, "Research on Structural Lay-up Optimum Design of Composite Wind Turbine Blade," *Energy Procedia*, vol. 14, p. 1, 2012.

[79] Altair Engineering, "Integrating HyperWorks into the Development and Optimisation of Wind Turbine Rotor Blades," 04:30:47 UTC.

[80] C. Kong, T. Kim, D. Han, and Y. Sugiyama, "Investigation of fatigue life for a medium scale composite wind turbine blade," *Int. J. Fatigue*, vol. 28, no. 10, pp. 1382–1388, Oct. 2006.

[81] G. C. Larsen, P. Berring, D. Tcherniak, P. H. Nielsen, and K. Branner, "Effect of a damage to modal parameters of a wind turbine blade," in *EWSHM-7th European Workshop on Structural Health Monitoring*, 2014.

[82] A. G. Dutton, M. Clarke, and P. A. Bonnet, "Modelling of static and fatigue failure in wind turbine blades using a parametric blade model," in *Proc European wind energy conference, Warsaw*, 2010.

[83] H. Hosseini-Toudeshky, M. Jahanmardi, and M. S. Goodarzi, "Progressive debonding analysis of composite blade root joint of wind turbines under fatigue loading," *Compos. Struct.*, vol. 120, pp. 417–427, Feb. 2015.

[84] A. Kimiaeifar, H. Toft, E. Lund, O. T. Thomsen, and J. D. Sørensen, "Reliability analysis of adhesive bonded scarf joints," *Eng. Struct.*, vol. 35, pp. 281–287, Feb. 2012.

[85] A. Kimiaeifar, E. Lund, O. T. Thomsen, and J. D. Sørensen, "Reliability Analysis of Adhesive Bonded Stepped Lap Composite Joints Based on Different Failure Criteria," in *18th International Conference on Composite Materials*, 2011.

[86] L. Mishnaevsky, P. Brøndsted, R. Nijssen, D. J. Lekou, and T. P. Philippidis, "Materials of large wind turbine blades: recent results in testing and modeling: Materials of large wind turbine blades," *Wind Energy*, vol. 15, no. 1, pp. 83–97, Jan. 2012.

[87] R. Cazacu and L. Grama, "Overview of structural topology optimization methods for plane and solid structures," *Fascicle Manag. Technol. Engine Ering*, no. 3, Dec. 2014.

[88] L. I. U. Wang-yu and Y. ZHANG, "Network study of plant leaf topological pattern and mechanical property and its application," *Adv. Nat. Sci.*, vol. 3, no. 2, pp. 82–92, 2010.

[89] S. Joncas, "Thermoplastic composite wind turbine blades: an integrated design approach.," [s.n.], S.l., 2010.

[90] L.-C. Forcier and S. Joncas, "Development of a structural optimization strategy for the design of next generation large thermoplastic wind turbine blades," *Struct. Multidiscip. Optim.*, vol. 45, no. 6, pp. 889–906, Jun. 2012.

[91] "Structural Analysis Solver for Linear & Nonlinear | Altair OptiStruct." [Online]. Available: https://altairhyperworks.com/product/optistruct. [Accessed: 28-Apr-2018].

[92] N. Buckney, A. Pirrera, S. D. Green, and P. M. Weaver, "Structural efficiency of a wind turbine blade," *Thin-Walled Struct.*, vol. 67, pp. 144–154, Jun. 2013.

[93] N. Buckney, S. Green, A. Pirrera, and P. M. Weaver, "On the structural topology of wind turbine blades," *Wind Energy*, vol. 16, no. 4, pp. 545–560, May 2013.

[94] R. H. Barnes and E. V. Morozov, "Structural optimisation of composite wind turbine blade structures with variations of internal geometry configuration," *Compos. Struct.*, vol. 152, no. Supplement C, pp. 158–167, Sep. 2016.

[95] M. Capuzzi, A. Pirrera, and P. M. Weaver, "Structural design of a novel aeroelastically tailored wind turbine blade," *Thin-Walled Struct.*, vol. 95, pp. 7–15, Oct. 2015.

[96] C. C. Liao, X. L. Zhao, and J. Z. Xu, "Blade layers optimization of wind turbines using FAST and improved PSO Algorithm," *Renew. Energy*, vol. 42, pp. 227–233, Jun. 2012.
[97] K. Cox and A. Echtermeyer, "Structural Design and Analysis of a 10MW Wind Turbine Blade," *Energy Procedia*, vol. 24, pp. 194–201, 2012.
[98] M. Jureczko, M. Pawlak, and A. Mężyk, "Optimisation of wind turbine blades," *J. Mater. Process. Technol.*, vol. 167, no. 2–3, pp. 463–471, Aug. 2005.
[99] E. Lund and J. Stegmann, "On structural optimization of composite shell structures using a discrete constitutive parametrization," *Wind Energy*, vol. 8, no. 1, pp. 109–124, Jan. 2005.
[100] O. R. Shah and M. Tarfaoui, "The identification of structurally sensitive zones subject to failure in a wind turbine blade using nodal displacement based finite element sub-modeling," *Renew. Energy*, vol. 87, pp. 168–181, Mar. 2016.
[101] Y. M. Ji and K. S. Han, "Fracture mechanics approach for failure of adhesive joints in wind turbine blades," *Renew. Energy*, vol. 65, pp. 23–28, May 2014.

3 Blade FE modelling tools

"Import antigravity" – *Randall Munroe*

Chapter summary: In this chapter, tools for creating FE models for wind turbine blades are discussed. First, an overview of existing tools and their limitations is given. Next, approaches to create conventional shell models are presented. Firstly, an approach that relies on automating the Abaqus/CAE pre-processor is discussed, along with its challenges and limitations. Subsequently, a novel, stand-alone, slice-based approach is presented. In a second part, approaches to create models using solid elements are presented. First, the challenges regarding this process are described. This is followed by an attempt to extend the slice-based approach to allow solid models to be created. However, the resulting method has several limitations. To counter these, a novel block-based approach was created. This is presented in detail at the end of the chapter and is based on the paper "High-fidelity finite element models of composite wind turbine blades with shell and solid elements" in the Composite Structures journal.

3.1 Introduction

3.1.1 Motivation for the use of modelling tools

The previous chapter demonstrated the state-of-the-art and the importance of FE modelling of wind turbine blades. It is apparent that the quality of the results depends on the quality of the model. Unfortunately, creating models of wind turbine blades can be a challenge. This is because of the level of detail and complexity inherent to these structures. This complexity is found at several levels:

- The shape of the blade is typically lofted from a sequence of transformed airfoil sections. This results in a doubly curved surface.
- The layup of a typical (MW scale) blade typically consists of hundreds of layers in the composite layup.
- The positions of layers in the layup are typically described in a fashion that is unique for wind turbine blades. These positions cannot easily be calculated by hand.

FE models are typically created using dedicated pre-processor tools. These are software packages that typically provide the user with a graphical user interface (GUI) to prepare models and simulations. As a first step a computer-aided design (CAD) model is created or imported. This component is subsequently partitioned. Partitioning is needed to divide the part in regions to allow the properties of those regions to be assigned. Partitioning is also used to divide the part features into simpler sub-features onto which the desired meshing strategy can be applied. In a subsequent stage an assembly is made, where a single part, different parts or possibly several instances of the same part are defined. Next, simulation steps are assigned. These steps are linked to the type of simulation and which solution method is used. At this level, interactions such as ties and contact are defined. As a final result of the pre-processor, an input file is written. This is typically a plain text file consisting of keywords and values describing the full FE simulation. This file can be fed to a solver, which will process the model and attempt to create a converged solution for the simulation. To simplify this time-consuming process, tools have been developed.

3.1.2 Structure of this chapter

This chapter is written with the following structure. First, the existing tools for the creation of FE models of wind turbine blades are discussed along with their strengths and weaknesses. Subsequently, in a second part, the novel tools that were created in this work are discussed.

These tools are discussed in sequence of refinement and complexity. For every tool the limitations are discussed and these elements form the motivation for the

subsequent approach. First an approach based on the use of a pre-processor is presented. Next, a stand-alone tool that uses a slice-based approach is presented. This tool is first created to produce shell models and later extended to allow for the creation of slice-based solid models. This leads to the last approach, which is based on blocks consisting of cells, which is the final approach developed in this work.

3.2 Wind turbine blade FE modelling tools: state-of-the-art

3.2.1 Existing tools

Because of the level of detail required to obtain high fidelity blade models, various tools have been developed and described in the international literature. An overview of existing tools is provided in Table 4. These will be discussed in the following sections.

Table 4: Overview of existing tools for the creation of 3D FE models of wind turbine blades. Cells marked with a "?" represent information that is unclear from the available literature.

Tool		FOCUS [3]	NuMAD [2]	BMT	Dutton et al. [6]	Botasso et al. [7]	NSE Blademesher [9], [10]
Pre-processor		Stand-alone	ANSYS [4]	PATRAN [5]	Stand-alone	Hypermesh [8]	Stand-alone
Key locations		Detailed	Chord-fraction based	?	?	?	Chord-fraction based
Laminate	Shell (BOT)	yes	yes	-	yes	yes	-
	Shell (MID)	-		-	-	yes	-
	Shell (TOP)	-		-	-	yes	-
	Solid	-	-	yes	-	yes	yes
Adhesive	Web joint	-	-	yes	-	yes	yes
	TE joint	-	-	yes	-	yes	yes
	LE joint	-	-	-	-	-	-

3.2.1.1 Parametric models

Various authors have made parametric versions of wind turbine blade models. These are often very simplistic. The structural layout is typically very basic. For example, Bechly and Clausen [1] used a FORTRAN routine to create a parametric model consisting of linear shell elements on the OML and solid elements representing the adhesive and filler material. This was applied to a 2.5 m blade and resulted in a simple structured mesh. Similarly, Jureczko et al.[2] created a parametric blade model. Meshes created with these methods can be seen in Figure 39. With a similar approach, Bonnet and Dutton [3] developed a tool to generate FE models using a python script. The script creates the OML shape and generates a FE mesh. A fully structured swept mesh is produced consisting of shell elements on the OML. Solid elements can be generated to represent the adhesive bonds connecting the shear webs with the OML. Resulting meshes can be seen in Figure 40. Both linear and second-order as well as reduced and full integration elements are available. The main advantages of the approach are the possibility to do a parameter study without the use of the tools within a pre-processor. The main limitations of these approaches lay in the limited level of detail that can be incorporated in the models. The number of partitions are very limited, while the structural layout is simplistic.

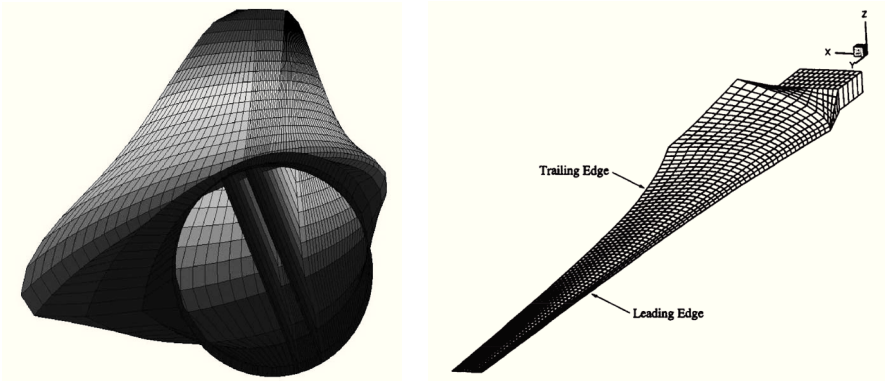

(a) (b)

Figure 39: Meshes of parametric blade models. The level of detail in these models is very limited. (a) FE mesh result obtained using the method developed by Jureczko et al. [2]. (b) FE mesh result obtained using the method presented by Bechly and Clausen [1].

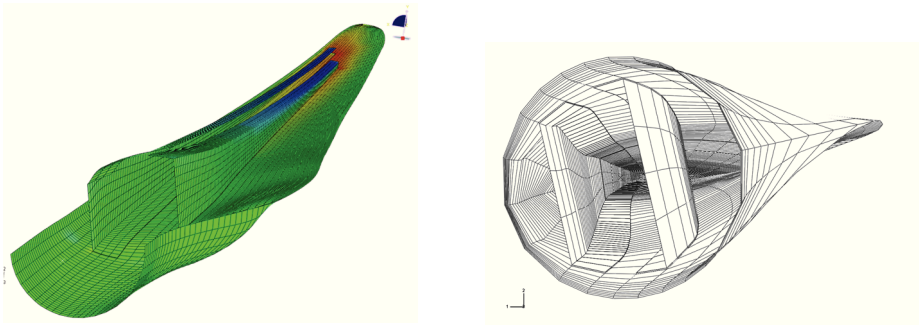

(a) (b)

Figure 40: Meshes of a parametric blade model of a 5MW reference turbine blade generated by the tool created by Dutton et al. [3] The OML surface is meshed using shell elements, while the adhesive joining the shear webs to the girders is modelled using cohesive elements. The level of detail included in the model is limited. (a) View of the blade with the SS shell hidden. (b) View of the blade from the root end.

3.2.1.2 NuMAD

The "Numerical Manufacturing And Design" (NuMAD) tool was developed by Sandia National Laboratories. It is a stand-alone tool that is based on MATLAB [4] to create a script which can be used in the ANSYS mechanical APDL commercial finite element engine [5]. It is complete with a Graphical user interface (GUI), seen in Figure 41. It is also able to generate meshes for aerodynamic simulations and provide inputs for other tools. The tool can create blade models with shell elements on the OML. All types of shell elements can be used. The structural layout is not pre-defined and partitions do not have to span the full blade length. However, the method for partitioning the blade does not appear to be very accurate. First, the partitioning at different span-wise positions requires the creation of airfoil stations. As such, the OML shape and topology of the model are not independent of each other. Furthermore, the partitions appear to depend on the airfoil station control points. For example in Resor and Paquette [6], the number of airfoil points was reduced to improve the model. In addition, the chord positions of the partitions were calculated by means of a spreadsheet. This seems neither fast, accurate or user friendly.

3.2.1.3 FOCUS

An alternative is FOCUS, a commercial tool developed by WMC in the Netherlands [7]. It is a complete blade design suite that includes a GUI, modules for aero-elastic load computations and other modules. The tool features a module allowing the creation of FE models with shell elements on the OML. The blade layout is not pre-defined. It is widely used in industry for the design of blades. The software first constructs an OML shape of the blade, after which it is

partitioned by functions running over the full length of the blade. This results in different panels being formed to which a layup is assigned. These are meshed with shell elements. The mesh consists of nodes positioned on span-wise slices. Triangular elements are used to vary the mesh density. The main limitation of this software is that only OML shell models can be produced. Furthermore, the resulting meshes seem to consist of nodes positioned on a series of slices. Consequently, mesh transition relies on the use of triangular elements.

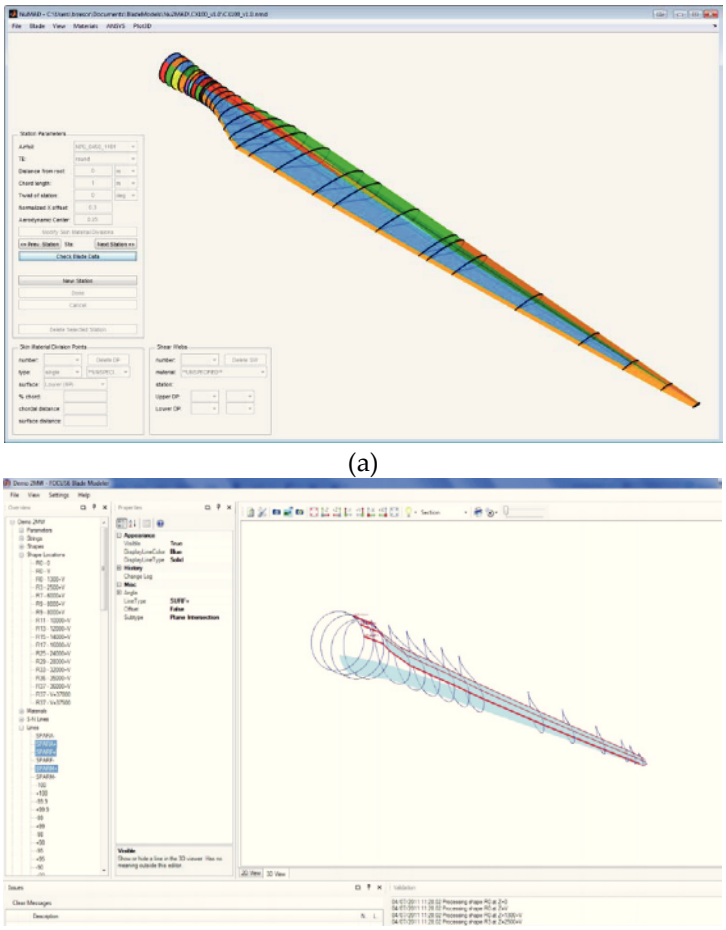

(a)

(b)

Figure 41: Graphical user interfaces of blade model creation tools. (a) The "Numerical Manufacturing And Design" tool (NuMAD). Reproduced from Ref. [5] (b) FOCUS. Reproduced from Ref. [7]

3.2.1.4 NSE Blademesher

Further, the "NSE Blademesher" [8] is a tool capable of producing blade FE models consisting mainly of solid elements. It uses a pre-defined structural layout to produce a fully structured mesh that is swept in the blade length direction. Solid elements with an equivalent (homogenized) material section are used for the laminate and adhesive of the blade, while shell elements are used to represent the trailing edge and web, as shown in Figure 42. The tool is used in a study in which a novel wind turbine blade employing blade sweep is developed [9]. The tool first calculates splines of the OML shape. On these splines, key-positions are calculated according to the layout. Subsequently, nodes are created in between the key-positions. These are subsequently used to calculate the position of additional offset nodes by extruding inwards. These nodes are then connected to form layers of solid elements. Two material orientation systems are used. One system is oriented so that the 1-direction aligns with the radial direction and the other follows the path of the leading edge. These systems use the 'OFFSET TO NODES' option within Abaqus [10]. This allows the elements to use a vector parallel in 3D space to the nearest leading-edge (LE) element as 1-direction.

However, there are several limitations with this tool, as discussed in Ashwill et al. [9]. First, intersections occur at the TE panel between the core on the SS and that on the PS. Moreover, the model is limited to the part of the blade beyond the position of maximum chord, where the section already has a regular airfoil shape. Also, the linear elements with a single equivalent material section do not allow investigation of the behavior of the individual plies. Furthermore, the simulations conducted in that study were geometrically linear, whereas various authors have demonstrated the importance of geometrically non-linear analysis.

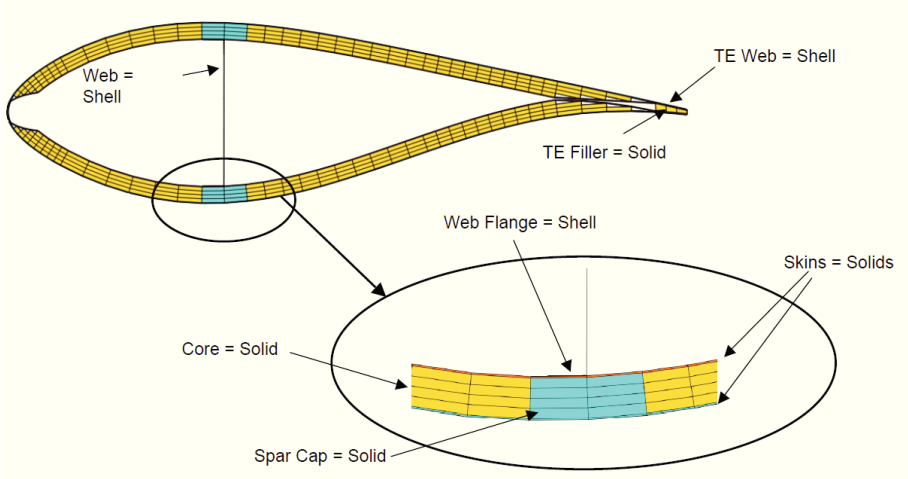

Figure 42: Schematic view of mesh section produced by the NSE Blademesher. The tool produces a fully structured swept mesh consisting mostly of linear solid elements. Reproduced from reference [8].

3.2.1.5 Bottasso et al.

Another approach is used by Bottasso et al. [11]. A tool was created to obtain both shell and solid models for an automatic multi-tier optimization loop. The tool relies on HYPERMESH [12] for CAD operations and meshing. The method works by first calculating a NURBS representation of the OML surface. This is then partitioned using HYPERMESH. The different faces are subsequently offset depending on their layup. When creating a solid model, a surface mesh is first produced on the OML and subsequently projected onto the inside surface as shown in Figure 43. This results in a model that can consist entirely of solid elements. Linear, layered solids are used to represent the laminate. The mesh consists primarily of hexahedral elements, with some wedges in specific regions. Advanced material orientations are calculated on an element-by-element basis by providing each surface with an orientation vector. The centroid of each element created on the face can subsequently be used to evaluate the normal at that position. This information is sufficient to calculate a complete material orientation system. It is unclear if the structural layout is completely pre-defined or not. Furthermore, it is unclear how flexible the presented tool is in terms of possible structural layouts.

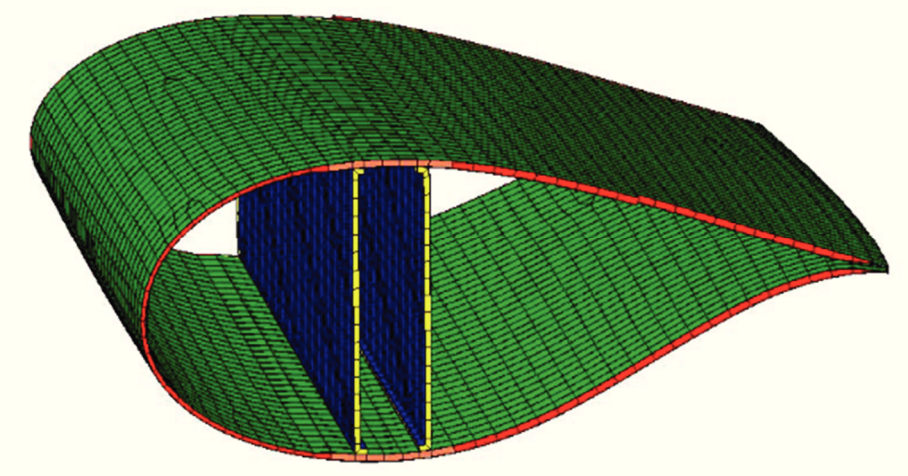

(a)

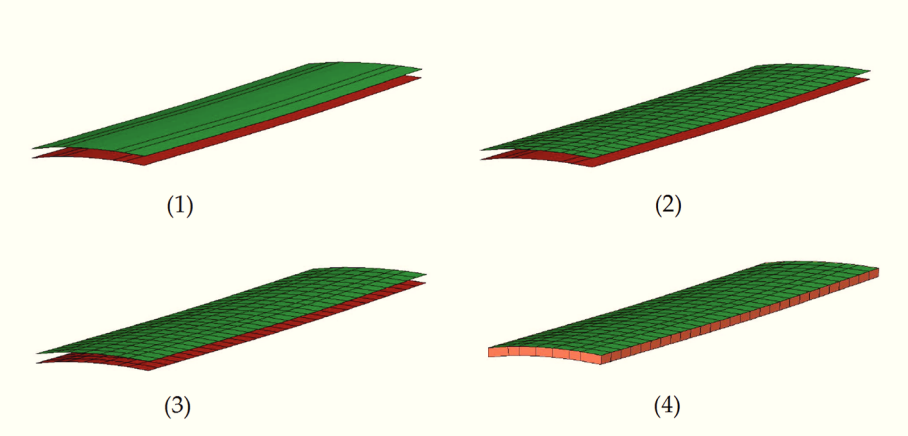

(b)

Figure 43: Meshing approach used by Bottasso et al. [11] to obtain a solid model using HYPERMESH [12]. (a) Resulting cross section of a blade. (b) The employed meshing strategy: first, surfaces are generated for the top and bottom of the material. Next, one surface is meshed. This mesh is projected onto the other surface and the nodes on one surface are connected to their projections to form solid elements. 1: Calculation of an offset surface, 2: Meshing of the base surface, 3: projection of the mesh from the base surface to the offset surface, 4: Creation of solid elements from the mesh on the surfaces.

3.2.1.6 BMT

Likewise, a tool called "Blade modelling tool" (BMT) was developed by DTU in Denmark to create solid models [13]–[15]. It uses input from a spreadsheet and creates a script which can be used to create the blade model in the PATRAN pre-processor [16]. The tool works by first calculating the OML geometry. Next a pre-defined structural layout is applied. It is unclear how the locations for the key-positions in this layout are calculated. The layout can be seen in Figure 44. The layup for every component in the layout is read from the input spreadsheet, allowing the thickness to be calculated for every panel. Interpolating surfaces are then calculated. After which the resulting collection of cells is meshed. The result is a blade FE model consisting completely of solid elements. The meshing algorithms included in PATRAN allow for a mesh with variable densities consisting purely of hexahedral first or second order layered solid elements to be constructed. The main limitation of this approach is that it relies on a fully pre-defined layout.

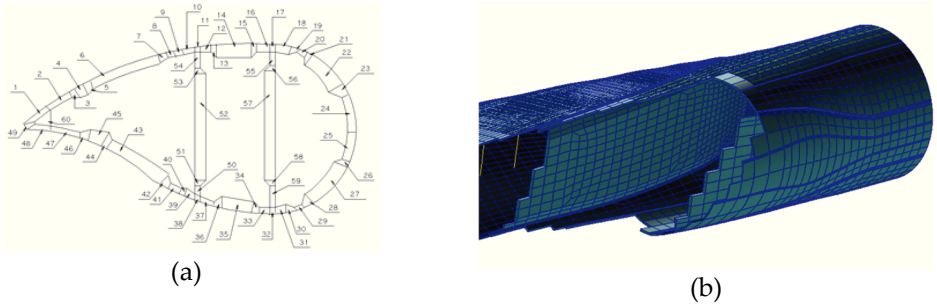

(a) (b)

Figure 44: Pictures of the Blade modelling tool (BMT) developed at DTU. The tool creates solid FE models by creating a script for the PATRAN pre-processor. (a) Schematic view of the pre-defined layout. (b) Resulting mesh with some elements hidden to show the internal features. The mesh consists entirely of solid hexahedral (brick) elements.

3.2.2 Conclusions

There are a number of tools dedicated for creating blade FE models. This again reinforces the assessment that automation tools are a necessity when creating blade models. The majority of these tools produce a script which can be used with a specific, commercial pre-processing software package to obtain the final blade model. They are therefore explicitly dependent on that particular pre-processor. In addition, the existing tools have limitations. First of all, some do not include the capabilities required to accurately calculate key locations on the blade surface, but rather rely on the user to provide chord-ratios at a limited number of stations. Secondly, most tools do not provide the user with the ability to choose between shell and solid models, but are dedicated to one specific type of output. Tools

dedicated to the creation of OML shell models typically allow for an un-structured layout that is not pre-defined. Tools capable of creating solid models typically rely on a specific pre-defined structural topology to create the model. Finally, most tools are not easily extendible to account for additional details and many are limited to shell models.

In this work, there is a need for both shell and solid models. The purpose is to have the capability to investigate both the global behavior of the structure as well as to allow detailed modelling of specific regions of interest such as the joints. In this respect the capabilities of the existing tools are not deemed sufficient. Several of the existing tools are commercial and black-box. Therefore, extending their capabilities is not a viable option. However, there are several tools where the source code can be accessed. Yet, it is not in the interest of the OptiWind project to invest in the tools that are property of others. Therefore, it was concluded that novel tools should be developed.

3.3 Application of the conventional modelling method

To demonstrate the practical limitations of modelling a blade using the conventional approach of manually directing a commercial pre-processor, this method was used to create a detailed FE model of a commercial 49 m blade using the Abaqus/CAE pre-processor software. In a first step, the blade's outer mold layer (OML) surface was imported from a CAD file. This surface had to be partitioned to allow the composite layup to be assigned. Positions on the blade surface were calculated using the CAD software SolidWorks [17]. The OML surface was first intersected with many planes perpendicular to the blade's length direction. On the resulting intersection curves, 3D offsets were applied to find the desired positions in 3D space. This approach is shown in Figure 45. While this method allows for the calculation of key-positions on the OML shape, it is highly time consuming to the user. Subsequently, the CAE was used to partition the OML along the chord-direction and to manually select the regions for every single ply in the layup. This manual process was found to take days. Furthermore, it was found to be difficult to do correctly. In addition, it is very likely that the resulting model contains several human errors. Finding and fixing these is a challenge on its own.

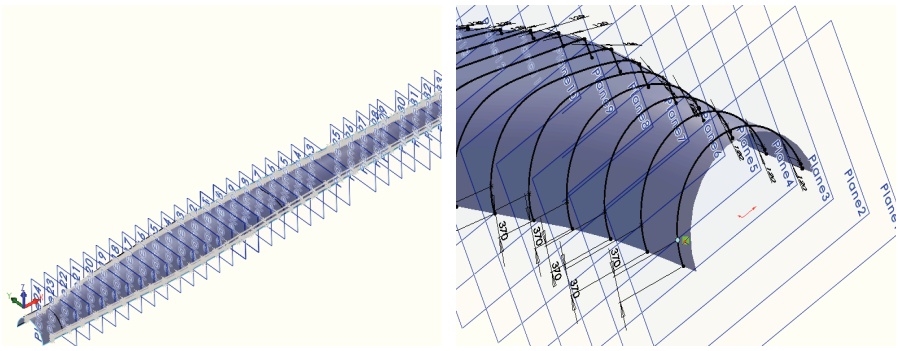

(a) (b)

Figure 45: Calculation of key positions on the blade outer surface positions using SolidWorks [17]. The OML surface is intersected with planes. On the resulting curves points are calculated by offsetting from the LE and TE. (a) Overview showing the full blade length. (b) Close-up view showing how each point was calculated.

It is therefore clear that the consequence of the amount of complexities in the blade is that the user-time required to produce a good, detailed FE model using a pre-processor is huge. Consequently, using a manual approach, user time limitations would limit the level of detail and fidelity of the models. Furthermore, creating a blade model manually involves several boring, repetitive tasks such as partitioning the OML surface and assigning each ply in the composite layup to its region. These tasks provide an opportunity for automation. Moreover, repetitive work is prone to human error. Therefore, automation of these processes is not just an opportunity, but a necessity, as detecting and fixing human errors is not always straightforward. Therefore, it can be concluded that the use of tools to (semi-) automate the creation of blade models would be highly beneficial.

3.4 Automated pre-processor

3.4.1 General approach

A first logical step to reduce the time needed for the creation of FE models is to retain the modelling process using a pre-processor, but automate the repetitive actions. In this way, these tasks are no longer a problem to the user. This increases the achievable level of detail for a given amount of user time. Such approach is similar to some of the existing tools discussed earlier.

For this approach the Abaqus/CAE pre-processor was used. It contains a Python interface which can be used to produce every action that can be done using the GUI. In this way, a complete model can be created using Python commands. Other pre-processing software tools (such as ANSYS, PATRAN and others) typically provide a similar scripting capability.

The typical process of creating a blade model consists of the following steps:

1. Creating or importing the blade's OML geometry
2. Partitioning the OML along the length of the blade
3. Partitioning the OML along the chord of the blade
4. Assigning each layer in the composite layup to the correct region
5. Meshing
6. Calculating material orientations

The main time-consuming tasks are the partitioning and layup application steps. Therefore, they are the main focus of the automation.

3.4.2 Automated pre-processor

The process to create a model using the automated pre-processor is divided in a series of steps. An overview can be seen in Figure 46. In a first step, the blade OML shape is partitioned along the length of the blade. To do this accurately, the description of the blade shape and ply edges was used to calculate datum points at a large number of positions. These datum points could then be projected onto a sketch in which they could be connected by an edge which is subsequently used to partition the surface by projecting. Once the span-wise partitioning is complete, different regions have to be assigned manually. These are stored and used later for assisting in the layup application.

The model is subsequently partitioned at all the desired span-wise positions. This was done for each position by creating a datum plane at the desired position perpendicular to the blade length direction and partitioning the OML surface with this plane. The resulting assembly of the 49 m blade can be seen in Figure 47.

Once the blade model is fully partitioned, the composite layup is assigned. This is done by selecting the correct region of the blade and assigning the desired ply. The selection process uses a bounding box method.

Next, a global mesh size is imposed and a quad dominated mesh is generated using the default meshing tools. Similarly, local material orientations are assigned using built-in methods. This is either done based on a single coordinate system or on an element-by-element basis by using the "discrete" methods available in the Abaqus/CAE [10].

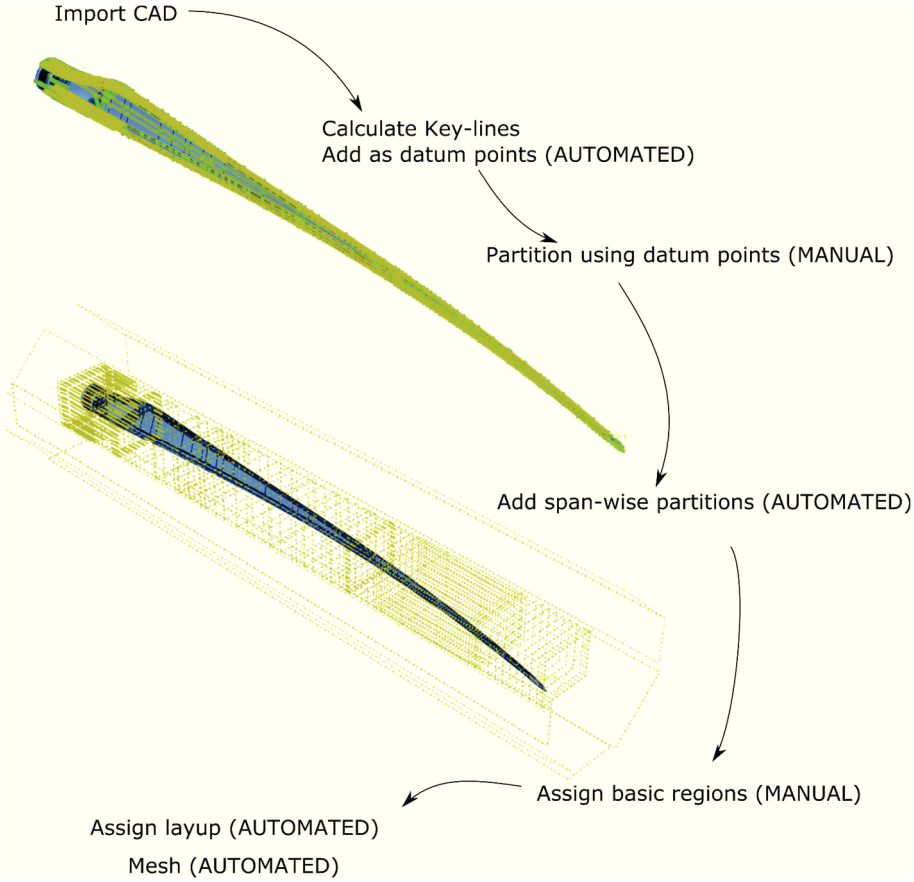

Figure 46: Schematic overview of the model creation process used with the automated pre-processor. First, a OML surface is imported as a CAD file. Datum points are subsequently added to represent the key-lines. These can then be used to accurately partition the surface along its length. At that point, basic regions can be added, from which a sub-selection is made for each ply defined in the layup using a bounding box. Lastly, the model is meshed and material orientations are assigned.

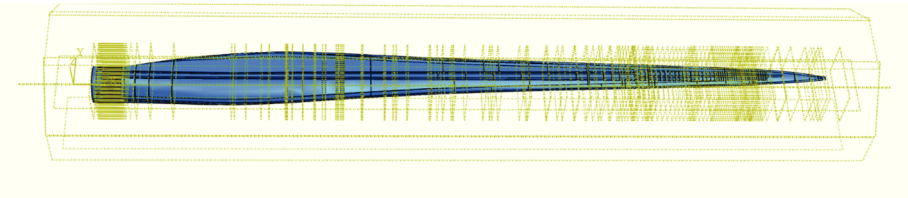

Figure 47: Model of a 49 m blade in the Abaqus/CAE pre-preprocessor. Python scripting was used to automate the partitioning of the model. The model is partitioned using datum planes and the layup is applied using a bounding box selection method.

3.4.3 Discussion of the approach

The automated approach was successfully applied to two large scale blades. Vast amounts of time can be saved when creating such models. There are however some issues with the automated version of the Abaqus/CAE pre-processor. First of all, the software becomes excruciatingly slow once a large number of features are added. The size of the pre-processor ASCII files becomes huge (over 300 Mb) and loading or saving these files can take over 30 minutes on a quad-core laptop with a solid state hard drive. A possible explanation for this phenomenon is that the pre-processor handles the part features in a tree structure. This allows actions to be undone and features to be suppressed, but consumes a large amount of memory and requires updating of the state of the part.

Secondly, the partitioning often fails. While the reasons for this issue vary, one common reason is that the CAD model of the blade OML surface consists of multiple geometric surfaces, while partitioning can only be performed on a single geometrical surface. Furthermore, the pre-processor was found to crash for unclear reasons while performing certain actions. This issue can be solved by creating a new OML surface from the blade planform.

Further, in some regions partitions cross each other. This can result in faces with very sharp corners. When left untouched, these corners would result in triangular elements with excessively high aspect ratio's, exceeding 1000/1. This would result in errors when running the simulation. Avoiding these issues required manual intervention.

3.4.4 Conclusion

While the automation of the Abaqus/CAE pre-processor allows for the creation of far more detailed FE models for a smaller amount of user-time, this approach suffers from severe limitations. The best way to avoid these issues appears to be the use of stand-alone software which generates the model creation up till the level of the final blade mesh. This mesh can then be imported and used for the further process.

3.5 Slice based model generating tool

3.5.1 Approach to create shell models

To avoid the drawbacks of using a pre-processor as mentioned previously, a stand-alone software tool was developed. This tool uses a number of user-inputs to generate a complete FE model in the form of an Abaqus input file. This input file is a plain text file with keywords and values in a specific structure. In the stand-alone software, the modelling process consists of the same steps to create the blade model as the manual and automated pre-processor approaches. An overview can be seen in Figure 48.

The advantages of a complete stand-alone tool are that unlike a commercial pre-processor, the tool is not a black-box and every action can be controlled. On the other hand, modern commercial pre-processors include a large number of valuable features such as meshing algorithms and tools for CAD operations that are well implemented and reliable. In the stand-alone software, none of these features are readily available.

The software is structured to have different components which each handle a modelling task. A first component calculates the OML shape. A second component calculates the partitions along the length of the blade, also known as the key-lines. All the required span-wise locations are then collected and intermediate partitions are calculated. At each of these positions a slice of the OML is calculated and nodes are created. Other components calculate the layup and local material orientations. These are then connected with elements to form the model. Each of these steps is explained in more detail in the following paragraphs.

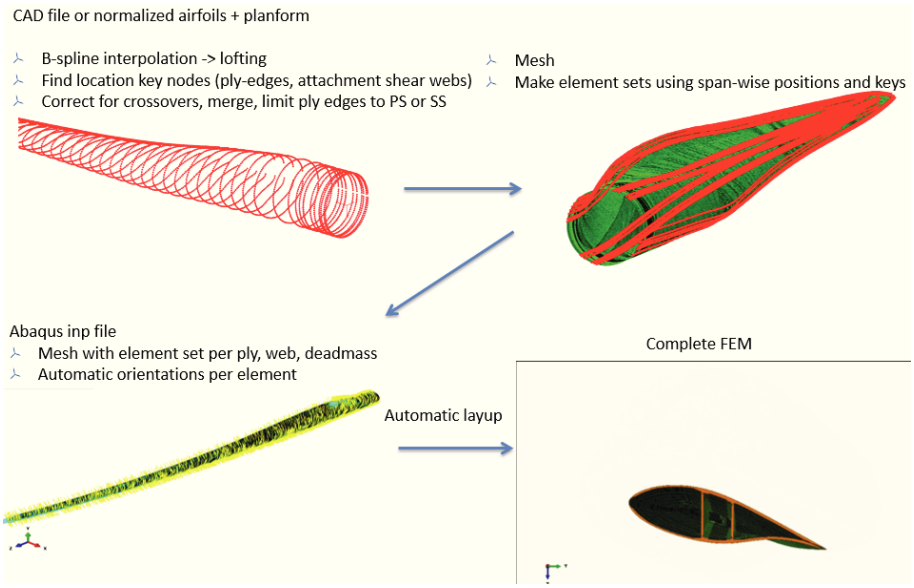

Figure 48: Schematic overview of the newly developed stand-alone slice-based software approach.

3.5.1.1 *Calculation of blade OML surface slices*

As previously discussed, usually only the OML shape of wind turbine blades is described. This outside shape is typically described by a series of airfoil stations. This can be seen in Figure 49. These each consist of an airfoil shape that is transformed. This transformation includes scaling the shape with the chord length, twisting it to match the pitch-angle and displacing the shape to its desired spatial position. To calculate intermediate slices, the following procedure is used: First, on every airfoil station a user-specified number of points is calculated. Next, these points are used to construct a series of splines that each connect all airfoil stations, with parameter set to the span-wise position. Finally, the resulting shape is evaluated by evaluating the series of splines at the same parametric position. This returns a slice of the OML shape. Using this method any blade shape can be created. As shown in Figure 50, this includes blades with pre-bending or sweep.

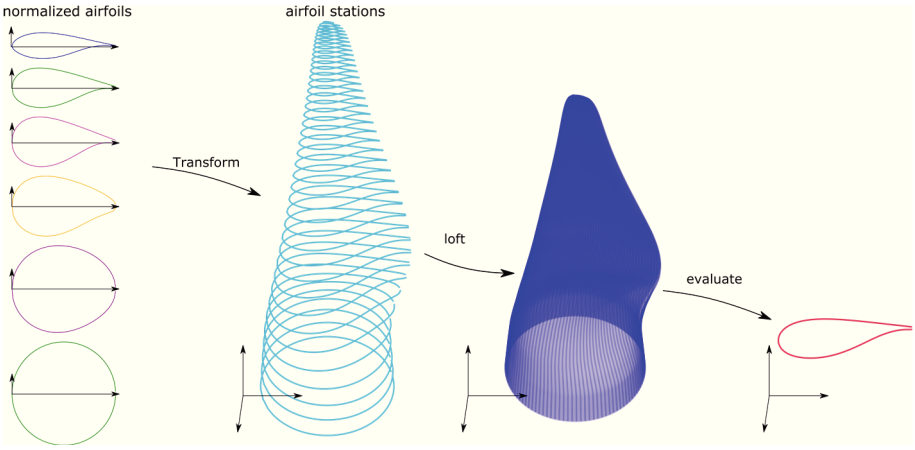

Figure 49: Schematic overview of how the blade's OML shape is calculated from airfoil sections. Normalized airfoils are transformed by translating, scaling and rotating to the desired airfoil stations. These stations are lofted together using curves along the length of the blade. These can subsequently be evaluated to obtain the shape for any slice at any span-wise position along the length.

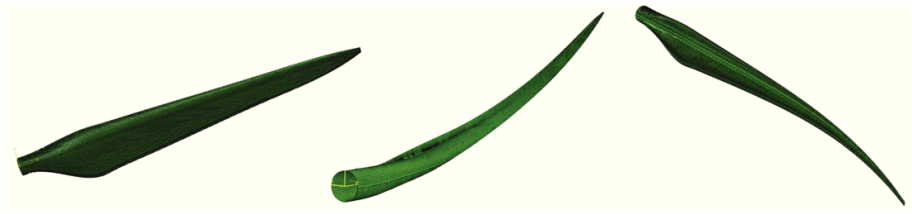

(a) (b) (c)

Figure 50: Meshes of different blades with elements positioned on the OML, created with the slice based approach. (a) straight blade shape (b) blade including pre-bend (c) blade including sweep.

3.5.1.2 Calculation of key-positions

To partition the blade along the length, "key-lines" are defined. These are functions on the blade OML surface. Examples of these functions can be seen in Figure 51 and Figure 52. At each spanwise position, these functions have one point, referred to as a "key-position". A key-line therefore exists as a series of key-positions. Key-lines are calculated based on references such as the LE, TE, reference planes or surfaces. A more detailed explanation is given together with the final software approach later in this chapter.

No structural layout is imposed and key-lines can coincide or cross each other. In the case of crossings, a single key-point is determined where the lines coincide, to avoid issues in the resulting mesh.

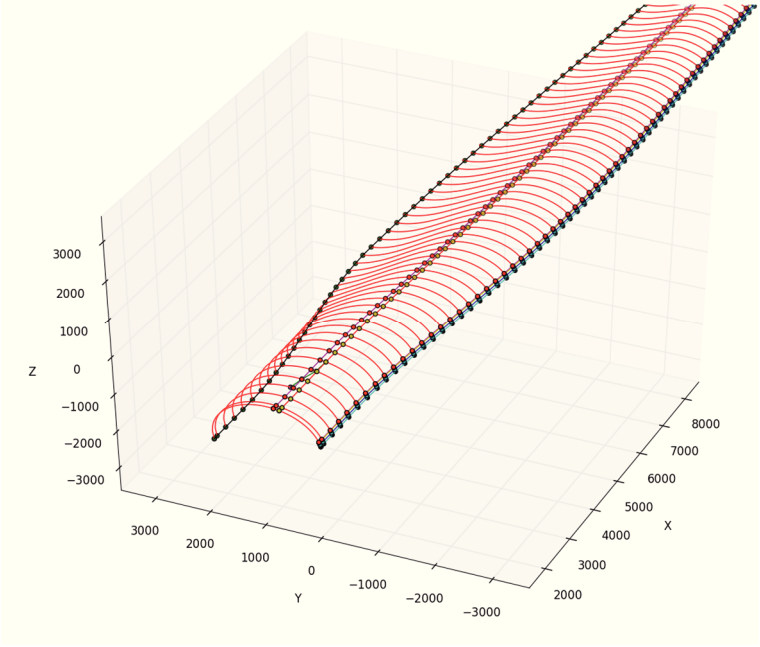

Figure 51: 3D plot of a PS half of the OML of a blade in the form of slices (red). A number of key-lines are shown, connecting a series of key-positions.

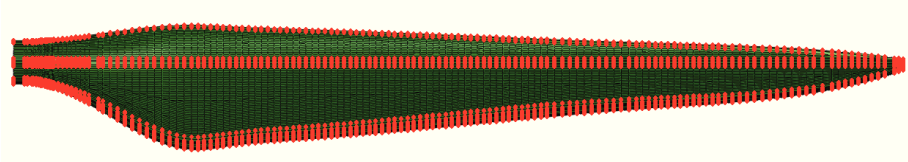

Figure 52: A blade model with key-lines indicated in red.

3.5.2 Meshing

As mentioned, one of the challenges with a stand-alone tool is that the meshing capabilities of pre-processors are not available. For this reason, the meshing strategy employed within the software was kept very simple. The meshing process for connecting two subsequent slices can be seen in Figure 53. Two subsequent slices each consist of a number of segments that are to be connected. One pair of segments is meshed at a time. First, all segments are seeded with the desired element size. Subsequently, triangles are made from the segment pair, minimizing the worst angle of the triangles. Next, the triangles are recombined, to form a combination of triangles and quadrangles. These are used as three and four node shell elements. The recombination strategy has the advantage that the mesh uses the optimal number of triangles at the best positions to create mesh transition. In the case of a skewed panel for example, triangular elements are

formed at the sides of the panel, allowing quads with a good shape to be formed in the center of the panel.

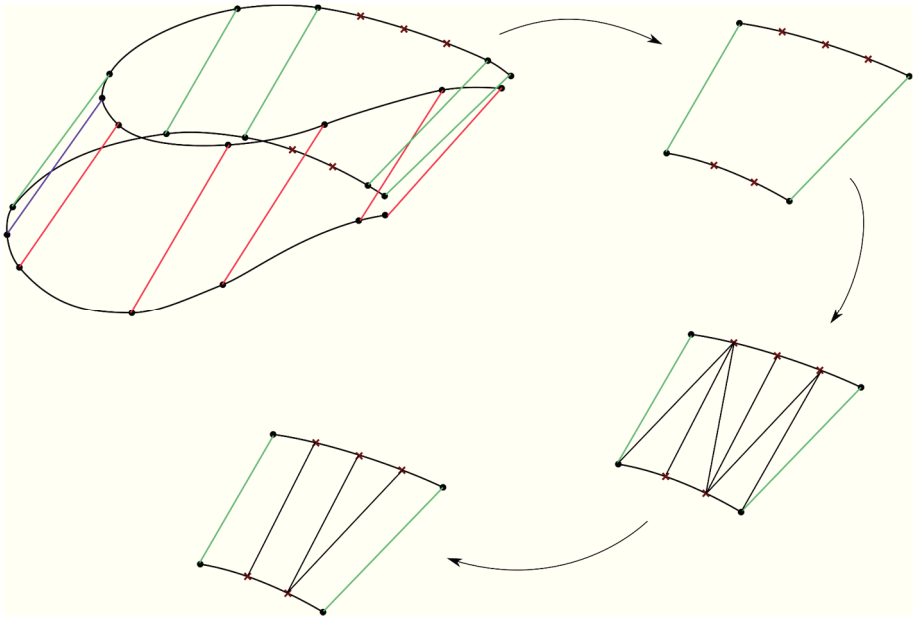

Figure 53: Schematic overview of how a mesh is created between two subsequent slices of the blade model. The segment is split in different panels by the key-lines. Each edge is first seeded and the nodes are calculated. Next the panels are meshed by triangulation and recombination. This allows mesh transition and avoids overly skewed elements.

The mesh density of the blade model can be varied, albeit not as locally as when a typical general-purpose pre-processor is used. A mesh density is set for the span-wise direction and chord-direction. Variations in mesh density can be seen in Figure 54. As mentioned in earlier approaches, there can be key-lines which cross each other at very sharp angles. This would result in very sharp elements with high aspect ratio's being formed. To avoid this issue, nodes that are within a user-specified proximity of each other are merged together. An example of the resulting mesh can be seen in Figure 55.

An advantage of the use of nodes positioned on a series of span-wise slices is that this allows the mesh to be used to prepare input files for the cross-section analysis tool BECAS [18].

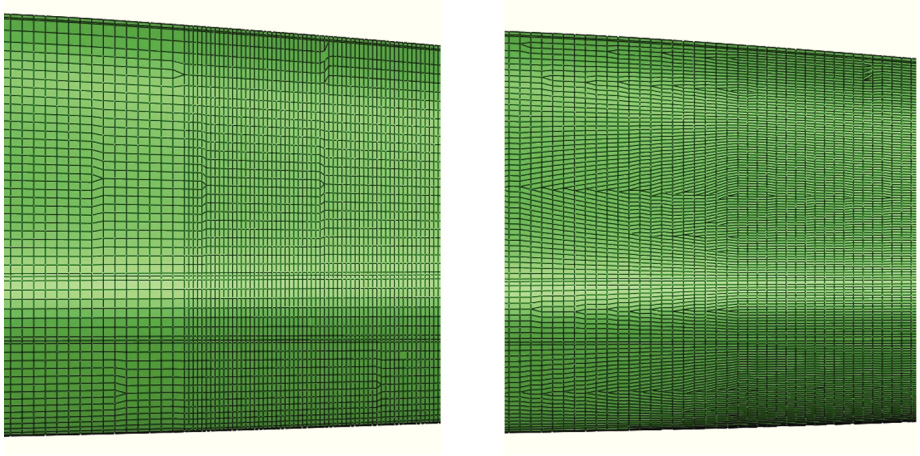

(a) (b)

Figure 54: Details of meshes produced by the slice based stand-alone software that contain a change in mesh density. (a) Span-wise variation in mesh density. (b) Chord-wise variation in mesh density.

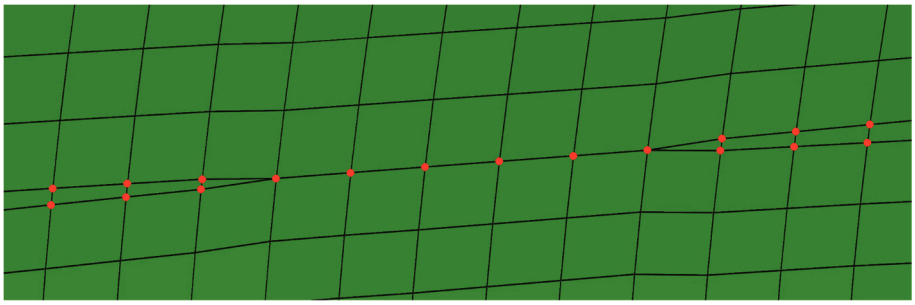

Figure 55: Close-up view of the mesh in a region where two key-lines are crossing each other slowly, creating a very sharp shard which would lead to elements with a very high aspect ratio. To avoid this, nodes that are within a certain proximity are pinched together with a user-defined tolerance.

3.5.2.1 Layup assignment

The layup is assigned in an automated fashion. The region for every ply is described by means of two bounding key-lines and two span-wise positions. This allows the layup to be specified by defining each individual layer and is independent from the level of detail in the layout.

3.5.2.2 Material orientations

The resulting mesh can be imported in the pre-processor, where material orientations can be assigned using conventional methods. However, one of the

blades considered in this work includes sweep in the planform. This sweep exists to introduce twisting deformation as the blade experiences high loads. This lowers the angle of attack of the outer portion of the blade and thereby lowers its lift coefficient, reducing the experienced load. Such a system is passive and responds very fast. To achieve this both the mold and the composite material directions are adapted. More specifically, the fiber mats which constitute the blade are not kept straight as in a conventional blade but follow the sweep. This deformation is applied to the dry fabric before infusion. This means that the main fiber direction is parallel to the sweep path. To model this correctly, local material orientations have to follow this path. To account for this effect, the software has the capability to calculate local material orientation systems in an element-by-element fashion, by using a single vector for the 1-direction at every slice in the FE mesh. This vector can be calculated from the sweep path. For every element on that slice, the normal vector is calculated and a Cartesian material orientation system is subsequently defined. The resulting material orientations on the XA21 blade models can be seen in Figure 56.

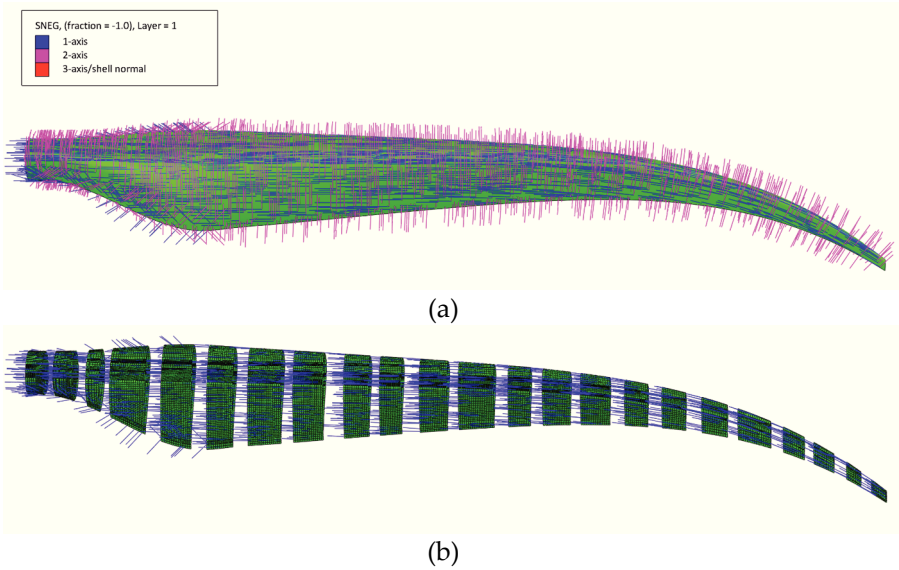

Figure 56: Plots of the XA21 shell FE model produced using the slice-based software tool. Local material orientations are plotted. The material 1-directions are shown in blue, while the 2-directions are shown in red. (a) Side view of the blade model. (b) Side view of the blade model with some slices of elements hidden for clarity.

3.5.2.3 Discussion

The advantages of the approach are considerable. Very accurate partitioning of the blade is obtained, while manual intervention is no longer required. This allows rapid modification of the model. Furthermore, the model can be considered

parametric, but unlike other studies claiming to use a parametric layout, the amount of partitions can be very high and the layout is not pre-defined or structured. The approach was therefore successfully applied to three different blades. This led to the observation of the following limitations:

- The included meshing algorithms are very basic. Because nodes are produced solely on individual slices, inevitably, variations in mesh density have to be handled by using triangular elements. In general, FE experts prefer to avoid using these elements, because a much higher mesh density is required to obtain a converged solution.
- Structural details such as the adhesive bonds are not included
- The output is limited to OML shell models

The typical run time of the program varies strongly depending on the number of key-lines, number of plies in the layup and the requested mesh size. However, on a regular laptop, the total process typically only takes a few minutes.

3.5.3 Conclusion

The newly developed software tool is excellent at creating shell models on the OML surface. It is fast and accurate, allowing high levels of detail. Furthermore, it does not impose any pre-defined layout. The mesh and geometry are independent and high quality meshes are produced in a very limited amount of time. However, the discussed method so far only reaches the level of detailed shell models. The challenges of correctly incorporating adhesive joints as well as producing solid models remain. Therefore, since the presented approach proved successful for shell models, the software is extended to produce solid models.

3.6 Extending the slice based software to produce solid models

3.6.1 Motivation

As already explained in the previous section, the conventional blade FE models with shell elements on the OML surface have several limitations. The lack of inside surface results in issues regarding the representation of the internal features such as the shear webs and adhesive bonds. Furthermore, several authors have reported that these models produce erroneous torsional predictions. In addition to these facts there is interest to obtain more detailed FE simulations. These are of interest for local regions such as near interfaces or for sub-modelling purposes. Moreover, the rapid increase in computational power can be expected to compensate for more computationally expensive solid models in the future.

The chosen approach is to first calculate a mesh on the OML as previously described. In a second step, the nodes are offset inwards to obtain layers of solid elements. This approach is similar to what is used in the NSE Blademesher [8].

3.6.2 Challenges for creating models with solid elements

Creating models other than those with shell elements on the OML, poses a unique set of additional challenges. These are explained in the following paragraphs.

3.6.2.1 *Mesh requirements*

When modelling the laminate of a blade with solid elements, certain modelling options and their corresponding consequences and requirements have to be considered. In Table 5 an overview of solid modelling options is provided. Firstly, for the laminate portion of the blade, either elements with a single, equivalent, material section or layered elements can be used. For the laminate, a single material section means that equivalent section properties must be calculated. However, this reduces the value of the output since it does not provide layer by layer results and does not allow the inter-laminar interactions to be considered. Therefore, it is preferable to use layered elements. Within Abaqus only brick shaped solid elements have layered variants. Wedge shaped elements are not available. This therefore removes the possibility of using mesh transition with triangles (or wedges). Alternatively, so-called continuum shell elements (solid-shells) can be used. These come only as linear elements which are layered and exist as 8-noded bricks and 6-noded wedges. However, to avoid locking effects, multiple linear elements should be stacked in the thickness direction. This causes an additional difficulty regarding the layup. As shown in Figure 57, the full layup is repeated in every element. This means that the layup should first be split up in the thickness direction to allow it to be assigned to the correct individual elements.

Alternatively, locking effects can be avoided with second order elements (of which only the layered solid brick variant is an option). For the elements representing the adhesive, general purpose solid elements with a single material section can be used.

Table 5: Overview of the available solid elements and their features. The main issue with each element type is indicated in bold.

Type of element	Available types	Available order	Available output
Layered solid	**Only brick elements, no wedges**	Linear and second order elements	Layer by layer output
Regular solid (equivalent section)	Brick, wedge, tetrahedral	Linear and second order elements	**Equivalent section output**
Continuum shell	Brick, wedge	**Only linear elements**	Layer by layer output

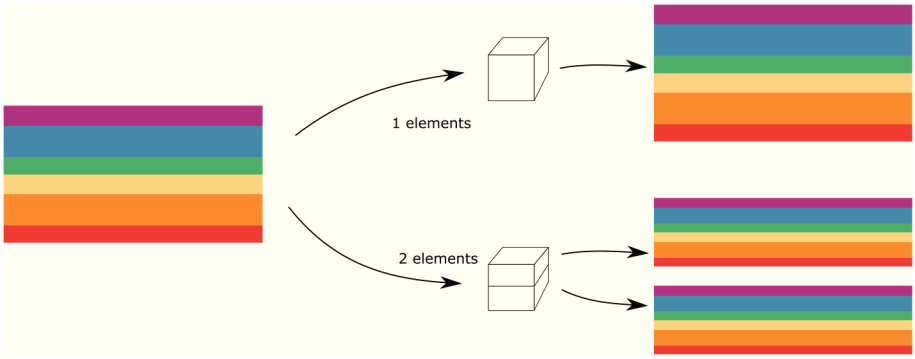

Figure 57: A challenge with the use of layered solid elements. Each element contains the full layup assigned from the material section. This complicates refining the mesh in the thickness direction.

Furthermore, the mesh has certain limitations in terms of quality. One requirement is that the element's thickness direction is parallel to how the composite layup is stacked. This can be seen in Figure 58. This also means that the mesh should consist of a matching pattern on the top and bottom surfaces. In addition, the elements should not be overly distorted. For continuum-shells and regular layered solid elements, different limitations apply. For continuum shell elements for example, the difference in normal at the corners should be limited to

less than 20 °. However, the shell nature of the continuum shells allows for a much thinner element to be acceptable. The aspect ratios of layered solid elements by comparison are much more easily exceeded.

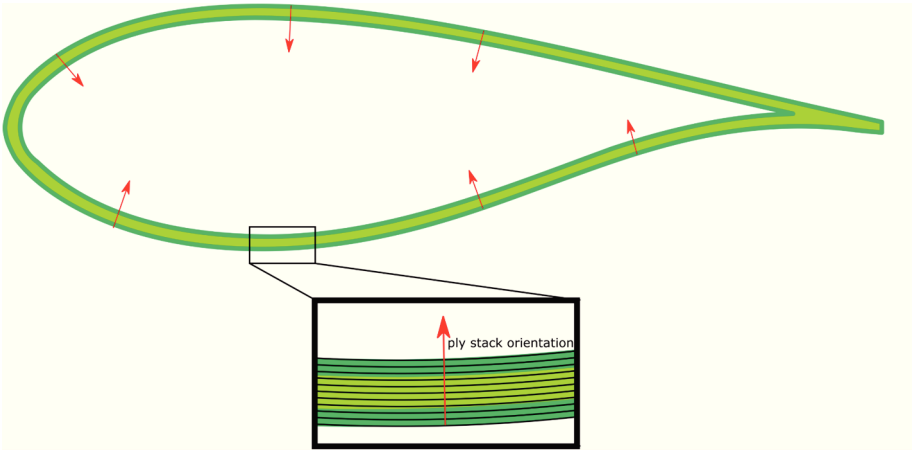

Figure 58: Schematic view of a blade cross-section. The ply stack orientation is parallel to the normal to the OML surface. Consequently, the solid elements should have their normal along this direction.

Further, the mesh on the PS and SS needs to be compatible in regions where the two sides are somehow connected. This can be for example, at the trailing edge where the adhesive joins the laminate of both sides. As an alternative, non-conformal meshes could be used and the elements representing the adhesive could be attached by means of tie constraints. However, these can be expected to drastically increase the number of iterations needed to obtain convergence within every time step, resulting in an increase in computational time. A compatible, continuous mesh without the need for constraints results in a single stiffness matrix being formed which would be much more computationally efficient.

3.6.2.2 Offsetting challenge

When models other than those consisting of shell elements positioned on the OML surface are created, new surfaces must be calculated by offsetting from the OML. These surfaces are dependent on the layup. Since the total thickness at any point is the sum of the thicknesses of a discrete number of plies in the layup, the surfaces are, in theory, not continuous. This is especially true if the ply-drops are grouped to simplify the modelling process. In reality however, ply-stacks are given a gradual drop-off to avoid stress concentrations. In Laird et al. [19] it is suggested to use a number of discontinuous surfaces and join them together with tie constraints. However, Branner et al. [20] discovered that this results in artificially

stiff bending behavior. Bottasso et al. [11] on the other hand tried using continuous offset surfaces, removing the need for constraints.

One challenge when creating models consisting of continuum elements is that offsetting the blade OML surface can result in both global and local self-intersections. Local self-intersections occur due to regions of high curvature in the original curve or surface, while global self-intersections result from different points on the curve or surface being offset to the same location. Offsetting is an active field of research and is important for CAD/CAM applications [21]. The main challenges are typically to avoid intersections and maintain the parametrization of the base curve. In general, two main approaches exist. The first is to directly calculate the offset curve from the base curve and its normal vectors and subsequently trim bad regions [22]. While this maintains parametrization, the trimming process can be difficult. The other approach is to calculate a signed distance field and use that to evaluate a curve at the given offset. This approach avoids all intersections, but loses the original parametrization. As shown in Figure 59, local self-intersections are often present at the LE while global self-intersections tend to occur towards the TE. In Ashwill [9] intersections at the TE core are noticed, but no solution is provided. It is worth noting that the global intersections are the result of an unrealistic layup in certain regions. This is also the case for models using shell elements, but often does not become apparent.

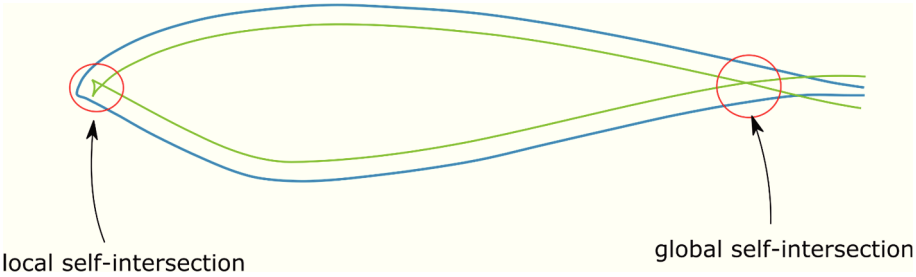

Figure 59: Airfoil section and offset curve containing local (at the LE) and global (at the TE) self-intersections.

3.6.2.3 Trailing edge region

Another challenge in creating solid models is the trailing edge region. Specifically, in the area where the transition is made from a circular root section to an airfoil shaped section. One difficulty here is that different faces are connected by the adhesive, as can be seen in Figure 60. Furthermore, a sudden transition is undesirable for the sake of mesh quality. Because of this difficulty, the transition region was not modelled in Ashwill [9]. In both BMT [23] and Bottasso et al. [11]

a TE configuration, which offsets the pressure and suction side panels according to the bisector is used. This can be seen in Figure 61. The same configuration can be used along the full span of the blade. However, neither seem to incorporate the over-lamination of the adhesive.

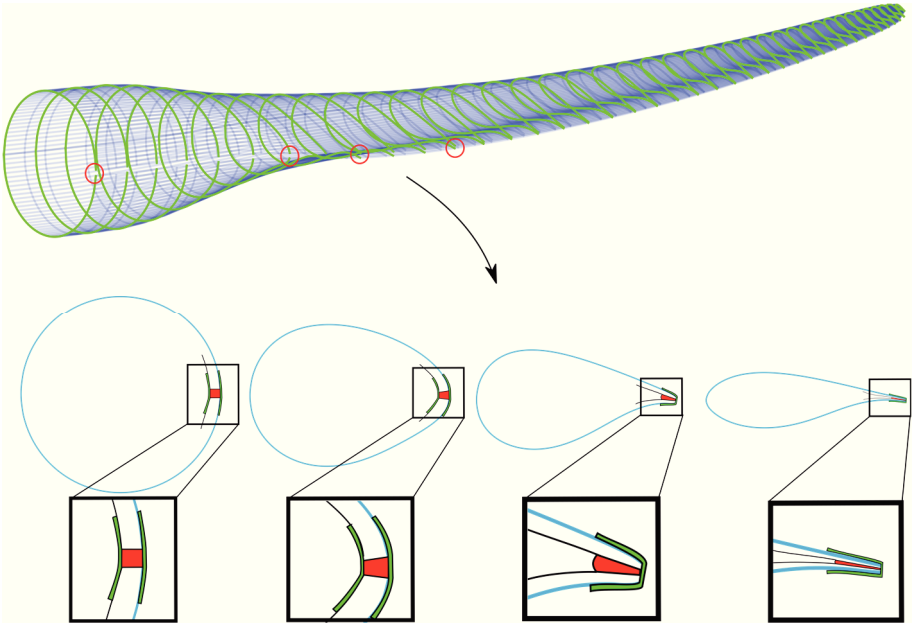

Figure 60: Overview of the change in trailing edge composition going from the circular root towards an airfoil shape at the position of maximum chord. The adhesive (indicated in red in the close-up figures) connects only the sides of the laminate while further out it connects the top faces of the laminate. Frequently, the adhesive joint is over-laminated (indicated in green) from the root up till the position of maximum chord.

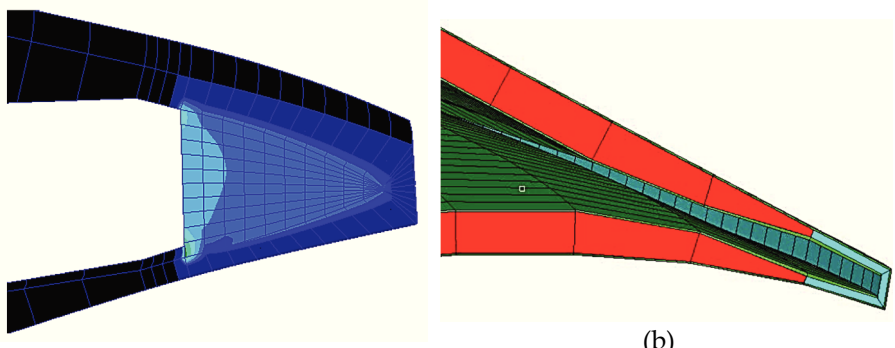

(a) (b)

Figure 61: Trailing edge modelling approaches as found in literature. (a) BMT trailing edge. Reproduced from Ref. [23]. (b) Trailing edge mesh as presented by Bottasso et al. [11].

3.6.2.4 Thickness calculation challenge

In the case of shell elements at the OML, the material thickness at every position only affects the thickness present at each element. In this sense, the thickness can make discrete jumps from one element to the next. This is however a problem in the case of a solid variant or even for a mid-thickness shell variant. In such cases, the surface at which the nodes are positioned depends on the material thickness. Since a continuous surface is desired, a single thickness should be calculated at the corners. More than simply the need to calculate a single value, the layup and its thickness should still be accurately represented. This means that in some regions, additional partitions of the OML are required to obtain an accurate model. An overview of different options to calculate the thickness at the interface between two regions can be seen in Figure 62.

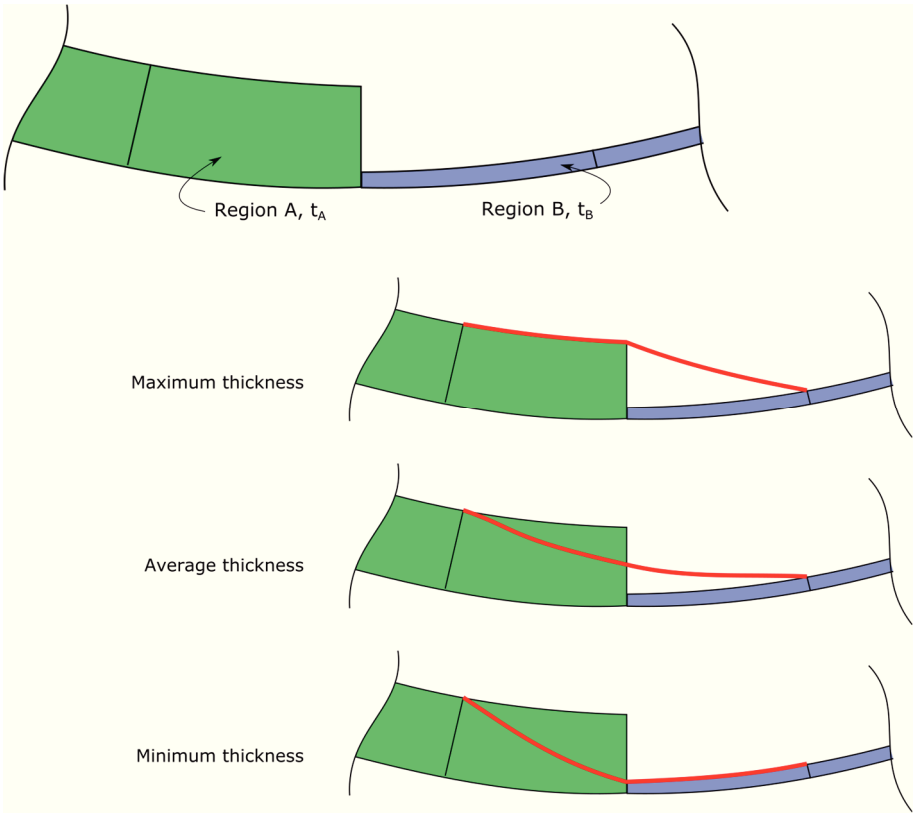

Figure 62: Schematic overview of the thickness calculation options at the interface of two regions with a different thickness. In real wind turbine blades, thickness changes are always very gradual to avoid stress concentrations.

3.6.2.5 *The web connection challenge*

A further challenge is the correct positioning of the webs. The position of the webs is initially calculated on the OML surface. However, if the normal is used for offsetting the surface, this no longer matches the plane onto which the shear web is supposed to reside. For this reason, simply offsetting along the normal is not sufficient. Instead an offset vector along the shear webs' reference plane vertical direction should be used. This can be seen in Figure 63. Therefore, it should be possible to modify the offset vector and still obtain the surfaces at the correct offset distance.

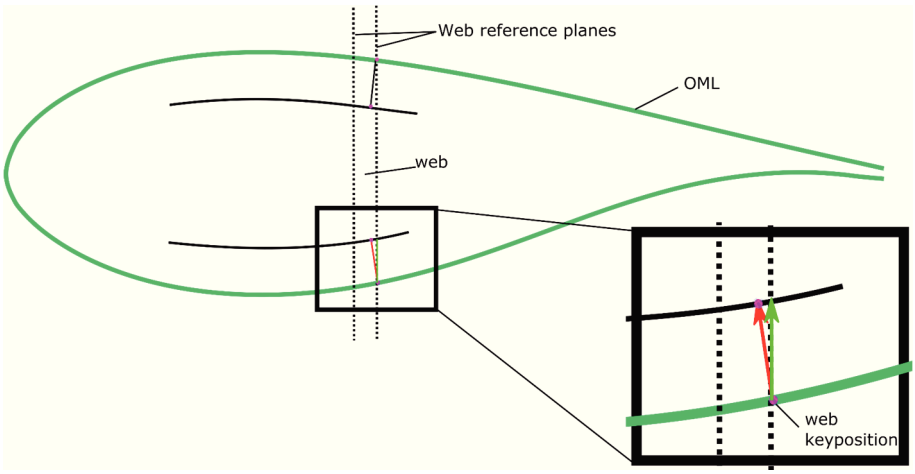

Figure 63: Schematic view of a blade cross-section. The keyline for connecting a shear web is calculated at the OML, but the web should attach at the plane with which the plane coincides. As a consequence the original offset vector, normal to the OML (shown in red) should not be used, but rather a vector within the shear web plane(shown in green).

3.6.3 Limitations of the slice based modelling approach

The previously discussed challenges became apparent while attempting to extend the slice based software to create solids. While extending the approach was in the end successful, the resulting tool has severe limitations. An example of the resulting mesh can be seen in Figure 64. Many of the challenges are not resolved for the general case.

To avoid the need for a tie constraint, a compatible mesh is required at the PS and SS in the TE area. This is needed for the elements representing the TE adhesive. A resulting drawback is that this removes some of the freedom of the unstructured approach. More specifically, intersections in this region have to be actively removed and the seeding needs to be imposed to allow a structured adhesive mesh to be formed.

A second limitation is that the offsetting process is limited to the use of the normal vector. If a different offset vector is imposed, as would be required to accurately position the webs, an inaccurate material thickness is obtained. Consequently, the shear webs, which are created based on their key-positions on the OML, are not correctly positioned. The side faces of the webs do not fully coincide with their intended plane.

A third limitation is that the thickness transitions are applied within a single element. Consequently, the size of the element affects the size of the transition. Therefore, the (inside) geometry is mesh dependent. This is undesirable since it

influences the results of a mesh refinement analysis, while the geometry should match the actual blade to achieve proper fidelity.

Further, the transition from the root to the maximum chord position at the TE is not clean. In the root region the offset is calculated along the normal vector, whereas for an airfoil, the bi-sector is used. In the latter case, the element closest to the TE is shaped rather poorly. The transition from a circular root to a general airfoil shape is handled by a sudden step from one configuration to another, resulting in one poorly shaped slice.

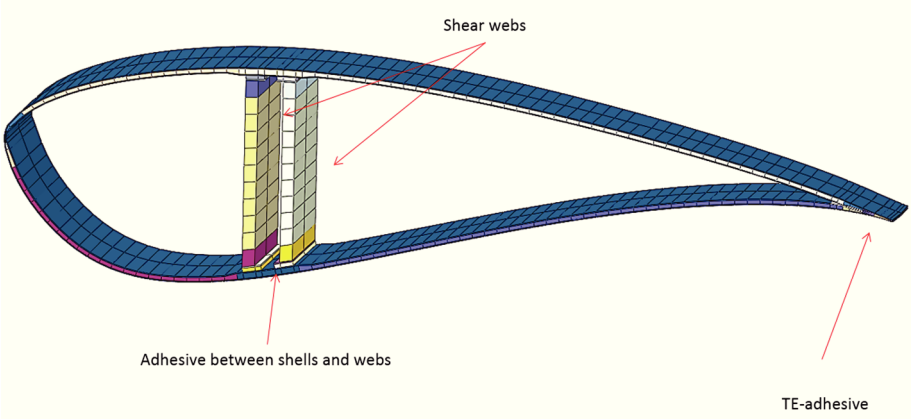

Figure 64: Solid blade mesh obtained using the slice based approach. Multiple linear solid elements are created through the thickness. The adhesive bonds are included with a single element through the thickness.

3.6.4 Conclusion

The slice based approach works well for the creation of OML shell models, but models consisting of solid elements bring their own unique set of challenges. These should be accounted for early in the modelling approach. The result is that extending the slice based approach is not really successful since the resulting modelling possibilities are limited. As argued by Bottasso et al. [11], the offsetting should be applied to a geometric level rather than by directly extruding the mesh. Furthermore, the requirement for mesh compatibility explains the fact that tools able to provide solid models rely on pre-defined structural layouts. In addition, the need for gradual transitions in the mesh could be handled by first creating cells which are then meshed so that the change in individual element shape is smooth. This sort of approach also resolves the mesh dependency of the thickness transitions. For these reasons, a different approach was developed, which focusses on first creating geometric entities such as faces and cells instead of mesh slices.

3.7 Block based approach able to create advanced shell, solid and hybrid models

3.7.1 Approach: parametric blocks

A final new approach was developed, capable of handling the issues with solid elements in the slice based software. This means that instead of producing slices of mesh, all operations are oriented towards first creating a set of geometric entities such as faces and cells. These are subsequently meshed to obtain the FE model. However, the goal is to do this without imposing a pre-defined structural layout. Therefore, instead of considering the blade as a single entity, it is considered in the novel approach as a collection of pre-defined parametric blocks. Each block consists of several components that each consist of a cell or face and have their own layup, as shown in Figure 65. To account for different regions and modelling strategies, a library of block types is available. Each block type has a different configuration and serves single or two opposing panels (one on the PS and one on the SS). For example, there is both a block type that creates a single face from a panel (that is later meshed with shell elements) and a block type that creates a single cell (that is later meshed with solid elements). More advanced block types create multiple cells and faces through the thickness. In this way there are also block types creating a trailing edge by modelling the entities representing the laminate on the PS and SS as well as that on the TE side and the adhesive connecting them. The same goes for the shear webs and their flanges. A schematic overview of some different block types can be seen in Figure 66.

Other software tools that can create models other than those with shell elements on the OML, typically consider a fixed pre-defined chord-wise topology for the blade. On the contrary, the novel approach allows the creation of both OML shell, mid-thickness shell and solid models as well as combinations of those without imposing a pre-defined layout. Figure 67 and Figure 68 show an example of how a collection of blocks can be used to model a blade section.

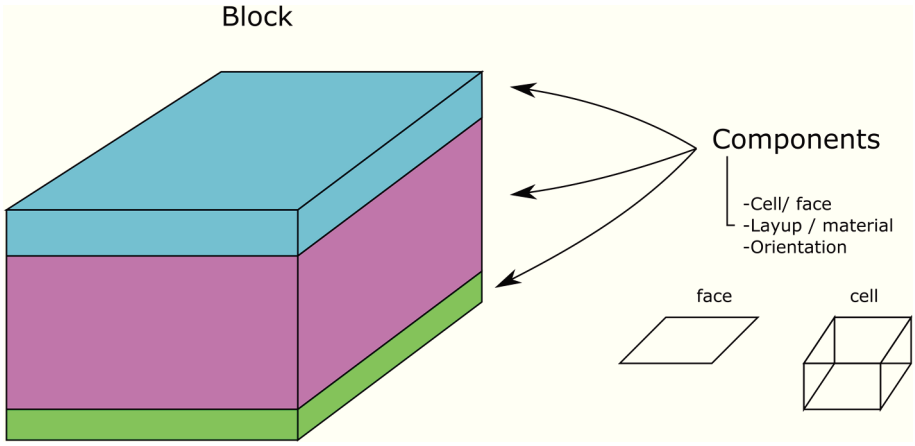

Figure 65: A schematic view of a block. Each block consists of one of more components. Each component consists either of a face or a cell, has a material or layup assigned to it as well as an orientation system. In the approach presented in this section, blade models are created as collections of these parametric blocks.

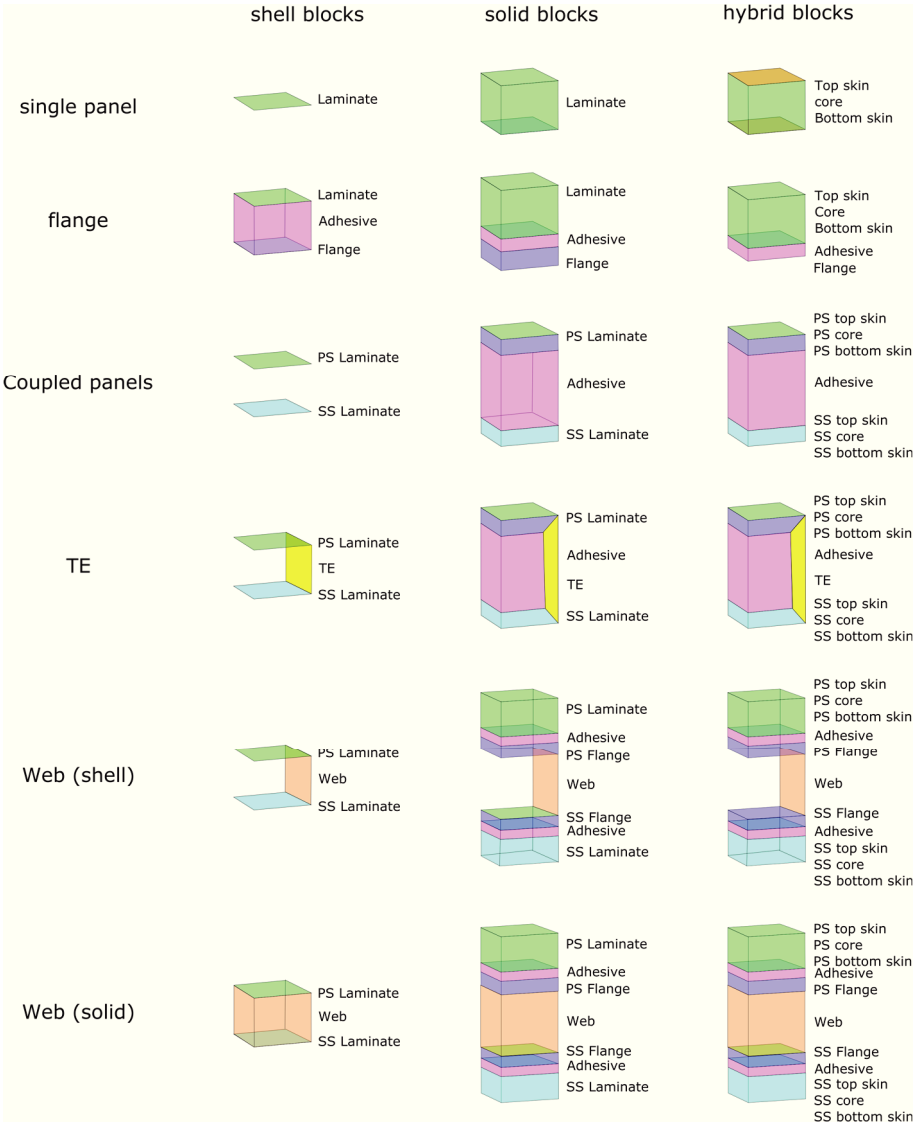

Figure 66: Schematic overview of blade blocks. Three main compatible categories are shown (shell, solid, hybrid). A single panel block is assigned only to a single panel, while other blocks are assigned to a combination of a panel on the SS and a panel on the PS. Various blocks are available to model different features.

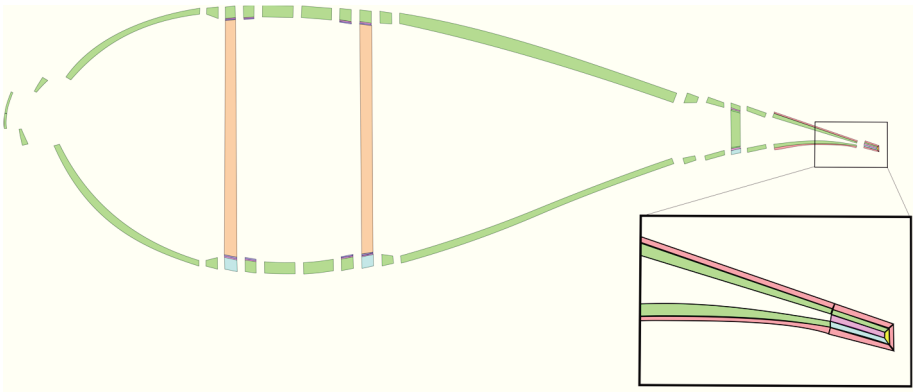

Figure 67: Schematic example of how a few compatible blocks result in a cross-section of a high fidelity solid model. The close-up provides a detail of the TE assembly.

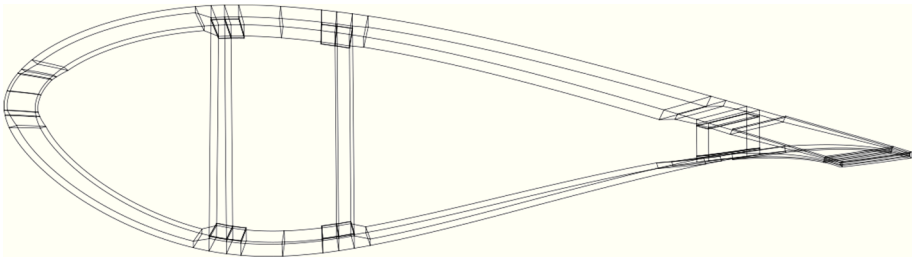

Figure 68: Example assembly of several blocks that together produce a section. The image is generated from the software at the meshing stage.

3.7.2 Software structure

The novel approach is implemented as an object-oriented software tool. It was developed in Python 3 for fast implementation. The tool consists of over 30 000 lines of code (excluding tests). A divide and conquer approach is used. Therefore, the software is broken down in several modules able to handle the different tasks. Each module's workings are verified by means of unit-testing. The software is documented in html files that are generated from the class documentation present in the code. This was done using Sphinx [24]. Furthermore, each component in the software contains plotting functions to allow visualization of the data. An overview of the different stages in the modelling process can be seen in Figure 69. At each of the stages the model data can be saved to a file. These data can later be loaded back into memory to skip re-calculating the same objects. In this paragraph, a brief overview of the different parts of the software is given. Further in this section, specific features are discussed in detail. As a first task, a parametric surface is created from the OML shape. As a second task, this surface is partitioned. This is done in a two-step process. The surface is first partitioned by

means of functions along the length of the blade and subsequently at a series of span-wise positions. The result is a "map" of the blade. This map represents the topology and consists of vertices, edges and panels. On this map, each ply in the composite layup can be assigned to the correct region. It is worth noting that this intermediate result is independent of the desired output model. Once the topology is clear, blocks can be assigned to the panels. This allows that the actual features such as faces and cells can be created. As final tasks, these features are meshed and material orientations can be calculated. This results in a complete FE model that can be imported in Abaqus. However, the format of the input files of most FE software is very similar. Therefore, it would be very simple to enable the software to produce input files for another FE solver. In its current version the software does not have a GUI and the user inputs have to be provided in a python script. This script consists of a number of functions to group inputs (blade geometry input, key-line input, blade map input, material data input, layup inputs and block assignement inputs). While this is perhaps not the most elegant solution, the initial purpose is to provide functionality. Furthermore, the use of a python script for user inputs has the inherent advantage that logic and functions are readily available. This is useful for providing the inputs in a clear, concise manner and also aids in the debugging of models.

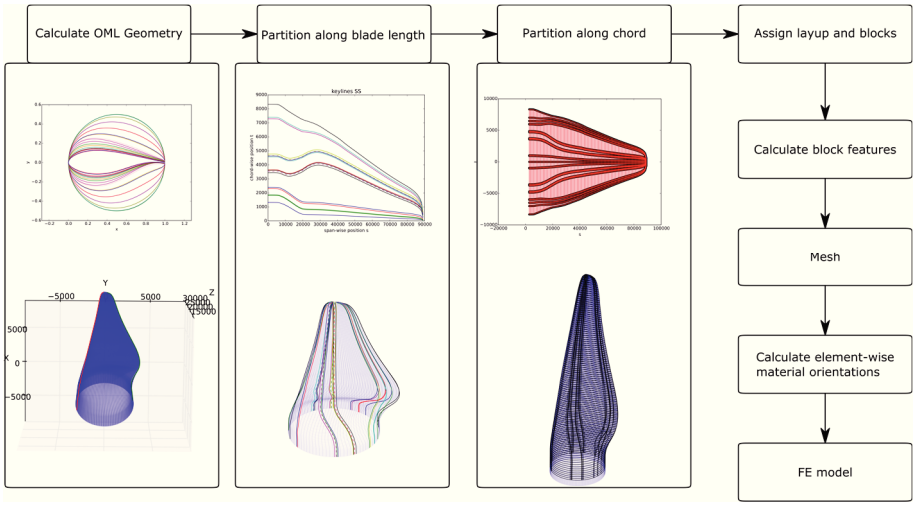

Figure 69: An overview of the different stages of the process of generating a FE model of a wind turbine blade with the proposed approach.

3.7.3 Calculation of the OML shape

A first requirement is the calculation of a parametric surface for the blade OML shape. Unlike in the slice-based approach, this is not a sequence of slices, but a parametric surface.

The procedure to create this surface goes as follows:

1. Normalized airfoils are created from files or by blending other airfoils
2. Values for the transformation from a normalized airfoil to the required airfoil station (chord length, relative thickness, pitch, pitch-axis, XY-offsets etc.) are specified at several span-wise positions.
3. Interpolation functions are calculated to obtain values for the transformation details at intermediate positions. Interpolation possibilities include piecewise linear functions, quadratic and cubic spline interpolation. To avoid overshoots while obtaining smooth functions, a piecewise cubic hermite interpolating polynomial (PCHIP) is available.
4. The shape of the blade is evaluated at many span-wise positions. This results in a grid of coordinates which is used to calculate a parametric spline surface.

An overview of the different interpolation methods for calculating the blade shape is shown in Figure 70.

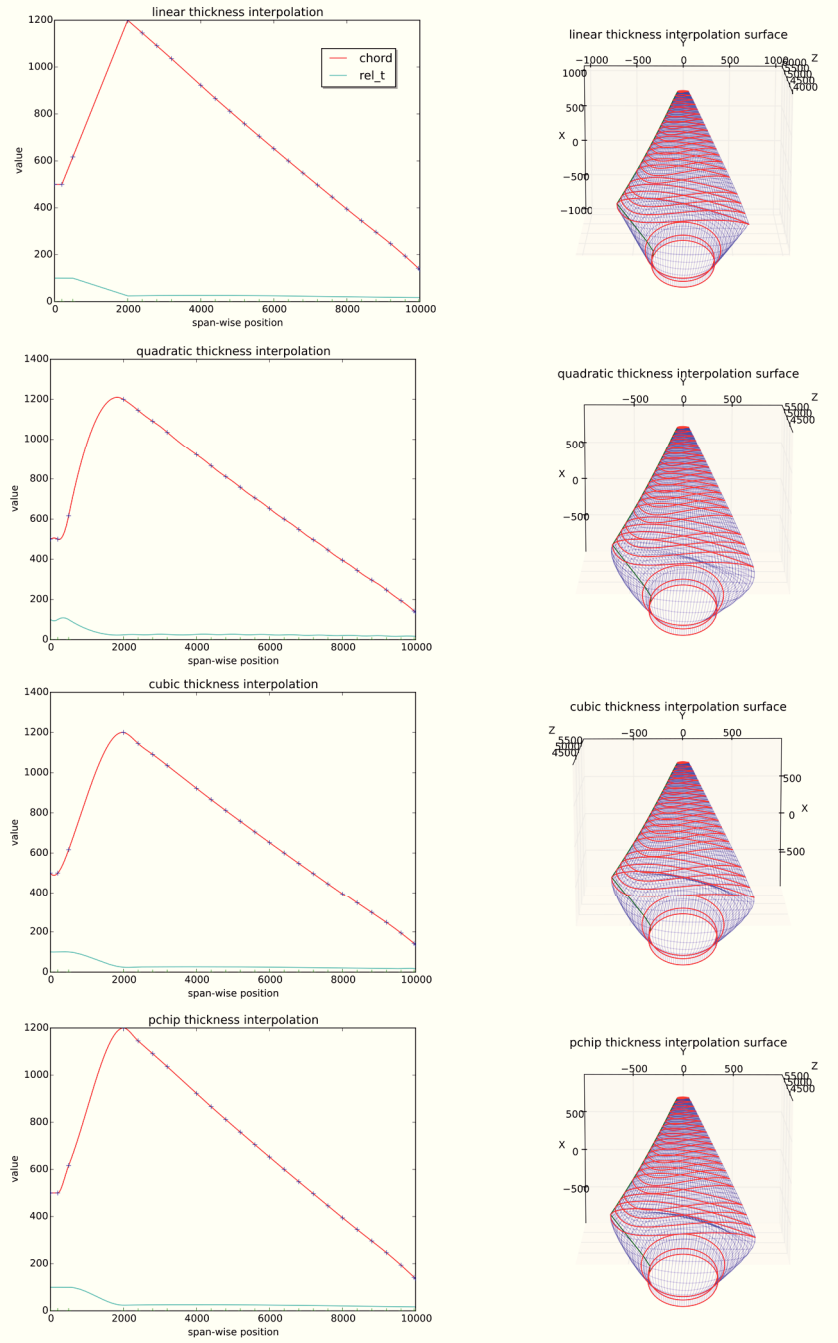

Figure 70: Overview of the different thickness interpolation methods available in the novel block based modelling tool.

3.7.4 High fidelity partitioning of the OML shape

To produce high fidelity models, accurate partitioning of the OML surface is needed. Existing tools often rely on the user to specify chord-ratios at a limited number of positions. A superior approach is to define functions on the OML surface, which can be evaluated at any span-wise position to accurately calculate partitioning positions. Furthermore, these functions need to represent positions in terms of arc-lengths because many plies are made of rolls of material with a constant width.

The importance of this last statement can be demonstrated by a simple example. Assume that a blade has a main girder made from a roll of uni-directional (UD) fiber material with a constant width of 650 mm. To model this blade, the boundary curves of the plies have to be calculated. In a first approach, both boundary curves are defined by the intersection of the OML and a plane. The two planes are positioned 650 mm apart. In a second approach, one curve is calculated by the intersection of the OML with a plane, while the other is calculated by adding an arc-length offset (of 650 mm) from the first curve. The resulting curves can be seen in Figure 71. While the curves seem similar, the difference reaches up to 41 mm which is more than 6 % of the width of the girder. Considering that this is the most important structural component, this deviation could have a significant effect. For this reason, in the presented approach, the OML surface is calculated so that it can be evaluated both in parametric (u,v)-space (where u and v are in [0,1]) and parametric (s,t)-space, with s the span-wise position and t the circumferential position on the slice at position s. This allows curves to be calculated in arc-length space, resulting in accurate partitioning.

Several methods to describe a key-line are included in the software:

1. By directly specifying the function in (u,v) or (s,t)-space by providing a number of coordinates and selecting an appropriate interpolation function.
2. By providing a reference such as a plane. At every span-wise position the closest position to the reference on the OML is calculated. This is done iteratively by means of a recursive method.
3. By specifying a previously included key-line and specifying a variable arc-length offset
4. By specifying multiple key-lines and describing in which region which key-line is active along with how the transition from one region to another is handled

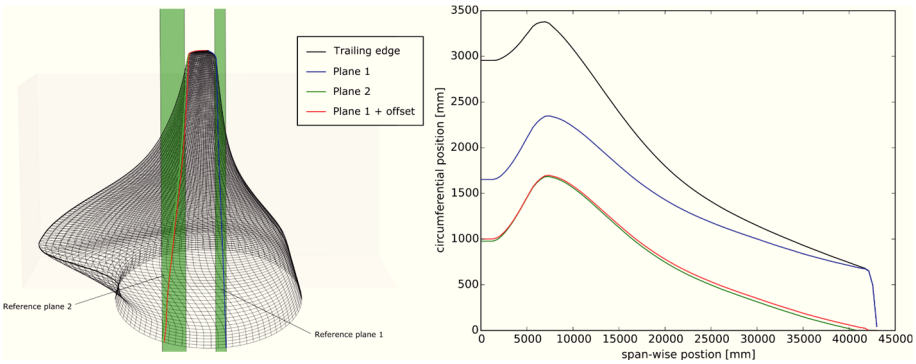

Figure 71: Comparison of methods to calculate the boundary curves of a girder with a constant width of 650 mm. The boundary on the LE side is calculated from the intersection with a plane. The boundary on the TE side is calculated in one approach by means of a second reference plane and in another approach by offsetting from the curve on the LE side. The difference in width reaches up to 41 mm.

3.7.5 Topology of the blade as a map

As mentioned, partitioning of the blade results in a map, describing the topology. An example of a blade map, represented both in 2D parametric space and 3D Cartesian space is shown in Figure 72 and Figure 73 respectively. Unlike in other software, this does not fully define the final output since the assigning of blocks will determine which cells and faces are produced. At the map level, the layup can be assigned and blocks can be assigned to the desired regions. The map serves as a layer that considers the information that should be shared over multiple blocks. For example, the thickness of each component is calculated in every corner of every panel from the thickness values of the layups in the adjacent panels. This allows the blocks assigned to these panels to have matching thicknesses at their corners and create continuous meshes.

The layup is applied at the map level in an automated fashion. Regions are specified in terms of the bounding key-lines and span-wise positions. This information makes it possible to determine rapidly which panels belong to the region. This approach differs from most other software tools, where typically the layup is specified at the level of the features. The advantage lies in the fact that in highly detailed models, the number of panels (usually between 2 000 and 10 000) is typically much higher than the total number of layers in the layup (usually a few hundred). Furthermore, the number of panels may be modified to change the level of detail without requirement to alter the layup definition.

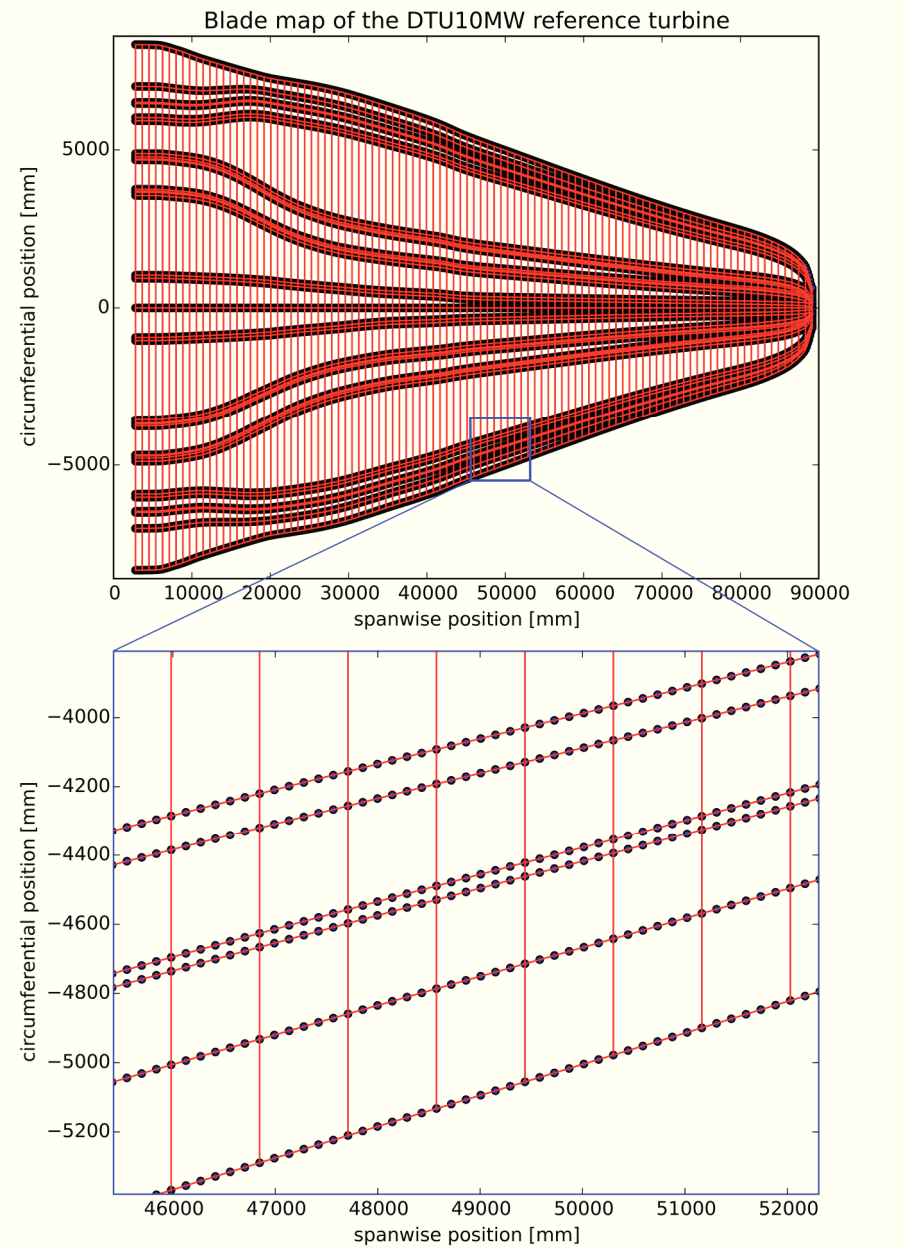

Figure 72: Example of a blade map made for the DTU10MW reference turbine blade [25]. The map is shown in 2D (s,t)-space, with s the span-wise position and t the arc-length circumferential position on the blade OML shape. Individual control points are shown in blue, these are connected with edges (shown in red) to form panels. This blade map example contains 19 833 points, 6 532 edges and 3 200 panels.

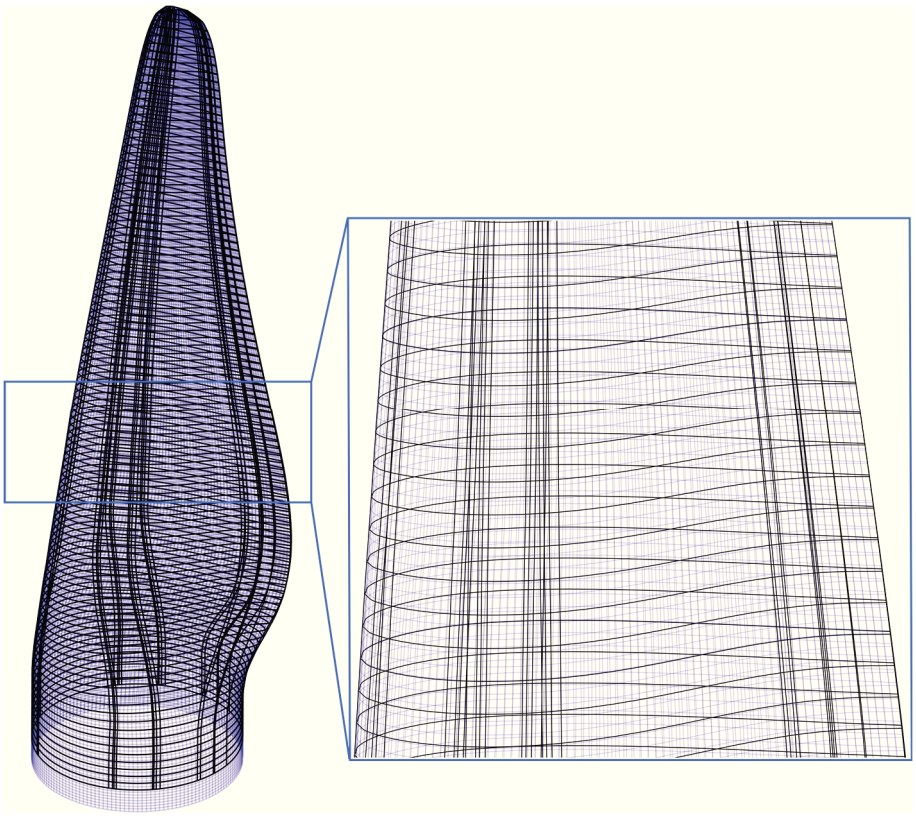

Figure 73: Example 3D plot of a blade map made for the DTU10MW reference turbine blade [25]. For clarity, only the OML surface (blue) and the edges of the map (black) are plotted.

3.7.6 Trailing edge region

For the trailing edge, a general-purpose trailing edge block is developed that allows a smooth transition from the circular root to the max chord region and beyond. A schematic view of the block can be seen in Figure 74.

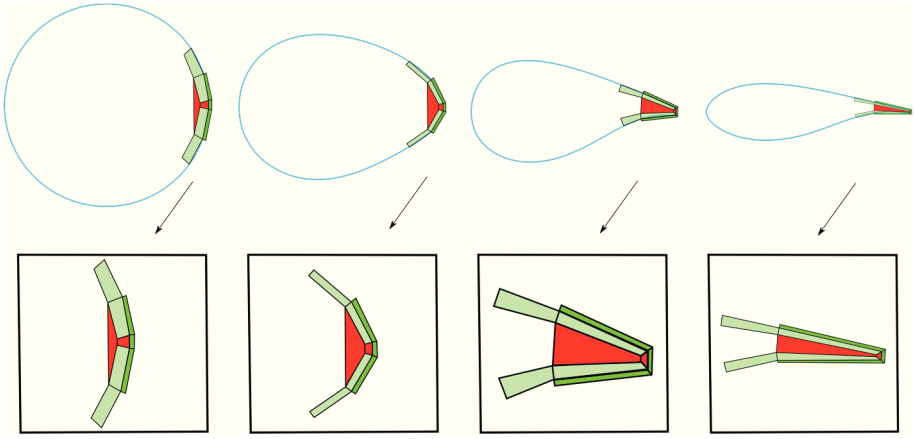

Figure 74: A Schematic view of the general-purpose trailing edge block implemented in the block based software. It allows the transition from the circular root region, where the laminate from the PS and SS is joined from the side faces, to the airfoil region, where the laminate on both sides is joined by connecting the top faces. The adhesive cell at the inside of the blade is typically not present at the root section. It is solely included in this overview to demonstrate the topology of the block.

3.7.7 Creating offset surfaces

To create solid models, the inner surface has to be created by offsetting from the OML surface. However, unlike in most CAD/CAM applications, the offset distance is not uniform for the full shape. Different thicknesses are required for different segments and continuous variations in thickness are desired. However, maintaining parametrization is desired to some extent in order to reach a good quality mesh. This requires that the shape of elements stays within certain bounds from regular bricks and wedges. In Ref. [9] the mesh is directly extruded inwards from the mesh on the OML surface. In Ref. [11] it is pointed out that this is not a good approach. Instead this is done at the geometry level. Offset surfaces are calculated and used to create faces or cells. However, as mentioned earlier, the offsetting process can be challenging. Therefore, the process is simplified with the approach shown in Figure 75. Instead of offsetting a full surface, the offset surface is calculated as a sequence of offset curves. Furthermore, the offset curves are calculated in the plane of the considered blade section, by projecting the offset normal vectors onto the plane and compensating the offset thickness.

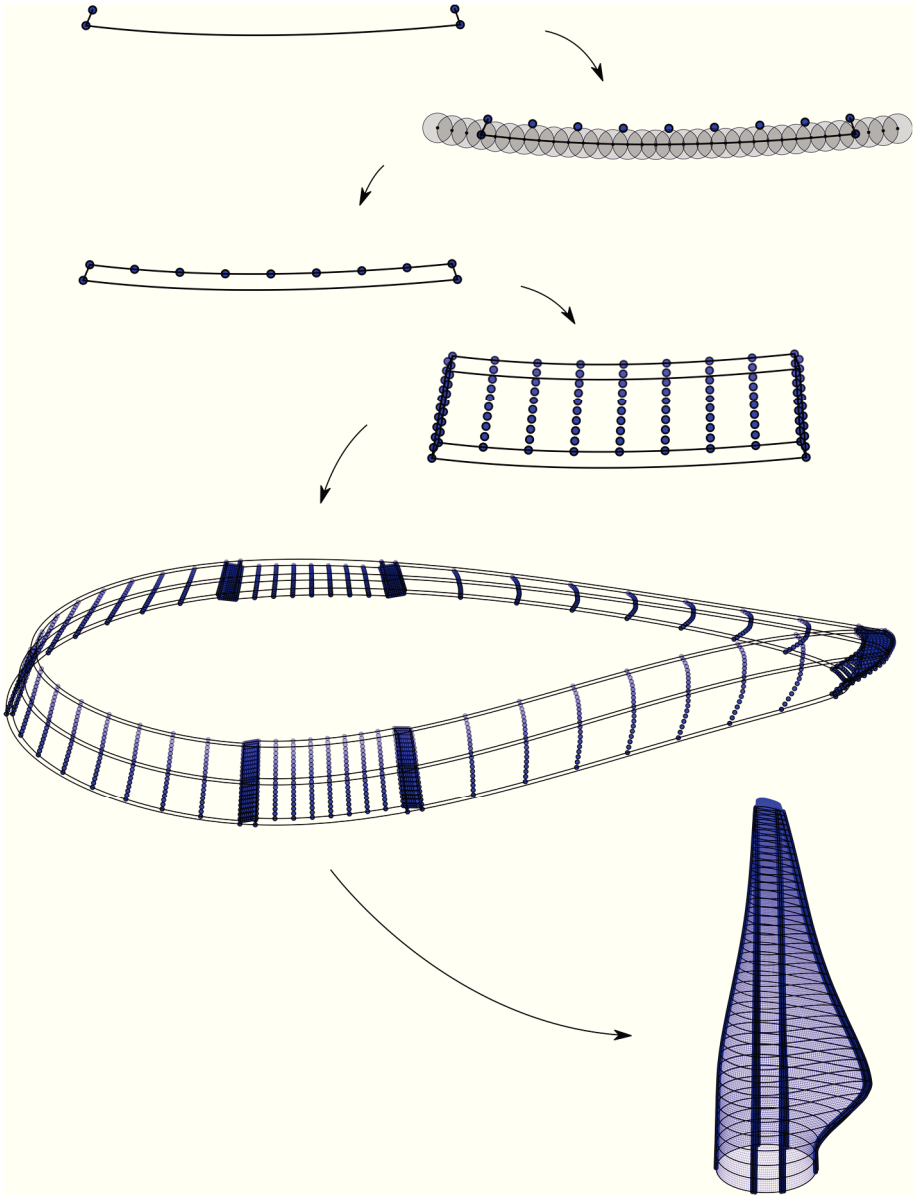

Figure 75: Schematic overview of how a blade model is created by offsetting. Offset curves are calculated between two offset vertices by means of a distance field based algorithm. Offset surfaces are created as a sequence of offset curves. These surfaces are used to create the required faces of the blocks. The blocks are subsequently combined to create a full model.

Additionally, the offset curves are calculated as a sequence of offset segments. First, the bounding vertices of the offset curve are calculated by directly offsetting from the base curve. Next, a smooth connecting curve is calculated considering the distance field. In this way self-intersections are avoided in between the bounding vectors while the parametrization is largely maintained. This allows the creation of a good mesh and accurate offset curves. In addition, this solves another challenge which was mentioned earlier, namely the need to offset along a different vector than the normal vector. This is both the case for vectors at the TE and vectors of a shear web. With the given approach, the offset vectors are simply modified to have the desired orientation. The offset distance is then automatically compensated to result in the same material thickness and offset curves connecting the vectors are calculated considering the distance field.

3.7.8 Meshing

Once the blade model is created in terms of faces and cells, these features need to be meshed to create the final blade model which can be used for numerical simulations. Various commercial and non-commercial tools exist to create FE meshes. Of these tools, Gmsh [26] in particular was considered because of its ability to create geometrical models from scripts. These scripts are simple, readable plain text files. Moreover, this allows the geometry of the model to be constructed without the typical CAD approach where a tree structure is maintained for a part and its features. Furthermore, Gmsh comes with advanced meshing algorithms and provides very good performance. For these reasons, the application was used to create simple blade models consisting of elements on the OML, shown in Figure 76.

In addition, it was used to create meshes for the TE adhesive, shown in Figure 77. The purpose was to tie the created elements to the laminate of an FE model using the Abaqus/CAE pre-processor. However, an issue with Gmsh is that the geometric features created with the scripting interface cannot be made to exactly match a global spline surface. A high-fidelity model should consist of OML faces which exactly match the OML surface. In addition, as discussed in Paragraph 3.6.2.1, a mesh consisting of solid elements should consist of layers of elements stacked in the laminate's thickness direction. This essentially means that a matching mesh is expected on the top and bottom surface. This should be possible while allowing for a change in mesh density and for wedge shaped cells to be meshed. Even though Gmsh was found to be very handy and versatile, these last requirements were not met. For this reason and the reason that using a third-party tool creates additional dependencies, the choice was made to create a custom meshing package.

The custom meshing package was integrated as part of the software tool. Geometric features and topology are defined, seeded and meshed. Edges can be

created with line segments, splines, arc segments or as a curve on a surface. In the latter case, the curve is evaluated to obtain coordinates in the parametric space of the underlying master surface. An example of such a curve can be seen in Figure 78 (a). For the creation of blade models specifically, this feature makes it simple to create edges that are positioned on the OML surface. Likewise, for faces, the underlying geometric surfaces can be surfaces using transfinite interpolation (resulting in ruled surfaces for the case where two of the edges are straight lines), spline surfaces or surfaces positioned on another surface. An example of such a surface can be seen in Figure 78 (b). This last feature is used to allow adjacent faces of the blade models that are positioned on the OML to have perfectly smooth transitions. This approach makes the geometry of the OML independent of its partitioning. This would not be the case if every face on the OML had its own underlying spline surface.

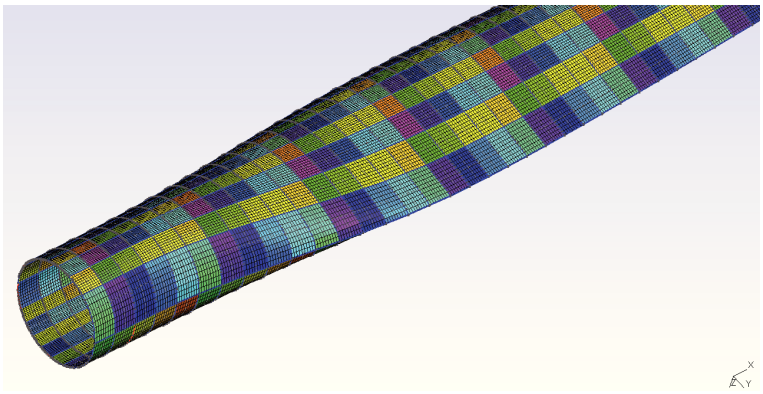

Figure 76: Simple blade mesh created using the in-house software output to create a model using the ".geo" format in Gmsh. The faces use transfinite interpolation and are therefore not exactly corresponding to the original, global OML surface.

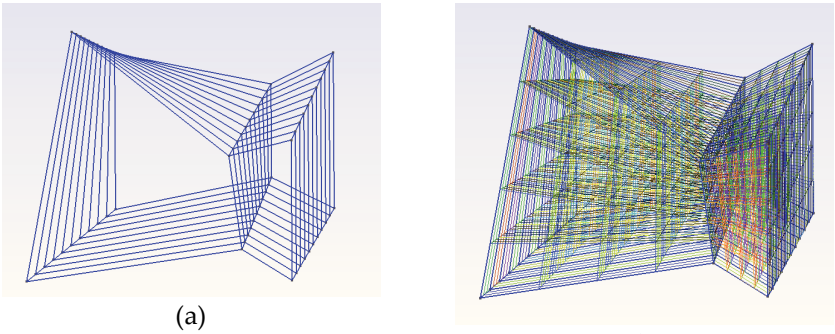

(a) (b)

Figure 77: Model for the TE adhesive to be added to an OML shell model, created using Gmsh. (a) geometry of a limited section. (b) Resulting structured volule mesh.

The package uses a simple mapping approach based on transfinite interpolation (TFI). Meshing takes place in parametric (u,v,w)-space and the resulting parametric mesh is subsequently mapped to 3D Cartesian space. This works for both structured and simple transition meshes as can be seen in Figure 79. The software includes the possibility to create both linear and second order shells and solids.

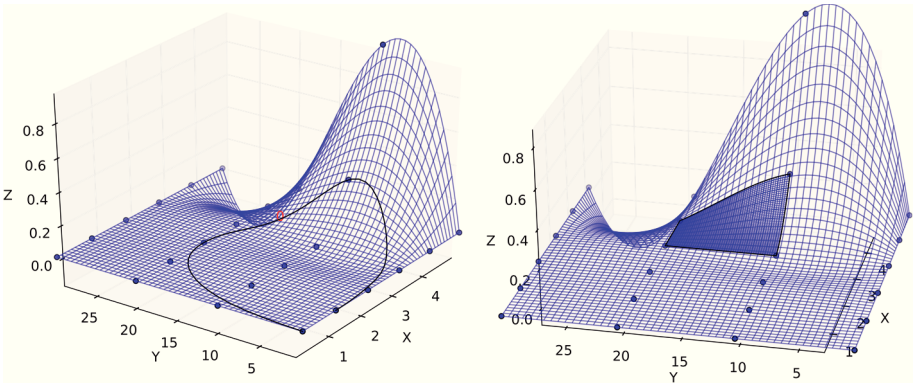

(a) (b)

Figure 78: 3D plots of examples of geometric entities available within the custom meshing package that are positioned on a master surface. These allow edges and faces to be defined that are positioned exactly on the OML surface. This allows for smooth transitions between adjacent faces and avoids dependencies between the geometry and topology. The control points of the master surface and the surfaces themselves are shown in blue, while edges are plotted in black. (a) A curve on the master surface. (b) A surface on the master surface.

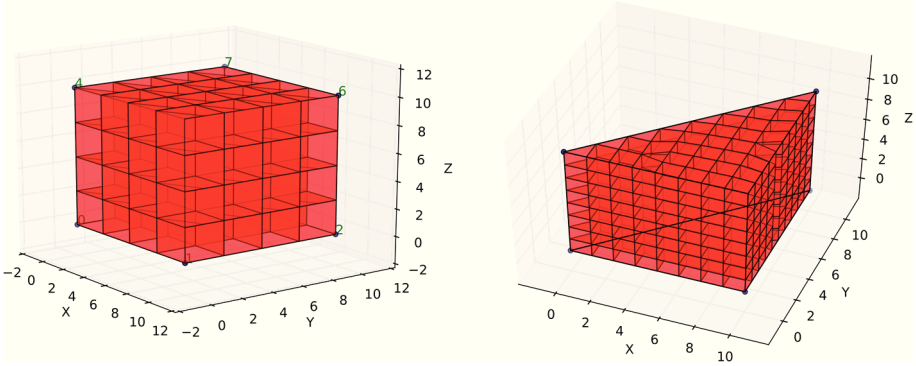

Figure 79: 3D plots of meshes on simple cells created using the custom meshing package. (a) Structured mesh on a box shaped cell. (b) Transition mesh on a wedge-shaped cell.

The TFI methods were first presented by Gordon et al. [27] and later by Erikson [28]. Further developments such as smoothing are suggested in Ref. [29]. These mapping methods allow a surface to be calculated analytically by evaluating its corners and edges. Similarly, it allows a volume to be calculated analytically from its corners, edges and faces.

In general, the TFI starts from a vector function $f(u,v,w)$

$$f(u,v,w) = [x(u,v,w), y(u,v,w), z(u,v,w)]$$

Which is known only on the outer lines of the region where:

$$u_1 \leq u \leq u_2$$
$$v_1 \leq v \leq v_2$$
$$w_1 \leq w \leq w_2$$

For this function, the TFI gives an algebraic interpolation under the form of a mapping. For the simplest case, we can apply this method to a cube with an interpolation of degree 1 and obtain a field $\tau_c(u,v,w)$:

$$\begin{aligned}\tau_c(u,v,w) \quad = {} & (1\text{-}u)\, f(0,v,w) + u\, f(1,v,w) + (1\text{-}v) f(u,0,w) + v\, f(u,1,w) \\ & + (1\text{-}w) f(u,v,0) + w\, f(u,v,1) \\ & - (1\text{-}u)[(1\text{-}v) f(0,0,w) + v\, f(0,1,w)] \\ & - u[(1\text{-}w) f(u,0,0) + w\, f(u,0,1)] \\ & - v[(1\text{-}w) f(u,1,0) + w\, f(u,1,1)] \\ & - (1\text{-}w)[(1\text{-}u) f(0,v,0) + u\, f(1,v,0)] \\ & - w[(1\text{-}u) f(0,v,1) + u\, f(1,v,1)] \\ & + (1\text{-}u)[(1\text{-}v)[(1\text{-}w) f(0,0,0) + w\, f(0,0,1)] \\ & + v\,[(1\text{-}w) f(0,1,0) + w\, f(0,1,1)]] \\ & + u[(1\text{-}v)[(1\text{-}w) f(1,0,0) + w\, f(1,0,1)] \\ & + v\,[(1\text{-}w) f(1,1,0) + w\, f(1,1,1)]]\end{aligned}$$

This results in an algorithm that allows a position in a volume to be calculated from its corners, edges and faces. This process is demonstrated in Figure 80.

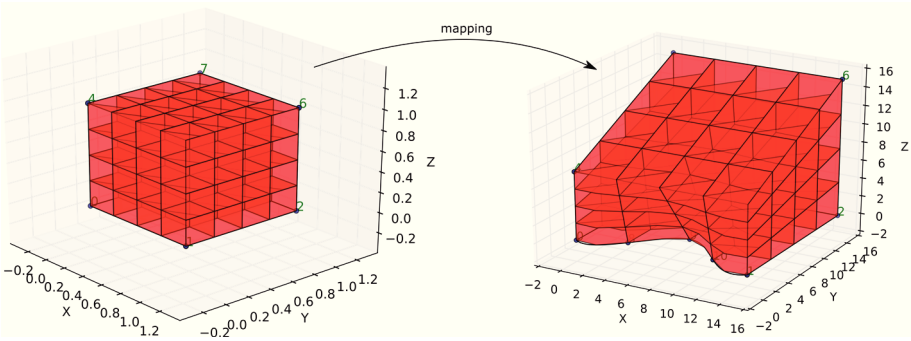

Figure 80: Example of the mapping used in the block based software. Meshing is applied to a box in parametric space shown on the left. This is then mapped to the real space shown on the right.

Examples of resulting meshes can be seen in Figure 82. Both first and second order meshing is available while both structured and transitional meshes can be created. Furthermore, both solid, shell and solid-shell elements can be created. A class diagram of one of the packages that were developed can be seen in Figure 81.

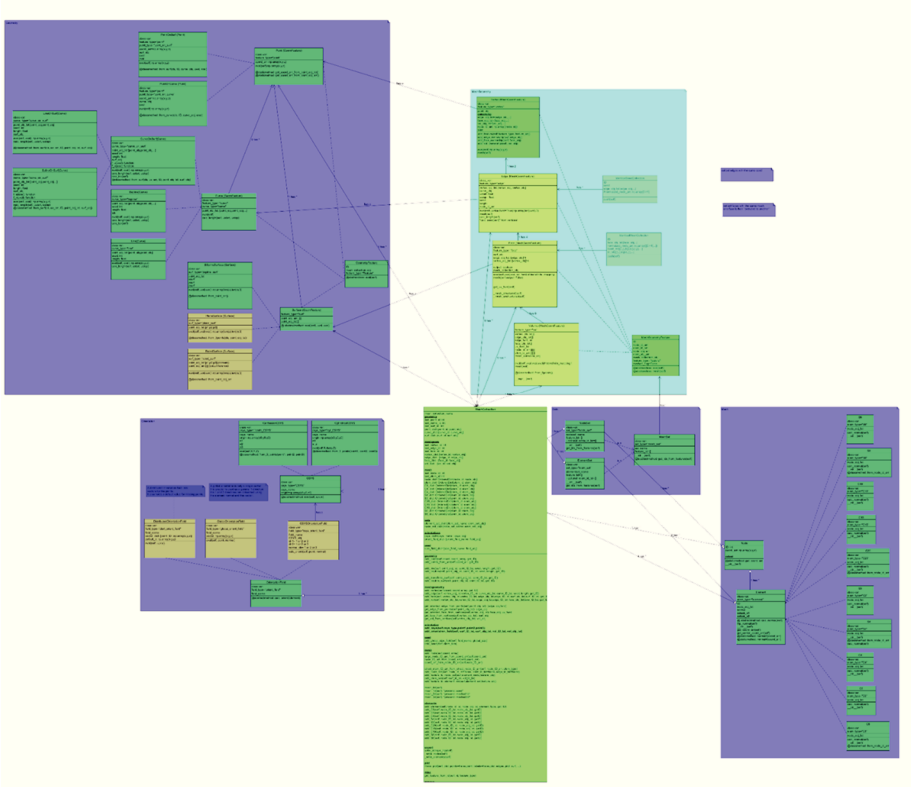

Figure 81: Class diagram of the developed meshing package, showing the structure of the software component.

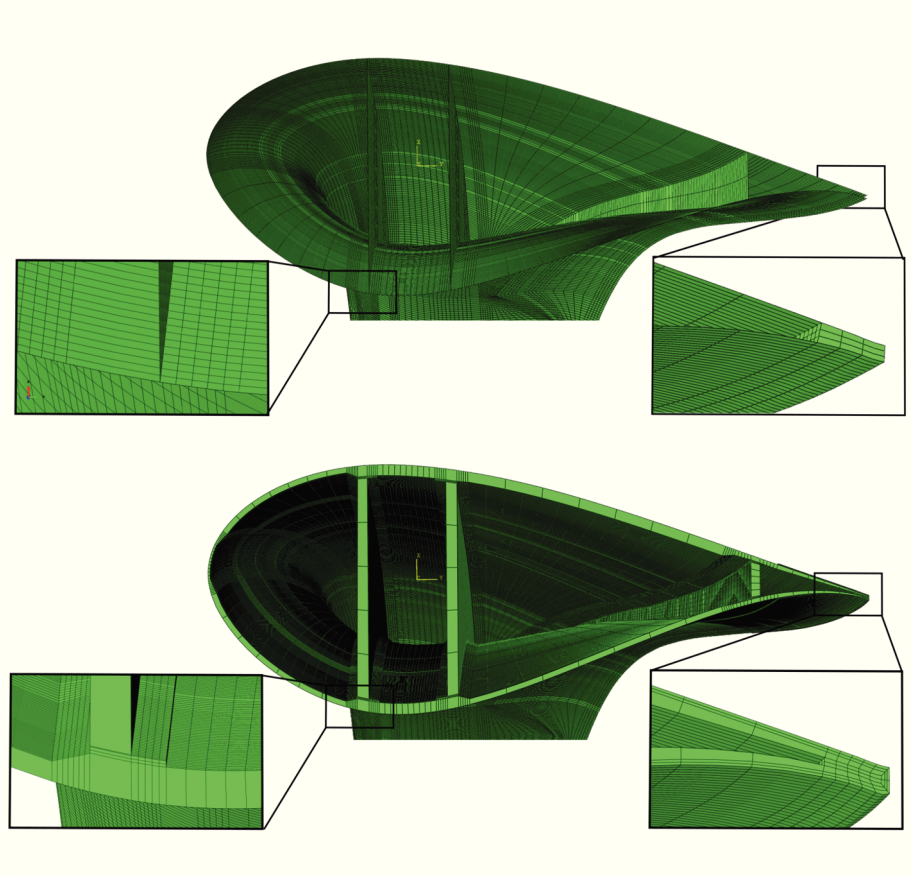

Figure 82: Meshes produced by the software along with details of the trailing edge joint and web-girder connections. (top) Shell output with solid elements to model the adhesive. (bottom) Second order solid output.

3.7.9 Creating a blade model from blocks

To obtain a useful model from a collection of pre-defined blocks, the adjacent blocks have to be compatible. This means that the interfaces between adjacent blocks should match, so that a continuous mesh can be formed. Compatibility is on one hand determined by the type of block, in the sense that there are different families of compatible blocks. An example of such a family are shell blocks, since they are compatible with other shell blocks, but not (directly) with solid blocks. In addition, the vertices on the edges that are adjacent to other blocks have to coincide with the vertices of those blocks so that they are stitched together and a single compatible mesh can be formed. This requires that both the offset normal and distance are identical for the adjacent blocks. Therefore, at the map level, the component thicknesses and offset normal vectors are calculated in every corner,

based on the values of the adjacent panels. These values are then used by the individual blocks.

The presented approach is very flexible, since changing the way a specific part of a blade is modelled is as simple as assigning a different block type. Furthermore, the assignment of blocks is the final user input, meaning that this does not require any other inputs to be modified. In addition, the approach is easily extendable. All that is required to provide additional functionality is adding new block types. Furthermore, it is very straightforward to create detailed sub-models of specific regions of interest. Also, the block approach allows for flexibility in topology which is typically not available in other software tools able to create solid blade models. This approach is also very general and could therefore also be applied to the model creation process of different components such as for example airplane wings.

3.7.10 Calculation of advanced material orientations

The most accurate material orientation available with most FE solvers is by means of a local orientation system for every element individually. An approach was developed to calculate these orientations based on key-line definitions. The assumption is made that fibers that were parallel in the original fiber mat stay parallel in terms of arc-length when placed on the blade mold. Therefore, parallel fibers will be parallel to a ply edge. This means that shearing within the fiber mats is neglected. However, these effects are assumed to be very small. Using this assumption, an orientation system can be defined based on any key-line. The key-line can be evaluated at any position on the blade surface and arc-length parallel curves can be created for any position on the OML. An example can be seen in Figure 83. Therefore, at any position on the OML, from this key-line the 1-direction of the material can be calculated as a 3D vector. Together with the normal which is evaluated from the OML surface, a full material orientation system is calculated as shown for a slice in Figure 84. Using this approach, as many orientations can be created as there are key-lines in the model. Subsequently, every component of every block can be assigned a (different) orientation using this method.

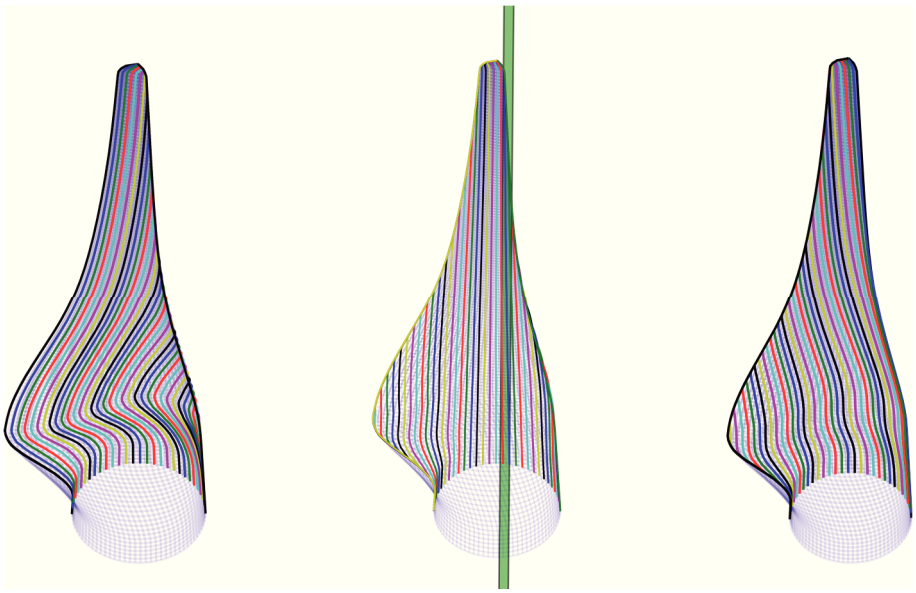

(a) (b) (c)

Figure 83: Curves representing parallel fibers according to the arc-length un-wrapping of the OML surface. (a) Curves parallel (in st-space) to the TE. (b) Curves parallel (in st-space) to the intersection of the OML with a plane. (c) Curves parallel (in st-space) to the LE.

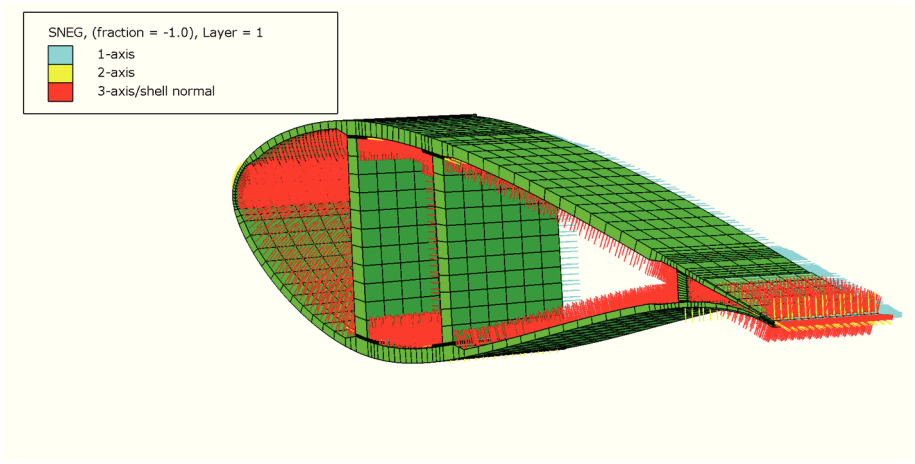

Figure 84: 3D plot showing the local material orientations on a blade slice. These can be calculated accurately on an element-by-element basis using the presented approach.

3.7.11 Additional possibilities

The software also includes solid blocks that can have a cell representing the wet layup (over lamination of the adhesive bonds). This can be seen in the examples shown in Figure 67 and Figure 82. However, this cell can also be used for different purposes, such as to represent icing on the blades or the rubber layer usually placed in between a blade and fixtures used for load introduction during static testing. Further, more advanced web blocks are possible, containing a circular, elliptical or V-shaped cut-out. In addition, these web blocks could consist of a much larger number of components (faces or cells with a different layup) to include more design details as shown in Figure 85. Furthermore, the block approach provides a very straightforward tool for using global-local sub-modelling. This can be done by first creating a global shell model and subsequently considering a more refined (solid) model for the region of interest. Or, ideally, a coarse solid global model can be used and regions of interest can be investigated further with a refined local solid model.

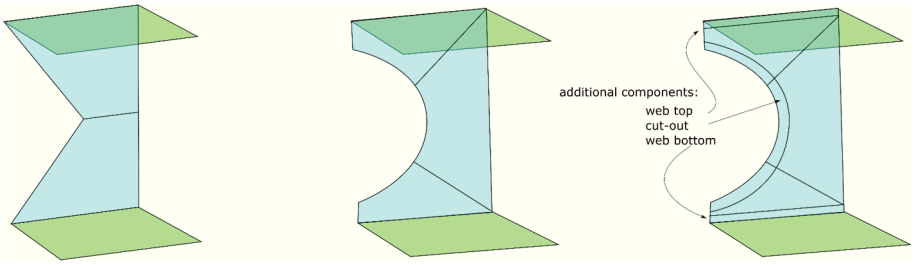

(a) (b) (c)

Figure 85: Schematic examples of other web block configurations. (a) V-cut out. (b) Elliptical cut-out. (c) Elliptical cutout with more components to provide additional detail.

3.7.12 Model debugging methods

It is valuable to compare the models that are created by the tool to some known data, in order to verify the fidelity and diagnose issues that would lead to a mismatch. To this extent, the software includes the possibility to calculate the mass distribution in space and over the different constituting materials. For this purpose, the volume of every solid is calculated. For elements containing only a single material, the density of that material is used to calculate the element mass. For elements containing a layup, the total mass is calculated using the relative thickness of each ply and the density of the corresponding material. A similar approach is used for shell elements. This way, the total volume, surface area, surface area per ply type, total mass, center of gravity and the total mass per

material is be calculated and reported to the user. An example of a resulting mass distribution can be seen in Figure 86.

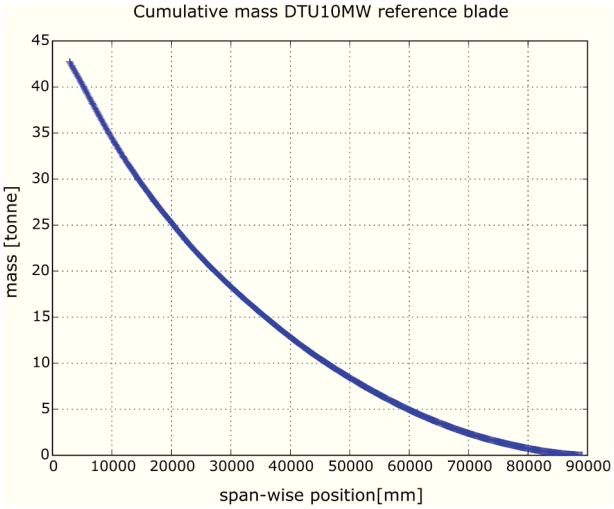

Figure 86: Automatically generated plot of the cumulative mass of a model produced by the block based software approach. For this example, the DTU10MW reference blade was used.

3.7.13 Typical runtime

The typical runtime of the software is highly dependent on the level of detail in the user inputs. For a model consisting of over 8 000 panels in the map, resulting in a solid model of 184 105 second order solid elements, the runtime is about 24 minutes on a laptop with a 2.4 GHz quad-core processor and 8 Gb of RAM. The calculation time is spent on the OML surface (1 %), key-lines (2 %), creating the map (15 %), calculating geometry for the blocks (7 %) and meshing (75 %).

3.7.14 Investigation of specific regions of interest

In the analysis of wind turbine blades, specific regions are often of interest. One approach which allows this type of investigation to be performed efficiently is using the sub-modelling technique. In that approach the result from a coarse global model is used to impose boundary conditions on a detailed and refined local model. Such an approach is computationally efficient. One assumption however is that the details in the local model (which are not present in the global model) do not affect the behavior of the global model. If this is not the case, alternative approaches using constraints or couplings can be used.

An example of the sub-modelling approach applied using the developed software can be seen in Figure 87. In Figure 88, the resulting strain distribution is shown.

An advantage of using solid elements (over shells) is that the stress distribution in the thickness direction is available.

Since manufacturing defects occur frequently, numerically studying their effect can be of great value. Wetzel [30] for example advocated that blades should be designed considering damage tolerance. For this purpose, the block based software could prove to be an asset, since including defects such as a local reduction in bond width or a lack of adhesive material could easily be modelled. Figure 89 gives an example of a local model with a reduced bond width at the PS of the LE shear web.

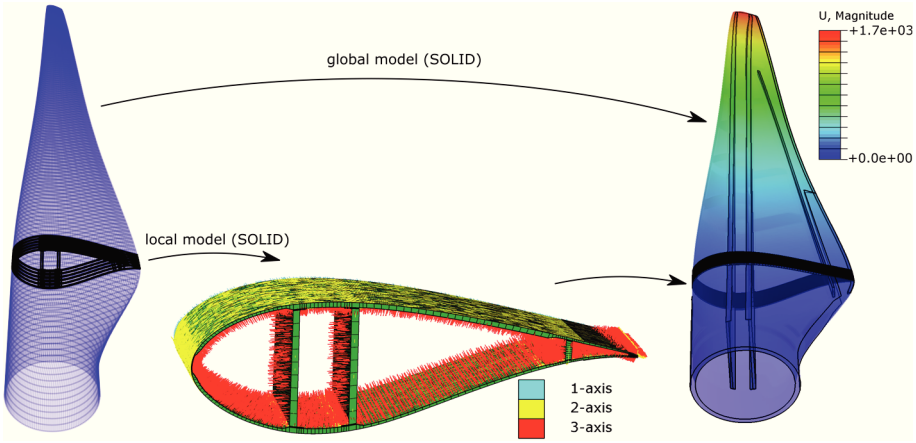

Figure 87: An example of a global-local approach which is feasible using the novel block based approach. The full blade is modelled using the software. A global solid model is created for the full blade and a local solid model is created for a 1 m long section. The global model is used in a static analysis and the nodal displacements are used as boundary conditions in the sub-model.

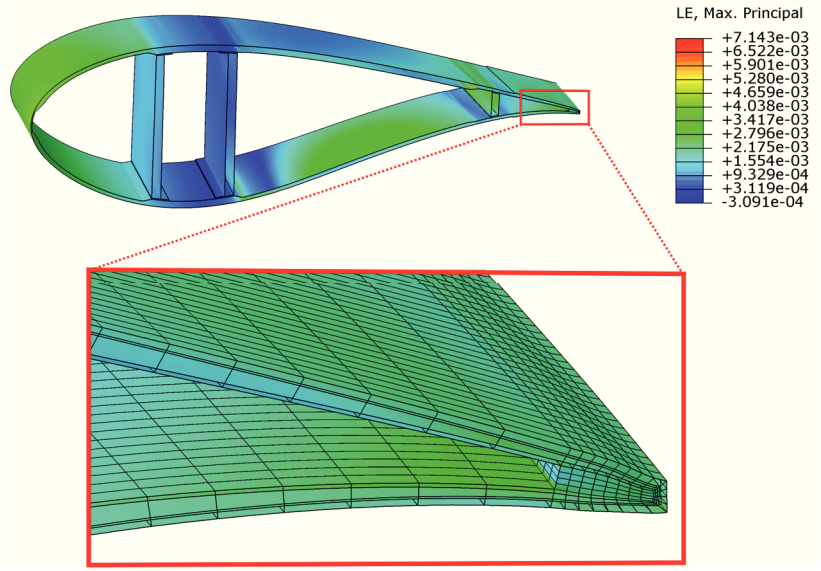

Figure 88: Contour plots of the maximum principal strain values on the local blade model. Stress values are available in all directions including the thickness direction. A close-up view of the trailing edge joint is provided with the mesh visible.

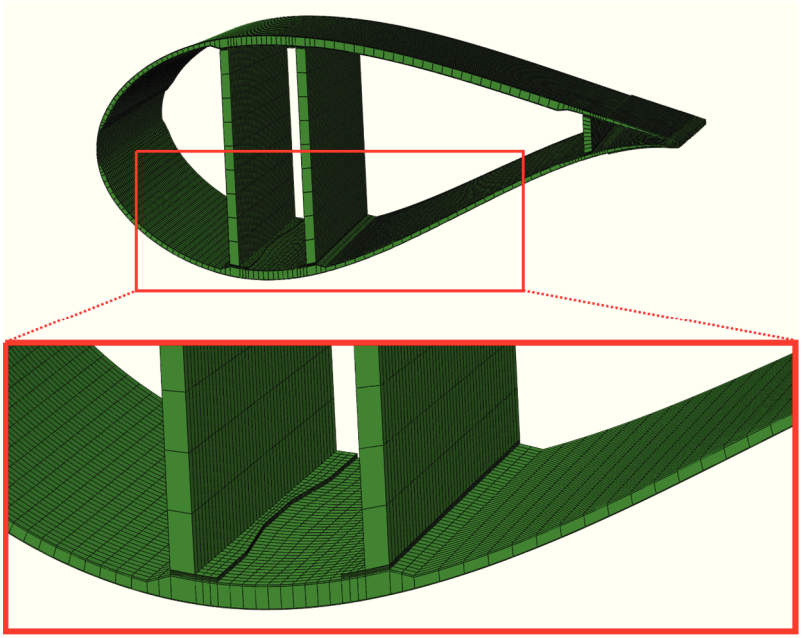

Figure 89: Plot of the mesh of a modified sub-model that has a local reduction in bond width at the joint of the LE shear web. This type of model would allow the investigation of the effect of this type of manufacturing defect.

3.7.15 Limitations of the approach

In the current state, the software does not allow for crossing key-lines to be passed onto the topology as no blocks have been included for triangular panels. An approach in which triangular panels were allowed was initially tested, but the number of panels that arise from a few angled key-lines quickly escalates as can be seen in Figure 90. To avoid such situations, human intervention would be required. However, as an alternative, blocks could be added that consist of pairs of wedge shaped cells. In this way, the layup can accurately be represented. This would allow crossing partitions, with an approximate accuracy, while the rest of the layout is not affected.

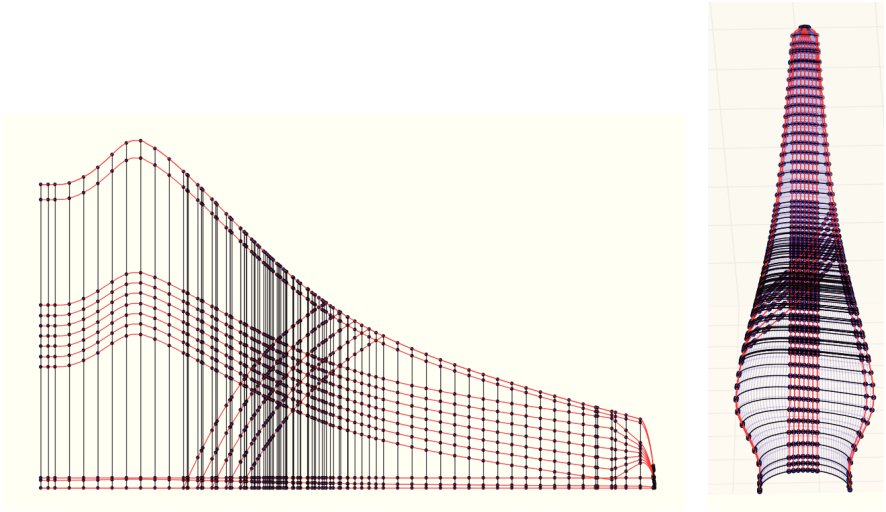

(a) (b)

Figure 90: Blade maps for a test model including some crossing key-lines. At every crossing between key-lines the span-wise position is added to the blade map. This rapidly escalates, resulting in an excessive number of panels. (a) 2D blade map in (s,t)-space. (b) 3D blade map.

3.7.16 Conclusion

The increasing dimensions of wind turbine blades, cascade effects in the costs of the turbine and current failure ratios make the use of advanced FE modelling of the blades desirable. Current modelling efforts appear to be limited in detail and fidelity because of the difficulty to obtain them. The newly presented approach divides the modelling process in a number of steps and allows for a variety of models to be created.

The approach allows:

- Accurate partitioning of the OML surface by means of key-line functions
- Creation of a map containing the topology of the OML partitioning
- Creating models by combining pre-defined parametric blocks
- Assigning the layup and blocks at the map level
- Creating shell models (on the OML, at mid-thickness or on the inside surface)
- Creating layered continuum (solid or solid-shell) models
- Calculating element-wise material orientations based on key-lines

The approach is flexible since it allows various topologies to be modelled. Likewise, different outputs can be created by modifying only the user inputs in the last stage of the model creation process. In addition, the approach is highly extendible. Additional functionality can be created by simply adding a new type of block to the available collection.

3.8 Bibliography

[1] M. E. Bechly and P. D. Clausen, "Structural design of a composite wind turbine blade using finite element analysis," *Comput. Struct.*, vol. 63, no. 3, pp. 639–646, May 1997.

[2] M. Jureczko, M. Pawlak, and A. Mężyk, "Optimisation of wind turbine blades," *J. Mater. Process. Technol.*, vol. 167, no. 2–3, pp. 463–471, Aug. 2005.

[3] P. A. Bonnet and G. Dutton, "Parametric Modelling Of Large Wind Turbine Blades," in *Abaqus UK regional user meeting*, 2007.

[4] "MATLAB - MathWorks." [Online]. Available: https://nl.mathworks.com/products/matlab.html. [Accessed: 19-Feb-2018].

[5] J. Berg and B. Resor, "Numerical manufacturing and design tool (NuMAD V2. 0) for wind turbine blades: User's guide," *Sandia Natl. Lab. Albuq. NM Tech. Rep. No SAND2012-728*, 2012.

[6] B. R. Resor and J. Paquette, "A NuMAD Model of the Sandia TX-100 Blade," Sandia National Laboratories, Albuquerque, New Mexico, SAND2012-9274, Oct. 2012.

[7] ECN, "FOCUS6 - The integrated wind turbine design suite." 2016.

[8] D. M. Hoyt, "Rapid FEA of Wind Turbine Blades - Summary of NSE Composites' structural analysis capabilities for blades," May-2008.

[9] T. Ashwill, "Sweep-Twist Adaptive Rotor Blade: Final Project Report," Sandia National Laboratories, SAND2009-8037, Jan. 2010.

[10] *Abaqus 6.14 Online Documentation, Dassault Systèmes*. 2014.

[11] C. L. Bottasso, F. Campagnolo, A. Croce, S. Dilli, F. Gualdoni, and M. B. Nielsen, "Structural optimization of wind turbine rotor blades by multilevel sectional/multibody/3D-FEM analysis," *Multibody Syst. Dyn.*, vol. 32, no. 1, pp. 87–116, 2014.

[12] Altair Engineering, "HyperMesh," 2017. [Online]. Available: http://www.altairhyperworks.com/product/HyperMesh. [Accessed: 04-Apr-2017].

[13] A. Corona, "Quantitative sustainability assessment of bio-based materials for wind turbine rotor blades," MSc in Materials Engineering, Technical University of Denmark, 2013.

[14] A. Karakalas *et al.*, "New morphing blade section designs and structural solutions for smart blades," D2.23, Jun. 2016.

[15] G. C. Larsen, P. Berring, D. Tcherniak, P. H. Nielsen, and K. Branner, "Effect of a damage to modal parameters of a wind turbine blade," in *EWSHM-7th European Workshop on Structural Health Monitoring*, 2014.

[16] "Patran." [Online]. Available: http://www.mscsoftware.com/product/patran. [Accessed: 06-Feb-2018].

[17] "Solidworks: 3D CAD Design Software." [Online]. Available: https://www.solidworks.com/. [Accessed: 05-Apr-2018].

[18] "BECAS," *http://www.becas.dtu.dk*. [Online]. Available: http://www.becas.dtu.dk/. [Accessed: 05-Apr-2018].
[19] D. Laird, F. Montoya, and D. Malcolm, "Finite Element Modeling - old," 2005.
[20] K. Branner, P. Berring, C. Berggreen, and H. W. Knudsen, "Torsional performance of wind turbine blades–Part II: Numerical validation," in *16th International Conference on Composite Materials*, 2007, pp. 8–13.
[21] S. Liu and C. C. L. Wang, "Fast Intersection-Free Offset Surface Generation From Freeform Models With Triangular Meshes," *IEEE Trans. Autom. Sci. Eng.*, vol. 8, no. 2, pp. 347–360, Apr. 2011.
[22] J.-K. Seong, G. Elber, and M.-S. Kim, "Trimming local and global self-intersections in offset curves/surfaces using distance maps," *Comput.-Aided Des.*, vol. 38, no. 3, pp. 183–193, Mar. 2006.
[23] F. M. Jensen, "Structural enhancers for rotor blades and their impact on O&M costs," presented at the 3rd International Conference Advances in Rotor Blades for Wind Turbines, Bremen, Feb-2014.
[24] "Overview — Sphinx 1.8.0+ documentation." [Online]. Available: http://www.sphinx-doc.org/en/master/. [Accessed: 04-Apr-2018].
[25] C. Bak *et al.*, "Light rotor: the 10 MW reference wind turbine," in *Proceedings of EWEA 2012 - European Wind Energy Conference & Exhibition*, 2012.
[26] C. Geuzaine and J.-F. Remacle, *Gmsh Reference Manual*. 2016.
[27] W. J. Gordon and C. A. Hall, "Transfinite element methods: Blending-function interpolation over arbitrary curved element domains," *Numer. Math.*, vol. 21, no. 2, pp. 109–129, Apr. 1973.
[28] L. E. ERIKSSON, "Generation of boundary-conforming grids around wing-body configurations using transfinite interpolation," *AIAA J.*, vol. 20, no. 10, pp. 1313–1320, 1982.
[29] C. B. Allen, "Towards automatic structured multiblock mesh generation using improved transfinite interpolation," *Int. J. Numer. Methods Eng.*, vol. 74, no. 5, pp. 697–733, Apr. 2008.
[30] K. K. Wetzel, "Defect-Tolerant Structural Design of Wind Turbine Blades," in *50th AIAA/ASME/ASCE/AHS/ASC Structures, Structural Dynamics, and Materials Conference*, American Institute of Aeronautics and Astronautics, 2009.

4 Construction of blade models for reference blade and commercial blade designs

"Whatever good things we build end up building us."- Jim Rohn

Chapter summary: In this chapter, the blade designs considered in this study are presented and the created models are validated in terms of their shape, mass and stiffness distribution. The values obtained from natural frequency extraction analyses are compared to the available design and experimental values. Furthermore, influences on these values are considered.

4.1 Introduction: reference blade designs vs. commercial blade designs

In practice, many studies have only limited access to actual blade designs. Moreover, the level of detail in commercial designs is often so high that it complicates scientific studies. For these reasons several research blades have been developed. An overview of such reference blades is provided in Table 6. A frequently used example of such a blades is the NREL5MW turbine blade [1], which is based on the turbine used in the Dutch offshore wind energy converter (DOWEC) study [2], [3]. A mass and stiffness distribution are available for this blade and further details have been released more recently [4]. Similarly, for the UpWind study [5] a blade design for a 20 MW turbine was created [6]. Its layup can be found in Ref. [7]. In a similar fashion in Ref. [8] a blade for a 5 MW offshore rotor is designed as part of a Chinese research project. Further, the USA based institute SANDIA has developed several designs for blades of 100 m length. The details of a GFRP design (referred to as SNL100-00) are found in Ref. [9] while the details for a design incorporating CFRP (named SNL100-01) can be found in Ref. [10]. Furthermore, during the INNWIND project a 10 MW reference turbine was developed at DTU. Full details on the blade can be found in Ref. [11].

Table 6: Overview of existing reference blade designs available in literature.

Blade design	Length [m]	Rating [MW]
DOWEC	62.7	6
UpWind	122	20
NREL5MW	63	5
OffWindChina 5 MW	65	5
SNL100-00	100	13.2
SNL100-01	100	13.2
DTU10MW	86.5	10

One could argue that these designs should be used as much as possible when investigating basic scientific effects, for the simple reason that the blade details should be publicly available to allow presented results to be reproduced by others. However, there are certain limitations associated with the use of these blade designs. First of all, their structural layups are greatly simplified compared to their commercial counterparts. Manufacturability is typically not accounted for. This is visible in the limited number of panels the structure is divided in and the resulting rapid changes in layup. Furthermore, reinforcements are often placed at the TE where normally, some space should be allowed to allow for the mold to be

closed during manufacturing. Likewise, the shear webs often start at the root connection. Secondly, these blades do not show the complexities that are present in commercial blades such as the use of plies that are cut off at an angle different from perpendicular to the blade's length direction. Secondly, reference blades are typically not converted into physical prototypes. Consequently, the results obtained from numerical modelling can never be validated with experimental data. This allows for a mismatch between the models and real-world circumstances to exist. Furthermore, several arguments can be named that speak in favor of the use of detailed commercial designs. Firstly, these designs demonstrate the actual state of the art. They are extensively optimized and account for real world practical issues. For example, commercial blades typically feature certain reinforcements in the areas where they are held during transport and installation. In this sense, the collaboration with industrial partners and the use of commercial blade designs is a great opportunity.

4.2 Blades modelled in this work

In this work, several blades have been modelled in high detail. These range from relatively simple reference blades to detailed commercial designs. In this section an overview and further details of the considered blades are provided. This can also be seen in Table 7.

Table 7: Overview of the blade designs considered in this work.

Blade	Length	Level of detail in design	Layout
DTU10MW	86.5 m	Reference blade (DTU)	Stressed shell
PowerComposites blade	49 m	Commercial (PowerComposites)	Stressed shell
XA21	10 m	Commercial (XANT)	Stressed shell
CTC43b	43 m	Commercial (CTC engineering)	Stressed shell

4.2.1 The DTU10MW blade

The DTU10MW blade is part of the DTU 10 MW reference wind turbine (RWT), which was used within the European INNWIND project. The details of the turbine are available online along with several detailed and coarse models. These data include a description of the blade planform along with the normalized airfoils that are used. Furthermore, the total thickness of every material in the layup is given for every panel in the layout. In this regard, manufacturing considerations have not been taken into account as ply drops are not gradual and the thickness values

are continuous as opposed to discrete multiples of that of a single ply. The turbine is designed for the IEC Class 1A wind regime and consists of a glass fiber epoxy construction with balsa wood as core material. Different views of the blade shape can be seen in Figure 91.

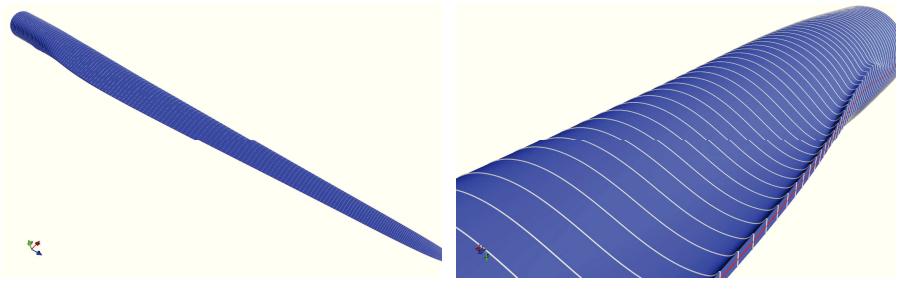

(a) (b)

Figure 91: The DTU10MW blade with gurney flaps. (a) Full view of the blade. (b) Close up view showing the gurney flaps at the TE. Reproduced from Ref. [12].

4.2.2 The PowerComposites 49 m blade

PowerComposites Limburg manufactured a blade for a wind turbine with a diameter of 100 m. The company closed down around the time that the SBO project started. The turbine is designed for the IEC Class 2A wind regime and consists of a glass fiber epoxy construction with balsa wood and polyvinyl chloride (PVC) as core materials. Figure 92 shows renderings of the blade. A CAD file of the OML surface and the structural layup were provided along with the first flap and edgewise eigenfrequencies.

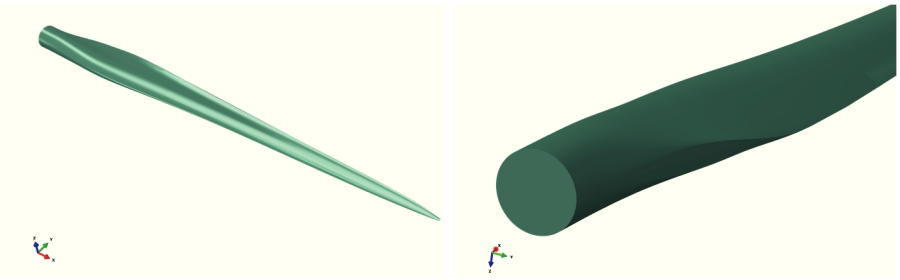

(a) (b)

Figure 92: Renderings of the 49 m blade considered in this study. (a) Global view. (b) Close-up view of the blade root showing the flatback region.

4.2.3 The Xant 10 m blade

Another blade design that is used in the investigations is the 10 m blade of the XANT. It is used on a turbine that has a rated power of 100 kW and is intended for local use and use in remote areas. For this reason, it is made for simplicity and reliability. Erection can be performed using a simple winch system while the turbine uses a down-wind configuration and fixed pitch stall control. The rotor has a cone angle for stability under changing wind directions. Figure 93 shows a XANT turbine installed in Harelbeke, Belgium. A CAD representation of the blade's outer surface, normalized airfoil files and the description of the planform were provided by the company along with material properties and the structural layup.

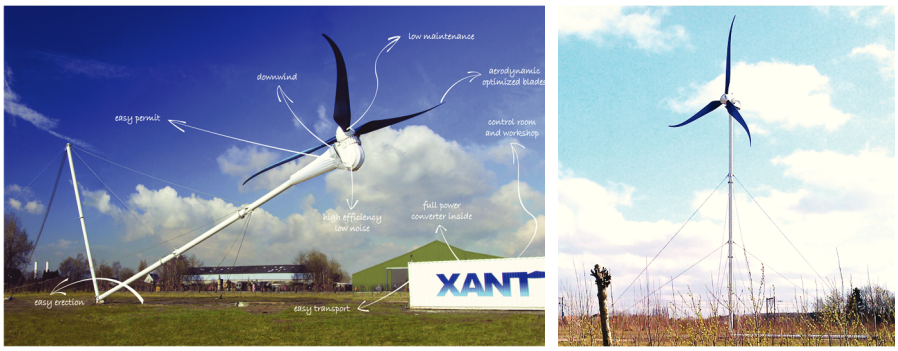

(a) (b)

Figure 93: Photographs of a XANT wind turbine located in Harelbeke, Belgium. The 100 kW turbine is intended for local use or for use in remote areas. It uses a down-wind configuration and blades incorporating a swept planform. (a) Turbine during erection using the Gin pole system. Reproduced from Ref. [13]. (b) Erected turbine. Reproduced from Ref. [14].

4.2.4 The CTC 43 m blade

The 43 m blade considered in this study was designed by CTC engineering in the Netherlands. It is a blade for a conventional pitch regulated turbine. Figure 94 shows renderings of the blade. The turbine consists of a glass fiber epoxy construction with PVC as core material. Detailed information regarding the shape, layup, materials, overall mass and stiffness properties as well as the results of static tests were shared by the company.

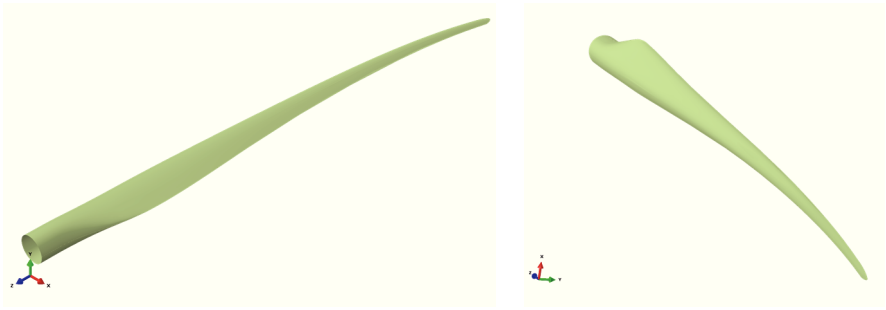

(a) (b)

Figure 94: The CTC43b wind turbine blade designed by CTC engineering in the Netherlands. The blade incorporates pre-curving to increase the inherent tower clearance. (a) Iso-parametric view of the blade. (b) Other view of the blade.

4.3 Validation of the blade models

For the blades mentioned in the previous paragraph, detailed models have been constructed using the developed tools. In the following paragraphs, these are validated at different levels. A first, simple and straightforward validation is the comparison of the produced mesh with the CAD file of the blade to ensure a match in outside shape. Subsequently, mass properties are validated. Comparisons are done for the total mass, center of gravity (COG) and mass of the constituent materials. In addition, the eigenfrequencies are extracted and compared to the expected values. These frequencies depend on the overall mass and stiffness distribution. Modal analyses are essentially eigenvalue problems and are typically computationally cheaper than static analyses with large deformations.

The eigenfrequencies are of importance since wind turbine blades are structures that are subject to cyclic loads during an expected lifetime of at least 20 years. One major threat to the life expectancy of the blade is resonance. Excitation of the rotor occurs due to various sources, but a strong and regular excitation originates from the tower passing frequency. To avoid resonance, blades are designed to have their first (typically flap-wise) eigenfrequency above the value of the first tower passing frequency. This latter value is typically referred to as the "1P" value, while the "3P" value originates from the three different blades on the rotor.

The higher modes are difficult to predict accurately. Especially for the first torsional mode discrepancies have been reported [15]. Due to issues with the torsional behavior of OML shell models, manufacturers are often using beam models for these calculations.

The eigenfrequencies of the blades are typically also measured during certification tests. Information about the experimental measurement of wind turbine blade eigenfrequencies can be found in Refs. [15]–[17].

4.3.1 The blade of the DTU10MW RWT

The blade of the DTU10MW reference turbine was modelled using the developed tools. A match in geometry and mass was obtained with the Abaqus model that is part of the available resources. However, due to the lack of validation possibilities and the simplicity of the layup and layout, it was decided to not use the model for more advanced investigations as preference was given to the commercial designs.

4.3.2 The 49 m blade of PowerComposites

Blade models were created for the 49 m blade using the developed tools. For this purpose, the constitutive airfoil stations and planform details were extracted from the CAD representation of the OML surface. The blade shape of the resulting models is compared to the original CAD drawings in Figure 95. A good match is obtained. The mass of the blade models is shown in Table 8 and is somewhat lighter than the design due to the fact that the bolts of the root joint and lightning protection system are not included in the models. The eigenfrequencies are compared in Table 9. The first flapwise frequency falls below the expected range, while the first edgewise frequency does agree with the expected design value. This is suspected to be due to a mismatch between different versions of the design. Furthermore, while the shell and solid models closely agree for most modes, a significant difference can be observed for the first torsional frequency. The shape of the first ten eigenmodes can be seen in Figure 96.

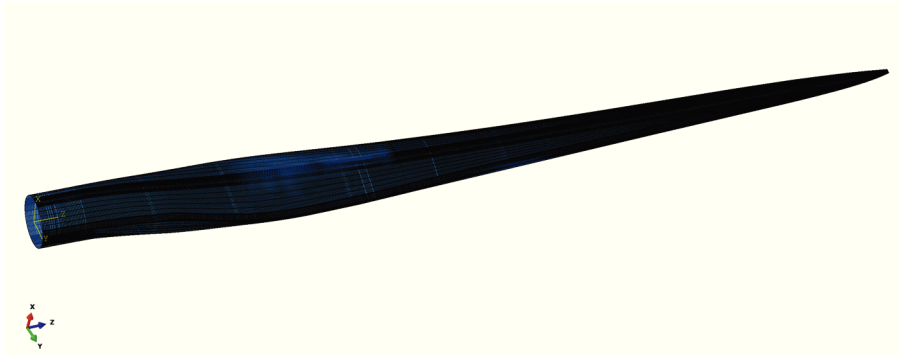

Figure 95: Comparison of the blade shape produced by the novel developed tools with the blade shape defined in the design CAD model. A very good match is obtained. Rendering the surfaces in high detail and making section cuts reveals that the distance between both is minimal.

Table 8: Overview of the total mass and COG of the 49 m blade

Representation	Total mass [tonne]	Span-pos COG [m]
Design	9.750	Approx. 15
Shell model	9.589	14.9
Solid model	9.429	15.2

Table 9: Overview of the eigenfrequencies of the 49 m blade, comparing the design values to the shell and solid models. The models show a lower first eigenfrequency than expected from the design. Further, the shell and solid models show different results for the first torsion frequency.

Eigenmode	Design [Hz]	Shell model [Hz]	Solid model [Hz]
1 (1st flap)	0.74 - 0.91	0.678	0.686
2 (1st edge)	1.01 - 1.35	1.174	1.229
3	-	1.967	2.046
4	-	3.485	3.716
5	-	3.756	3.984
6	-	5.933	6.141
7 (1st torsion)	-	7.114	7.722
8	-	7.849	8.397
9	-	8.548	8.689
10	-	11.299	11.314

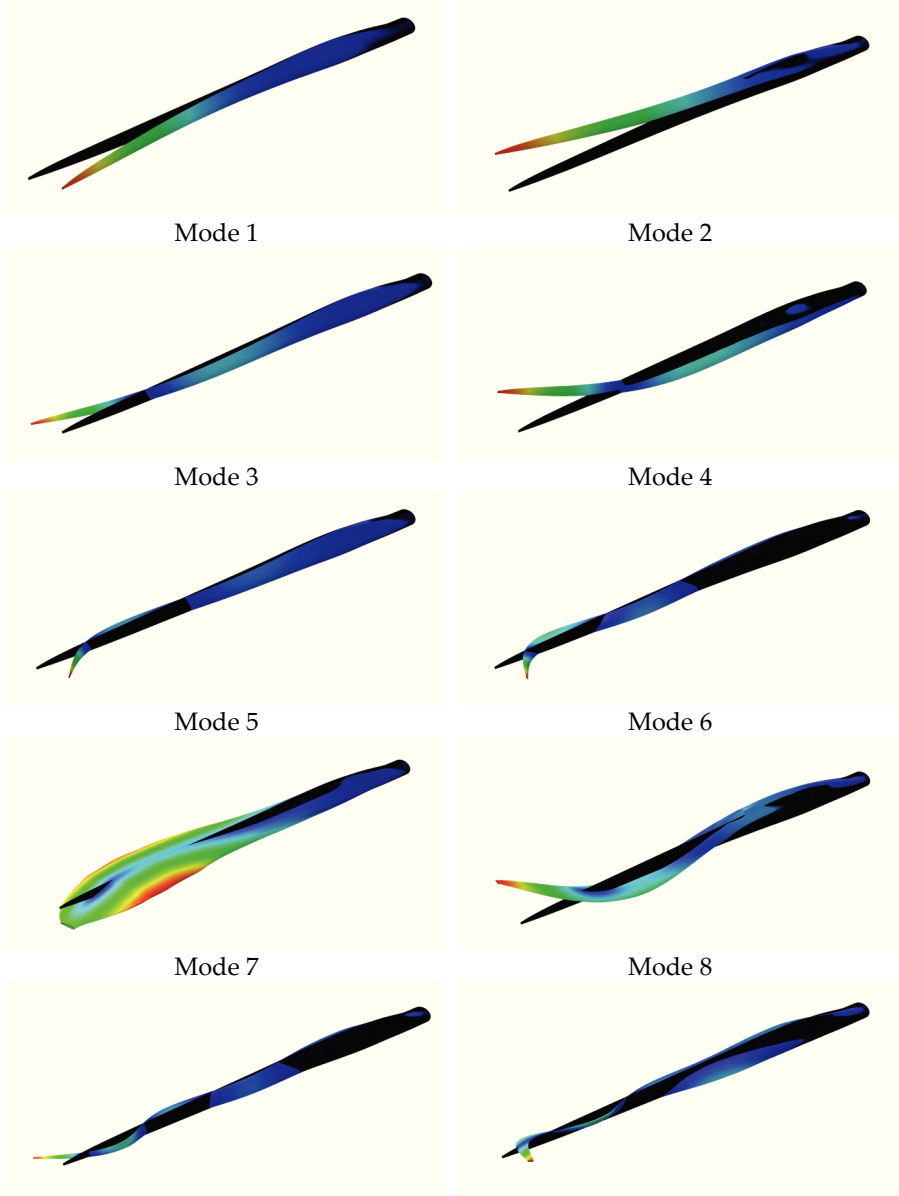

Figure 96: Contour plot of the displacement magnitude on different eigenmodes of the 49 m blade. Both the un-deformed and deformed shapes are plotted. For visibility, a large scale factor is applied to the displacements.

4.3.3 The 10 m blade from XANT

Blade models were created for the 10 m blade from XANT. The blade shape of the resulting models is compared to the original CAD drawings as can be seen in Figure 97. A good match is obtained. In Table 10 the mass and COG of the final model are compared to the design, while in Table 11 the eigenfrequencies are compared. The shapes of the corresponding eigenmodes can be seen in Figure 98. Differences can be observed between the models, design and experimentally measured values. An explanation for this is that there are (minor) differences between the design that was produced and that which was initially calculated. The deviations in eigenfrequencies are larger for the HAWC2 model of the blade.

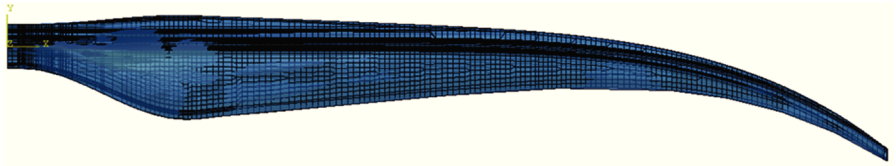

Figure 97: Comparison of the blade shape produced by the novel developed tools with the blade shape defined in the design CAD model. A very good match is obtained. Rendering the surfaces in high detail and making section cuts reveals that the distance between both is minimal.

Table 10: Overview of the total mass and COG of the 10 m blade

Representation	Total mass [tonne]	COG [m]
Design	252 kg	2.99
Shell model	255 kg	2.99

Table 11: Overview of the eigenfrequencies of the 10 m blade

Eigenmode	Design [Hz]	Experiment [Hz]	Shell model [Hz]
1 (1st flap)	3.52	3.53	3.29
2 (2nd flap)	7.13	-	6.86
3 (1st edge)	9.30	6.11	8.06
4	-	-	15.04
5	-	-	19.60
6	-	-	23.92
7	-	-	31.32
8	-	-	35.93
9	-	-	38.82
10	-	-	44.30

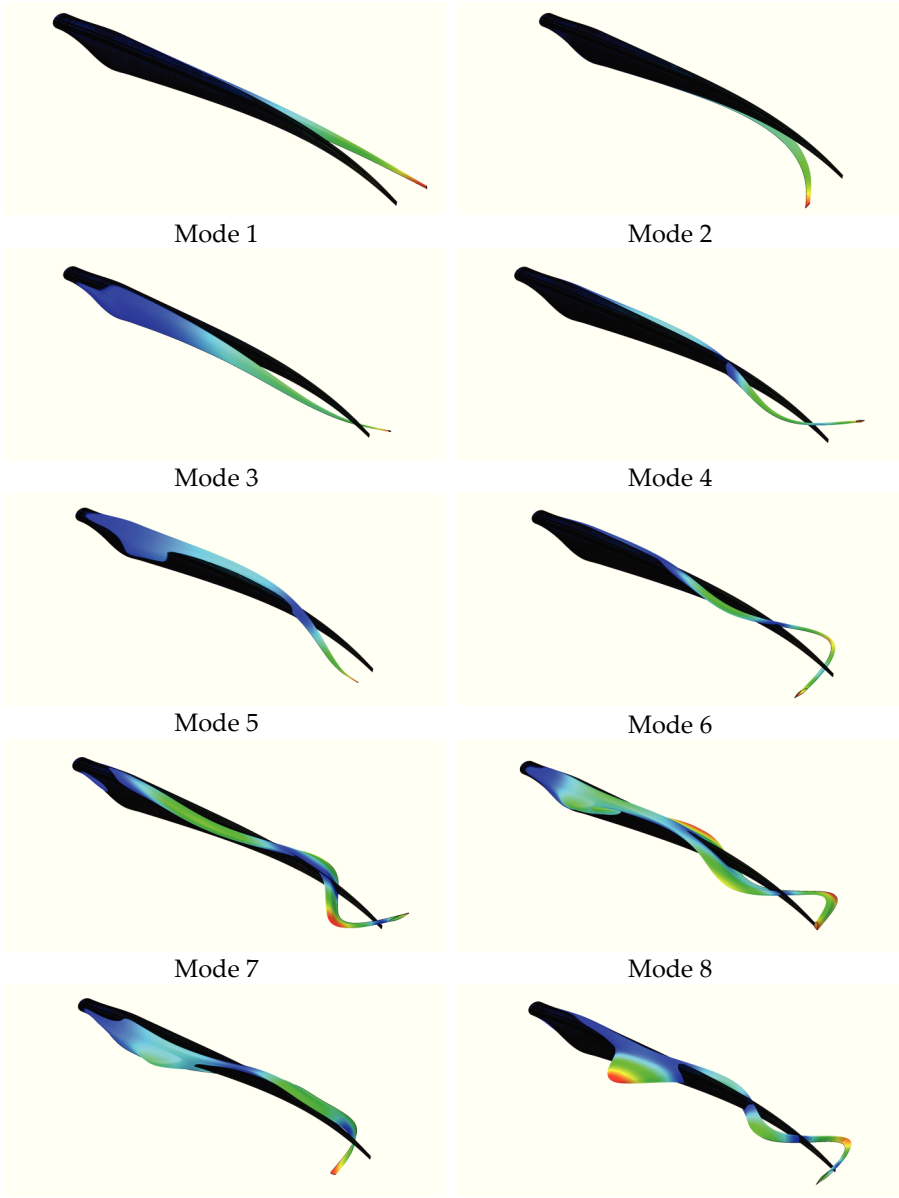

Figure 98: Contour plot of the displacement magnitude on different eigenmodes of the 10 m blade. Both the un-deformed and deformed shapes are plotted. For visibility, a scale factor is applied to the displacements.

4.3.4 The 43 m blade from CTC engineering

The 43 m blade designed by CTC engineering in the Netherlands was modelled. The blade shape of the resulting models is compared to the original CAD drawings as can be seen in Figure 99. A good match is obtained. In Table 12, the mass and COG of the models is compared. Table 13 shows the eigenfrequencies for the blade. The frequencies resulting from the models are slightly higher than the design values, which could be explained by the slightly lower mass of the models. This difference is due to the dead masses of the lightning protection system and balancing box not being included in the models. In addition, a difference can be seen between the torsional frequencies predicted by the shell and solid models. The corresponding eigenmodes can be seen in Figure 100.

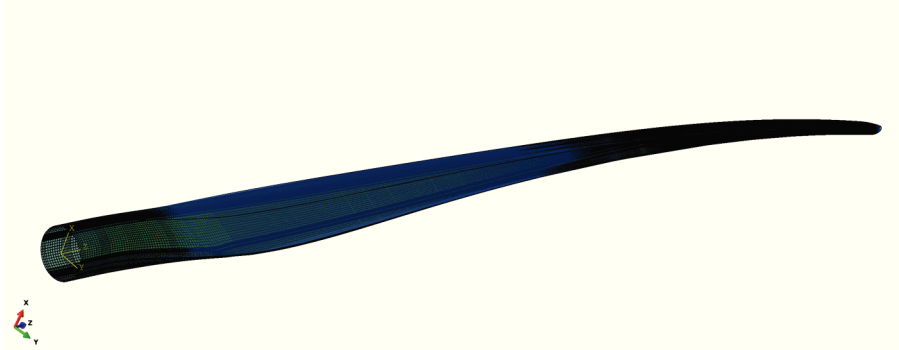

Figure 99: Comparison of the blade shape produced by the novel developed tools with the blade shape defined in the design CAD model. A very good match is obtained.

Table 12: Overview of the total mass and COG of the 43 m blade. The mentioned models are built using the block based approach.

Representation	Total mass [kg]	Spanwise position COG [m]
Design	6350	13.3
Shell model	6240	13.5
Solid model	6180	13.5

Table 13: Overview of the eigenfrequencies of the 43 m blade. The difference between the models and design can be explained by the slightly lower mass. This is due to the lightning protection system and balancing box which are not included in the models. In addition, a difference in torsional frequency can be seen between the shell and solid models.

Eigenmode	Design [Hz]	Shell model [Hz]	Solid model [Hz]
1 (1st flap)	0.77	0.806	0.813
2 (1st edge)	1.06	1.076	1.037
3 (2nd flap)	2.15	2.222	2.252
4 (2nd edge)	-	3.056	3.003
5		4.2896	4.368
6		6.8462	6.754
7		7.0748	7.322
8		10.45	10.956
9		12.004	12.122
10 (1st torsion)	15.1	12.544	14.317

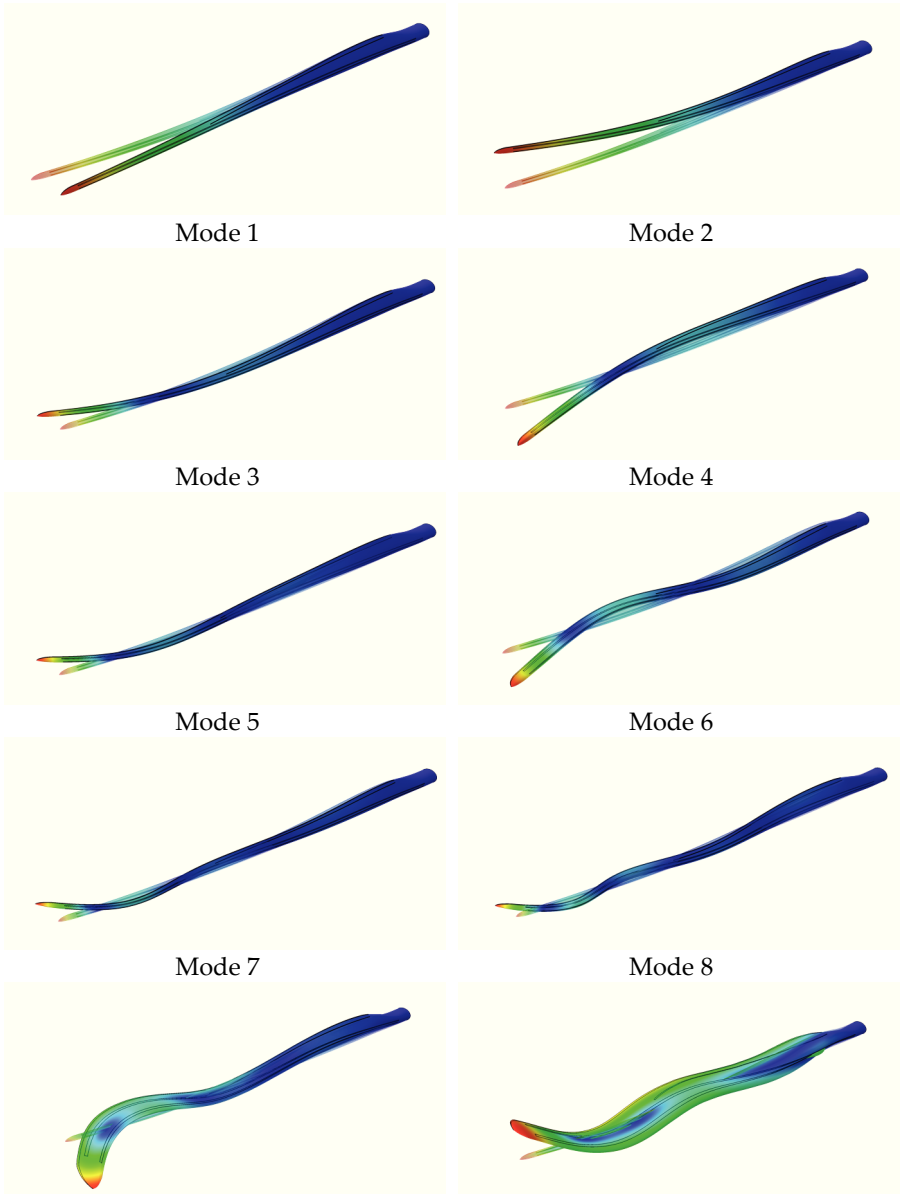

Figure 100: Contour plot of the displacement magnitude on different eigenmodes of the 43 m blade. Both the deformed and un-deformed shapes are plotted. For visibility, a scale factor is applied to the displacements.

4.3.5 The influence of the material orientations

To investigate the importance of accurate material orientations, calculations were conducted using the 10 m blade from Xant. This blade incorporates blade sweep, which the UD fibers in the spar caps follow. Calculations were performed using both accurate element-wise material orientations calculated using the developed tools and simplistic orientations along the blade direction. This has a strong effect as can be seen from Table 14.

Table 14: Eigenfrequencies obtained with models employing a simple material orientation system compared to eigenfrequencies obtained using accurate material orientation systems

Eigenmode	Eigenfrequency with simple material orientations [Hz]	Eigenfrequency with advanced material orientations [Hz]
1	3.12	3.29
2	6.29	6.86
3	7.68	8.06
4	13.67	15.04
5	18.78	19.60

4.4 Conclusions

Both commercial blade designs and academic reference designs exist. While the use of reference blades benefits the reproducibility of the results, the designs are simplistic compared to actual blades. Furthermore, the reference blades lack validation possibilities. In this regard, conducting investigations with commercial designs provides opportunities. One reference blade and three commercial blades were modelled in this work. The blade models used in this study were validated. First, their shape was compared to the available CAD files. Subsequently, the total masses, COG and mass distributions were compared. For the shape comparison, a good agreement was found for all the considered models. Some deviations in mass were present. These are the result from the lightning protection system and balancing box not being included in the models. Furthermore, for the PowerComposites and Xant blade some differences exist between different versions of the structural design.

Further, the eigenfrequencies were extracted from the different models that were employed. The resulting values were compared to the design and available experimental values. This validated the overall mass and stiffness distributions.

Furthermore, the influence of the assigned local material orientations systems was investigated for the blade incorporating sweep. It was found to have a significant influence on the obtained eigenfrequencies. This is logic, considering the

anisotropic properties of the UD material that is used in the spar caps and the rapid change in stiffness with its orientation.

In addition, the values obtained from shell models were compared to the values obtained from solid models. It was found that for the lower eigenfrequencies a good agreement is obtained, while a discrepancy appears for torsional modes.

4.5 Bibliography

[1] J. Jonkman, S. Butterfield, W. Musial, and G. Scott, "Definition of a 5-MW reference wind turbine for offshore system development," NREL/TP-500-38060, Feb. 2009.

[2] H. B. Hendriks *et al.*, "DOWEC concept study; evaluation of wind turbine concepts for large scale offshore application," Jan. 2000.

[3] H. J. T. Kooijman, C. Lindenburg, D. Winkelaar, and E. L. van der Hooft, "DOWEC 6 MWPRE-DESIGN: Aero-elastic modelling of the DOWEC 6 MWpre-design in PHATAS," DOWEC-F1W2-HJK-01-046/9, 2002.

[4] B. R. Resor, "Definition of a 5MW/61.5m Wind Turbine Blade Reference Model," SAND2013-2569, Apr. 2013.

[5] "UpWind: Design limits and solutions for very large wind turbines," Mar. 2011.

[6] J. Peeringa, R. Brood, O. Ceyhan, W. Engels, and G. de Winkel, "UpWind 20MW Wind Turbine Pre-Design," *ECN Pap. No ECN-E–11-017*, 2011.

[7] R. Nijssen, G. D. de Winkel, J. M. Peeringa, and R. DATE, "WMC5MW laminate lay-out of reference blade for WP 3," *Knowl. Cent. Wind Turbine Mater. Constr.*, 2007.

[8] Z. Sun, M. Sessarego, J. Chen, and W. Z. Shen, "Design of the OffWindChina 5 MW Wind Turbine Rotor," *Energies*, vol. 10, no. 6, p. 777, Jun. 2017.

[9] D. T. Griffith and T. D. Ashwill, "The Sandia 100-meter all-glass baseline wind turbine blade: SNL100-00," SAND2011-3779, 2011.

[10] D. T. Griffith, "The snl100-01 blade: Carbon design studies for the sandia 100-meter blade," *Sandia Natl. Lab. Tech. Rep. SAND2013-1178*, 2013.

[11] C. Bak *et al.*, "Light rotor: the 10-MW reference wind turbine," presented at the Proceedings of EWEA 2012 - European Wind Energy Conference & Exhibition, European Wind Energy Association (EWEA), 2012.

[12] C. Bak *et al.*, "Design and performance of a 10 MW wind turbine," *J Wind Energy*.

[13] A. De Broe and W. Coppye, "A naked turbine for hash environments," presented at the International Wind-Diesel Conference, 2011.

[14] L. Huysmans, "Xant plaatst eerste commerciële Belgische windmolen," 01-Oct-2015. [Online]. Available: http://trends.knack.be/economie/bedrijven/xant-plaatst-eerste-commerciele-belgische-windmolen/article-normal-613797.html. [Accessed: 23-Apr-2018].

[15] G. C. Larsen and Forskningscenter Risø, *Modal analysis of wind turbine blades*. Roskilde: Risø National Laboratory : available from: Risø National Laboratory, Information Service Department, 2002.

[16] D. T. Griffith and T. G. Carne, "Experimental modal analysis of 9-meter research-sized wind turbine blades," in *Structural Dynamics and Renewable Energy, Volume 1*, Springer, 2011, pp. 1–14.

[17] S. Reese, D. T. Griffith, M. Casias, T. W. Simmermacher, and G. A. Smith, "Modal testing of the TX-100 wind turbine blade.," SAND2005-6454, 920816, May 2006.

5 Aero-elastic blade simulations

"We are all just looking out for something real" – Blade Runner

Chapter summary: In this chapter, tools to conduct simulations of wind turbine blade structures under aero-dynamic loads are presented. Such load cases represent a coupled challenge as the deformation of the rotor affects the surrounding airflow and thus the aerodynamic loads that affect the structure. In a first approach, a simple aerodynamic model using blade element momentum (BEM) theory is combined with a detailed shell FE model. The results are compared to a typical aero-elastic model used to calculate the turbine's load envelope. In a second approach a refined computational fluid dynamics (CFD) model is combined with a refined FE model.

5.1 Motivation for aero-elastic simulations

While experimental testing of blades occurs on test stands where the structure is loaded at a few discrete positions, the blades that are put into service experience distributed loads. These include gravitational, gyroscopic and centrifugal components as well as an aerodynamic load, spread over the outside surface. This last component takes place as the result of a coupled system: the aerodynamic load and the deformation of the blade mutually affect each other. The aerodynamic load, resulting from the airflow over the blade affects the deformation of the structure, which in turn affects the flow and thus the load. This results in a so-called fluid-structure-interaction (FSI) system. To account for the real-world load cases, this problem must be taken into account and cases with distributed loads should be considered. Furthermore, current blade designs try to implement strategies to reduce the loads resulting from turbulence. Since the blades are part of the rotor, which is at the beginning of the energy conversion chain, load reductions at this level result in a cascade towards other components. Lower loads at the rotor level result in reduced loads at the level of the bearings, gearbox, generator, all the way down to the tower and foundation. All together limited reductions in load can result in much larger savings at the level of the overall turbine [1]. Methods for reducing the rotor loads are applied with several different approaches, which are discussed in the following paragraphs.

5.1.1 Minimizing the blade mass

A first approach to generally reduce the loads from the turbine is minimizing the mass of the blades. For this purpose, the layup is optimized and the planform modified. Often more slender planforms are preferred in combination with a higher tip speed ratio (TSR) since this allows a reduction in chord length. This could mean less material and a lower mass. However, as discussed in Bottasso et al. [2] reduction of the chord length results in a reduction of absolute thickness of the blade shape, which in turn results in an increase in spar cap thickness to compensate for the lost bending stiffness. Similarly, increasing the chord length results in larger panels that can buckle, requiring additional core material, resulting in a mass increase. This means there is an optimum chord length.

5.1.2 Active load reduction

Another approach is the use of active load reduction measures. Most frequently, modern wind turbines have an active pitch regulation system that pitches the blades towards feathered position with increasing wind speed. The loads can be reduced by cyclic pitching. Further reducing the loads is possible by pitching each blade individually. Alternatively, the blade shape can be altered to respond to changing conditions. Examples of approaches that are under development are the use of trailing edge flaps and slats. In proof of concept experiments these have shown to result in large decreases in fatigue loads [3]–[6]. Alternatively, telescopic

blades have been suggested and investigated [7]–[11]. These consist of multiple segments which can be retracted into each other to reduce the length of the blades and thus the swept area of the rotor. Wind turbine blades with novel active load control features can be seen in Figure 101.

(a) (b)

Figure 101: Examples of active load reduction strategies that are being researched. (a) Wind turbine blade with trailing edge flaps. Reproduced from Ref. [3]. (b) An example of a telescopic wind turbine blade. The blade consists of two segments that can be retracted into each other to reduce the diameter of the rotor, which reduces the loads at a higher wind speed. Additional equipment for measuring the wind speed is present. Reproduced from Ref. [7].

5.1.3 Passive load reduction

An approach to cause passive load reduction is causing a twisting deformation of the blade under loads. This is done either by introducing elastic couplings by using off-axis fibers in the composite layup or by using a swept planform [12]. Both approaches cause the blade to deform in torsion as it deflects, resulting in a change in angle of attack (AoA) of the airfoils towards the tip. This deformation can be designed to twist the blade towards stall or more commonly towards feather as shown in Figure 102. The advantages of passive load reduction methods are their very fast response time and low maintenance.

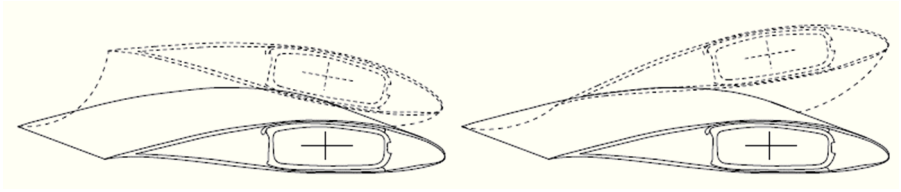

(a) (b)

Figure 102: Schematic view of twist deformations that can be obtained by introducing elastic couplings in the composite layup of the blade. (a) Deformation towards stall (b) Deformation towards feather. Image reproduced from Ref. [13].

5.1.3.1 Wind turbine blade bend-twist coupling

Various studies have been conducted, investigating the possibility of bend-twist couplings. For example, Bottasso et al. [14] investigated the optimal use of bend-twist coupling using off-axis fibers and an optimization approach. Different configurations were considered. It was found that the weight is lowest when the off-axis fibers are used both in the spar caps and the skin. Furthermore, it was found that weight could be saved by limiting the off-axis material to an outboard portion of the blade. Finally, the passive coupled blade is combined with an active individual pitch controller, which was found to result in a synergy. Similarly, Wetzel [15] performed a parametric study to investigate the use of off-axis fibers in the spar cap of a 37 m rotor blade. Both the angle of off-axis fibers and their concentration was varied. It was concluded that the optimal angle for the fibers was close to 7.5 ° and that a higher concentration of off-axis material was more useful outboard. Furthermore, Fedorov [13] investigated bend-twist couplings using both numerical and experimental methods. Tests and analyses were performed on a blade section and prismatic beams. In addition, Cox and Echtermeyer [16] investigated how the potential for bend-twist coupling scales with blade length by designing blades of different lengths. It was found that there is no dependence with scale. In all configurations the same tip twist and relative load reduction were observed.

5.1.3.2 Wind turbine blade sweep

An alternative approach is to use geometric sweep to move the aerodynamic center away from the elastic center. Aerodynamic lift will then create a torsional moment in the blade. This approach has also been investigated in several studies. In the sweep-twist adaptive rotor blade (STAR) study [17], a blade having a geometrical sweep is designed. A prototype is built and tested.

Most frequently, blades with a swept planform only incorporate a backward sweep towards the tip. However, this can result in a large torsional bending moment towards the root. Wetzel et al. [18] proposed that in addition to the backward sweep at the tip, a forward sweep could be added to the inboard section to trigger a torsional load in the opposite direction, thereby reducing the resulting load at the root. A comparison between the typical and proposed planforms can be seen in Figure 103.

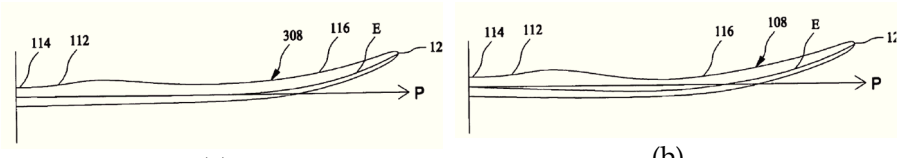

Figure 103: Schematic overview of the innovative blade sweep proposed in Wetzel et al. [18] (a) Conventional blade incorporating a planform that is swept backwards towards

the tip. (b) Innovative swept planform with a forward sweep on the inboard portion of the blade and a backward sweep towards the tip. This reduces the twisting moment at the root.

5.2 Fluid structure interaction simulations

The interaction between the blades and the airflow results in an implicit system called a fluid-structure interaction (FSI). This system can be solved by iterating between the aerodynamic and structural problems. Depending on the desired result, different coupling schemes are possible. If only steady-state cases are investigated, a so-called "weak" coupling is sufficient. In such a case the aerodynamic model and structural model are simulated only once per load incrementation step. If the investigation of more complex transient effects is desired, the use of more advanced iteration schemes is required.

In practice, aero-elastic simulations are used to calculate the load envelope for the turbine under a sequence of design load cases. In these calculations the structural side is typically modelled using beam elements, while the aerodynamics side is handled by a simple model using blade element momentum (BEM) theory. This is a computationally efficient approach, which allows many load cases to be considered.

On the other side of the spectrum, very detailed FSI simulations exist. These typically rely on advanced computational fluid dynamics (CFD) models and 3D structural FE models. The structural models are typically not that advanced. However, this total results in computationally expensive simulations.

A few studies have suggested the use of a combination of the best of both worlds. Specifically, by combining BEM on the aerodynamics side with a FE model on the structural side, advanced structural behavior can be investigated at an acceptable computational effort.

Two approaches are presented in this chapter. In the first approach, the tools are developed to allow a cost-efficient combination between a BEM model and a FE model to be used. This approach is demonstrated on a swept wind turbine blade. The second approach is combination of a refined CFD and a refined FE model. This approach was used under the FWO project in a collaboration with the department of Flow, Heat and Combustion Mechanics of Ghent University. The work was performed by Gilberto Santo as part of his PhD and is briefly discussed. The simulations use the structural models created within this research.

5.3 Development of a fluid-structure interaction method combining a BEM code and a finite element model

5.3.1 Introduction: the need for a simple FSI method

As mentioned, traditional FSI methods are either computationally demanding or designed for capturing the global behavior of the blades at an acceptable computational effort by using beam models. To obtain detailed structural behavior at an acceptable computational cost, a new coupling was created between the FE solver Abaqus and the aerodynamics code HAWC2aero which uses BEM theory.

Recent efforts have allowed the use of beam elements with fully populated stiffness matrices. These appear once pre-curving or material couplings occur [19]. However, these models were not available at the time of doing the research. Furthermore, these beam models are still not sufficient to account for local effects or to include non-linear effects such as those resulting from advanced material models.

5.3.2 Materials and methods

For this investigation, the Xant 10 m wind turbine blade is used. OML shell models of the blade, created using the slice based approach discussed earlier were used. Both a linear thickness interpolated shape and a b-spline interpolated shape were constructed, as shown in Figure 104. The models were created to obtain a high level of detail and fidelity. Initially a model using linear elements (type S4R and S3) was used.

The original plan was to couple the HAWC2 model with the Abaqus FE model. For this approach, the coupling scheme can be seen in Figure 105. However, HAWC2 is an aero-elastic code consisting of both a structural and aerodynamic solver. A discussion with the developers of HAWC2 made it clear that using this approach would not be possible as desired. As an alternative, HAWC2aero, the BEM-code component of HAWC2 was used. By using HAWC2aero together with Abaqus the structural and aerodynamic parts are nicely separated and additional computational costs due to iterations within HAWC are avoided. The final coupling scheme is shown in Figure 106.

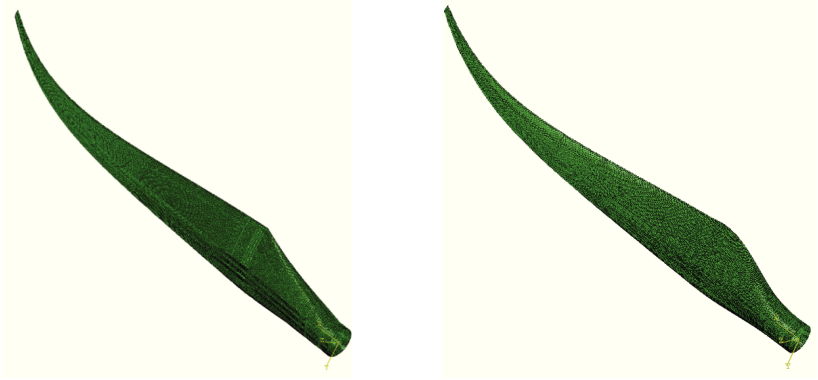

(a) (b)

Figure 104: 3D plots of the newly created FE models for the 10 m blade. (a) 3D OML shell FE model with the OML shape obtained using linear thickness interpolation. (b) 3D OML shell model with the OML shape obtained using b-spline interpolation.

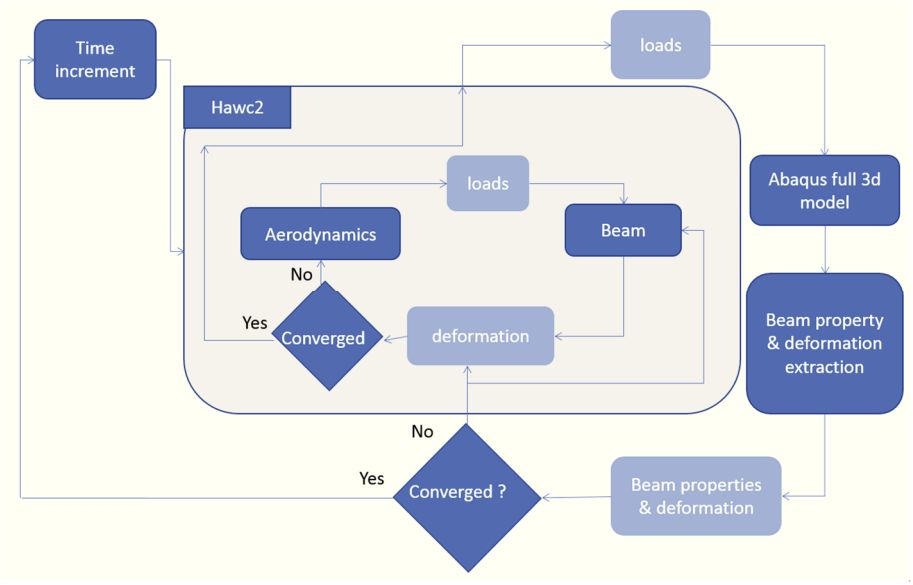

Figure 105: Initial coupling scheme, providing a weak coupling between the aero-elastic code HAWC2 and the finite element package ABAQUS.

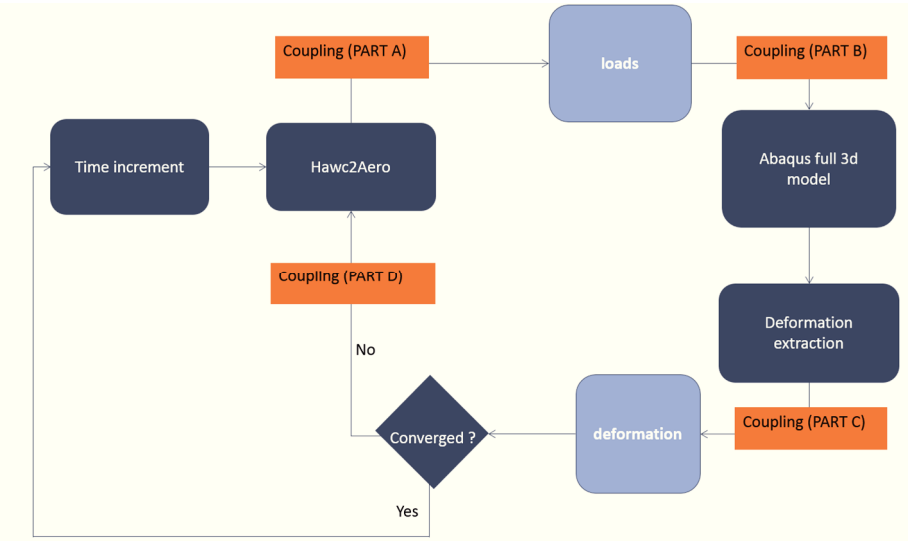

Figure 106: Final coupling scheme, providing a weak coupling between the BEM code HAWC2aero and the finite element package ABAQUS.

In the FE model, the blade is positioned to correspond to the position in the HAWC2aero model, which can be seen in Figure 107. The centrifugal effect is accounted for by means of a volumetric body force about an axis that accounts for the cone-angle of the rotor. In addition, the aerodynamic loads are calculated by HAWC2aero for a rigid configuration of the blade. These loads are interpolated using b-spline functions as shown in Figure 108. This function is subsequently used to calculate the forces to apply to each of the sections, as shown in Figure 109. The calculated loads are introduced to the FE model using concentrated forces at the centerlines, in the middle of the spar structures, on both the pressure and suction sides.

Further, to allow the extraction of the total resulting root bending moment, all the nodes at the root of the blade were connected to a reference point at the origin of the assembly by means of a multi-point constraint (MPC) of the type “beam” [20]. Essentially this coupling introduces rigid beam elements between the master node and all the slave nodes and thereby constrains the displacement and rotation of those nodes. The total reaction forces and moment can hence be extracted from the master node in the result of the simulation.

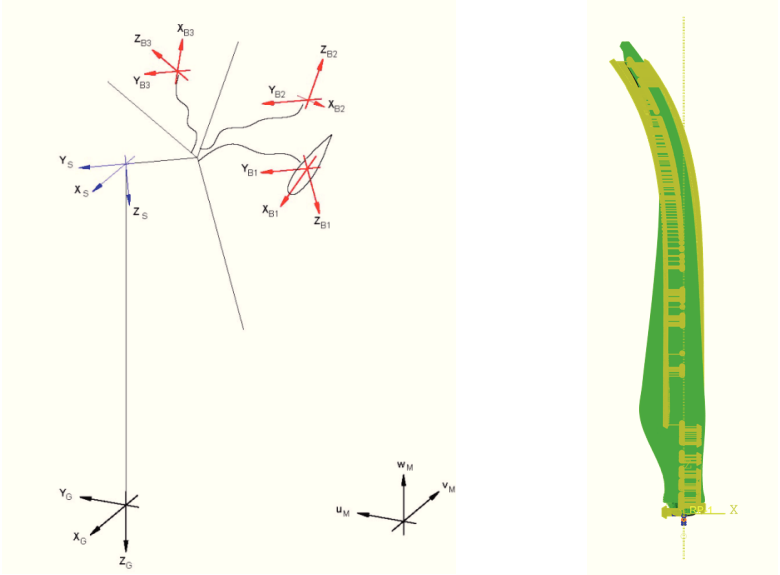

(a) (b)

Figure 107: Overview of the orientation systems that are used. (a) Schematic view of the coordinate system used by HAWC2 and HAWC2aero [22]. (b) The assembly set-up of the structural model.

After running the structural solver, the deformation of the blade is extracted from the output database using Python scripting. The deformation of the blade is extracted using the displacement of the nodes at the LE and TE along the full span of the blade. These data are used to calculate the angle of attack along the span under the deformed configuration. The updated configuration of the rotor is then sent to the aerodynamic solver for a subsequent iteration.

For reference, the aero-elastic code HAWC2 is used to calculate the behavior of the blade under aero-elastic loads. The total mass and center of gravity (COG) of both models can be compared in Table 15.

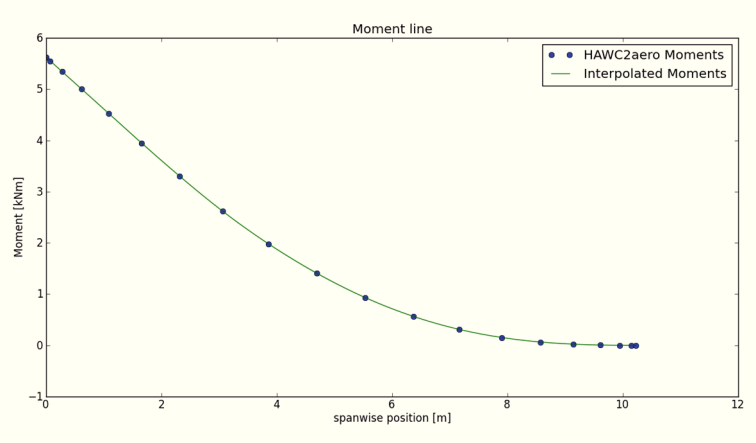

Figure 108: Plot of the moment over the blade span calculated by HAWC2aero. The moments at specific stations are interpolated using b-spline functions. This leads to a smooth result. The graph shows the given moments as dots and the interpolated moments as a continuous curve as a function of span-wise position.

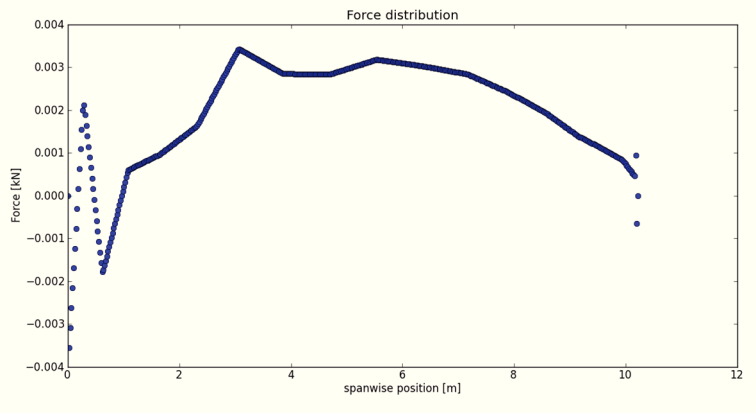

Figure 109: The interpolated moment line is used to calculate the forces required to obtain that exact moment line. The graph shows the forces as a function of the span of the blade.

Table 15: Comparison between the mass and center of gravity of the HAWC2 model used in the design of the blade and the newly created Abaqus 3D FE model.

	HAWC2 model	Abaqus slice based model
Total mass	261 kg	255 kg
C.O.G. spanwise position	3,0 m	2,9 m

5.3.3 Results and discussion

5.3.3.1 Convergence of the iterations

While it was possible that the deformations resulting from exposing the blade to a large wind load would result in an instable iteration, this was not the case. The simulations are found to converge rapidly. It sufficed to iterate four times before the change in angle of attack dropped below 2 % and the change in rotor power changed less than 0.5 % between subsequent iterations.

5.3.3.2 Coupling results

The coupling scheme was used to simulate a wind ramp, meaning a series of increasing wind speeds were simulated. For each wind speed, the aerodynamic and structural models were iterated until the results converged before moving to the next wind speed. The resulting values were compared to those obtained from aero-elastic simulations using the HAWC2 model used in the blade design. The HAWC2 simulations were conducted by Simon Reijniers from TU Delft who was doing his thesis at the Xant company. In Figure 110, the power is plotted as function of the surrounding wind speed. A good match is obtained between the two approaches. A similar match is found in the thrust and torque curves presented in Figure 111 and Figure 112.

In Figure 113 the resulting root bending moments are compared. A mismatch can be observed between the root bending moments calculated using the newly developed coupling and the values obtained using HAWC2. For the moment about the x-axis (Mx), the mismatch disappeared after updating the mass properties of the model representation in HAWC2 [21]. Furthermore, in a later phase, the HAWC2 model was updated with beam properties obtained using BECAS. This lead to most of the discrepancies disappearing, resulting in a good match between both models.

Furthermore, in Figure 114 the rotational speed of the rotor is compared for both simulations. This value is imposed in the HAWC2aero modelling while in the HAWC2 modelling it is a resulting value. Further, in Figure 115 the tip twist is compared. A different twist behavior is observed at the blade tip. However, when the values from the HAWC2 model are calculated using the coordinates of the

nodes, a similar pattern appears [21]. In addition, in Figure 116 and displacements are compared.

Furthermore, the deformed blade configuration can be seen in Figure 117. The blade deforms in torsion towards the tip, resulting in a reduced AoA. This indicates that the intended deformation to reduce blade loads takes place. In Figure 118 the corresponding maximum principal strains are shown.

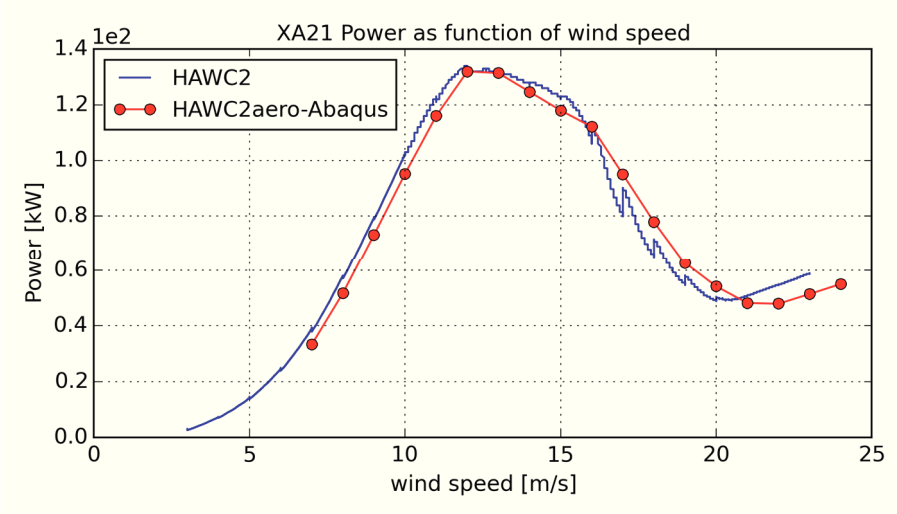

Figure 110: Rotor power as a function of wind speed obtained via both the coupling between HAWC2aero and Abaqus and via HAWC2. A very similar pattern is obtained.

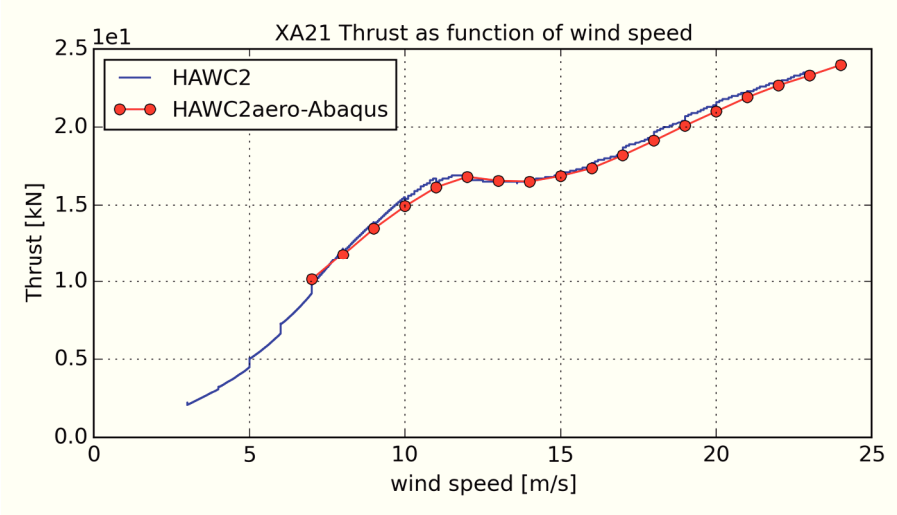

Figure 111: Total thrust on the rotor as a function of wind speed obtained via both the coupling between HAWC2aero and Abaqus and via HAWC2.

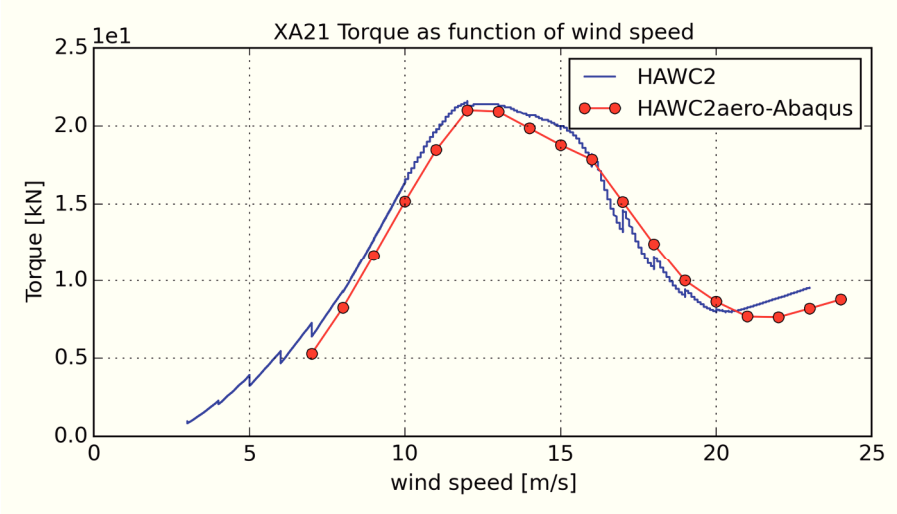

Figure 112: Resulting torque as a function of wind speed obtained via both the coupling between HAWC2aero and Abaqus and via HAWC2.

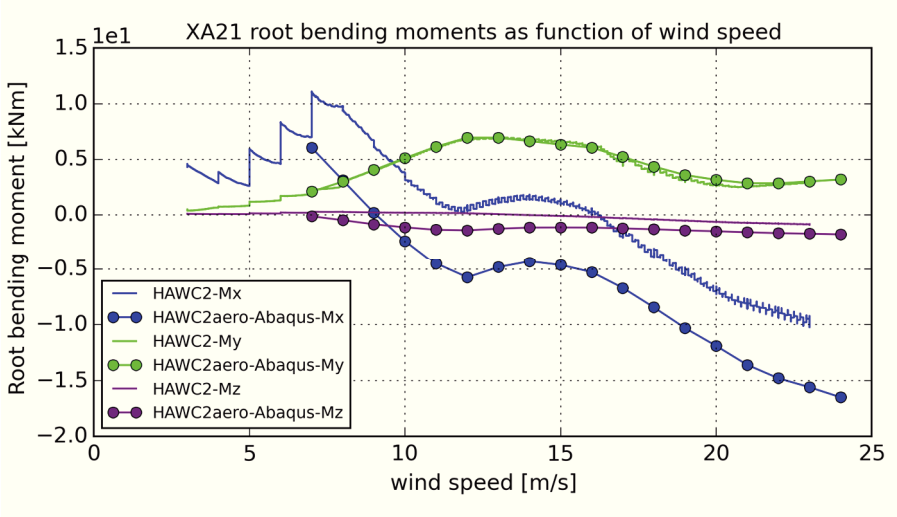

Figure 113: The resulting root bending moments as a function of wind speed: Mx, My and Mz as a function of wind speed for the standard glass-epoxy XA21 blade, obtained via both the coupling between HAWC2aero and Abaqus and via HAWC2.

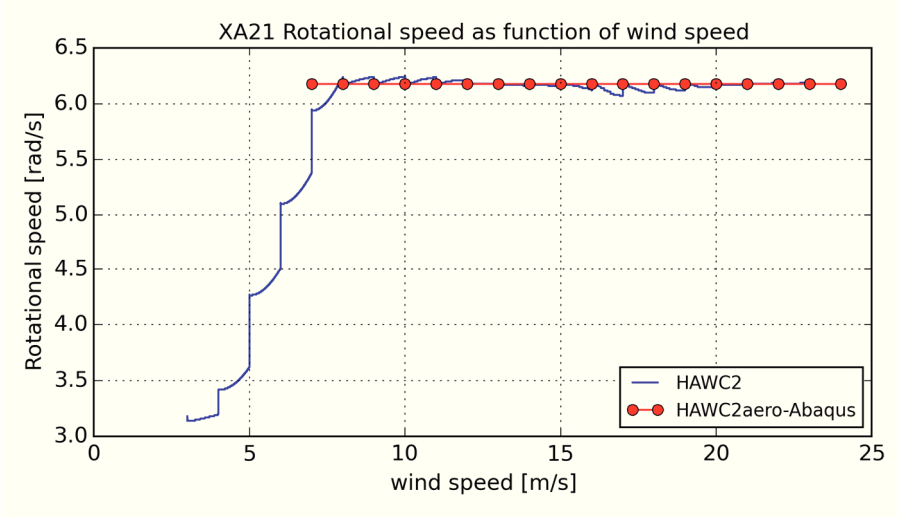

Figure 114: Comparison of the angular velocity of the rotor in the HAWC2 simulation and the coupled HAWC2aero – Abaqus simulation for the standard glass-epoxy XA21 blade. At wind speeds above 7 m/s the angular velocities match.

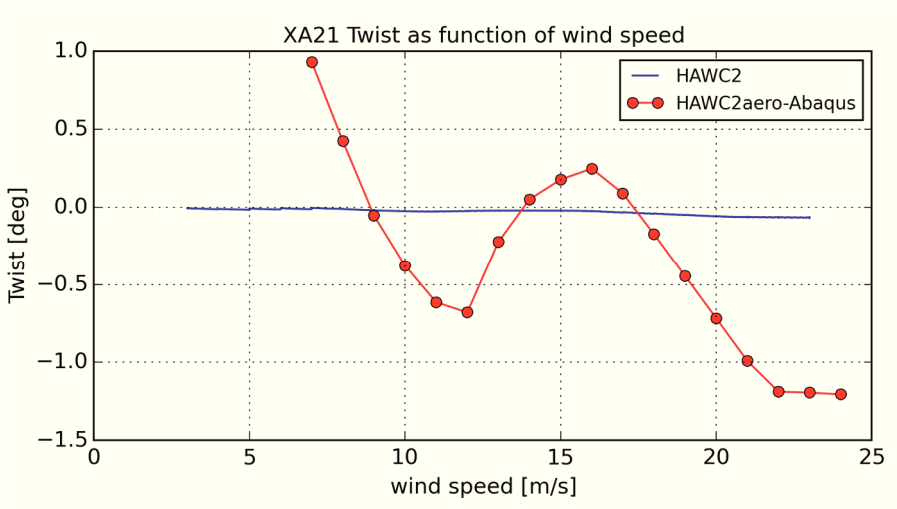

Figure 115: Comparison between the twist at the tip of the blade as predicted by the HAWC2 beam models and the Abaqus-HAWC2aero shell model for the standard glass-epoxy XA21 blade.

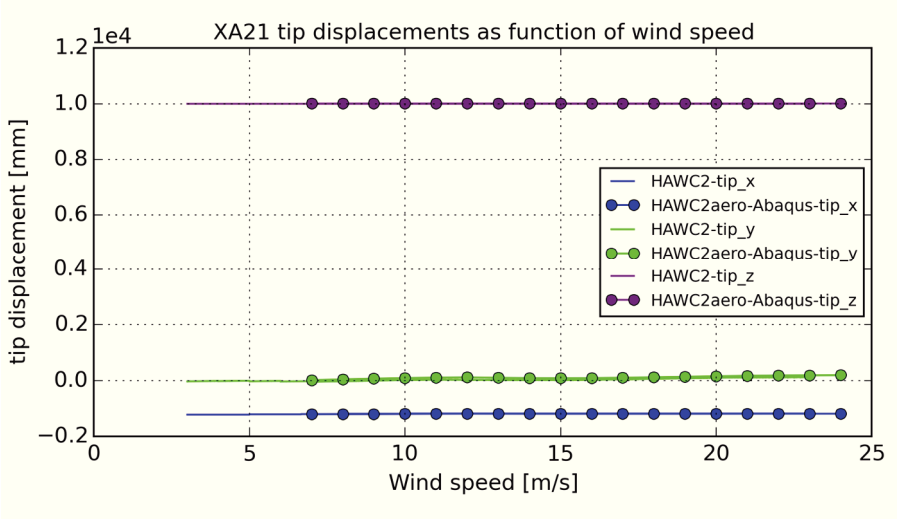

Figure 116: Comparison between the downwind tip deflections as predicted by the HAWC2 beam model and the Abaqus-HAWC2aero shell model for the default glass-epoxy XA21 blade.

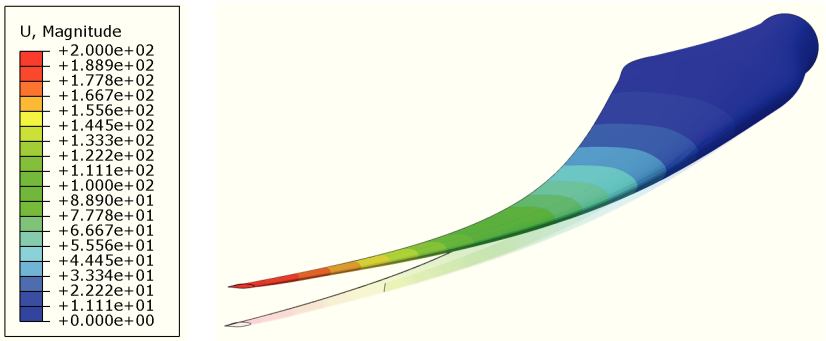

Figure 117: A contour plot of the displacements of the 10 m blade under a wind speed of 24 m/s. The original configuration is plotted transparent while the deformed blade shape is shown opaque.

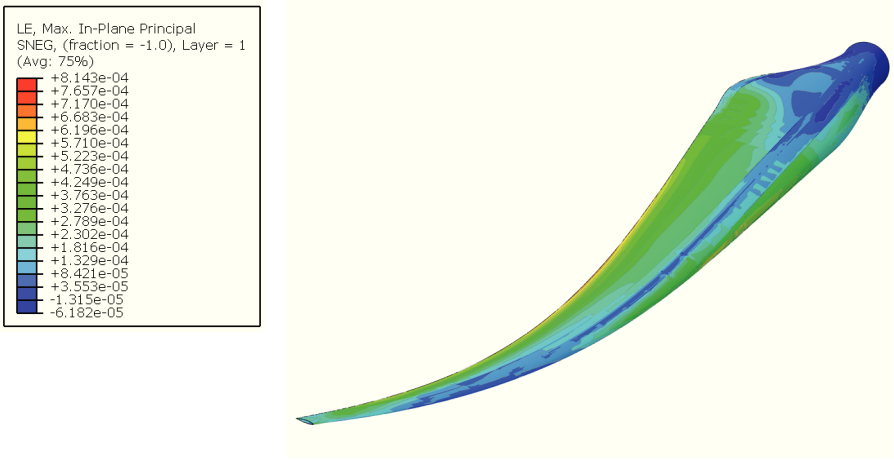

Figure 118: Contour plot of the maximum principal true strain distribution over the outside surface of the 10 m swept wind turbine blade considered in this study under aero-elastic load.

5.3.4 Conclusions

The conclusions of this part can be summarized as follows:

- Development of the tools to allow cost effective FSI calculations:
  - An FSI approach that couples a simple aerodynamics code using BEM theory (HAWC2aero) to an advanced 3D FE model was successfully developed. This approach allows cost effective FSI simulations to be conducted. Especially on the structural side, detailed effects are captured and useful are obtained.
- Demonstration of the approach:
  - The approach was successfully demonstrated by calculating the steady state behavior of the rotor at different wind speeds.
  - The resulting power, thrust, torque and tip displacement and twist values were compared to those resulting from aero-elastic HAWC2 simulations. These rely on a beam representation of the blade. A good correlation was found between both cases. However, discrepancies exist between the torsional root bending moments resulting from both methods.
  - Better agreement was found between both approaches after updating the beam properties of the blade with values obtained using BECAS.

5.4 Fluid structure interaction by means of coupled CFD-CSM approach

5.4.1 Introduction

The interaction between the flow field and a wind turbine structure is a highly complex problem. Different computational models can be used, resulting in different levels of fidelity. To consider the effects that take place in a direct fashion, advanced numerical methods are required. For example, while accurate wind loads can be computed by means of aero-elastic codes that rely on BEM theory, tip losses are included using an analytical or semi-empirical approach. To consider these effects directly, a full 3D flow field must be calculated using CFD. The same applies for 3D flow effects caused by centrifugal and Coriolis forces. Furthermore, typical aero-elastic codes rely on beam models and a fixed set of airfoils, of which the shape is assumed to remain unaltered. These do not account for a change in cross-section as the blade deforms and do not account for the change in aerodynamic behavior this causes. To accurately include these effects both a detailed 3D FE model and a 3D CFD model are required. Such an approach has been used in the work of Gilberto Santo. Using the models of the 49 m blade created by the author as structural models, a detailed fluid structure interaction is created. This was done by coupling a detailed 3D CFD simulation to the Abaqus FE model.

5.4.2 Materials and methods

On the aerodynamics side, a large 3D CFD domain is created, as can be seen in Figure 119. The domain is several times larger than the rotor diameter to prevent unrealistic obstruction of the airflow. This region is discretized using a fully structured mesh. Furthermore, a fully structured local grid is provided for the boundary layer of the rotor region. Turbulence is included using a Reynolds-averaged Navier-Stokes (RANS) turbulence model. This approach allows for a computationally efficient way to include turbulence effects. Alternatives, such as large eddy simulation (LES) and direct numerical simulation (DNS) are computationally far more expensive.

As computational structural model (CSM) a slice based OML shell model of the 49 m blade, obtained using the slice-based modelling approach, was used. This model is presented in Figure 120.

A so-called “strong” coupling is created by using a stand-alone code, Tango [22], [23] which was developed during the PhD of prof. Joris Degroote [24] at the department of Flow, Heat and Combustion Mechanics of Ghent University. This tool allows coupling of separate commercial flow and structural solvers. Several iterations are possible within each time step, allowing the simulation of transient conditions. Unlike in earlier work, the flow field includes the atmospheric

boundary layer (ABL). This results in a variation in wind speed over the height of the domain, as occurs naturally in the real world. Preservation of the ABL in the direction of the flow is achieved by means of modified wall functions.

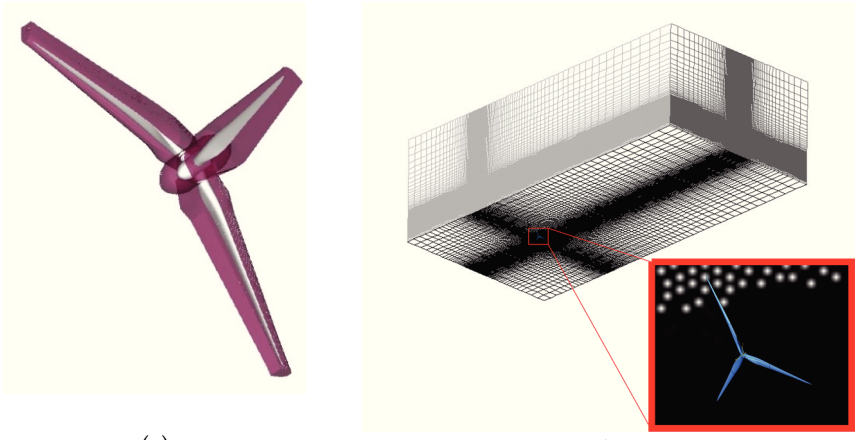

(a) (b)

Figure 119: Schematic overview of the employed 3D CFD grid. (a) The rotor with the cells for the boundary layer mesh indicated in magenta. (b) Overview of the total flow domain. The width and length of the domain are about ten and twenty times the rotor diameter respectively. Courtesy of Gilberto Santo, Ref. [25].

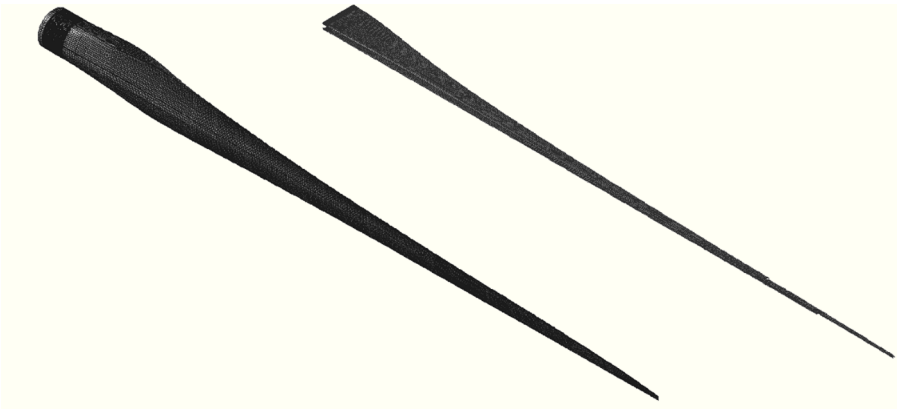

Figure 120: The blade structural model of the 49 m blade used as computational structural model (CSM) for the FSI simulations.

5.4.3 Results and conclusions

For details of the results, the reader is referred to Ref. [25]. As an example, the velocity magnitude of the resulting flow field can be seen in Figure 121.

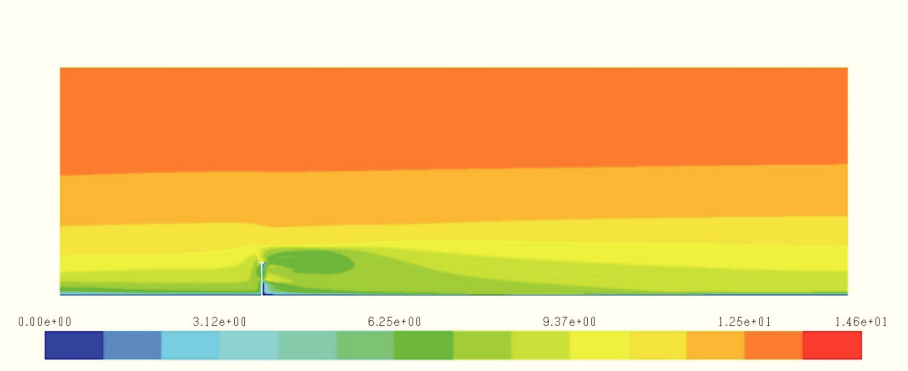

Figure 121: Contour plot of the velocity magnitude in a vertical plane through the tower and parallel to the incoming wind. Courtesy of Gilberto Santo Ref. [26].

In a nutshell, the approach successfully combines a stand-alone CFD solver, a stand-alone structural solver and a coupling code. The fluid structure interaction effects are significant, as the results differ between calculations using a rigid blade and the coupled approach. This can be seen in Figure 122, which shows the torque contribution from a single blade for both the rigid and flexible case as a function of the rotor position. The blades experience large deformations and a reduced power output is obtained. Including effects such as the ABL and gravity have a significant influence [26].

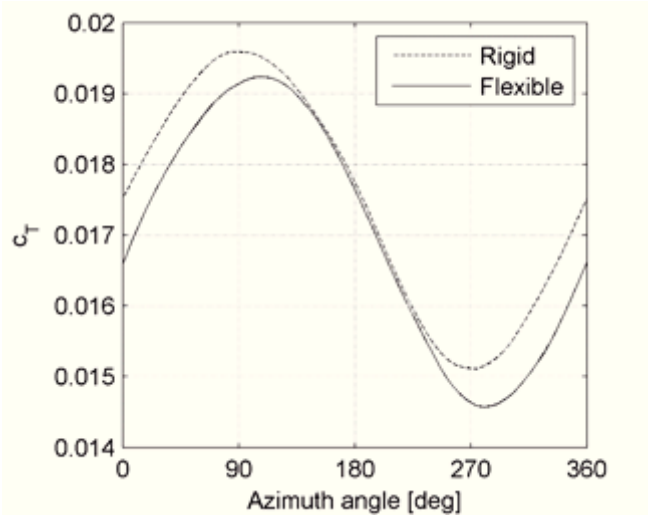

Figure 122: Single blade contribution to the rotor torque, showing a significant difference between the case in which the rotor is held rigid and that in which it is flexible. This proves the need to consider the FSI. Reproduced from Ref. [25].

5.5 Bibliography

[1] F. M. Jensen, H. Stang, and K. Branner, *Ultimate strength of a large windturbine blade*. 2009.

[2] C. L. Bottasso, P. Bortolotti, A. Croce, F. Gualdoni, and L. Sartori, "Aero-Structural Design of Rotors," presented at the Sandia Wind Turbine Blade Workshop, 2014.

[3] J. C. Berg, M. F. Barone, and N. C. Yoder, "SMART wind turbine rotor: data analysis and conclusions," *SAND2014-0712 Sandia Natl. Lab. Albuq. NM*, 2014.

[4] T. Barlas *et al.*, "Smart rotor blades and rotor control for wind turbines - State of the Art - Knowledge Base Report for UpWind WP 1B3," 2006.

[5] T. K. Barlas and G. A. M. van Kuik, "Review of state of the art in smart rotor control research for wind turbines," *Prog. Aerosp. Sci.*, vol. 46, no. 1, pp. 1–27, Jan. 2010.

[6] D. Castaignet *et al.*, "Full-scale test of trailing edge flaps on a Vestas V27 wind turbine: active load reduction and system identification: Full-scale test of trailing edge flaps on a Vestas V27 wind turbine," *Wind Energy*, vol. 17, no. 4, pp. 549–564, Apr. 2014.

[7] M. H. Dawson, "Variable Length Wind Turbine Blade," DE-FG36-03GO13171, May 2006.

[8] M. H. Dawson, "Final Technical Report," Energy Unlimited, Inc, Jun. 2005.

[9] M. Dawson and J. Wallace, "Variable Length Wind Turbine Blade Having Transition Area Elements," WO2010120595 (A1), 21-Oct-2010.

[10] M. Dawson and J. Wallace, "Mass-centralizing blade extension drive mount locations for wind turbine," US8231347 (B2), 31-Jul-2012.

[11] S. V. Pasupulati, J. Wallace, and M. Dawson, "Variable length blades wind turbine," in *Power Engineering Society General Meeting, 2005. IEEE*, 2005, pp. 2097–2100.

[12] T. D. Ashwill, "Passive load control for large wind turbines," *AIAA April*, 2010.

[13] V. Fedorov, C. Berggreen, S. Krenk, and K. Branner, "Bend-Twist Coupling Effects in Wind Turbine Blades," DTU Wind Energy, Denmark, 2012.

[14] C. l. Bottasso, F. Campagnolo, A. Croce, and C. Tibaldi, "Optimization-based study of bend–twist coupled rotor blades for passive and integrated passive/active load alleviation," *Wind Energy*, vol. 16, no. 8, pp. 1149–1166, Nov. 2013.

[15] K. K. Wetzel, "Utility Scale Twist-Flap Coupled Blade Design," *J. Sol. Energy Eng.*, vol. 127, no. 4, p. 529, 2005.

[16] K. Cox and A. Echtermeyer, "Geometric Scaling Effects of Bend-twist Coupling in Rotor Blades," *Energy Procedia*, vol. 35, pp. 2–11, 2013.

[17] T. Ashwill, "Sweep-Twist Adaptive Rotor Blade: Final Project Report," Sandia National Laboratories, SAND2009-8037, Jan. 2010.

[18] K. K. Wetzel, "Wind turbine rotor blade with in-plane sweep and devices using same, and methods for making same," US7344360 (B2), 18-Mar-2008.
[19] K. Branner *et al.*, "Anisotropic beam model for analysis and design of passive controlled wind turbine blades," DTU Wind Energy, 2012.
[20] *Abaqus 6.14 Online Documentation, Dassault Systèmes*. 2014.
[21] R. Simon, "RE: FW: Verification of the models."
[22] J. Degroote, P. Bruggeman, R. Haelterman, and J. Vierendeels, "Stability of a coupling technique for partitioned solvers in FSI applications," *Comput. Struct.*, vol. 86, no. 23–24, pp. 2224–2234, 2008.
[23] J. Degroote, M. Hojjat, E. Stavropoulou, R. Wüchner, and K.-U. Bletzinger, "Partitioned solution of an unsteady adjoint for strongly coupled fluid-structure interactions and application to parameter identification of a one-dimensional problem," *Struct. Multidiscip. Optim.*, vol. 47, no. 1, pp. 77–94, 2013.
[24] J. Degroote, "Development of algorithms for the partitioned simulation of strongly coupled fluid-structure interaction problems," dissertation, Ghent University, 2010.
[25] G. Santo, M. Peeters, W. Van Paepegem, and J. Degroote, "Dynamic load and stress analysis of a large Horizontal Axis Wind Turbine using full scale fluid-structure interaction simulation," *Renewable Energy*, p. Under review.
[26] G. Santo, M. Peeters, W. Van Paepegem, and J. Degroote, "The effect of gravity in transient fluid-structure interaction simulations of a large wind turbine with composite blades," presented at the 8th International Conference on Textile Composites and Inflatable Structures, 2017.

6 Modelling of wind turbine blade static certification tests

"Keep your eyes on the stars and your feet on the ground." - *Theodore Roosevelt*

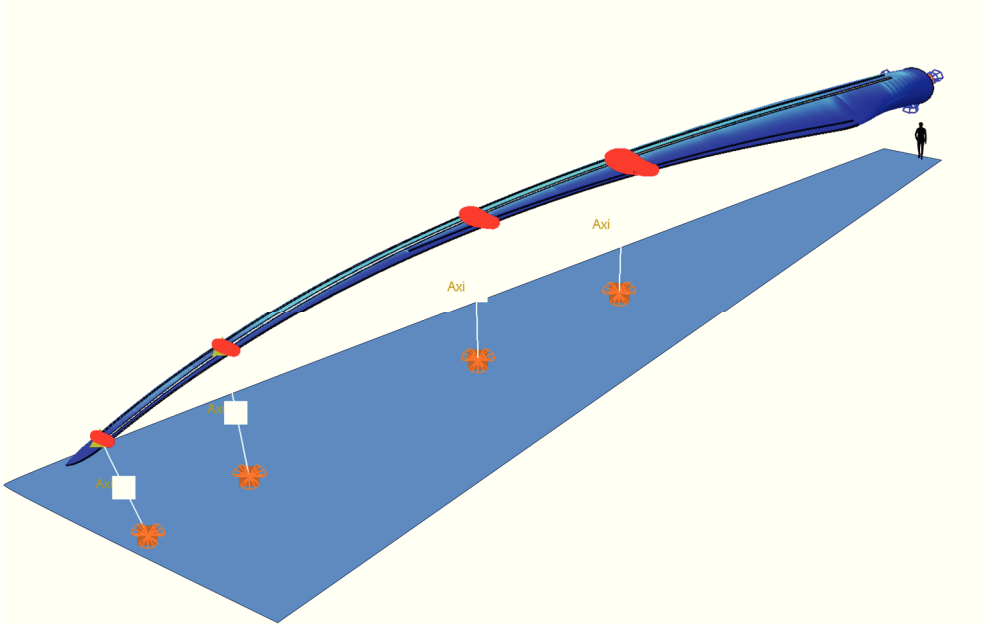

Chapter summary: In this chapter, the modelling of static certification tests for wind turbine blades is investigated. The certification tests for a 43 m blade are analyzed using FE models and the results are compared to data from the experimental tests. This is done using both conventional shell and advanced solid models. It is found that for the specific blade and load case, both modelling methods result in displacement and strain values that align with the experimental results.

This chapter is based on the paper "Comparison of Shell and Solid Finite Element Models for the Static Certification Tests of a 43 m Wind Turbine Blade" in the Energies journal [1].

6.1 Introduction: Wind turbine blade static tests

To provide confidence in a new blade design, a full-scale prototype is typically manufactured and tested under static loads. These loads are calculated from the extreme loads that are obtained as a result from aero-elastic calculations, amplified by safety factors (SF). This kind of testing is typically required as part of the blade certification process, in which a third party assesses the soundness of the design. Often, the test procedure is elaborate and consists of static tests in the main four directions (LE to TE, TE to LE, PS to SS and SS to PS), followed by a fatigue test and a subsequent repetition of the static tests. This proves the ability of the blade design to survive the extreme loads even at the end of its design life.

6.2 Modelling of the static blade tests

The static tests are often modelled using the FE method. This happens for two reasons. Firstly, the certification process of a blade represents a significant financial investment. Secondly, along with the static blade tests, the certification bodies typically require the manufacturer to present expected strain and deformation levels for the static tests in order to certify the design. The most accurate way to obtain these values is by means of FE modelling. In addition, the modelling of the static tests provides a rare opportunity to validate the blade models with experimental values. The static tests are conducted in a laboratory, where the applied boundary conditions are known and the applied loads are accurately measured. Furthermore, the blade is accessible and a wide variety of measurement equipment can be used. This stands in sharp contrast to a rotor blade in operation. In such case, the blade itself is not easily accessible making it much more difficult to apply measurement equipment. In addition, the loads exerted on the rotor by the surrounding airflow are typically not known and are therefore difficult to model.

6.3 Investigation of the static certification tests of a 43 m blade

6.3.1 Materials and methods

6.3.1.1 Experimental static tests

The 43 m blade was experimentally tested under static loads at a certified test center. The tests were conducted by bolting the test blade onto a reaction block using the normal T-bolt root connection. Figure 123 shows the position of the reaction block, which lifts the blade of the laboratory (LAB) floor and tilts the blade to an angle relative to the lab floor. Fixtures, also referred to as “saddles”, are mounted onto the blade. These are made of wood, cut to fit precisely on the outside of the blade, covered by a steel frame. A layer of rubber is placed in

between the blade and the saddle to provide friction. These are placed at four different span-wise positions. Subsequently, cables are attached to the fixtures and connected to pulleys on the lab floor. The cables are attached at such a position on the fixture that the applied force is approximately in line with the shear center of the blade section, as shown in Figure 124. The pulleys are positioned so that at maximum load the cables connecting the pulleys to the fixtures are approximately vertical.

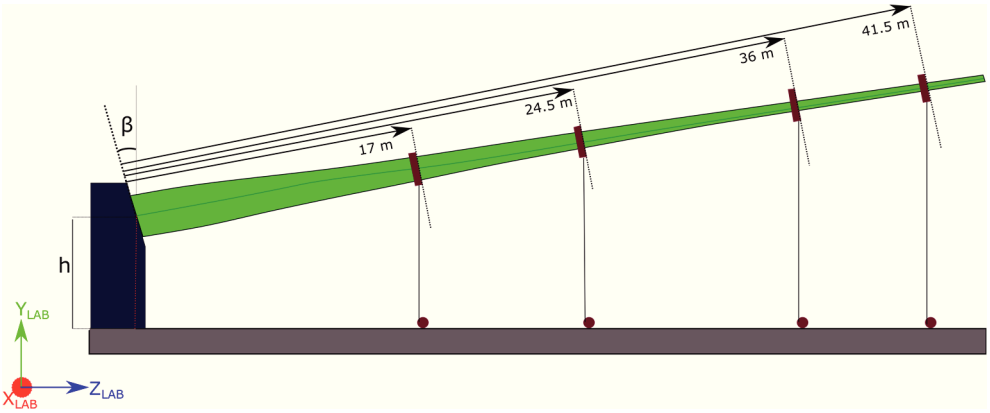

Figure 123: Schematic overview of the static test setup. The blade is positioned onto the reaction block at a height h of approx. 4.5 m at an angle of 13 °. The lab coordinate system is positioned as indicated. Different load cases are created by mounting the blade onto the test stand under a different pitch angle.

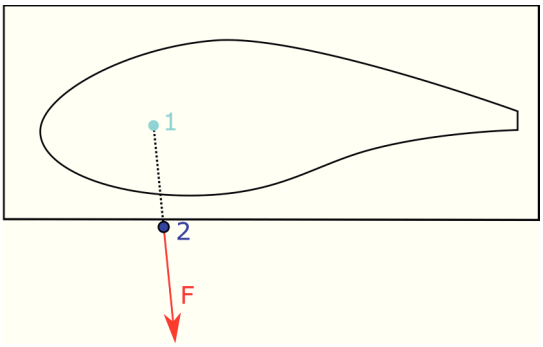

Figure 124: The cables are attached to the saddles at a position (2) which approximately results in the applied load (F) to be applied in line with the shear center (1).

Four different load cases are experimentally tested: positive flat-wise, negative flat-wise, positive-edgewise and negative edge-wise. These can be seen in

Figure 125. For each test case, the loads are incremented during five subsequent steps. Between increments, all data from measurement equipment are recorded. These data include: (i) the load on every individual cable, (ii) the reaction moments at the blade root, (iii) the displacement of each of the fixtures and (iv) strains at many strain gauge locations. The longitudinal strains are measured at a series of span-wise locations on the middle of each of the girders and near the leading edge (LE) and trailing edge (TE) as well as on the shear webs. Additionally, transverse strains are measured at several locations where high strains were observed in the results of preliminary calculations.

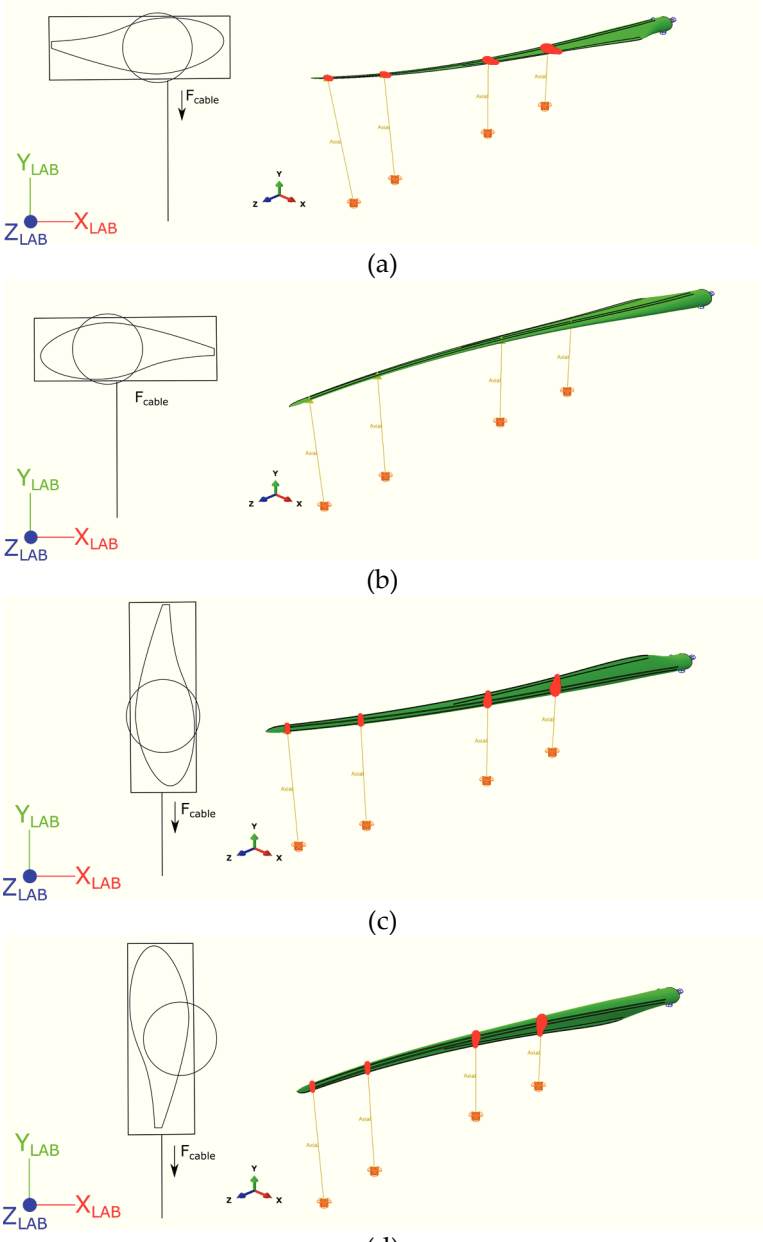

Figure 125: Schematic overview of the different load cases. The different loads are created by attaching the blade to the test stand at a different pitch angle. (a) Blade positioned for the positive flat-wise load-case. (b) Blade positioned for the negative flat-wise load-case. (c) Blade positioned for the positive edge-wise load-case. (d) Blade positioned for the negative edge-wise load-case.

6.3.1.2 *Models of a segment of the spar structure*

To limit the complexity, in a first step, a 10 m long portion of the blade's spar structure is modelled. This can be seen in Figure 126. The layup of the girders is simplified in this model to consist of only uni-directional (UD) GFRP material. At the inboard end of the model, a multi-point-constraint (MPC) of the type "beam" is applied, which rigidly connects the surface to a reference node. Similarly, at the outboard end, a master node is connected to the surface, but by means of a "continuum distributing coupling", which distributes the loads. Three different load cases are considered: pure-flap-wise load, combined flap-wise and edge-wise load and torsion. An overview of the load cases can be seen in Table 16.

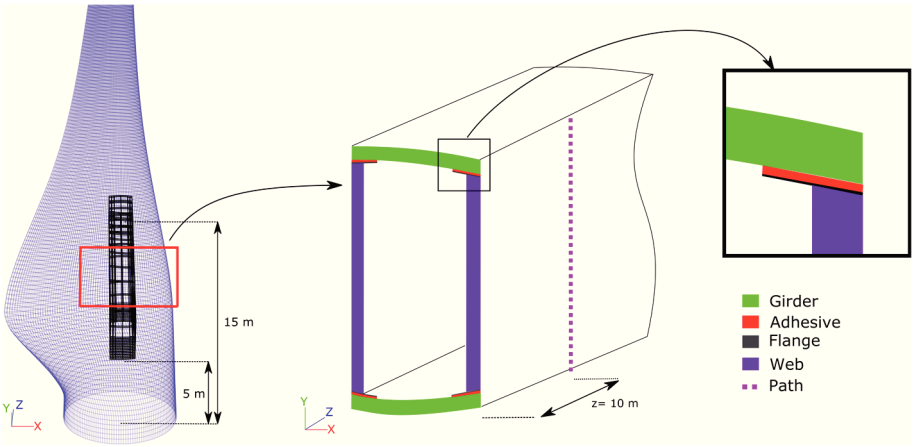

Figure 126: In a first approach, the model is limited to a portion of the spar. (left) Spar segment in the overall blade. (middle) Front view of the spar, showing the UD girders, shear webs with flanges and adhesive bonds. A path for the extraction of data from the simulations is added on the side of the model over the full height of the spar. (right) Close-up view of a corner of the spar segment.

Table 16: Overview of the considered load cases for the spar segment.

Load Case	**Tip Side Load**	**Load Magnitude**
Flapwise	Flap-wise concentrated force Fx	150 kN
Combined	Flap-wise and edge-wise concentrated force Fx, Fy	150 kN, 50 kN
Torsion	Torsional moment Mz	0.3 kNm

6.3.1.3 Full scale blade models

To model the full-scale blade tests, FE models of the full structure are created using the newly developed block-based approach. Both a model consisting of second order shell elements (type S8R) positioned on the OML and a model consisting of layered second order solid elements (C3D20R) are created. Second order shell elements are used for their more advanced transverse shear behavior. Second order solids are used to avoid locking issues. The models include accurate material orientations defined for every element individually. Cross-sections of these models along with the local material orientations on a slice of the mesh can be seen in Figure 127.

Data are extracted from the simulations in an automated fashion. At the blade root a single master node is rigidly connected to the circumference. Reaction moments and displacements are obtained from this node. Strain values are obtained from nodes at the blade OML surface. The strain values at the integration points are extrapolated to the nodal positions. For each node, the strain values are then calculated by averaging these values for the connected elements, considering only the top or bottom section point. For the longitudinal strain values on the girders, node sequences along the entire girder are used while for the other strain gauge positions individual nodes are used.

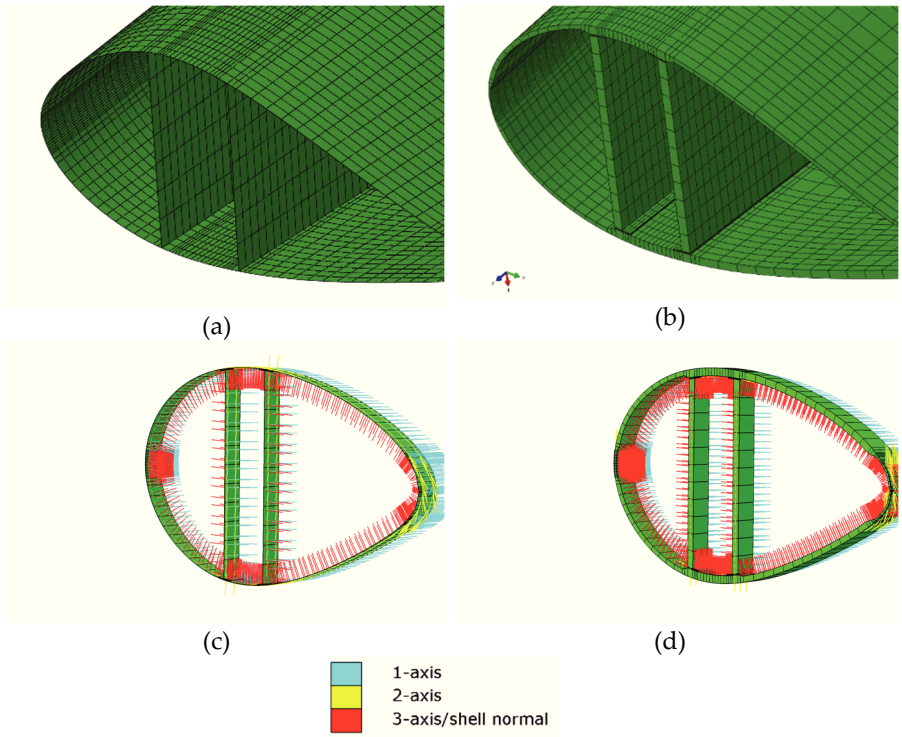

Figure 127: Cross-sections of the different FE models. (a) Conventional OML shell model, consisting of second order S8R elements. (b) Model consisting of second order, layered solid elements C3D20R. (c) Slice of the OML shell model showing the local material orientations. (d) Slice of the solid model showing the local material orientations.

6.4 Results and discussion

6.4.1 Investigation of the spar segment

To ensure validity in comparing the OML shell and solid models, the mass and center of gravity (COG) of both models are compared. It is found that these differ less than 1 %. In a subsequent step, mesh refinement analysis is conducted. Different mesh densities are produced and the displacement of the master node as well as strains along the top of the girders are extracted and compared. This is done separately for the length-wise and chord-wise densities as well as for the seeding in the spar's height direction for the webs, adhesive and girders. From the results it became apparent that the coarsest version of the mesh in longitudinal and chord-wise direction of average size of 100 mm was sufficient. Furthermore, the shear web mesh was found to be sufficiently refined with only two second-order elements over the height.

If we compare the displacements and rotations of the master node at the outboard end of the segment, we notice that the absolute differences are very limited. This means that the overall stiffness of the structure is accurately modeled using the OML shell approach. However, some differences appear when we compare the stress values along a path on the side of the spar at the half-length position, shown in Figure 126. In the resulting graphs, plotted in Figure 128, the presence of the adhesive bond and girders becomes apparent in the solid models, while the side wall of the OML shell model does not contain these features.

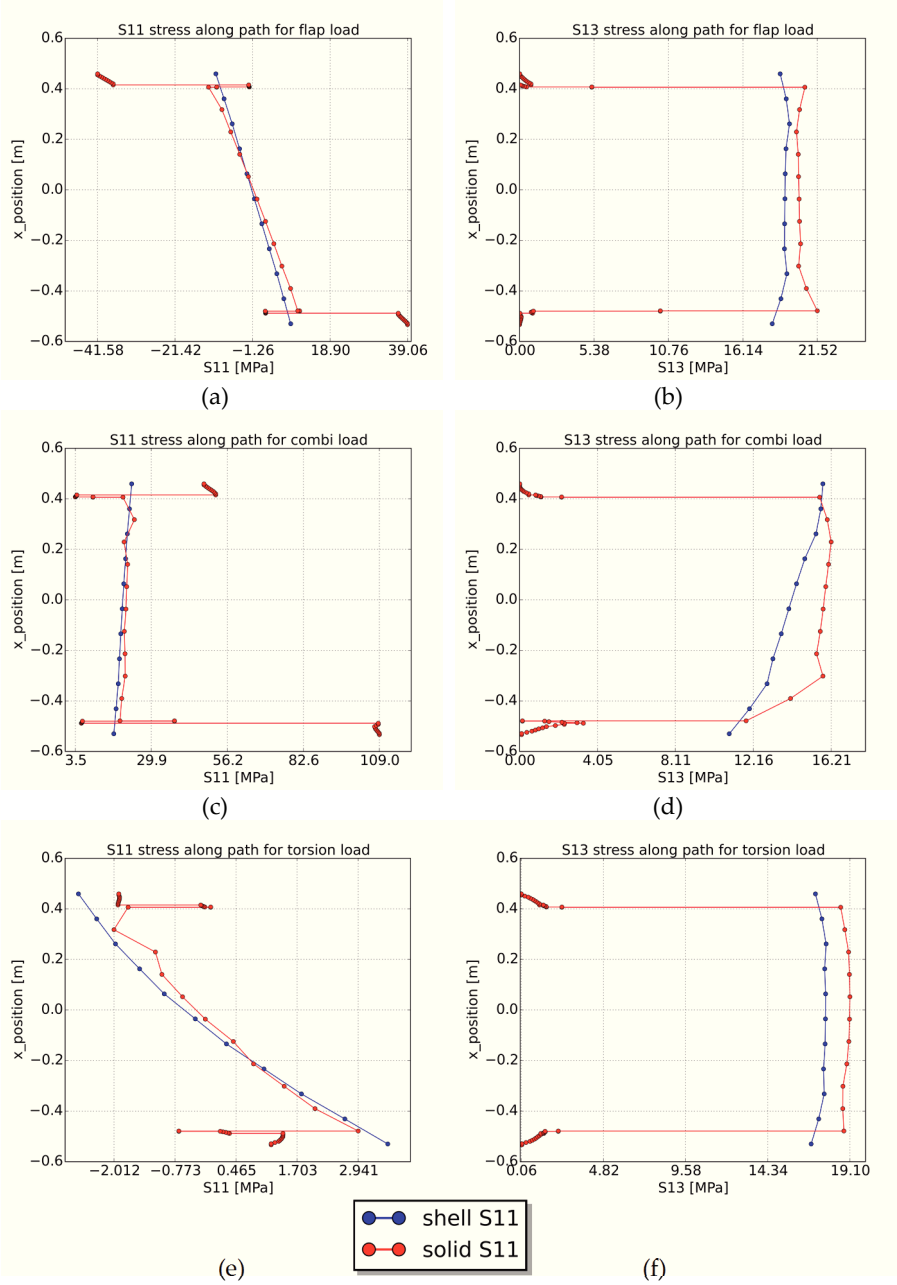

Figure 128: Plots of the stress values along a path on the side of the spar model for different load cases. (a) Longitudinal stress S11 for the flap-wise load case. (b) Shear stress S13 for the flap-wise load case. (c) Longitudinal stress S11 for the combined flap and edge-wise load case. (d) Shear stress S13 for the combined load case. (e) Longitudinal stress S11 for the torsion load case. (f) Shear stress S13 for the torsion load case.

6.4.2 Investigation of the boundary conditions for static tests

After exploring the modelling of a spar segment, the investigation can progress to the more complex full-scale case. First, the boundary conditions and settings for correctly modelling the static blade tests are explored. To mimic the tests as closely as possible, the models are spatially positioned to match the position of the blade in the LAB-coordinate system. This can be seen in Figure 125. This is relevant since the deformation under gravity load is significant. The strain gauges used in the experiments are zeroed after the blade is positioned and is only loaded by gravity.

As mentioned, at the blade root connection, an MPC is used to rigidly connect all nodes to a single central master node of which the displacements and rotations are fully constrained. This allows simple extraction of the root bending moment and mimics the behavior of the T-bolt root connection which prevents both displacement and rotation.

At the different load introduction positions, a master node is connected to a portion of the blade by means of a distributing coupling. This connection spreads the load of the master node over the slave nodes, without preventing deformation of the cross-section. As mentioned, cables are used to introduce the loads in the experimental tests. This means that the orientation of the force acting on the blade fixture depends on the deformation of the blade. To include this non-linear load introduction, the cables are modelled by means of axial connector elements. Applying a connector force to these elements results in a concentrated force pointing from one end to the other end of the connector, thereby mimicking the cable. Such an approach was also used in Haselbach et al. [2].

6.4.2.1 Importance of geometric non-linearity

Several authors have demonstrated the need for the use of non-linear geometry. Both options were applied to the conventional shell model. The resulting blade deformation differs significantly, as can be seen in Figure 129. This clearly demonstrates the need to use non-linear geometry.

6.4.2.2 The influence of the cables

To study the effect of modelling the cables used for introducing the loads, the AXIAL connector elements are replaced by concentrated forces along the LAB y-direction. These do not follow the rotation of the master node, but stay aligned with the y-direction. It is found that the difference in results is very limited. One exception is that the observed resulting root bending moment is slightly higher (less than 1 % in all cases) with the concentrated forces. This is not entirely unexpected since at full load, most cables are approximately, but not perfectly vertical and therefore introduce a very similar load as the concentrated forces.

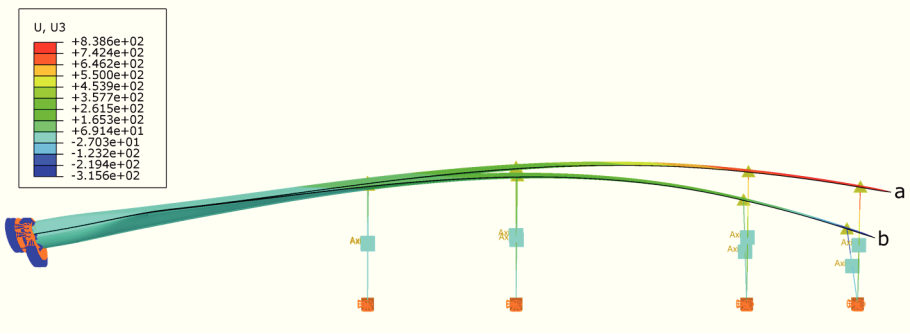

Figure 129: Contour plots of the displacements in the z-direction of the conventional OML shell model on the deformed shape under static load. (a) The result obtained from a geometrically linear calculation. (b) The result from a geometrically non-linear calculation.

6.4.2.3 *The influence of the coupling*

In literature, it has been suggested that the clamps at the load introduction points restrict the deformation of the blade cross-section and thereby influence the test [3]. To investigate this aspect, the fixture's distributing couplings were replaced by MPC's of the type beam [4], preventing deformation of the section. The results can be seen in Figure 130. It is clear that in the area of the fixtures, the transverse strains are forced to remain zero. However, strains at the locations with strain gauges do not show significant difference. It is worth mentioning that the position of the clamps is chosen based on the structural layup. Areas which are deemed critical to the design or which contain rapid changes in layup are typically avoided.

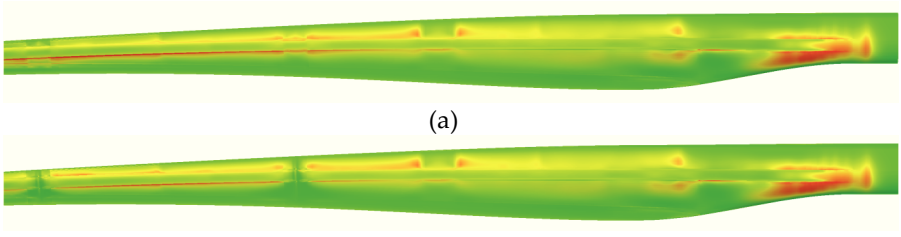

(a)

(b)

Figure 130: Contour plots of the transverse true strain values of the blade loaded under the negative flat-wise load case. Different methods are used to connect the blade to the master nodes at which the loads are introduced. The differences appear limited to the vicinity of the connections. (a) Result obtained using a "flexible" distributing coupling. (b) Result obtained using a "rigid" multi-point-constraint (MPC).

6.4.3 Comparison of shell and solid models: full scale blade

6.4.3.1 Root bending moment

The applied loads are validated by comparing the resulting root bending moments. As mentioned, the magnitude of the applied connector loads is based on measured load cell values during the actual experimental tests. The resulting root bending moment is therefore compared to the measured values, as can be seen in Figure 131. This shows good similarity for each of the different load cases.

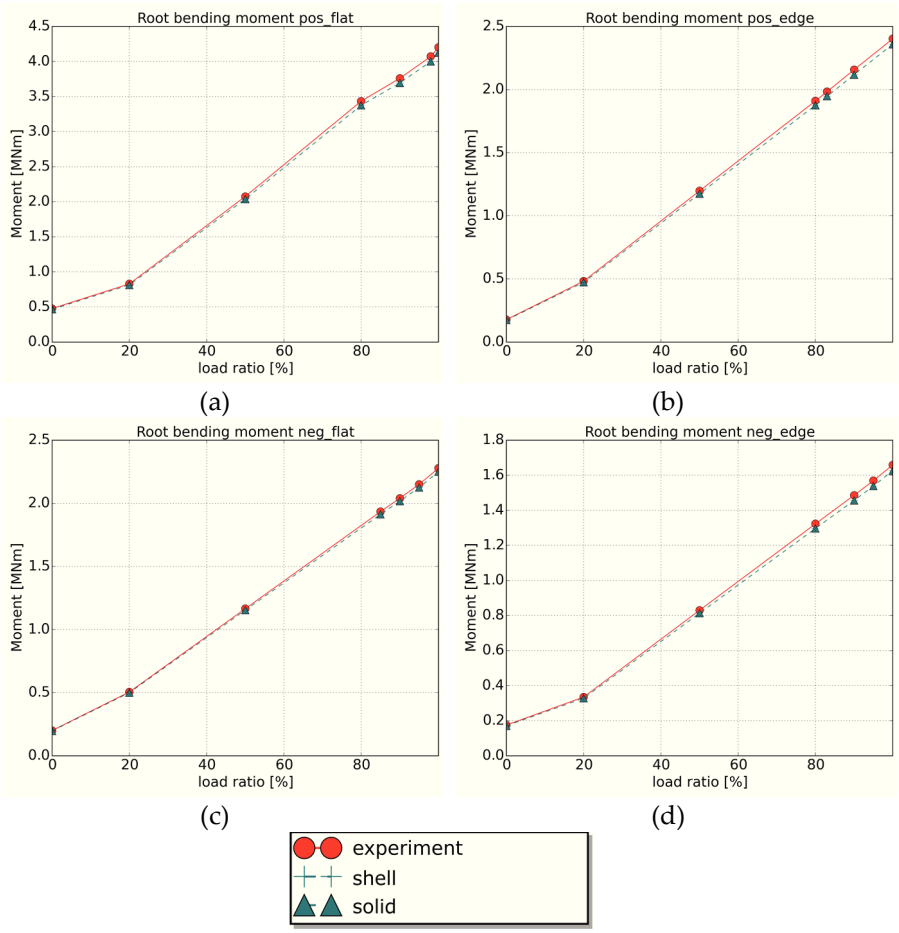

Figure 131: Root bending moment about the x-axis in the lab coordinate system for the different load cases. (a) Positive flat-wise load case. (b) Positive edge-wise load case. (c) Negative flat-wise load case. (d) Negative edge-wise load case.

6.4.3.2 *Displacement of the saddles*

Subsequently, the displacements of the master nodes of the fixtures are extracted and compared to the measured displacements of the saddles. The vertical displacements (LABy-direction) are shown in Figure 132, while the sideways displacements (LABx-dirction) are shown in Figure 133 and those in the LAB z-direction are shown in Figure 134. The shell and solid models provide very similar displacements in all directions. Some differences can be observed between the measured and predicted values. These appear most pronounced in the LAB x-direction. However, the absolute values of these displacements are very small. Furthermore, the differences may be a result of modelling assumptions, variations in material properties or tolerances of the blade, test set-up and measurements.

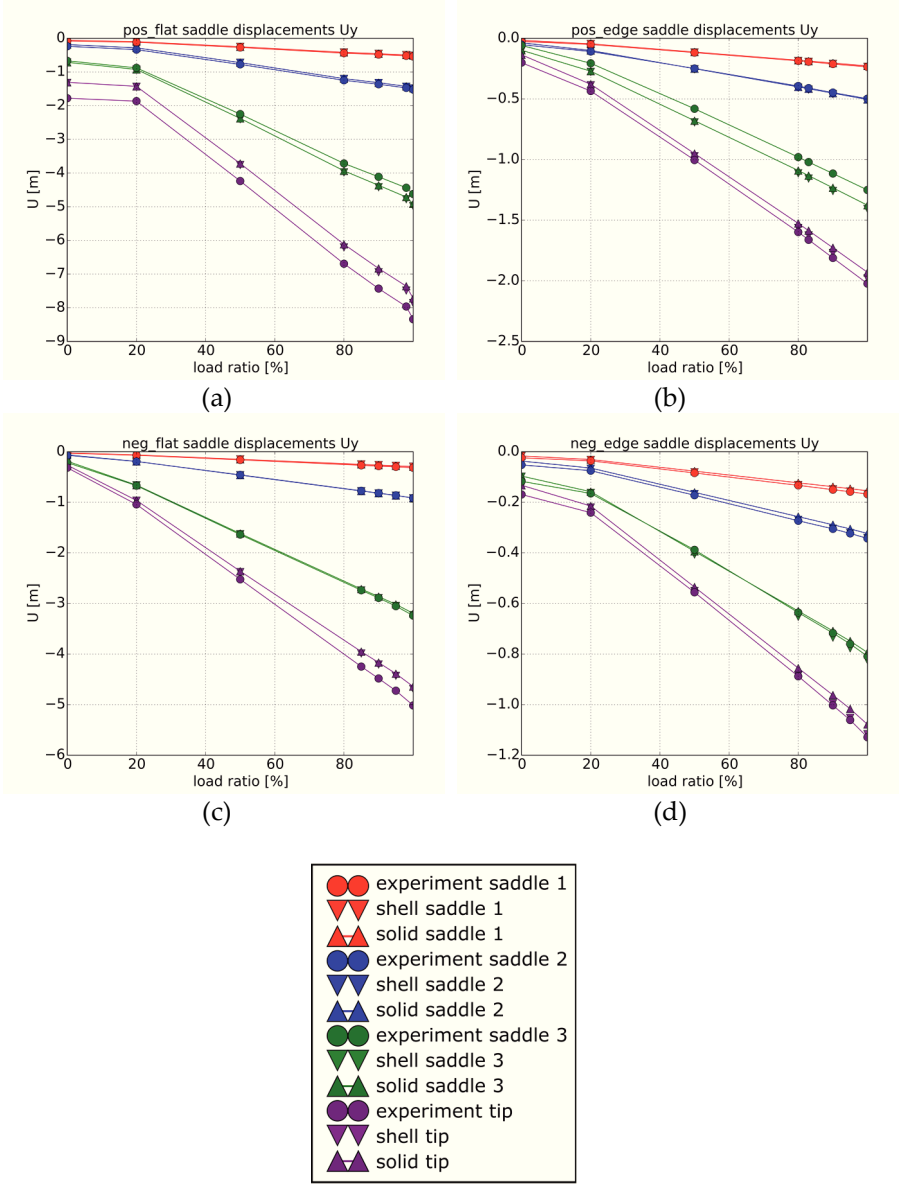

Figure 132: Saddle displacements Uy for the different load cases. The shell and solid models closely agree and correspond well to the experimental results. (a) Positive flat-wise load case. (b) Positive edge-wise load case. (c) Negative flat-wise load case. (d) Negative edge-wise load case.

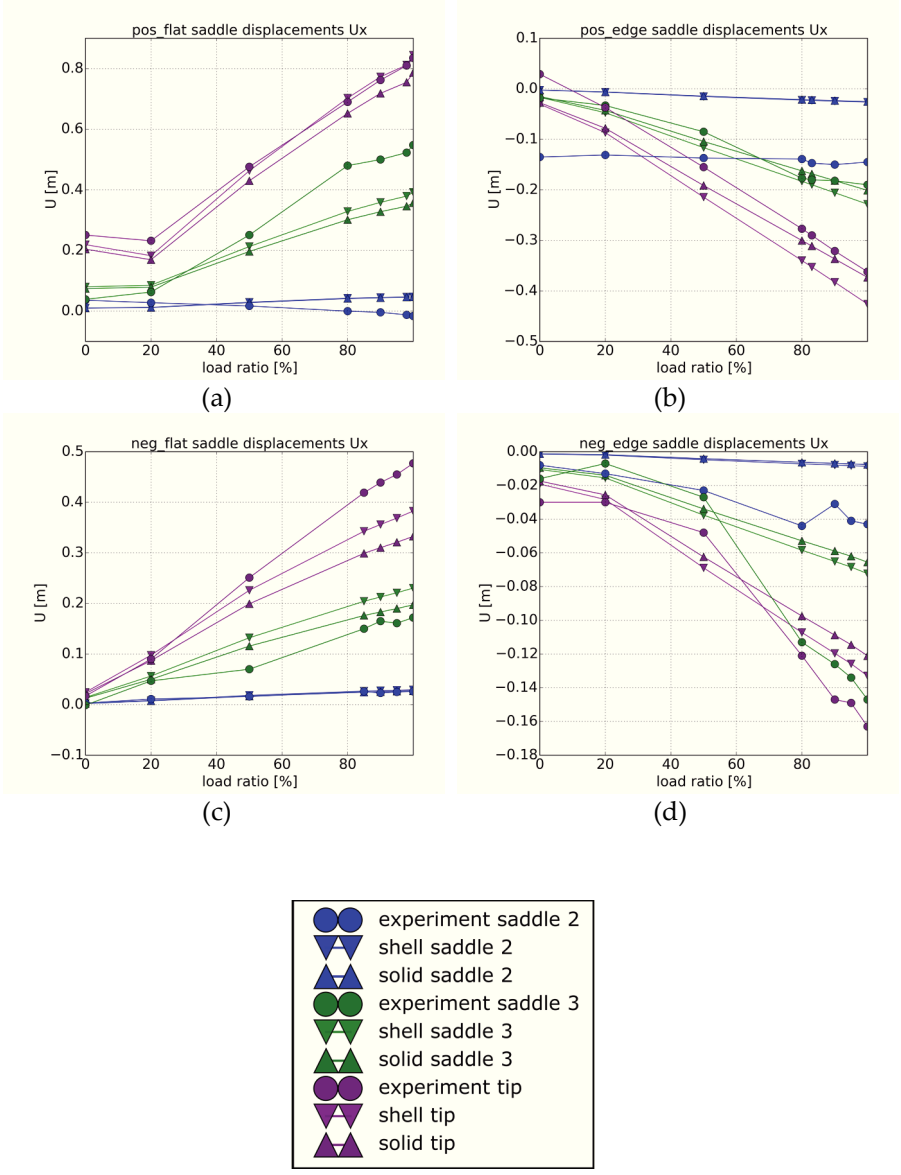

Figure 133: Saddle displacements Ux for the different load cases. Both the shell and solid models show similar patterns to the experimental values. (a) Positive flat-wise load case. (b) Positive edge-wise load case. (c) Negative flat-wise load case. (d) Negative edge-wise load case.

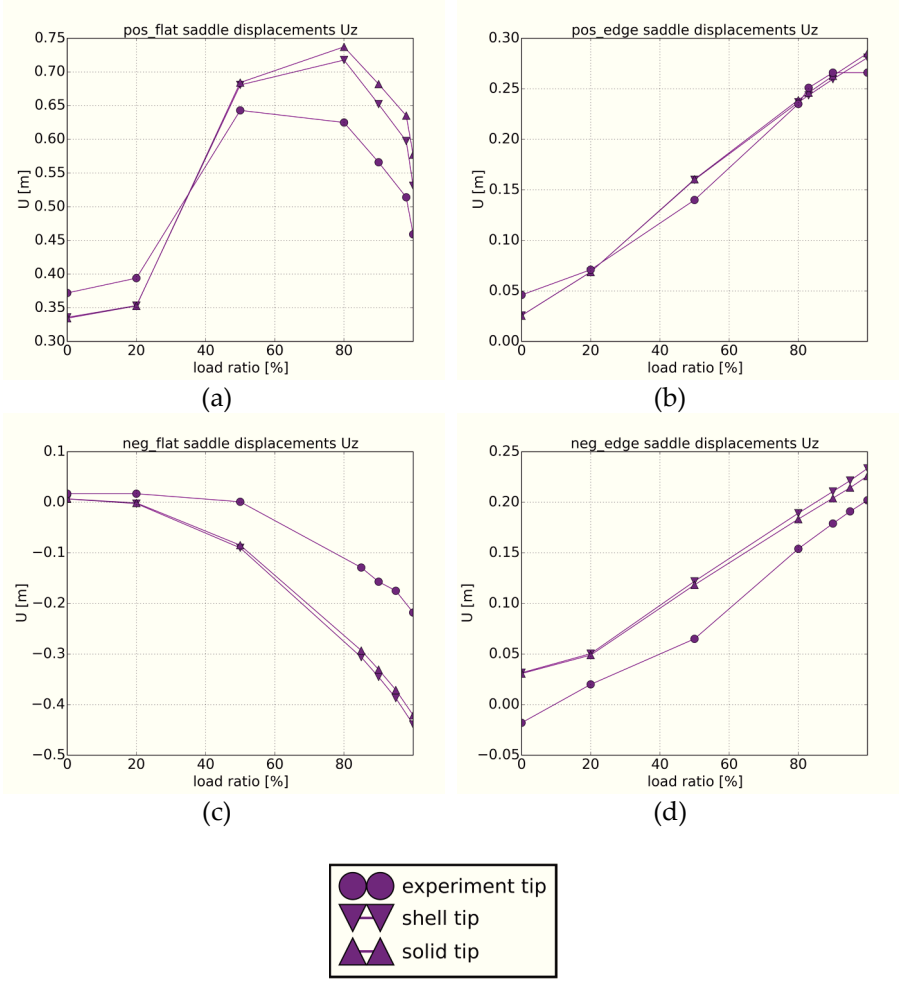

Figure 134: Saddle displacements Uz for the different load cases. The shell and solid models agree quite well and show a similar pattern as the experimentally measured values. (a) positive flat-wise load case. (b) Positive edge-wise load case. (c) Negative flat-wise load case. (d) Negative edge-wise load case.

6.4.3.3 *Longitudinal strain values*

Longitudinal strain values are measured during the static tests and data from paths on the mesh are extracted to allow comparison. The data for the strain values on the girders are presented in Figure 136 and Figure 137 while the data for the strain values along the LE and TE are presented in Figure 138.

The simulations show very similar values as the experiments. One path where this seems to differ is the TE girder on the SS, which can be seen in Figure 136. While

the simulations predict a symmetric behavior, the experimentally measured strain values show a different picture. One possible explanation for this discrepancy could be the over-lamination of the adhesive joint between the TE girders and TE web. Such features are typically used to reinforce the joint. An example can be seen in Figure 135. This kind of reinforcement is very effective. In Ref. [5] it was even concluded that such features can dramatically increase the fatigue life of the connection (by a factor of 30 for low cycle fatigue and 50 for high cycle fatigue). The over-lamination is present on both the PS and SS, but runs only for a very short distance on the SS, while on the PS it covers the full length of the shear web in this particular blade. This asymmetry is not included in the models and may explain the difference in longitudinal strain on the TE girders.

Furthermore, the data show a good match between the shell and solid models. While very slight discrepancies between both modelling approaches are present, it is not clear which method provides more accurate results.

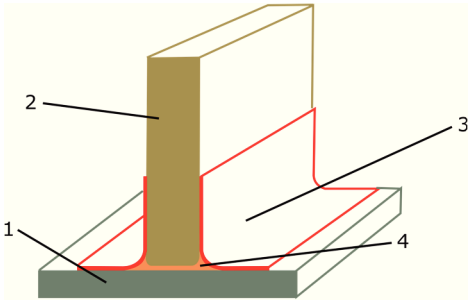

Figure 135: A joint between the outer shell and a shear web, that is over-laminated using hand layup in order to reinforce the adhesive joint. This drastically increases the fatigue life of the joint. (1) Outer shell laminate. (2) Shear web. (3) Over-laminate. (4) Adhesive.

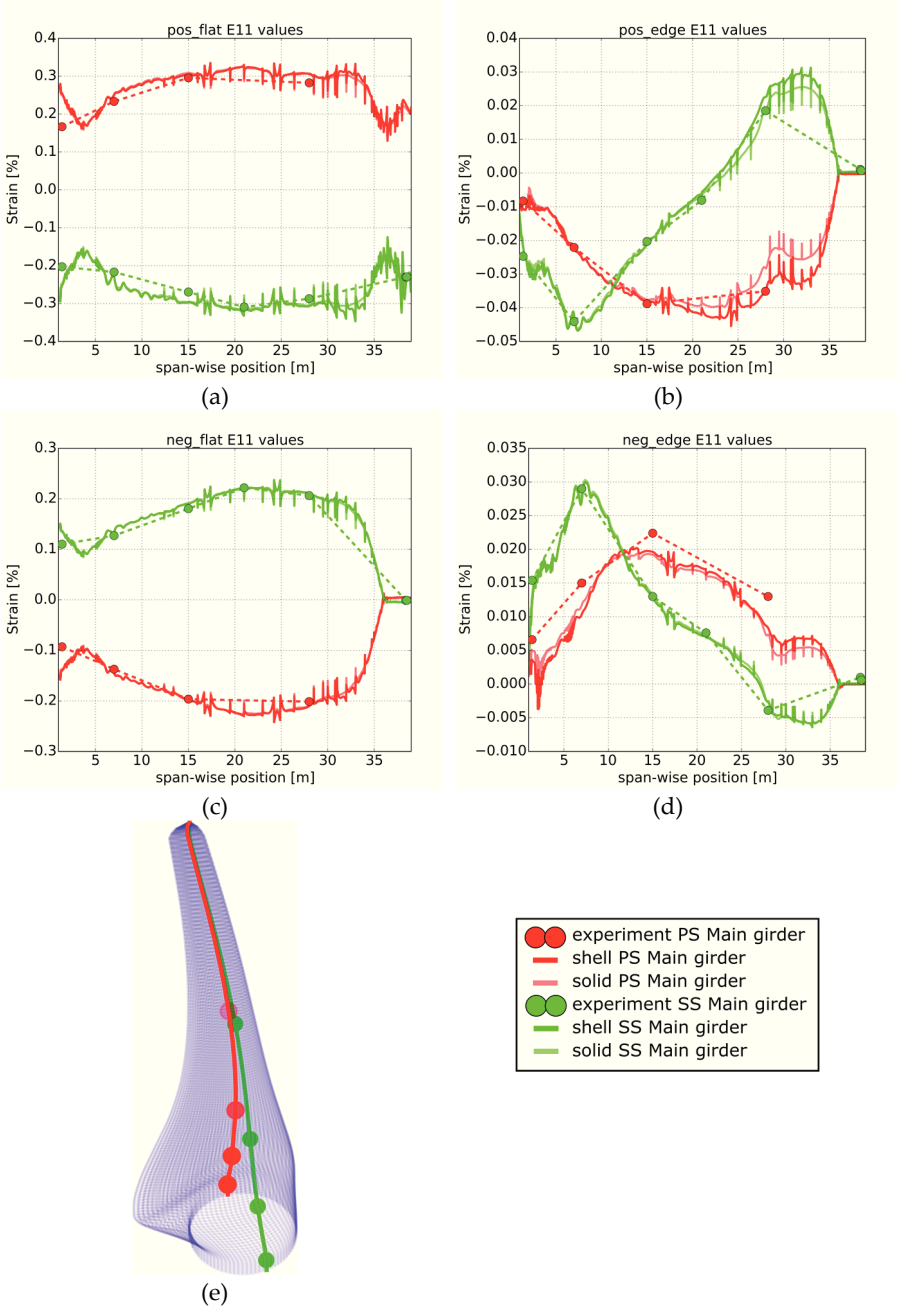

Figure 136: Overview of the true strain in the longitudinal direction along the different paths positioned on the main girders. (a) Positive flat-wise load case. (b) Positive edge-wise load case. (c) Negative flat-wise load case. (d) Negative edge-wise load case (e) 3D plot of the path and strain gauge locations on the blade OML surface.

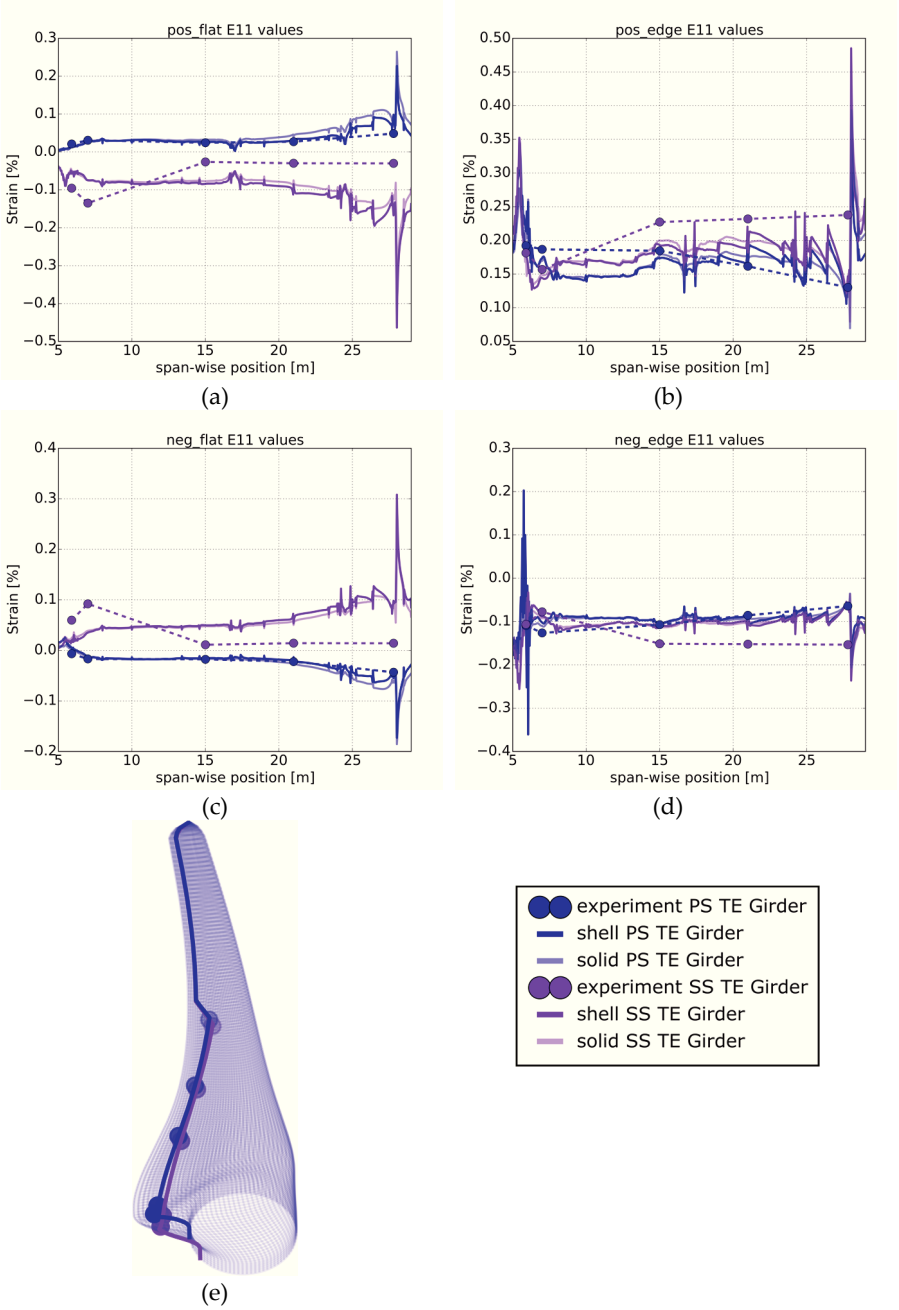

Figure 137: Overview of the true strain in the longitudinal direction along the different paths positioned on the TE girders. (a) Positive flat-wise load case. (b) Positive edge-wise load case. (c) Negative flat-wise load case. (d) Negative edge-wise load case. (e) 3D plot of the path and strain gauge locations on the blade OML surface.

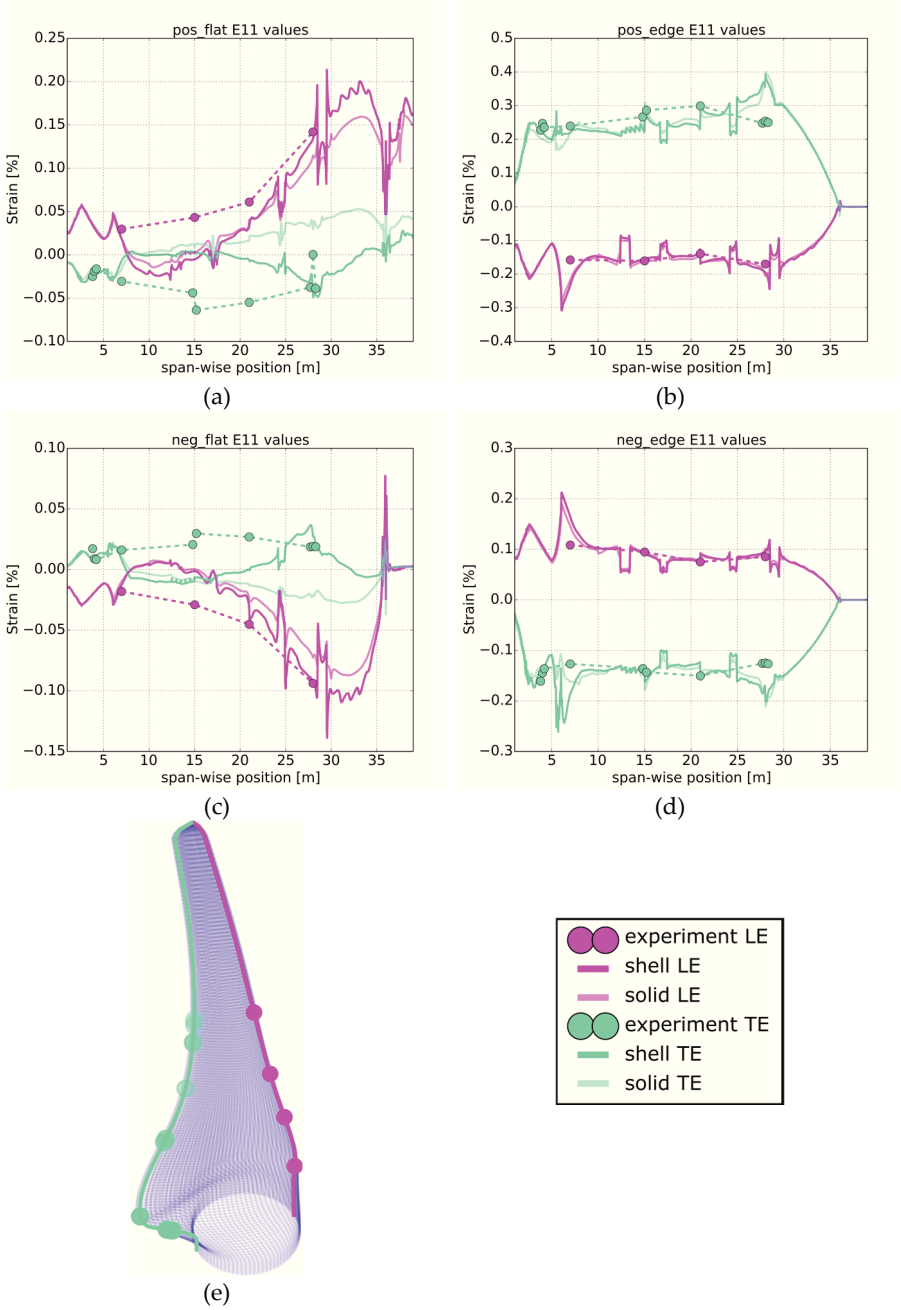

Figure 138: Overview of the true strain in the longitudinal direction along the paths on the LE and TE. (a) Positive flat-wise load case. (b) Positive edge-wise load case. (c) Negative flat-wise load case. (d) Negative edge-wise load case. (e) 3D plot of the path and strain gauge locations on the blade OML surface.

OML shell model	Solid model
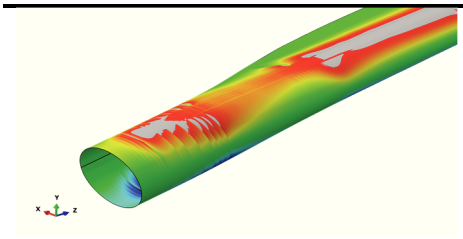	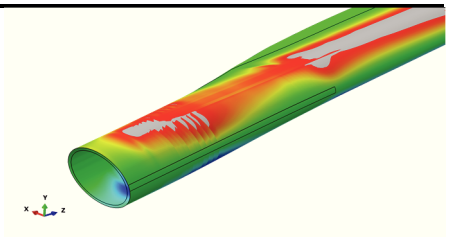
(a)	(b)
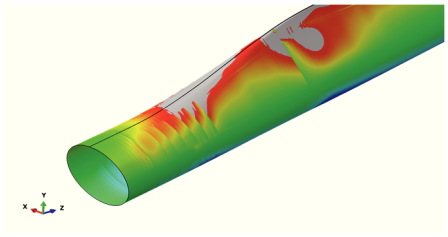	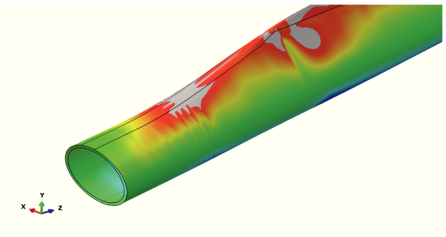
(c)	(d)
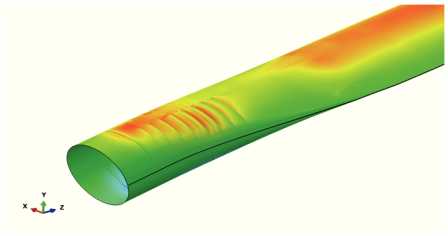	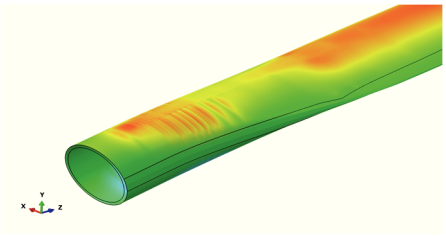
(e)	(f)
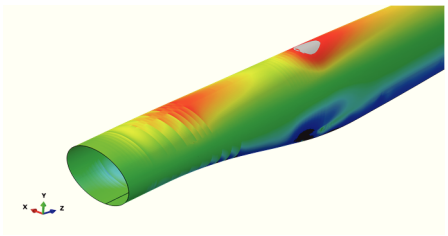	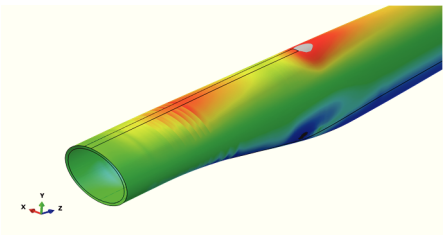
(g)	(h)

Figure 139: Contour plot of the longitudinal strain on the blade under the different load cases for the shell and solid models. (a) OML shell model under the positive flat-wise load-case. (b) Layered solid model under the positive flat-wise load-case. (c) OML shell model under the positive edge-wise load-case. (d) Layered solid model under the positive edge-wise load-case. (e) OML shell model under the negative flat-wise load-case. (f) Layered solid model under the negative flat-wise load-case. (g) OML shell model under the negative edge-wise load-case. (h) Layered solid model under the negative edge-wise load-case.

Furthermore, in Figure 139 contour plots of the longitudinal strain under negative flat-wise load case are displayed for the shell and solid models. While both plots show a very similar image, more rapid changes in strain value can be observed in the shell model. This can be explained by the fact that the solid model has a continuous thickness, with gradual transitions, whereas in the shell model, the thickness changes are instant.

6.4.3.4 Transverse strain values

Furthermore, strain values were measured in the transverse direction. These are compared to the values obtained at the same locations in the models. The strain values are found to be very large in some regions. This can be attributed to large non-linear deformations of the cross-section. Figure 140 and Figure 141 show strain values for the different load cases. Some differences between the results obtained from shell and solid modelling can be observed. In general, the differences between the shell and solid models are limited. Furthermore, the strains observed in the actual tests are larger than those observed in the simulations. An exception is in the strains measured next to the main girders. These correspond well to the results from the shell and solid models for the flat-wise load cases, but differ for the edge-wise load cases. The reason for this is unclear.

In Figure 142, contour plots of the transverse strains are shown for the negative flat-wise load case. A nearly identical strain distribution is observed. Again, slightly more gradual changes are visible in the solid model compared to the shell model, due to the gradual thickness transition inherent to the solid model. Hot spots are visible in the transition zone next to the main girder.

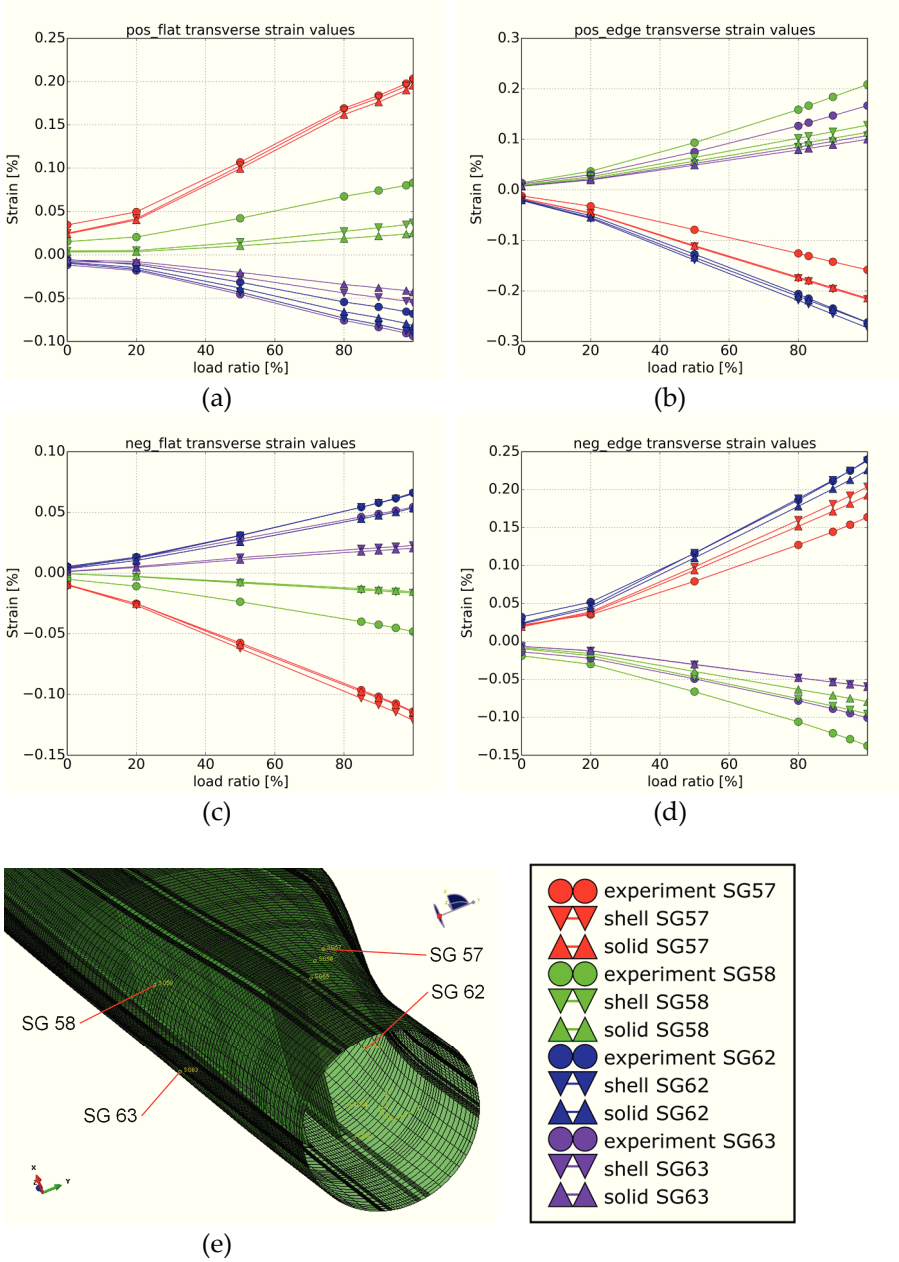

Figure 140: Overview of the true strain values in the transverse directions at four locations on the blade surface. (a) Positive flat-wise load case. (b) Positive edge-wise load case. (c) Negative flat-wise load case. (d) Negative edge-wise load case. (e) Overview of the strain gauge (SG) locations on the blade shape. The considered strain gauges are all positioned on the outside of the blade.

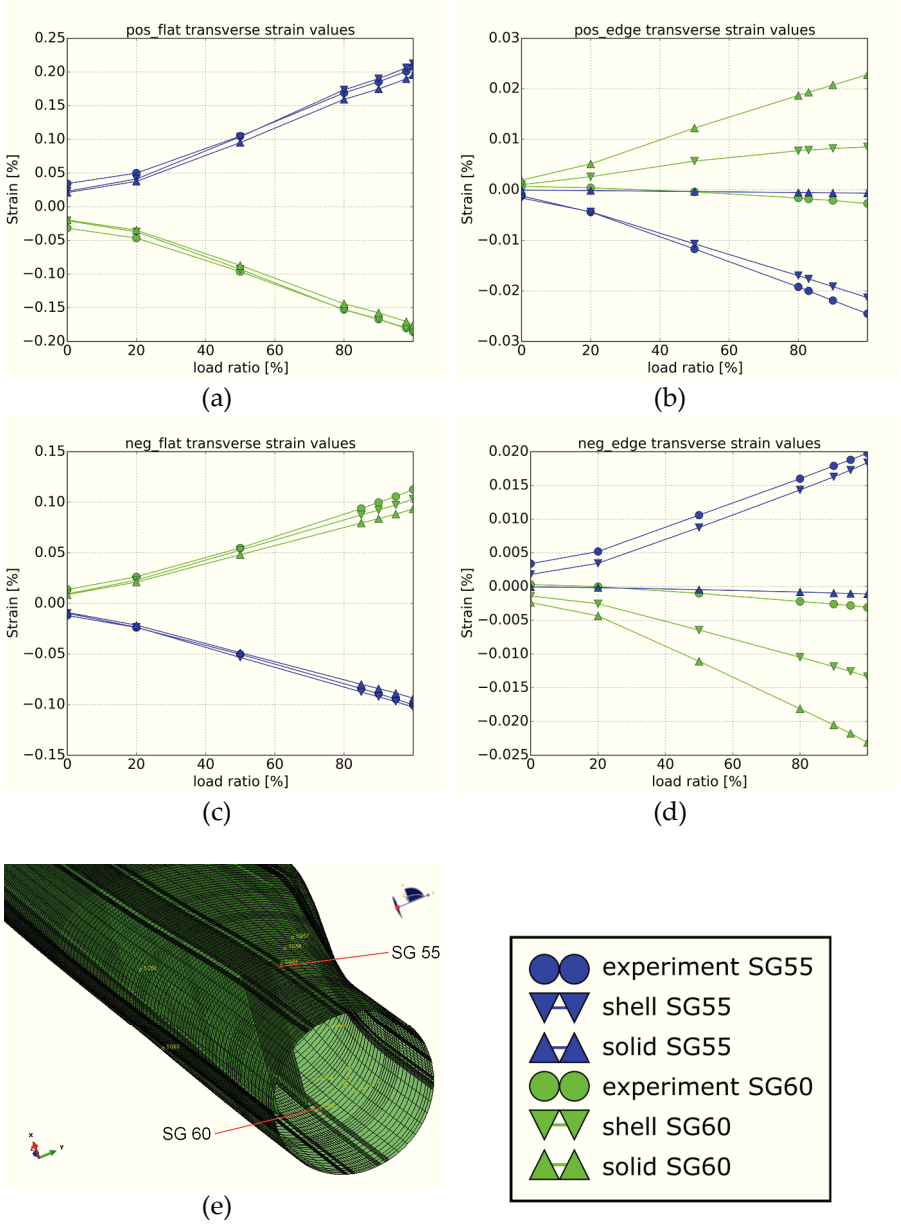

Figure 141: Overview of the true strain values in the transverse directions at two locations on the blade surface. (a) Positive flat-wise load case. (b) Positive edge-wise load case. (c) Negative flat-wise load case. (d) Negative edge-wise load case. (e) Overview of the strain gauge (SG) locations on the blade shape. The considered strain gauges are all positioned on the outside of the blade.

OML shell model	Solid model
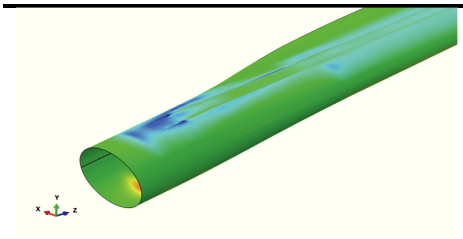	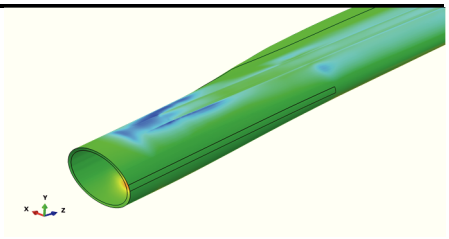
(a)	(b)
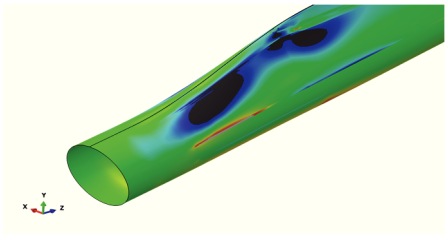	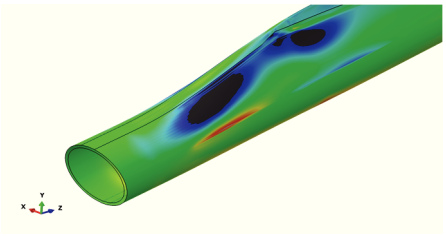
(c)	(d)
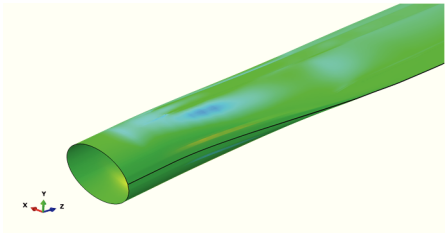	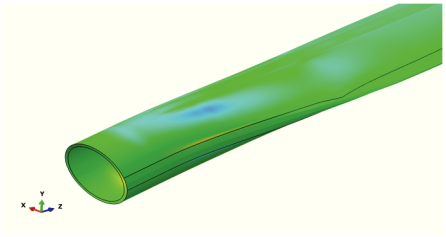
(e)	(f)
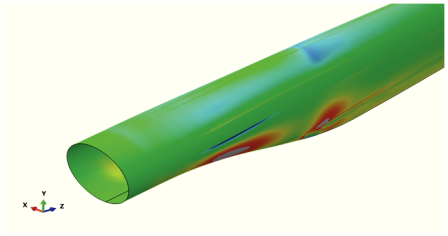	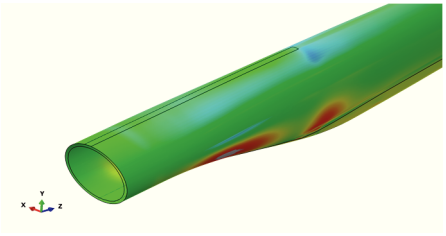
(g)	(h)

Figure 142: Contour plot of the transverse strain on the blade under the different load cases for the shell and solid models. (a) OML shell model under the positive flat-wise load-case. (b) Layered solid model under the positive flat-wise load-case. (c) OML shell model under the positive edge-wise load-case. (d) Layered solid model under the positive edge-wise load-case. (e) OML shell model under the negative flat-wise load-case. (f) Layered solid model under the negative flat-wise load-case. (g) OML shell model under the negative edge-wise load-case. (h) Layered solid model under the negative edge-wise load-case.

6.4.3.5 Strain differences between the inner and outer surfaces

In both the experiments and simulations significant differences are observed between the strain on the inside and outside surface at several locations on the blade. At two positions, strain gauges measuring transverse strain are placed on the in- and outside of the blade. Differences of over 1500 μstrain are observed. These differences result in a local rotation within the surface. In Figure 143 the deformation of several blade cross-sections is shown, magnified by a factor of 20. Strain differences between inside and outside surface result in local rotations.

As suggested in Jensen [3], these can be seen as local rotations. Causes are changes in thickness, layup and load paths. In addition, non-linear deformations result in deformation of the structure, such as the flattening of the cross-section due to the brazier effect.

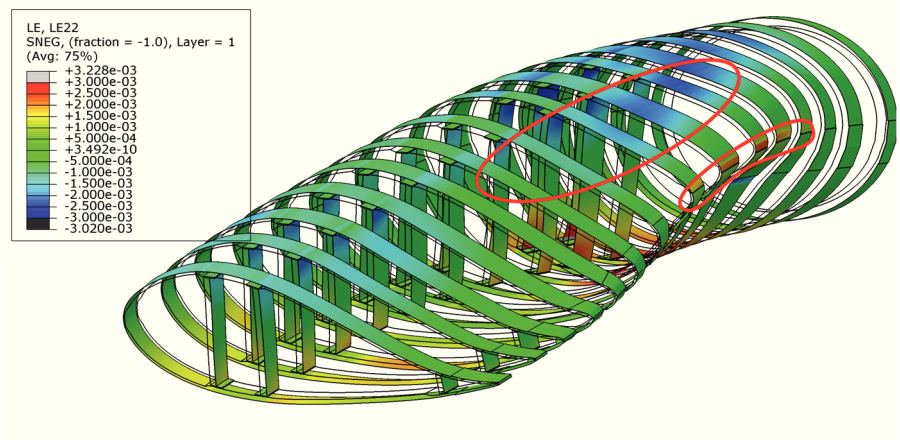

(a)

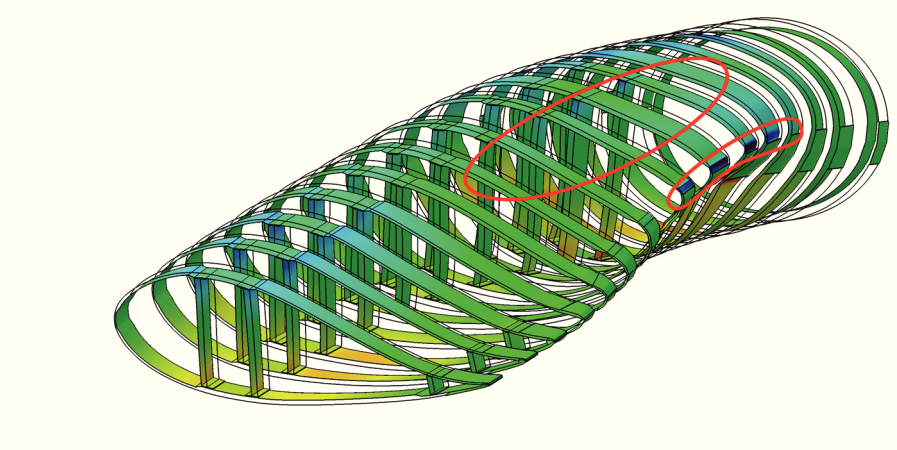

(b)

Figure 143: Contour plots of the transverse true strain values on a series of cross-sections of the solid model, deformed under the negative flat-wise load case. The deformation is scaled by a factor 20 for clarity. (a) Strain values on the outside surface. (b) Strain values on the inside surface.

6.4.3.6 Computational effort

While the observed displacements and strain distributions are very similar between the shell and solid models, the computational effort for the solid model was considerably higher. In Figure 144 the total CPU times are presented for the different load cases and models. The CPU time needed for the analyses using shell models was about 10 % of those using solid models. Furthermore, generating the final models with the in-house software took approximately 4.9 minutes for the shell model and 22.7 minutes for the solid model.

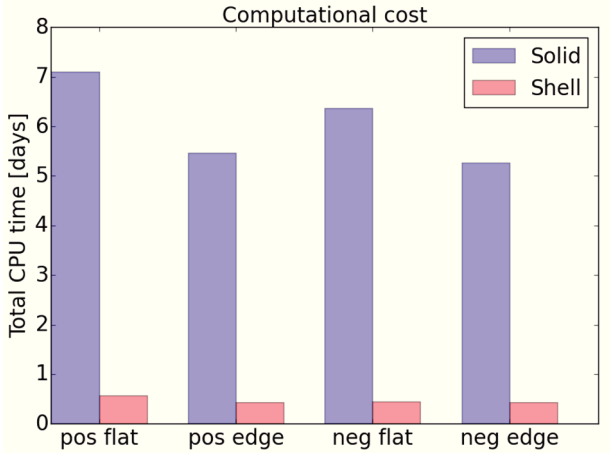

Figure 144: Comparison between the computational costs for the different load cases for the final shell and solid models considered in this study. The CPU time required to calculate the shell models is less than 10 % of that for the solid models. The analyses were parallelized over multiple CPU's. The simulations were conducted on a workstation with a 12 core CPU and 128 Gb RAM. The resulting wall clock time was about one twelfth of the total CPU time.

6.4.3.7 Modelling assumptions and implications

In the blade models, several assumptions are made. Firstly, the models represent an idealized, flawless structure. The experimentally tested sample was produced under factory conditions where manufacturing tolerances apply and flaws and defects occur. These are known to have a high prevalence. Furthermore, the models represent the blade design with the assumptions that the composite materials have the exact mechanical properties that were assumed during the design and that these properties do not vary within the structure. In addition, it was assumed that the blade did not sustain any damage throughout the tests and that the sequence in which the load cases were applied does not influence the results. These assumptions may explain some of the discrepancies between the results obtained from the models and experiments.

6.5 Conclusions

A commercial 43 m blade was statically tested. These tests were successfully modelled using FEM. First, different options for modelling the static tests were investigated. It was observed that the use of geometric non-linearity is a necessity. Furthermore, different methods of load introduction were considered. Connector elements that accurately represent the cables were compared to the use of concentrated forces. While the latter do not account for the change in orientation of the applied force as the blade deforms, the influence on the observed results

was limited due to the design of the test. Furthermore, the load from the cable was spread to a span-wise region by a "flexible" distributing coupling and by a "rigid" MPC. While it was found that the MPC prevented cross-sectional deformation, resulting in transverse strain values remaining zero in the region of the clamp, its influence was found to be restricted to the vicinity of the fixtures.

Subsequently, the use of shell and solid modelling was compared. In a first approach, only a segment of the spar structure was analyzed. A conventional OML shell model as well as a second order layered solid model were produced using the developed software tool. Despite the geometric mismatch between the OML shell model and reality, the predicted stresses along the side of the spar show similar values for the shear web. It can be argued that the overall behavior of the structure is accurately predicted because the shear stiffness of the shear web is close to the transverse shear stiffness of the girder combined with the adhesive bonds and flanges. In other words, the transverse shear deformation that takes place in the girder, adhesive and flange appears to be accounted for by the over-dimensioned shear web. Next, both a conventional OML shell model and a layered solid model were constructed for the full-scale blade. The obtained displacements and longitudinal strains are in good agreement with the experimental tests and little difference is observed between the shell and solid models.

The OML shell models were found to be both efficient and accurate. Layered solid models did not appear to provide big differences in the prediction of strains or displacements. It can therefore be concluded that for the considered blade and load cases, the solid model provides little additional value over a conventional OML shell model. However, since the study was applied to a specific commercial blade under specific load cases, the similarity between the results obtained using shell and solid models may not be present for other blades or other, more severe, load cases. The results merely indicate that shell and solid models can be constructed and analyzed resulting in a good match with experimental values. In addition, the results indicate that in many cases the shell modelling approach provides realistic results.

However, the use of solid elements is useful to obtain an accurate stress distribution in the adhesive bonds. Furthermore, several authors have successfully used solid models in load cases where damage developed. In such cases the stress in the thickness direction of the laminate is of great importance since it results in delamination and crack growth. The assumptions inherent to a shell model do not allow for these stresses to be observed. Further, a solid model proves useful when using a sub-modelling approach to investigate a specific area of interest. A sub-model contains multiple nodes in the laminate's thickness

direction. This allows for more accurate sub-modelling boundary conditions to be transmitted to the local solid model.

6.6 Bibliography

[1] M. Peeters, G. Santo, J. Degroote, and W. Van Paepegem, "Comparison of Shell and Solid Finite Element Models for the Static Certification Tests of a 43 m Wind Turbine Blade," *Energies*, vol. 11, no. 6, p. 1346, May 2018.

[2] P. U. Haselbach, M. A. Eder, and F. Belloni, "A comprehensive investigation of trailing edge damage in a wind turbine rotor blade," *Wind Energy*, vol. 19, no. 10, pp. 1871–1888.

[3] F. M. Jensen, H. Stang, and K. Branner, *Ultimate strength of a large windturbine blade*. 2009.

[4] *Abaqus 6.14 Online Documentation, Dassault Systèmes*. 2014.

[5] F. Sayer, A. Antoniou, and A. van Wingerde, "Investigation of structural bond lines in wind turbine blades by sub-component tests," *Int. J. Adhes. Adhes.*, vol. 37, pp. 129–135, Sep. 2012.

7 Conclusions and future research

"The Prologue And The Promise", Robert McCall

Chapter summary: In this chapter, the conclusions of the work are discussed and an overview is given of potential future research. This includes both potential additions to the developed software tools and opportunities for investigations that are feasible using the software. In addition, potential investigations for the development of blade segmentation joints are suggested.

7.1 Conclusions

7.1.1 State-of-the-art in wind turbine blade modelling

Wind turbine blades are complex structures in terms of shape and materials. To account for this level of refinement, both industry and academia have resorted to the use of FE modelling to investigate their structural behavior. Different modelling approaches have been used in literature. Their pros and cons are summarized in Table 17.

Table 17: Overview of the different types of models and their advantages and drawbacks.

Model	Advantages	Drawbacks
Shell models		
OML shell models	• Most frequently used. • Straightforward to produce: the surface is known from the mold. • Computationally cheap	• Poor torsional behavior according to several sources • Lack of inside surface affects modelling of internal features
Mid-thickness shell models	• Correct torsional predictions • Computationally cheap	• Hard to obtain since the surfaces depend on the layup • Lack of inside surface affects modelling of internal features
Continuum models		
Solid models	• Internal features are correctly represented • Correct torsional predictions	• Computationally expensive • Difficult to obtain
Hybrid models	• Internal features are correctly represented • Correct torsional predictions • Computationally more efficient	• Difficult to obtain

Most frequently, blades are modelled using shell elements with material offsets. This approach is logical, considering that the blades typically consist of a thin,

hollow structure of which the outside shape is clearly known, regardless of the layout and layup. Several authors have indicated that these models may not be appropriate when investigating the torsional behavior of the structure. Furthermore, due to the lack of inside surface inherent to the OML shell approach, internal features such as the shear webs and adhesive bonds are difficult to include. For these reasons, several alternatives have been proposed, including the use of models using continuum elements, models using shell elements without material offsets and models using a combination of shell and solid elements. The main drawbacks of these alternatives are the difficulty to obtain the models and the higher computational cost in the case of continuum elements.

7.1.2 Developed blade modelling tools

The modelling of wind turbine blades is a task with a series of very specific challenges. An attempt to create a blade model using the conventional manual approach was made. This made clear that tools are needed to make accurate and detailed models feasible. Various tools exist, but most present a black-box to the user. In addition, the development of tools that are property of other institutes was not desirable within the project. Throughout the work, several solutions were created that accomplish the task of creating blade models with high levels of detail. Each tool was built using the experience gained from prior versions.

First, an approach was used which automates the Abaqus/CAE pre-processor using the Python interface. This approach allowed the creation of detailed OML shell models. However, once a considerable amount of detail was introduced, the pre-processor became very slow and the files very large (file sizes would exceed 300 Mb and the loading time would reach over 30 min). Furthermore, minor issues occur sporadically that require manual intervention. This causes a bottleneck that limits the level of detail that can be achieved.

For this reason, a choice was made to build stand-alone software. First, a slice based tool was created that is able to generate detailed OML shell models. This tool is highly effective and flexible. It was used to create accurate, detailed models of several commercial blade designs. The tool was then extended to enable the creation of solid models. While this was successful, many limitations are present. Many challenges appear when making the transition towards solid models. These include problems with self-intersections, mesh quality aspects, correctly representing the internal geometry and compatibility between areas that are connected in the thickness direction.

These problems were addressed in a final, block based approach. This novel approach considers the blade as a collection of pre-defined parametric blocks. This enables a versatile, flexible and extendible divide-and-conquer design. The approach is implemented as an object-oriented, stand-alone software tool that

does not rely on any commercial software. The code is built up as several packages and consists of over 30 000 lines of code (excluding the many unit tests) to which documentation exists in a searchable html format.

The software is able to calculate the outer shape of any blade starting from normalized airfoil files and a planform description. The shape of the blade in between airfoil stations is calculated using thickness interpolation for which several interpolation functions are possible (including linear, quadratic, and cubic polynomials and piecewise cubic hermite interpolation functions). The tool is able to partition the surface of the blade in a very straightforward and accurate fashion using keyline functions that can be based on specific locations on the blade, on references or on other keyline functions. This allows very accurate positioning of plies and features. Furthermore, the software calculates a topology for the structure, onto which the layup and blocks can be assigned. The layup is assigned using the keylines, so that it remains unaltered if more partitions are introduced.

Thanks to the block approach, the tool can serve as a platform for creating detailed high-fidelity FE models for wind turbine blades. Within a single procedure, the creation of models with shell elements (with or without material offsets), solid elements, continuum element or combinations of those is possible. Furthermore, more possibilities exist than simply types of elements. For example, for the use of solid elements, some blocks represent the laminate in a single cell, whereas another family of blocks represents the laminate using three cells in the thickness direction. Using the right type of blocks allows the adhesive, flanges and webs to be represented in a way that is geometrically correct.

Further, the software contains newly developed modules that handle meshing. Both linear and second order shell and continuum elements can be produced and various element types such as regular solids, layered solids and continuum shell elements are available. While the current version produces input files specific to the Abaqus FE code, only limited work is needed to enable the creation of models for any FE solver as this only relates to the final export functions of the code.

Furthermore, the software is also able to calculate accurate material orientations which can be varied for each of the individual components of each block. These are calculated on an element-by-element basis and added to the models using a distribution. This is particularly important as anisotropic materials with a high stiffness modulus are often used for which the stiffness rapidly drops if the alignment is not correct.

Every module of the software tool is equipped with possibilities for visualizing the model data. This serves the purpose of debugging user inputs and provides useful visual material. A key advantage of using a stand-alone tool is that it is very flexible and easy to modify features. If a mistake would be made in the input or a

change was made to the design, updating the blade model is quickly done. This is often not the case for semi-automated approaches that rely on an external pre-processor. In addition, the software automatically calculates the mass distribution and center of gravity of the models it creates. Similarly, the total mass of each of the constitutive materials is calculated. These data allow rapid debugging and validation of the created models.

While the software runtime varies greatly with the level of detail in the provided inputs and requested outputs, typical times for the creation of blade models are 5 min for shell models and 20 min for solid models. To improve the performance, the results are stored at intermediate stages, allowing for example the assigned blocks to be changed without recalculating the blade shape. Furthermore, the software enables the creation of models that align closely with reality. Unlike in many approaches, the adhesive bonds which are typically a source of concern in the blade design are modelled at their geometrically correct location. Ply drop-offs and thickness changes can also be included in an accurate fashion. The software is also useful for the study of manufacturing flaws, as these can easily be added with the used approach while localized bending can be taken into account.

7.1.3 Validation of the blade models

Several commercial blades were modelled with the developed tools. An academic reference blade designed for a 10 MW turbine, a commercial 49 m blade, a commercial 10 m blade incorporating blade sweep and a commercial 43 m blade were modelled. These models were validated in terms of total mass, center of gravity and eigenfrequencies. The eigenfrequencies demonstrate the accuracy of the overall mass and stiffness distributions. It was found that the eigenfrequencies can be very sensitive to the local material orientations. Subsequently, the models were used for more complex analyses. These include the simulation under aerodynamic load and the simulation of static tests.

7.1.4 Modelling of aero-elastic blade behavior

For the investigation on the aero-elastic behavior of blades, the conclusions from existing literature can be summarized as follows:

- The aero-elastic behavior of blades is a fluid-structure-interaction (FSI) challenge.
- The FSI is typically accounted for in aero-elastic calculations used for the blade load calculations, by means of a model using BEM theory for the aerodynamic part and a beam representation for the structural side. This option is computationally cheap, but 3D effects have to be added artificially.

- An alternative approach is the use of FSI simulations with a detailed CFD model and a detailed FE model. This option provides a high level of fidelity but is computationally expensive.
- Alternatively, a BEM theory model can be combined with a FE model to provide a high level of detail on the structural side, while remaining computationally cheap on the aerodynamic side.

The conclusions from the new work can be summarized as follows:

- A coupling between HAWC2aero and Abaqus was successfully developed.
    - This allows FSI to be investigated at a computationally acceptable cost.
    - The coupling iterates between subsequent time steps and is limited to steady-state behavior.
- The coupling was used to model the behavior of the 10 m blade incorporating aft sweep.
    - A wind ramp was successfully simulated and the resulting data were compared to aero-elastic calculations obtained using HAWC2.
        - The resulting power, torque and thrust show a very similar behavior
        - A deviation exists for the twist of the blade tip, but this decreases with updated beam properties.
- Models for the 49 m blade created by the author were used for advanced FSI calculations at the department of Flow, Heat and Combustion Mechanics of Ghent University.

7.1.5 Modelling of static blade tests

The conclusions from the state-of-the-art can be summarized as follows:

- Static testing in four different directions is typically done as part of the blade certification process.
- For static testing, the blade is placed on a test stand and loaded while displacements and strain values are recorded.
- FE analysis is often used to predict the displacement and strain values.

The conclusions from the conducted work can be summarized as follows:

- The 43 m blade was statically tested at a certified test institute
- Based on preliminary simulations, the location for strain gauges was determined
- The static tests were modelled successfully.

- Both shell and solid models were produced for the blade.
- The cables were included using connector elements, but were found to have only a limited influence.
- The results for the resulting root bending moment, displacements and strains were extracted from the resulting output files in an automated fashion and compared to the data from the experimental tests.
    - The numerical root bending moments were in good agreement with the experiment
    - The numerical saddle displacements showed a similar pattern as the experimentally obtained values.
    - The strain values in the longitudinal direction showed a good match for most paths. An explanation for the deviation at the TE girders could be the asymmetric over-lamination of the joint.
    - The strain values in the transverse directions were high and the simulation values show mostly similar behavior as the measured ones.
    - Large differences were found to exist between the in- and outside surfaces of the blade in both the experiments and simulations. These strain differences result in local rotations of the laminate and are the result of changes in thickness and layup as well as nonlinear deformation of the cross-section.
- For the considered blade and load case, the solid model did not provide much additional value over the shell model since both models provided very similar data to the experiments. This conclusion should however not be generalized since this may be due to specific features of the considered blade (specifically the presence of a third, TE shear web) or the load case.
- The computation cost of the solid models was found to be about a factor 10 greater than that of the shell models.

7.1.6 Segmented blades

The research project initially envisioned a far-reaching investigation into possibilities to segment wind turbine blades. The work on this topic, presented in Appendix A of this dissertation, is limited to an investigation regarding the state-of-the-art. The reason for this is two-fold. On one hand, many of the critical challenges with blade segmentation are practical issues. For example, the assembly of blade segments is a very different challenge on-site compared to under factory conditions. On the other hand, it was deemed a priority to first investigate better modelling tools, apply these to single-segment blades of the

current generation and validate the results of the obtained models before investigation into segmented blades would be realistic. Nevertheless, the trends that sparked the idea of split blades continue to date. For this reason, there is still interest from industry and new patents keep being filed.

The investigation of the state of the art revealed the following:

- There is a vast amount of literature on the topic of blade segmentation in the form of patents and patent applications. These are filed by almost all major companies in the field of rotor blade design and manufacturing.
- Several segmentation strategies are possible. Each serves a different purpose.
    - Segmentation can be used to reduce the length of the components, which is for example critical for turning on smaller roads during transport.
    - A second approach is to reduce the width of the blade, which is closest to the maximum feasible dimensions for road transportation.
    - A third approach uses movable segments to influence the loading of the structure. Examples are the use of flaps and telescopic blades.
- In case of segmenting to reduce the blade length, structural joints are required to transfer very high loads. The options are:
    - Mechanical joints: in this regard much experience is present from the blade root joints and extenders and from tip brakes and winglets. The main challenges for mechanical joints are to be lightweight and require minimal maintenance.
        - Longitudinal bolts: in the case of longitudinal bolts, the number of bolts should be maximized in order to minimize the weight of the joint. In this sense, inserts have the advantage over T-bolt joints, where packing limitations are strict.
        - Transverse bolts: both rivets and bolts have been suggested. To improve the allowable load, fiber metal laminates (FML) have been considered.
        - Spar bridges: providing overlap between the structural spars of adjacent segments has been used successfully.
        - Other connections: other connection types, such as several relying on (pre-tensioned) cables or slings have been suggested.
    - Adhesive joints: these joints are structurally very efficient, but suffer from practical challenges regarding the in-field assembly.

- Detachable joints may provide opportunities for replacing segments instead of full blades

7.2 Possibilities for future research

7.2.1 Blade modelling tools

While the tools that have been developed in this work provide a wide range of capabilities, many possibilities exist to further extend and improve their capabilities. Several ideas regarding possible extensions are detailed in the following paragraphs.

7.2.1.1 Software extension: automatic generation of couplings

One possibility to extend the block based software tool is to include the automatic generation of constraints (such as tie-constraints) and couplings (such as shell-to-solid-couplings). This way, it would be possible to allow blocks that are not directly compatible to be combined effortlessly. Specifically, this would allow combinations of shell and solid blocks. This can be seen in the example presented in Figure 145. Such a model could reduce the required computational effort while providing accurate representations of the joints.

7.2.1.2 Software extension: additional blocks

The most straightforward approach to extend the existing block-based software tool is to include additional blocks. In particular, blocks could be added that provide a higher level of detail, by consisting of more components.

One area where this would be useful is a more advanced TE configuration. In the current blocks, the trailing edge adhesive is modelled as being flat. In some blade configurations, a specific shape is introduced into this joint to reduce the notch effect [2]. This could be accounted for by means of blocks like those presented in Figure 146.

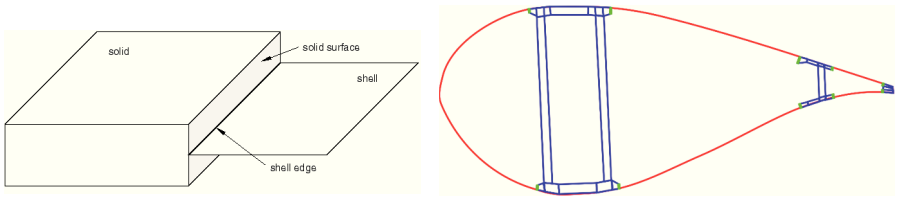

Figure 145: An extension of the software to automatically generate couplings to connect the necessary regions could allow the creation of blade models consisting of blocks of different families which are not inherently compatible. (a) Shell-to-solid coupling. Reproduced from the Abaqus v6.14 documentation [1]. (b) Schematic view of an example blade cross-section consisting of a series of shell (red) and solid (blue) blocks. At the interface (highlighted in green) between both types of blocks, a shell-to-solid coupling could be employed.

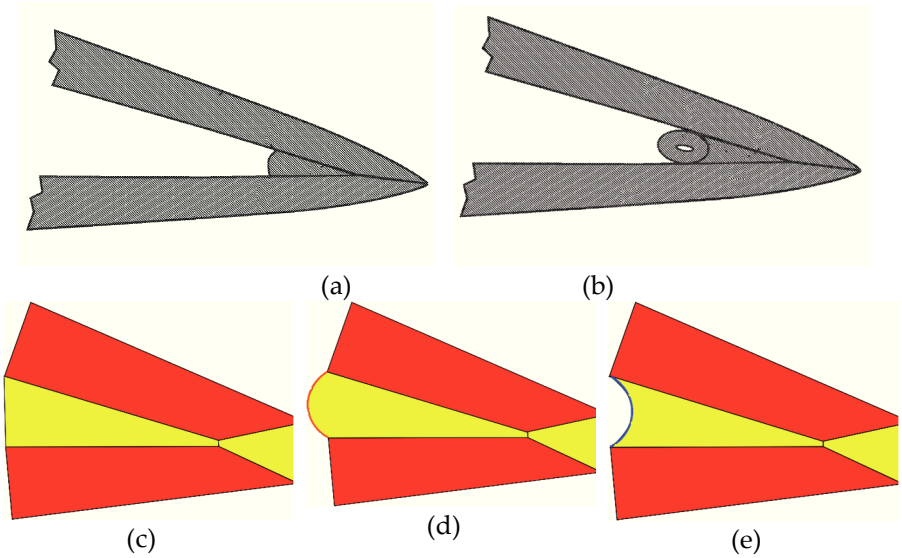

Figure 146: A schematic view of advanced trailing edge and TE block configurations. Actual adhesive bonds are typically formed by applying the adhesive and subsequently pushing the adhering surfaces towards each other. This results in an adhesive bond which bulges out towards the LE. However, this results in a weaker joint due to the notch effect at the top and bottom of the bulge. A better joint can be obtained by creating a dent towards the TE. An advanced trailing edge block could correctly model this detail. Additional cells for the wet-layup are removed for clarity. (a) Conventional TE configuration. Reproduced from Ref. [2]. (b) Trailing edge configuration suggested by Gill et al. [2]. (c) Trailing edge with a flat configuration. (d) Trailing edge with an outwards bulging configuration. (e) Trailing edge with an inward bulging configuration.

Similarly, the adhesive joints at the webs are typically not flat. In addition, the joints are often over-laminated. It has been demonstrated that this modification dramatically increases the life-expectancy of the joint [3]. A family of blocks could be created to allow these details to be included. Furthermore, the actual shape of the adhesive could also be incorporated.

Furthermore, specific blocks could be created to accurately model the adhesive joint at the LE. This joint is virtually never included in studies, while damages regularly occur in the LE region. Furthermore, this is an area in which manufacturing flaws are also likely to occur. Investigating their effect could be of interest. This joint can already be included using the current state of the software by using a combination of flange blocks to mimic the joggle lap joint. However, a special purpose block could enable the joint to be modelled more accurately. A schematic view of these LE joint modelling strategies can be found in Figure 147.

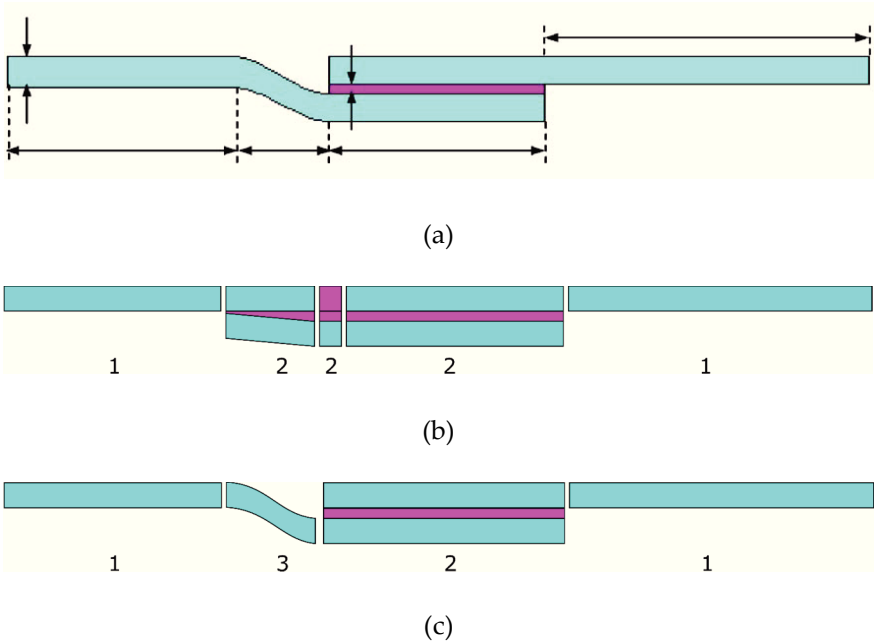

Figure 147: Schematic views of the joggle lap joint like that used at the LE of many wind turbine blades. Including the joint in the models would be an interesting addition. (a) Joggle lap joint configuration. Reproduced from Ref. [4]. (b) A combination of existing blocks to mimic the joint. (c) Joggle lap joint configuration with a new special purpose block. Numbers: 1: Conventional laminate block. 2: Conventional flange block. 3: Special purpose block for the joint.

Additionally, the tool should be extended to include split blocks, allowing more accurate modelling of plies that are cut-off at an angle. Schematic examples can be seen in Figure 148. Extending the current version of the block based tool to incorporate this type of feature would require only a very limited amount of work. An advantage of combining the two cells in a single block is that in this way, the mesh of both configurations could be made compatible, minimizing the number of wedge elements. However, even with these blocks it would be challenging to correctly incorporate the thickness change due to the ply drop-off. This issue is demonstrated in Figure 149. If an angled ply would drop off, the change in thickness would take place over a short distance. In practice, the software will spread the thickness transition over the full cell, reducing the accuracy of the representation.

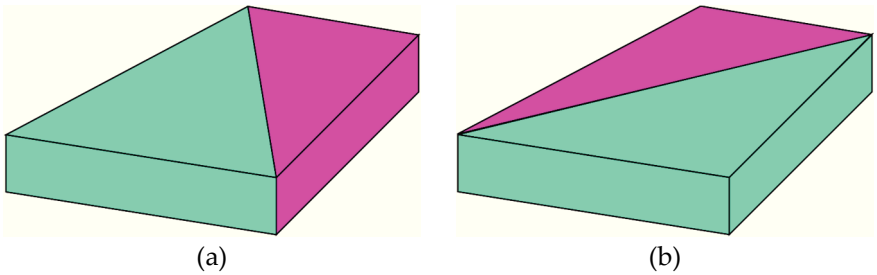

Figure 148: Split block configurations. The purple cell and teal cells each have their own layup. (a) Left split block. (b) Right split block.

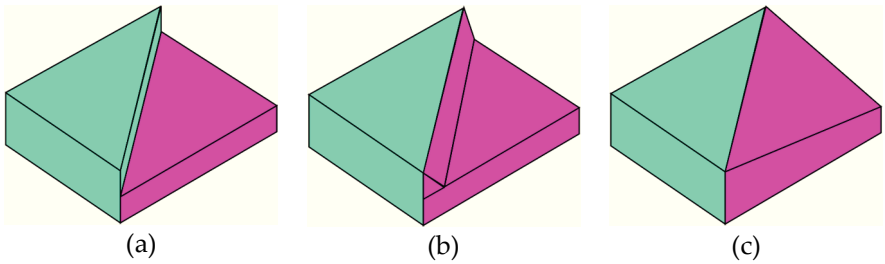

Figure 149: Schematic drawing to demonstrate the issue with ply drop-off for an angled ply on a split block. Due to the working of the software, the thickness transition would be spread over the entire cell with a lower thickness. This effect could be solved by using hybrid blocks, where the laminate change can be present in the layup of the shell elements, which do allow for a sudden thickness change. (a) Thickness for the different cells as input by the user. (b) Actual thickness as it would be present in the real blade. (c) Thickness resulting from the software. The change in thickness is spread over the full cell.

Another addition could be blocks that provide more detail when modelling the shear webs. An example can be seen in Figure 150. While blocks allowing for a shear web with a V-shaped cut-out are already implemented, elliptical cut-outs are most frequently used. In addition, the core tapers off towards the cut-out. Furthermore, at the base and top, the shear webs often use a thicker core.

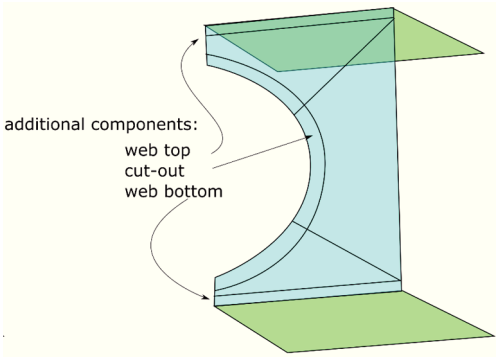

Figure 150: A schematic overview of advanced shear web blocks. Additional components allow more detail to be introduced. At the top and bottom of the webs a wider core is often used. Furthermore, the cut-out typically has an elliptical shape and the core material is chamfered towards it.

7.2.1.3 Software extension: advanced meshing strategies

A further feature that could be added in the future would be the implementation of more advanced meshing strategies. In this regard, several options are possible. Examples of advanced meshing algorithms are the blossom and blossom-quad algorithms [5].

More advanced meshing would allow for more mesh variation, while allowing almost fully hexahedral meshes. This has multiple advantages. Firstly, a much more refined mesh could be used in specific areas of interest. For example, the trailing edge region could be meshed finely, while keeping the rest of the mesh coarse. Secondly, in the current state, mesh transition relies on the use of wedge shaped elements. In the current version of Abaqus, the layered solid element library does not contain these shapes, but is limited to normal brick elements [1]. Wedge shaped elements are however available as continuum shell elements.

7.2.2 Blade simulations

While shell and solid models were compared for the 43 m blade, this was not a general investigation between the different modelling methods, but rather a comparison for a particular case of which validation data was available. The conclusions regarding the similarity between the shell and solid representation are therefore not applicable to the general case. Several features of the 43 m blade,

such as the presence of a TE shear web are suspected to have an influence on the similarity between the solutions of the different models. For this reason, a more general investigation of shell and solid representations would be desirable. The block based approach provides all the needed tools to conduct such investigation. Furthermore, besides the shell and single cell solid representations, more advanced representations such as the hybrid and solid representation with three cells in the laminate thickness direction could be considered.

Furthermore, it would be very interesting to include material failure criteria in the models. These were not used in the investigations presented earlier in this manuscript because the data for the specific material were not at hand. Various criteria are available in literature, of which several are readily available within commercial FE packages. Other criteria may need to be implemented using custom user subroutines. For example, during the course of this work, the author developed and implemented a bi-modular orthotropic material model using a user material (UMAT) subroutine. Failure criteria are useful to detect potential areas where damage could initiate.

Furthermore, in Chen et al. [6] failure criteria involving the behavior of the material in the thickness direction were advocated. It was argued that the debonding between skin and core and delamination require the behavior in the thickness direction to be accounted for. This does however require the use of solid elements or cohesive elements, which is a possibility using the developed software.

An additional topic for investigation is that of the adhesive bonds. While the developed tools allow the bonds to be included accurately by means of solid elements positioned at the physically correct location, the stress distribution within the bonds and how these are affected by changes in the blade design was not investigated.

In the same direction, another step forward would be to include progressive damage modelling in the investigations. If the material could degrade and detach, the influence of defects could be investigated. Specifically, this would be interesting for the adhesive, where a layer of cohesive elements could be introduced at the adhesive-laminate interfaces.

Furthermore, further investigation of the localized bending effects could be interesting, particularly in specific areas with rapid changes in layup and geometry, such as the area after the start/end of the girders or the root transition region.

7.2.2.1 *Investigation of specific regions of interest*

The developed tools are useful for the investigation of specific regions of interest. This can for example be done by creating advanced models with high levels of detail or by using a sub-modelling approach. Such an approach allows details to be considered at an acceptable computational cost. Furthermore, the flexibility of the modelling tool allows manufacturing defects to be investigated.

Further, while the work presented in this dissertation regarding wind turbine blade segmentation is limited to an investigation regarding the state-of-the-art, blade segmentation is a potential topic to research. In the master thesis of Stijn Ketele [7], which was supervised by the author, the T-bolt root connection of the 49 m blade considered in this study was investigated. A sub-modelling approach was used to investigate individual T-bolt connections represented by solid elements as shown in Figure 151. Using a similar approach, split blade connections can be investigated by means of the models the software can produce in combination with local joint models which can be created using conventional pre-processor approaches. For this purpose, the boundaries of the joint model could be calculated by the tool and exported to the pre-processor. If the effect on the behavior of the full blade proves limited, a sub-modelling approach can be used. Otherwise, constrains or couplings could provide a solution.

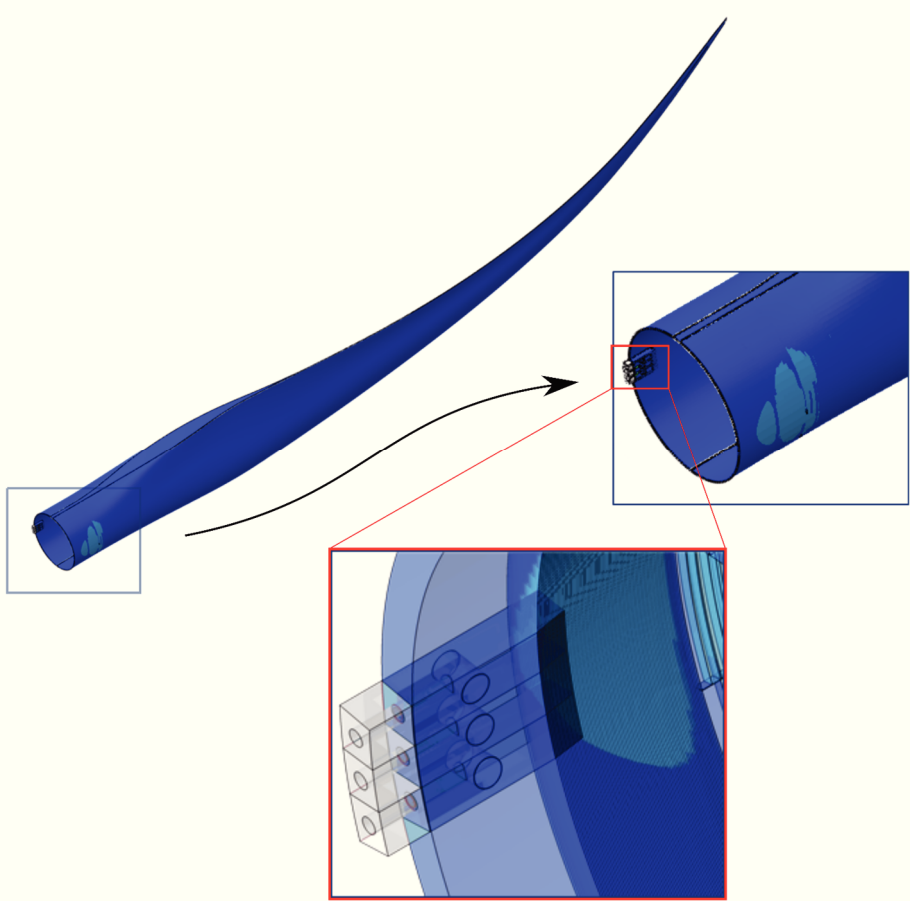

Figure 151: Overlay plot of the result of a global model of the 49 m blade under a static load case and a local model of T-bolt connections at the blade root, investigated in the master thesis of Stijn Ketele which was supervised by the author [7]. A similar approach could be used to investigate the joint of split blade designs.

7.3 Bibliography

[1] *Abaqus 6.14 Online Documentation, Dassault Systèmes*. 2014.

[2] A. Gill, "Assembly and Method of Preparing an Assembly," WO2010023140 (A1), 04-Mar-2010.

[3] F. Sayer, A. Antoniou, and A. van Wingerde, "Investigation of structural bond lines in wind turbine blades by sub-component tests," *Int. J. Adhes. Adhes.*, vol. 37, pp. 129–135, Sep. 2012.

[4] A. A. Taib, R. Boukhili, S. Achiou, and H. Boukehili, "Bonded joints with composite adherends. Part II. Finite element analysis of joggle lap joints," *Int. J. Adhes. Adhes.*, vol. 26, no. 4, pp. 237–248, Jul. 2006.

[5] J.-F. Remacle, J. Lambrechts, B. Seny, E. Marchandise, A. Johnen, and C. Geuzaine, "Blossom-Quad: a non-uniform quadrilateral mesh generator using a minimum cost perfect matching algorithm," *Int. J. Numer. METHODS Eng.*, 2010.

[6] X. Chen, X. Zhao, and J. Xu, "Revisiting the structural collapse of a 52.3 m composite wind turbine blade in a full-scale bending test," *Wind Energy*, vol. 20, no. 6, pp. 1111–1127, Jun. 2017.

[7] S. Ketele, W. Van Paepegem, and M. Peeters, "Detailed modeling of connections in large composite wind turbine blades," Ghent University, 2013.

Appendix A: Wind turbine blade segmentation: state-of-the-art

A.1 Introduction

As already mentioned, wind turbines are rapidly increasing in size. The resulting dimensions for the blades are causing challenges. This includes challenges with manufacturing, transportation, handling and installation. One approach to counter these issues is the concept of so-called segmented blades. These are blades that are manufactured to consist of several segments, which can be transported individually and assembled at a later point. In this chapter, the practical issues resulting from the present upscaling are discussed and the state-of-the-art in wind turbine blade segmentation is explained in detail.

A.2 Transportation of wind turbine blades

A.2.1 State-of-the-art

In general, wind turbine blades are manufactured at a production facility and subsequently transported to the installation site [1]. Due to local legislation, the total number of transports and various other factors, transportation costs are highly route dependent. Every haul requires investigation of the optimal route and transportation method [2].

While wind turbine blades are frequently transported by road, typically, lengths of over 45 m need to be transported as oversized and overweight (OSOW) load requiring specialized trucks with rear steering escorted by service cars [3]. The route has to be analyzed to ensure blade transport vehicles can be accommodated [3]. Furthermore, modifications to the road may be required and local regulations may restrict road transportation to night-time, specific weather conditions and may impose special licenses [4], [5]. Licenses with a limited validity period introduce lead-times and additional costs in the case of a delay [6]. Wind turbine blades can also be transported by rail. While blade lengths are not limited to the size of a single rail car, trains have to go slower when part of the blade is hanging over board [7].

Further, blades are also transported over waterways and seas. However, to prevent twisting of the ship from damaging the blades, expensive fixtures, custom to every blade type, have to be used [5].

As a last resort, blades can also be transported by air lifters. Because helicopters are expensive and risky, blimp like air lifting devices are under development [2]. A blimp is an aircraft similar to a zeppelin, but without the rigid internal structure. Increased difficulty of transporting larger blades results in a non-linear increase in costs. Beyond certain breakpoints there is a sudden steep increase [2]. On the road, transportation costs rise sharply for blade lengths over 46 m and can be prohibitive for blades longer than 61 m [8].

Furthermore, there are actual limitations to the dimensions of components that can be transported for each method [9]. These apply to the bounding box surrounding the blade. As can be seen in Figure 152, the height and width of the box is determined by the blade's maximum chord length and the blade root diameter as well as the amount of pre-bending and pre-curving. An overview of the maximum allowed dimensions and weights is given in Table 18.

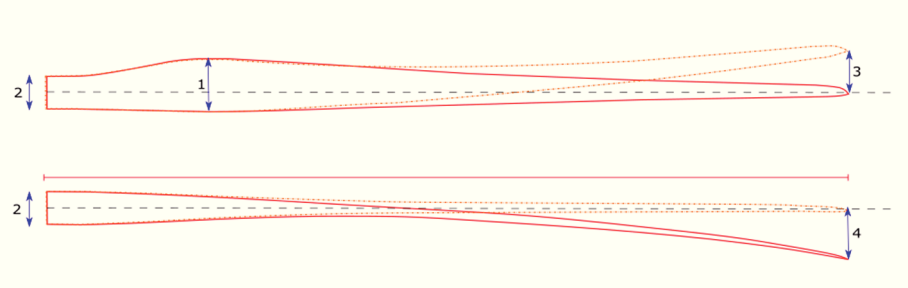

Figure 152: Top and side view of a modern wind turbine blade, giving an overview of blade transportation critical dimensions: 1: Maximum chord length. 2: Blade root diameter. 3: Blade sweep. 4: Blade pre-curving.

Table 18: Maximum allowed dimensions and weights for the transportation of wind turbine blades, based on Ref. [2].

transportation method	max. weight [tonne]	max. length [m]	max. height [m]	max. width [m]
Rail	163	27.4	4	3.4
Road (over weight)	36	45.7	4.1	2.6
Water (barge)	>200	76.2	-	16.5

A.2.2 Transportation improvements

Various improvements have been made to the conventional transportation methods. One possible approach is to make the position in which the blade is

carried variable. Jensen [10] suggested a system where the blade is suspended at both ends, which can each be lifted. This allows the blade to be lifted over small obstacles. Similarly, in Ref. [11] it was suggested to rotate the blade to pass under obstacles such as bridges. These systems can be seen in Figure 153. Likewise, Kawada et al. [12] proposed connecting only the blade root to a truck with a system that enables tilting the tip upwards. This allows larger blades to get past a narrow corner. Furthermore, Nies et al. [13] suggested tilting the blade and reducing the length of the carrying vehicle. Additionally, Pedersen et al. [14] improved upon these tilting concepts, allowing the blade tip to be in front of the truck while using a lighter vehicle. To allow larger blades to be transported by rail, Landrum et al. [15] proposed using two coupled rail cars and using a sliding support. Another approach is to deform the blade to alter its dimensions. Modern wind turbine blades are often pre-curved and swept. For larger blades however, the amount of pre-curving is less than desirable, due to the difficulty of transport [16]. This issue could be reduced by applying a load to "straighten" out the blades while they are transported [16]. In addition, to improve blade transportation by rail, in Ref. [7] it is advocated using bumpers to bend the more flexible outboard portion of the blades during turns so that there would be no overhang. An overview of these methods can be seen in Figure 154. Further, the transportation of blades over water is less restricted. In Ref. [5] it is proposed to take advantage of the similarity between blades and composite boats. When all gaps are sealed, the blades can float on the water and towed behind a ship. Alternatively, Ref. [17] investigated producing blades in a small on-site factory using material kits prepared at the main factory. However, there were difficulties with handling the blades at the temporary facility.

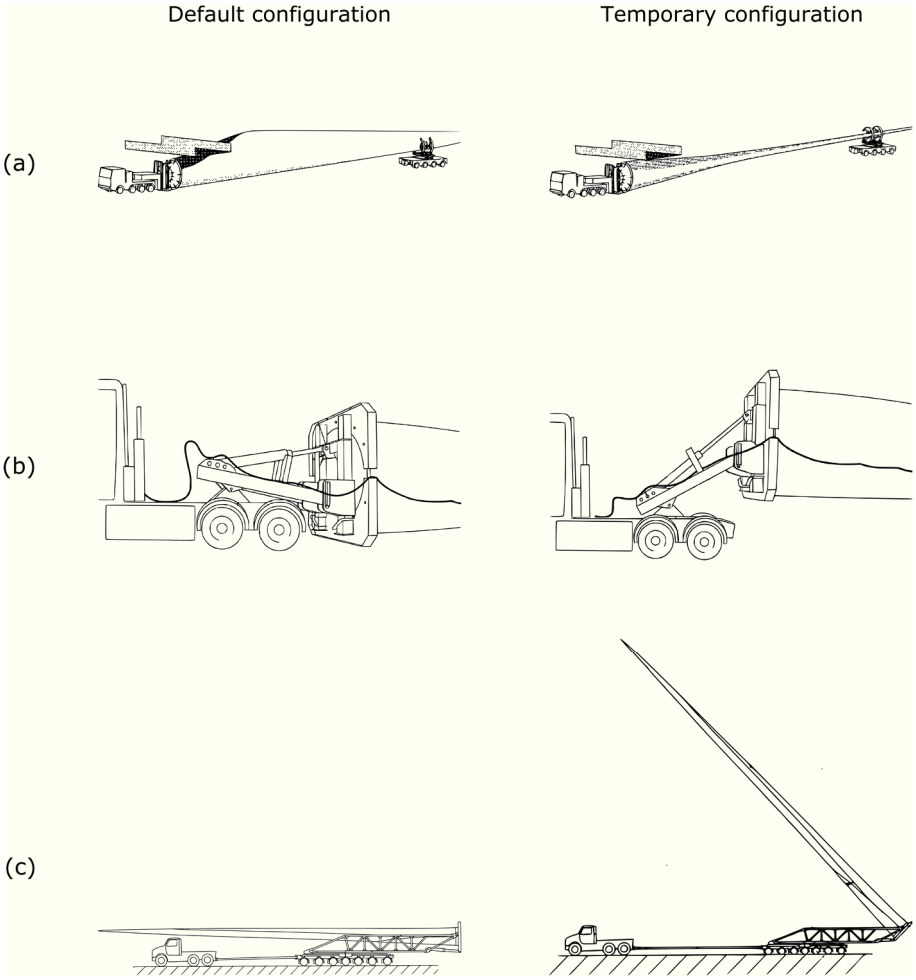

Figure 153: Blade road transportation solutions that temporarily change the way the blade is handled. (a) Solution where the blade can be rotated to pass under obstacles such as bridges or tunnels, as proposed in Ref. [11]. (b) System where the blade can be lifted to pass over low obstacles as proposed in Ref. [18]. (c) System where the blade can be tilted at the root as proposed in Ref. [19].

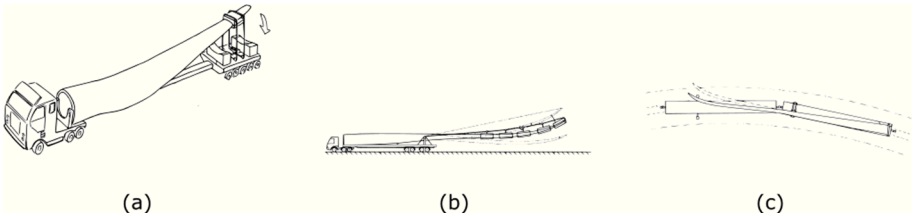

Figure 154: An overview of blade transportation solutions that deform the blade to ease transportation. (a) Straightening of the pre-curved blade to simplify transportation proposed in Ref. [16]. (b) Temporary deforming the blade to simplify transportation. (c) Deforming the outboard portion of the blade during rail transportation to prevent overhang during turns, as proposed in Ref. [7].

An alternative way to avoid transportation difficulties is to use airborne transport to deliver the blades to the site. This was advocated by several companies as a viable option. The US based company Aeros GmbH reported developing a blimp-like vehicle, called the Aeroscraft, to transport large components. The vehicle uses a balloon filled with helium which can be compressed and stored in high pressure tanks to regulate the balloon's density and thus its buoyancy. Similarly, a company investigated the option of lifting blades by means of balloons. These last concepts can be seen in Figure 155 and Figure 156.

Figure 155: The aeros blimp-like vehicle, suggested to be capable of transporting wind turbine blades. (a) Artist impression of the aeros transport vehicle transporting three wind turbine blades. (b) Picture of the developed prototype. Reproduced from Ref. [20] and Ref. [21].

Figure 156: Photo of a small-scale test of a blade transportation concept. Reproduced from Ref. [22].

Further, data was obtained from a company involved in blade transportation. The cost of the transport of blades of different lengths for a given journey, namely from Genk to Zeebrugge (approx. 190 km) can be found in Table 19. A significant part of this cost is related to the number of accompanying vehicles that are required. An overview of this requirement in accordance with Belgian legislation can be found in Table 20. It was clear from this data that the cost of road transportation was relatively low, even for blades of considerable length. The obtained values are lower than those reported in Dutton et al. [23] (shown in Table 21). However, this can be attributed to a different length of the routes. Furthermore, it is expected that the prices will rise sharply when certain limits are reached.

Table 19: Overview of the prices for the transport of blades of different lengths, obtained from communication with a company involved in the logistics of blades.

Type	**Max. blade length [m]**	**Max. payload [tonne]**	**Price [€]**
Normal truck	12	25	525
Special transport for 26,5 m blade	26.5	N.A.	1250
Special transport for 49 m blade	49	N.A.	2200

Table 20: Overview of the number of accompanying vehicles required by Belgian legislation for the transport of large and heavy components. Data from Ref. [24].

Category	Length [m]	Mass [tonne]	Accompanying vehicles
1	< 27	< 25	-
2	< 30	< 90	1
3	< 35	< 120	2
4	> 35	> 120	3

Table 21: Overview of transportation costs for blades of different lengths from LM Denmark to Hannover as reported in Ref. [23].

Blade length [m]	Price [€]
30	2600
40	5200
60	13000

A.3 Segmentation

The increase in size of the turbines has led to various issues with the production and logistics of several components. This has led to interest in dividing these components in pieces or "segments". By far the biggest component of a wind turbine is the tower. While these used to be built from at most a few parts of rolled steel, towers consisting of pre-cast reinforced concrete are now frequently used. In Ref. [2] several concepts to segmented and easier to erect towers are investigated. Such designs are also in use today [25], [26]. Other large components are the molds that are used to manufacture the blades. Segmented versions of these parts have been developed, allowing assembly and disassembly to ease transportation. Furthermore, some manufacturers have produced molds consisting of root, middle and tip segments [27].

In a similar fashion, so-called "segmented" blades are under consideration and development. In contrast to the conventional single piece blades, these are manufactured as a number of segments, which can be transported individually and assembled at the site of the turbine. While the "segmented", "split" or "modular" blade concept is not new, it has recently gained increased interest. In the following sections, an overview of the available concepts and related challenges is provided. Design options include span-wise or chord-wise segmentation, the location of the joint as well as the joint itself. The available

options are discussed along with their advantages and limitations. Furthermore, the feasibility of different methods is discussed.

A.3.1 Blade segmentation strategies

Blade segmentation can be done following different strategies. These are detailed in the following sections. An overview is provided in Figure 157.

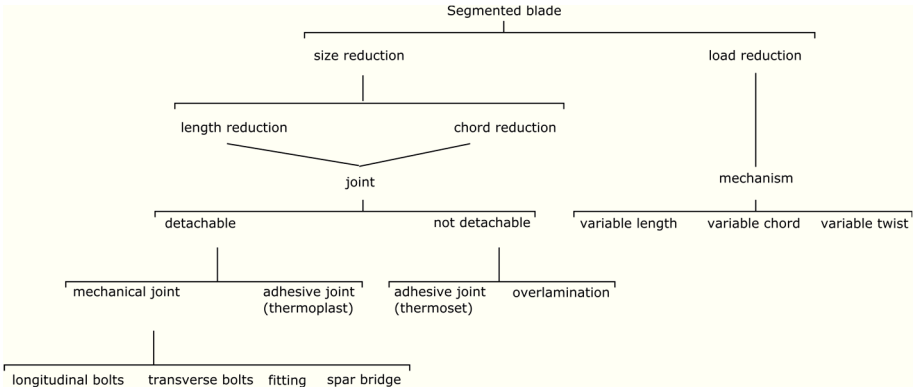

Figure 157: Schematic overview of a classification of segmented wind turbine blades. At a first level segmented blades are divided by the purpose of the segmentation. Reducing the blade dimensions requires a joint, while reducing loads requires a mechanism.

A.3.1.1 Segmenting to obtain a reduced component length

Large blades cannot get past narrow corners. This issue can be alleviated by splitting the blades into in-board and out-board segments. However, such a division requires the use of highly loaded structural joints to transfer loads between the segments. Introducing such additional joints goes against the historical trend in aerospace and wind energy of reducing the number of components [8]. Furthermore, fatigue design is better off without joints [28]. Additionally, there is a trend to produce more slender blades with higher tip speed ratios (TSR) and reduced chord lengths resulting in less space for a segmentation joint [29], [30].

A.3.1.2 Segmenting to obtain a reduction in width and height of the components

On straight roads, the width and height of the blade's bounding box are the main limiting factors. The area of maximum chord length is typically critical since it can easily reach a size of 6 m [31]. To counter this problem, Mikhail et al. [32] tried to alleviate the transportation issues by truncating a blade around the area of the maximum chord length. However, in this study, the prototype blade was found not to perform as expected. More beneficially, the blade can be segmented to

obtain a separate trailing edge segment [31], [33], [34]. This segmentation strategy can be applied without dividing the blade's structural spar. Therefore, the segmentation joints are not highly loaded and typically the trailing edge segment does not transfer loads coming from the tip region to the root. Alternatively, the blade can be split in a load-bearing structural spar and a non-structural aerodynamically shaped skin to reduce the width of the structure. Various authors [35]-[40] have suggested to consider the blade as a structure consisting of a load-bearing part (the spar) and an aerodynamic skin. In this approach it is possible to maintain a single part for the load bearing component, while making separate segments for the blade skin. However, conventionally, the skin transfers shear loads between the spar and trailing edge reinforcements originating from edge-wise loads. The decoupled skin concept should avoid to break up the structure that handles the edgewise loads [8].

A.3.1.3 Segmenting to obtain a variable rotor loading

Control strategies such as varying the blade pitch or the rotor speed are used to produce the maximum amount of energy while limiting the load to the turbine's rated power. Additionally, various strategies are used to reduce the extreme and fatigue loads on the rotor. Reducing the loads on the rotor can affect the loads on other components such as the bearings, gearbox and generator and could reduce the COE. Such strategies include cyclic pitch, individual pitch control and aero-elastic tailoring [41], [42]. Alternative strategies using the relative displacement of different blade segments are possible. One such approach uses telescopic blades. In that case, one segment is retracted into the other to vary the swept area of the rotor [43]-[46]. This allows the turbine to produce more power at low wind conditions while avoiding the extreme loading at high wind speeds. However, this requires a mechanism to perform the retraction that has to transmit all the loads from the outboard segment to the inboard segment. Alternatively, various active 'smart' control strategies are under development [41]. These use distributed sensors and actuators along the blades. The actuators include trailing edge flaps. Castaignet et al. [47] demonstrated this concept on a turbine with 13 m long blades. The average flap-wise blade root moment decreased by 14 % along with 20 % of the amplitude of the 1P loads (the loads resulting from the individual blade tower passing). Berg et al. [48], [49] tested trailing edge flaps on a turbine with 9 m blades. An average load reduction of 14 % was reported.

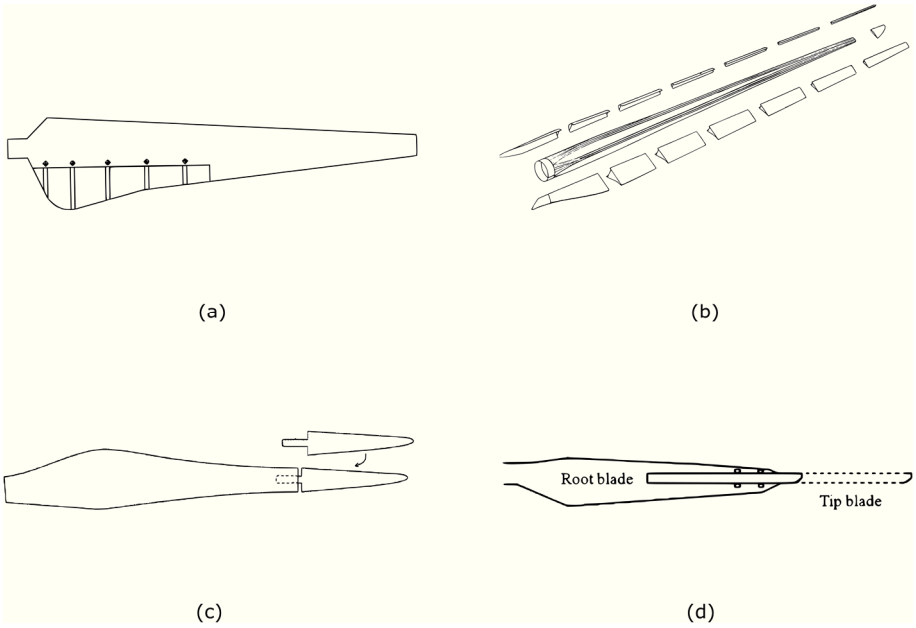

Figure 158: Different segmentation strategies. (a) Blade with a separate TE-segment to reduce the blades width. (b) Blade with separate LE and TE panel segments to reduce the blade width. (c) Blade divided to reduce the length of the components. (d) Telescopic wind turbine blade.

A.3.2 Cost of energy implications of blade segmentation

The overall aim of the wind energy industry is to provide energy at the lowest possible cost. This cost is affected by segmenting. Wind turbine blade segmentation inevitably affects the COE of such a turbine. In the following section the effects of segmenting are qualitatively assessed. This leads to a list of aspects to consider when devising a segmentation approach. The cost of energy (COE) can be modelled as suggested in Ref. [50], as shown in equation (10). The COE depends on the fixed charge rate (FCR), the initial capital cost (ICC), the net annual energy production of the turbine (AEP_{net}), the land lease cost (LLC), operations and maintenance (O&M) cost and the levelized replacement cost (LRC).

$$COE = \frac{FCR.ICC}{AEP_{NET}} + LLC + \frac{O\&M + LRC}{AEP_{net}} \qquad (10)$$

A.3.2.1 The initial capital costs

The ICC depends on manufacturing transportation and installation cost of the turbine. On one hand, manufacturing costs increase because of the additional

material, labor and production steps required for producing the joint and reinforcing the inboard part of the blade [23]. On the other hand, a cost reduction is possible due to economic benefits. Production facilities can be smaller [23], [51], [52] and components can be standardized. For example, a single root segment can be combined with different tip segments to obtain blades for different wind conditions [53], [54]. Additionally, using different materials at different locations along the span is economically interesting but requires a difficult transition. This can be simplified by segmenting [31], [55]. Furthermore, segmentation simplifies quality assurance for the individual segments [55].

Blade segmentation can decrease transportation costs [23]. Moreover, many sites that are suited for wind turbines are in complex terrain with poor infrastructure. Their development may become cost effective with segmented blades [56], [57].

Installation costs increase because of additional assembly steps required to make the final blade. In this respect, speed and simplicity of assembly are important.

A.3.2.2 Operations and maintenance cost (O&M)

The cost for operations and maintenance O&M increases because of additional inspections or maintenance. It may be required to verify the pre-stress of bolts or the protection against water ingress [58]. Minimal additional maintenance and good access and ease of inspection to the joint are required to limit this cost increase. Therefore, sensors can be included to monitor the joint as proposed in Ref. [59].

A.3.2.3 Levelized replacement cost (LRC)

The use of a detachable joint could allow replacement of a single segment rather than the complete blade in the case of damage [60], [61]. This would allow a reduction of the LRC, which represents the cost of replacements over the life of the turbine.

A.3.2.4 Net annual energy production (AEP_{net})

Further, the annual energy production (AEP) has a very strong influence on the COE since it has to offset all the costs including those not related to the rotor. The performance of the rotor will decrease by alterations to its outside shape. Therefore, joints should use holes that can be covered or blind holes from the inside of the blade [31]. A lower rotor inertia makes it easier for the control system to keep the ratio of the rotational speed of the rotor to the wind speed optimal under fluctuating wind conditions, thereby resulting in a higher AEP [62]. Additionally, the AEP will be decreased if a local stiffened portion is included [63].

A.3.2.5 Resulting considerations for segmented blades

In order to minimize the COE resulting from a segmented blade the different cost components have the following considerations based on references [23], [64].

- Initial capital costs (ICC)
  - manufacturing costs
  - tolerance requirements
  - production complexity and accuracy
  - ability to use with conventional production methods
  - quality control
  - positioning accuracy and speed of assembly
- Annual energy production (AEP)
  - reliability
  - aerodynamics
  - weight of the joint
- Annual operating expenses (AOE)
  - requiring minimal inspection
  - easy to repair during service
  - possibility of disassembly for replacing segments

Segmenting blades is useful if this results in a reduced COE. For example, Ref. [23] reported an expected increase in blade cost of approximately 19 % for a 60 m blade, while the transportation costs decreased only about 5 % of the total price of the blade, thus overall resulting in an elevated COE. However, from Dutton et al. [23] it is clear that the relative added cost of segmenting a blade decreases with the size of the blades. Further, at a turbine level, the optimum scale is determined by the ratio between capital costs and other costs [65]. Because the fixed costs are significantly higher for offshore turbines than for their onshore counterparts, the optimum size for offshore turbines is larger than onshore [65]. Additionally, for land based turbines, transportation costs may be extremely high for certain sites that do allow for a high AEP. Therefore, segmentation is most likely to be cost effective for either very large, typically offshore turbines or on-shore turbines that are installed on sites that allow a high yield but are otherwise difficult to access.

A.3.3 Joints

In the rest of this chapter, the focus will be placed on segmented blades that employ structural joints. This is mainly the case for blades which are divided to reduce the length of the individual components.

A.3.4 Adhesive joints in segmented blades

Adhesive joints can be structurally efficient, light and cheap. They have low stress concentrations and good damage tolerance. However, when used in segmented blades they result in high installation costs due to the need for specialized equipment and the number of added time-consuming steps during on-site assembly. Various approaches have proposed to alleviate these issues. One problem is the lack of inherent self-alignment of adhesive joints. This increases the complexity and time required to assemble the blade from its segments [66]. In Baker et al. [67] a system is presented to align blade segments on different carriers using laser positioning. Alternatively, Zirin et al. [68] suggested using brackets attached to the spar caps to ease alignment, after which the adhesive bond can be formed. Livingston et al. [69] proposed using alignment pins. Additionally, Baehmann et al. [70] and Riddell et al. [71] suggested using different types of overlapping portions to ease alignment. Further, Kyriakides et al. [72] proposed using joint portions that are offset in span-wise direction to create an overlap.

A second issue is the difficulty of producing a high quality bond on-site compared to under controlled conditions [61]. Surface preparation, temperature and humidity affect the quality of adhesive joints [73]. Good control over the bond thickness is important to avoid stress concentrations. In Ref. [74] the use of a bonding grid is proposed. This grid is incorporated into the joint to obtain a very accurate bond thickness. Zirin et al. [68] suggested using shims to ensure a constant minimum distance between the parts to be adhered. To ensure a perfect fit between two segments, Riddell [71] advocated producing the segments in a single mold. By folding in a vacuum bag with release agent the two adjacent segments can be manufactured while in contact with each other. Afterwards, they can be separated easily and will have a very good fit at the interface. Further, air entrapments can drastically reduce the strength of adhesive joints. Arelt et al. [75] suggested to put the connecting surfaces in place first, creating a cavity which can subsequently be flooded or infused to create the joint while avoiding air entrapments. Similarly, Ref. [70] suggests a segmented blade with overlapping spar caps, which cause the formation of a spar cap cavity, which is subsequently filled with adhesive. Another issue is the assembly time and requirement of specialized equipment such as ovens, heat tents and heater blankets to cure the bonds [76]. Up to ten hours at elevated temperature may be required to fully cure the adhesive [75]. Diver et al. [76] suggested the use of resistance heated bonds to

alleviate these issues. Also, the O&M costs are lower for adhesive joints compared to mechanical connections.

A.3.5 Implementations in segmented blades

Blade segments can be joined using structural adhesive bonds. An overview is given in Figure 159. The efficiency of the joint depends on the chosen geometry. Finger joints were used in the wood-epoxy blades of the MOD-5A turbine [77]. However, the use of this type of joint in modern fiberglass blades may be impeded by the higher modulus of elasticity and strains as well as issues with tooling. Similarly, diamond shaped splice-inserts can be adhered to the segments to form the joint [78]. Likewise, Bech et al. [79] improved upon this approach by using longer connections providing higher stiffness and strength. Ref. [80] used finite element modelling to investigate the option of bonded strap plates. For general geometries, scarf joints and stepped lap joints have the highest efficiencies [81]. Concepts using scarf joints were suggested by various authors [68]-[70], [74]. To avoid fragile protrusions, [82] proposed using a double scarf joint. Segmentation using stepped lap joints was suggested by Baker et al. [67]. Further, Frederiksen [83] suggested not infusing the fibers in the joint areas when fabricating the segments, so that they can be joined by overlapping, infusing and curing the dry fibers.

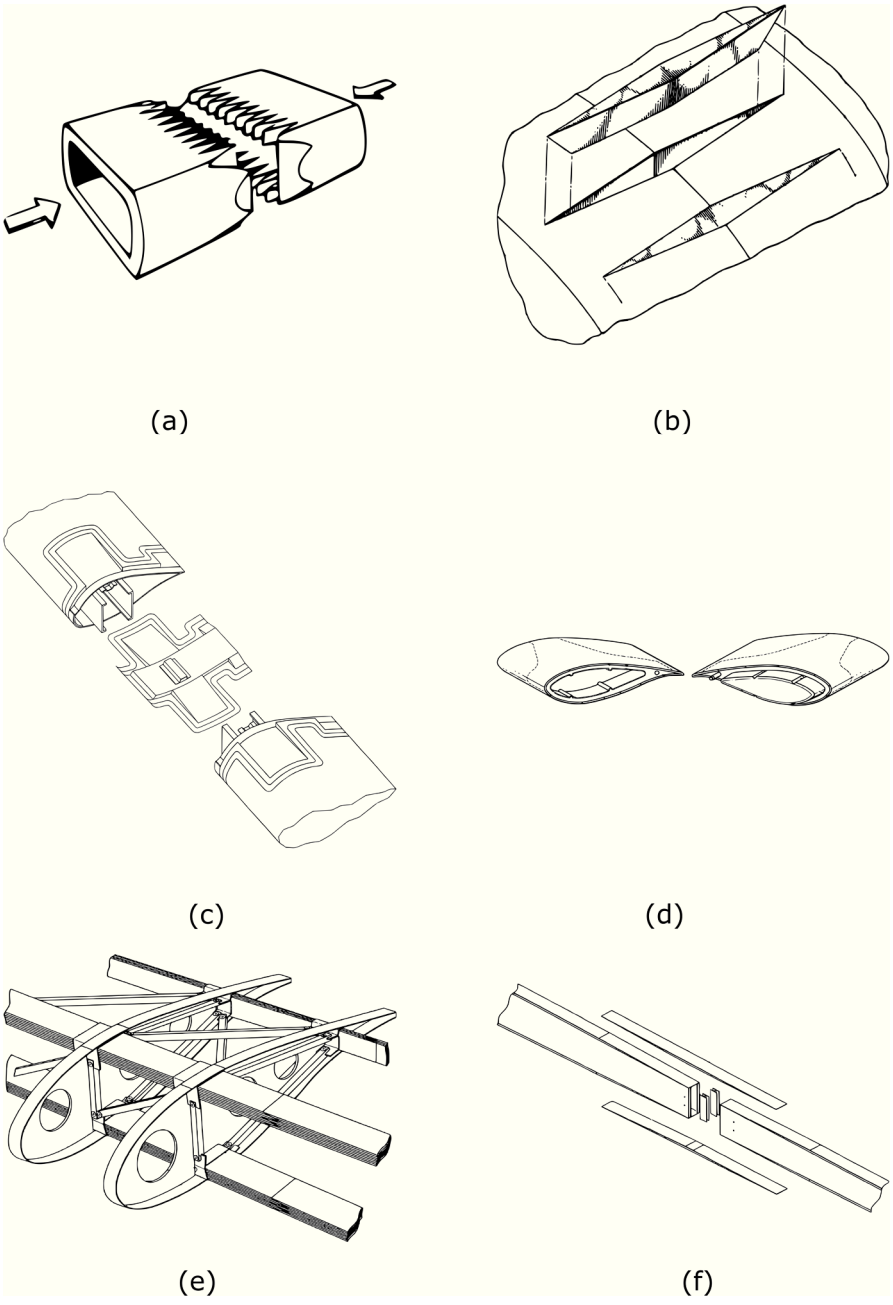

Figure 159: Blade segmentation concepts using adhesive bonds. (a) Finger joint. (b) Splice insert joint presented in Ref. [77]. (c) Adhesive cavity joint. (d) Single lap joint presented in Ref. [71]. (e) Stepped lap joint as presented in Ref. [67]. (f) Double scarf joint as presented in Ref. [82].

A.3.6 Mechanical joints in segmented blades

Mechanical joints are heavy and expensive, but are fast and easy to assemble [23], [52]. Furthermore, they are easy to inspect but require some maintenance.

A.3.6.1 Prior experience from blade root connections

Conventionally wind turbine blades are attached to a steel hub using a detachable mechanical joint. These root joints are highly loaded and experience a very high number of load cycles. Because of the existing experience in this field and the similarities with the joints for segmented blades these joint types are candidates for blade segmentation. The most frequent root types are seen in Figure 160.

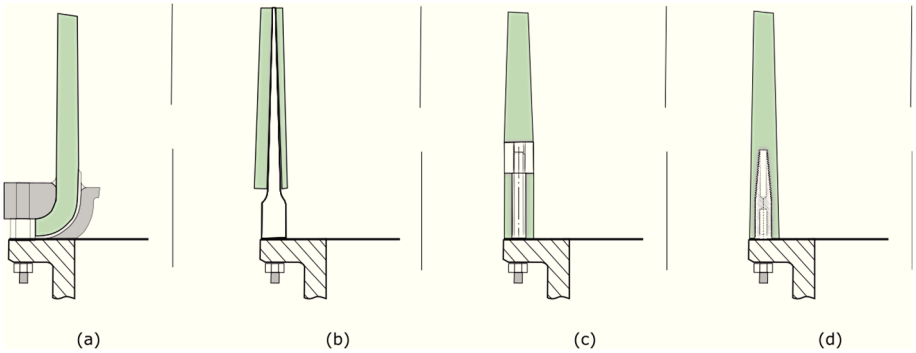

Figure 160: An overview of blade root joints. (a) Flange root connection. (b) Hub type root connection. (c) T-bolt root connection. (d) Stud root connection.

A.3.6.1.1 Flange type

Blades with a flange type root have a flange formed by molding the material outwards. This flange is then bolted to the hub. Bundles of fibers can be looped around bushings with the flange to capture them mechanically. This type of root is known as the Hütter root connection [84], [85]. An implementation of this joint can be seen in Figure 161.

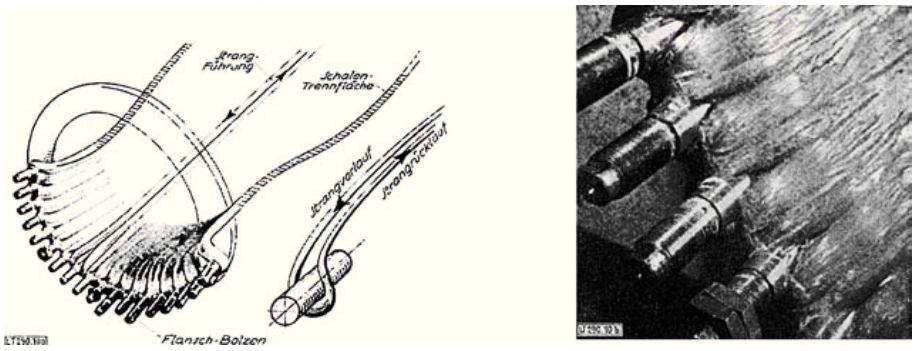

(a) (b)

Figure 161: The Hütter flange connection. Image from Ref. [86]. (a) Schematic drawing. (b) Photo of a joint in production.

A.3.6.1.2 Hub type

The hub type root connection uses a tapered metal cylinder embedded or adhered to the root laminate and bolted to the hub. Assuring correct bond thickness is difficult, but critical for the performance of the joint [17]. Strain incompatibilities are present, resulting in large stress concentrations. Furthermore, in some implementations the hub has a lower diameter than the actual root, reducing the structural efficiency of the joint [85]. Hosseini et al. [87] investigated the progressive de-bonding of a hub type joint.

A.3.6.1.3 T-bolt joint

T-bolt joints have cross-bolts positioned perpendicular to the root cylinder surface. Longitudinal bolts connect the hub to the cross-bolt [88]. T-bolts rely on the contact between the cross-bolt and the laminate to transfer loads. Martinez et al. [89] investigated the T-bolt joint both numerically and with experiments and concluded that the T-bolt joint is reliable and cheap but has a low structural efficiency, resulting in a high weight compared to other solutions such as inserts. Packing limitations exist and lead to a significant laminate build-up. Furthermore, the load factors of the bolts are critical to the integrity of the connection.

Multiple improvements to the conventional T-bolt joint have been suggested. Harismendy et al. [90] suggested the use of two longitudinal bolts for each cross bolt outside the blade laminate. While Quell et al. [91] suggested using other shapes of cross bolts than cylindrical. Additionally, Ref. [92] suggested using multi-row T-bolts in order to increase the packing limit. These concepts are presented in Figure 162.

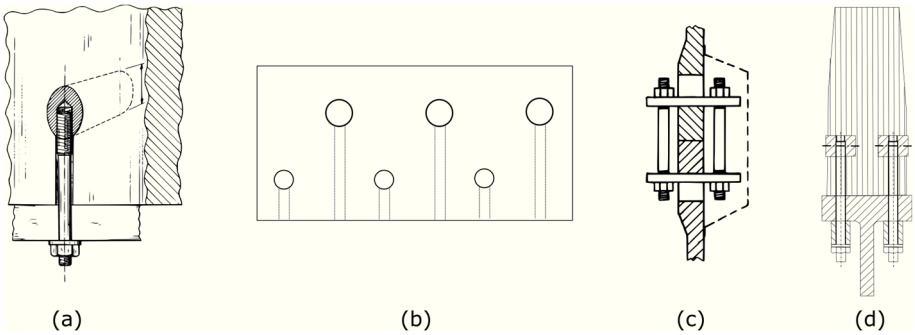

Figure 162: T-bolt improvements suggested in literature. (a) T-bolt joint with non-cylindrical cross-bolts as suggested in Ref. [91]. (b) T-bolt joint with alternating long and short longitudinal bolts as suggested in Ref. [92]. (c) T-bolt joint with two longitudinal bolts as suggested in Ref. [90]. (d) T-bolt joint with multiple parallel T-bolts, where the cross-bolt does not pass trough the full laminate as suggested in Ref. [93].

A.3.6.1.4 Stud/insert type

The stud or insert root joint relies on longitudinal bolts attached to studs or inserts. Typically, the inserts are female threaded and made of steel, causing a thermal and flexural mismatch [94]. This is countered by tapering the studs on the outside or inside and by using a thicker laminate. It was furthermore suggested to use a threaded insert made from a composite tube to improve compatibility to allow a reduced root wall thickness. Furthermore, to reduce the stress concentration at the tip of the inserts, Vronsky et al. [95] suggested using inserts of different lengths.

Often, the studs are glued into the blade. In wood composite blades the studs are placed in holes that are drilled, while in glass fiber blades the holes are preferably formed during fabrication [17], [96]. Positioning of the stud is vital to the quality of the joint as a non-uniform adhesive thickness causes stress concentrations [97]. Typically, fixtures are used to position and bond the studs simultaneously. Often, the adhesive is injected into the hole around the insert by using a secondary hole or through the gap between the laminate and the stud. Alternatively, modified studs can allow the adhesive to flow through the center of the insert to form the bond through the stud. Additionally, the joint quality can deteriorate because of macroscopic voids [17]. To avoid these voids, Raina et al. [97] suggests to improve the tru-stud bonding method to allow vacuum infusion by adding a second channel to the stud.

Alternatively, the studs can be directly embedded during the lamination process. This requires less fabrication process steps, tooling and allows the root laminate to be much thinner, but increases the complexity of the lamination process [17], [98]. Sørensen et al. [99] suggested using a holder with spaced

recesses to hold the bushings. As an alternative, Bendel et al. [100] and Kildegaard et al. [101] both suggested inserts that can easily be positioned and form a smooth outer and inner surface onto which the fiber mats of the root laminate can be applied.

In general, to provide sufficient pull-out strength, inserts are required to be long. Various improvements have been suggested to increase the pull-out strength, allowing shorter, lighter inserts. Ref. [102] suggested to include longitudinal grooves on the outside of the inserts to increase the contact area with the laminate. Further, in similarity with the Hütter root, Ref. [98] proposed to capture the inserts mechanically by looping fibers around it. Additionally, Feigl et al. [103] suggested putting fibers in between the inserts for a better contact, whereas Schmidt et al. [104] suggested stitching together the fibers surrounding the bushings.

A.3.6.1.5 Comparison: T-bolts vs. inserts

The blade root design is mainly driven by cost as it represents between 7 and 20 % of the total blade cost [89], [105]. The weight of the joint is less important, since it is added close to the hub and the center of rotation. Therefore, it does not have a big impact on the blade's eigenfrequencies, and edge-wise and dynamic loads. This is different for blade segmentation joints which are placed further outboard. Due to the superior fatigue performance of T-bolts and studs, other blade root designs have become rare. Jackson et al. [106] performed the preliminary design of a 50 m blade. Blade roots were designed considering a T-bolt joint and a stud joint. The stud connection allowed a larger number of connections because of packing limitations of T-bolts. This lead to a reduced root laminate build-up resulting in a lower weight and price, despite cheaper T-bolt hardware.

A.3.6.1.6 Implementations in segmented blades

The T-bolt joint has been used in several prototype segmented blades, seen in Figure 163. It was first used on the DEBRA-25 wind turbine [107]. T-bolts joined the blades to the hub and connected the C-spars of the two 8.5 m blade segments. The turbine was successful and needed only limited additional maintenance to verify bolt pre-tension. Dutton et al. [23] also investigated the use of a T-bolt joint for a segmented blade by using a single row of T-bolts in a prototype 23.3 m blade. The blade survived both static and fatigue testing. Later, Vionis et al. [56] also investigated the use of a T-bolt joint by using a double row of T-bolts in a 30 m segmented blade. The blade survived static testing but bolts at the spar caps failed during fatigue testing at one fifth of the 1E6 load cycles. Prototypes using inserts have also been made. Within the UpWind project, a 42.5 m sectional blade using inserts was developed [108]. This can be seen in Figure 164.

Figure 163: Prototype segmented blades using a T-bolt joint. (a) DEBRA-25 blade. Reproduced from Ref. [107]. (b) Split blade tested under the JOULEIII project. Reproduced from Ref. [23]. (c) Blade tested under the MEGAWIND project. Reproduced from Ref. [56].

Figure 164: Photos of the "Innoblade" segmented wind turbine blade developed by Gamesa. Still images produced from Ref. [109]. (a) Closeup view of the joint. (b) Transportation of the inboard segment.

A.3.6.1.7 Pre-tensioning methods for the bolts

When blades are joined by longitudinal bolts, these are typically pre-stressed, to improve their resistance to fatigue loads. One approach is to allow sufficient space to enable pre-tensioning as used in references [23] and [107]. Another approach relies on the use of an intermediate plate as shown in Figure 165. Both segments are then joined to the intermediate plate by bolts. The plate is then designed to allow access to the bolts to allow fixing and pre-tensioning them. This space requirement limits the number of bolts that can be placed, which as mentioned earlier should be maximized to minimize the weight of the joint. In references [54], [110] a joint is presented for blade segmentation that increases the number of connections by alternating long and short bolts. The joint design was dimensioned for a 61.5 m segmented blade.

Alternatively, in Ref. [111] an approach to join two blade segments is suggested that used a single bolt to join both sides without use of an intermediate plate. The bolts are therefore left-handed threading on one end and right-handed threading on the other. Furthermore, Monreal et al. [112] presented an approach which allows pre-tensioning of the bolts without access problems. Essentially, the segments are first connected by colts and later pre-stress is induced by closing an intermediate wedge which places tension on the bolts as shown in Figure 166.

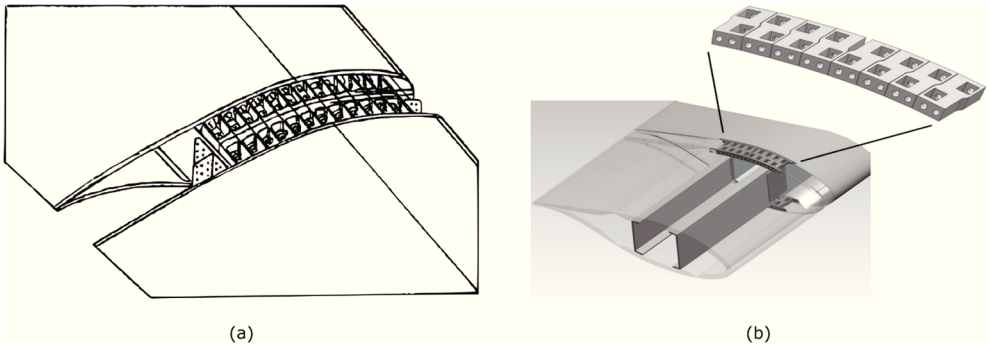

Figure 165: Prototype segmented blades using an intermediate plate. (a) Blade joint developed during the UpWind project. Reproduced from Ref. [59]. (b) Blade joint with alternating long and short bolts as suggested in Ref. [54].

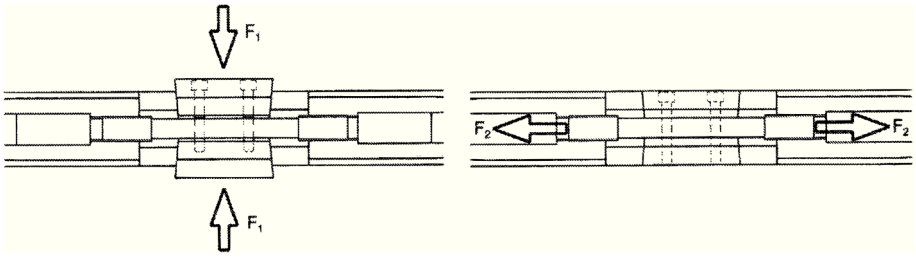

Figure 166: Schematic overview of the pre-tensioning method suggested in Ref. [112]. A wedge is inserted between the two segments, resulting in a pre-stress in the bolts. (a) Situation where the two segments are joined by a bolt, but pre- tension is not yet applied. The wedges are about to be pushed together. (b) Situation where the wedges are pushed together, pushing the segments away from each other, resulting in a pre-tensioning of the bolts.

A.3.6.2 Prior experience from blade root and hub extenders

To use existing blades on turbines at sites of a lower wind class than they were designed for, blade root extenders are placed in-between the hub and the blade roots, increasing the rotor diameter [113]. Blade extenders are generally made out

of metal but can also be manufactured from composite material [114]. They can incorporate a pre-coning [115] or sweep [116]. In a similar approach, the hub is extended, placing the pitching mechanism further out-board forming a hub extender or partial pitch system [55]. This concept was already used in the NASA Mod-2 turbine [117], [118].

Lu et al. [119] investigated a segmented blade of which the inboard portions were essentially blade extenders connected by a truss structure to reduce loads. Furthermore, to provide sufficient solidity at the blade root, an aerodynamic shape with a large chord length is required. This can be made feasible by using a root extender with an aerodynamic shape as suggested by Curtin et al. [120]. An overview of these methods is shown in Figure 167.

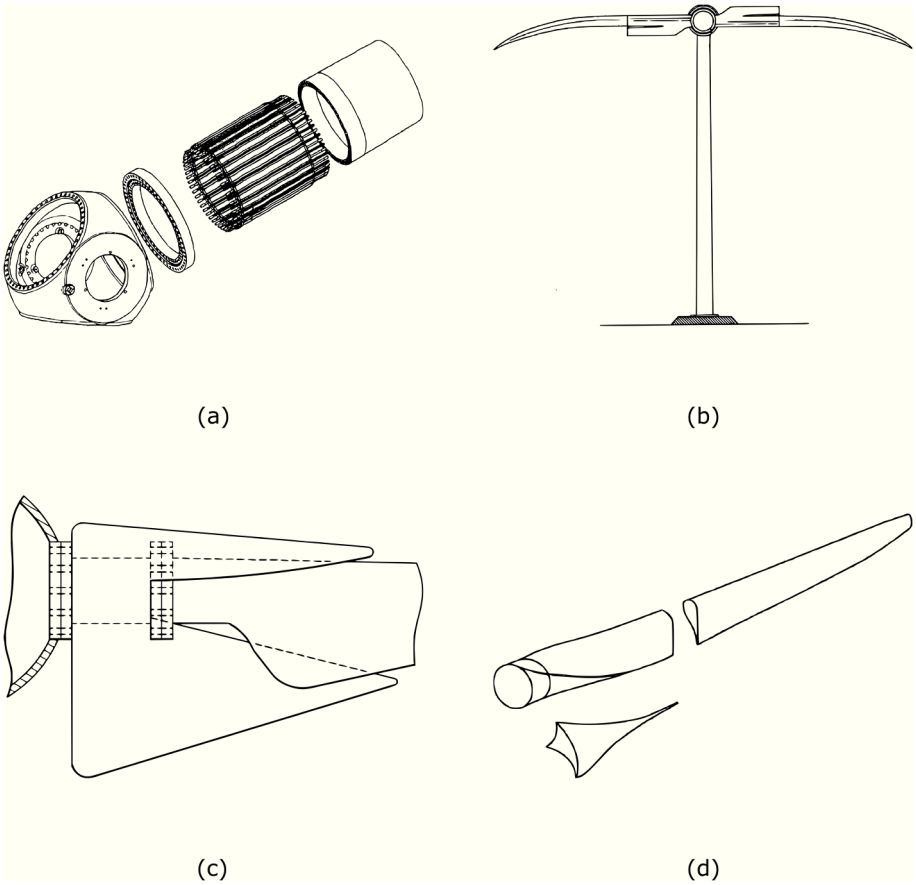

Figure 167: Blade extension methods. (a) Blade root extender as presented in Ref. [113]. (b) Partial pitch mechanism as presented in Ref. [55]. (c) Blade root extender with an

aerodynamic shape as presented in Ref. [120]. (d) Segmented blade with the inboard segment made from steel as presented in Ref. [31].

A.3.6.3 Prior Experience from rotor tips and glider wings

To reduce turbulence at the tips, aircraft often employ winglets. Similar tips are used on wind turbines to limit noise production [121]. However, such angled blade tips form delicate components during transportation and make manufacturing more complex and expensive. Therefore, they are often made as separate components and connected to the blades at the installation site. The blade tips can be connected by means of tubular guides and locked by means of a bolt, either transversely to the joint as suggested in Ref. [121] or longitudinally as suggested in Ref. [122]. Furthermore, in the past, tip brakes were used to prevent over-speed on rotors with stall control [84], [85], [123]. These can rotate 90 ° to create drag. They are typically connected by means of a tube. Similarly, [55] suggested to alleviate loads with a segmented tip. In addition, the fabrication methods, structural layout and slenderness of gliders and wind turbine blades are similar making joints used in gliders suitable candidates for blade segmentation [107]. Gliders often have detachable wings to allow easier transport and storage [124]. Modern glider carry-through structure configurations have one or two tongues next to each other to transfer bending loads [125]. Similar spar-bridge strategies with one or more protrusions have been suggested and tested for segmented blades. For example, [126] suggested a segmented blade that relies on joining the shear webs of a number of structural spars with shear pins. Loads are distributed using shear blocks attached to the webs. Segmented blades using spar-bridge joints were suggested in references [127]-[130]. Further, [23] designed and tested a 13.4 m blade with a connecting tube, which was attached to the blade using two bulkheads similar to the concept suggested by Finnigan et al. [131]. The blade was tested and performed well.

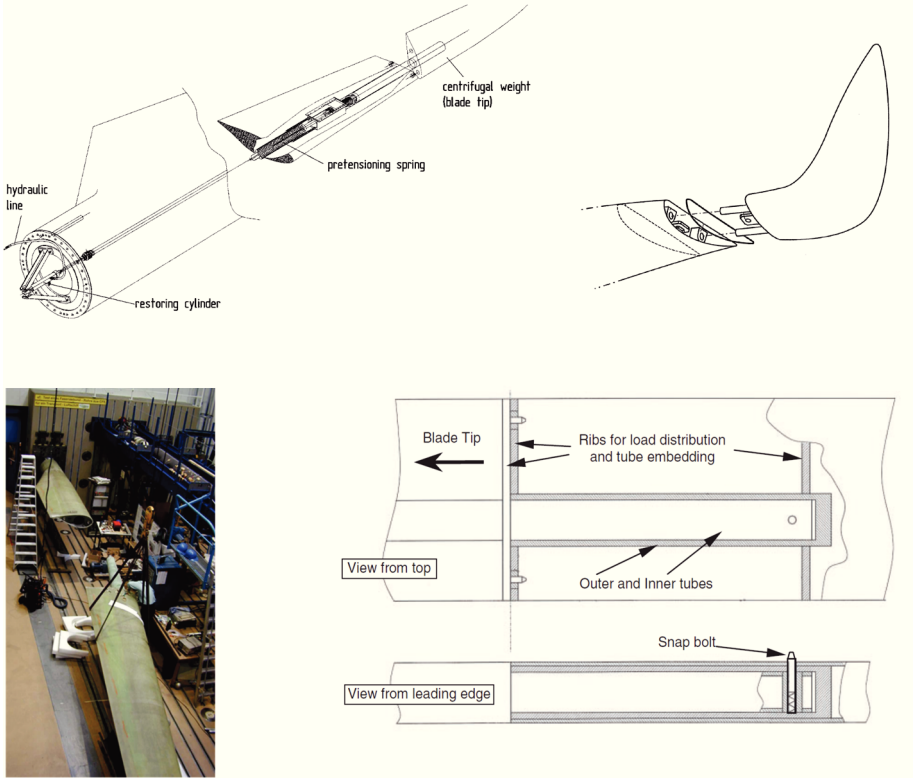

Figure 168: Rotor tips and glider wing joints.

A.3.6.4 Joints using transverse fasteners

Joining the segments with fasteners in a transverse direction has also been considered. Torres et al. [132] suggested joining the blades by riveting. Petri et al. [60] suggested transversely bolting overlapping plates to the segments. To increase the bearing strength of the laminate, [64] suggested using fiber metal laminate (FML) in the region of the joint. Llorente et al. [133] suggested using lugs to connect the spar of adjacent segments. These methods can be seen in Figure 169.

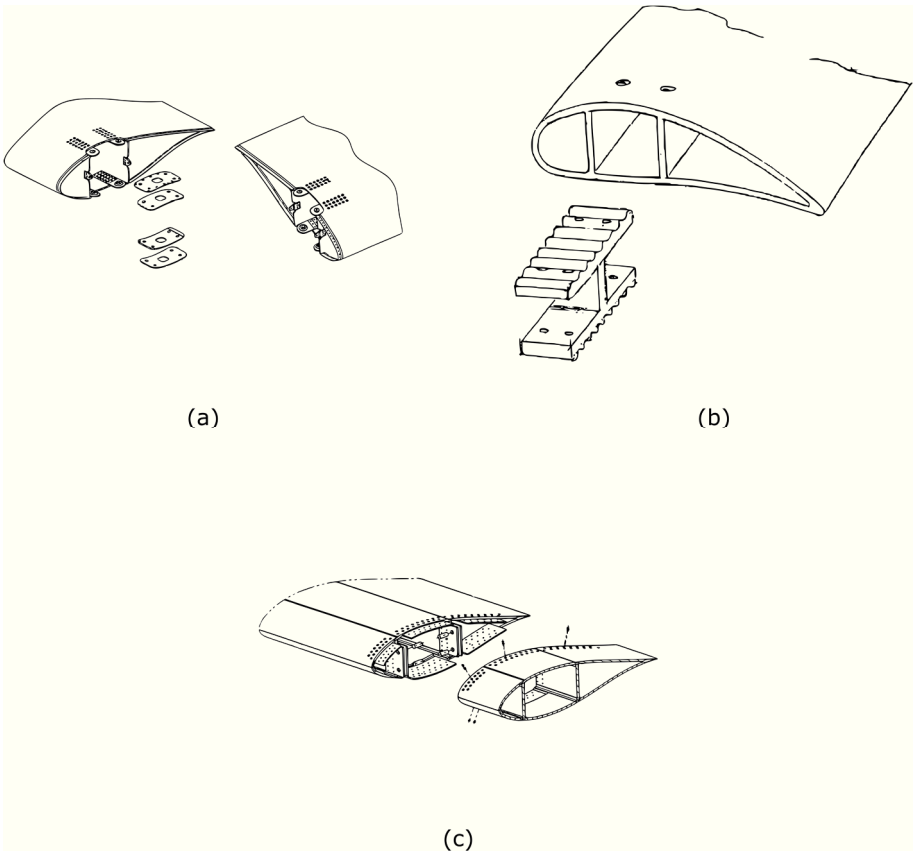

Figure 169: Transverse joining concepts. (a) Segments joined with lugs as proposed in Ref. [133]. (b) Segments joined by intermediate pieces as proposed in Ref. [60]. (c) Segments joined with rivets as proposed in Ref. [132].

A.3.6.5 Other concepts

Some blade segmentation concepts are not directly related to experience with other joints. An overview of these methods can be seen in Figure 170. There are several segmentation joints that rely on cables to form a connection. Wobben et al. [134] suggested using pre-tensioned straps to hold together eccentric transversal bolts, attached to neighboring segments. However, due to friction the pre-stress accuracy is limited and difficult to ensure [61]. Furthermore, this concept leads to high stress concentrations [75]. Alternatively, pre-tensioned cables can be used to hold the different segments together by pulling them towards the root. Kootstra et al. [135] proposed to incorporate a joining segment that is pulled towards the root using a pre-tensioned cable. Similarly, in Ref. [136] using pre-tensioned steel cables running through channels in the skin and shear

webs as an alternative to a structural spar is suggested. The cables are attached at the blade root and fastening points on every blade segment. Likewise, Cairo et al. [137] suggested using pre-tensioned cables running through conduits in the blade skin. Further, Klein et al. [138] suggested using U-shaped cable loops embedded into the laminate.

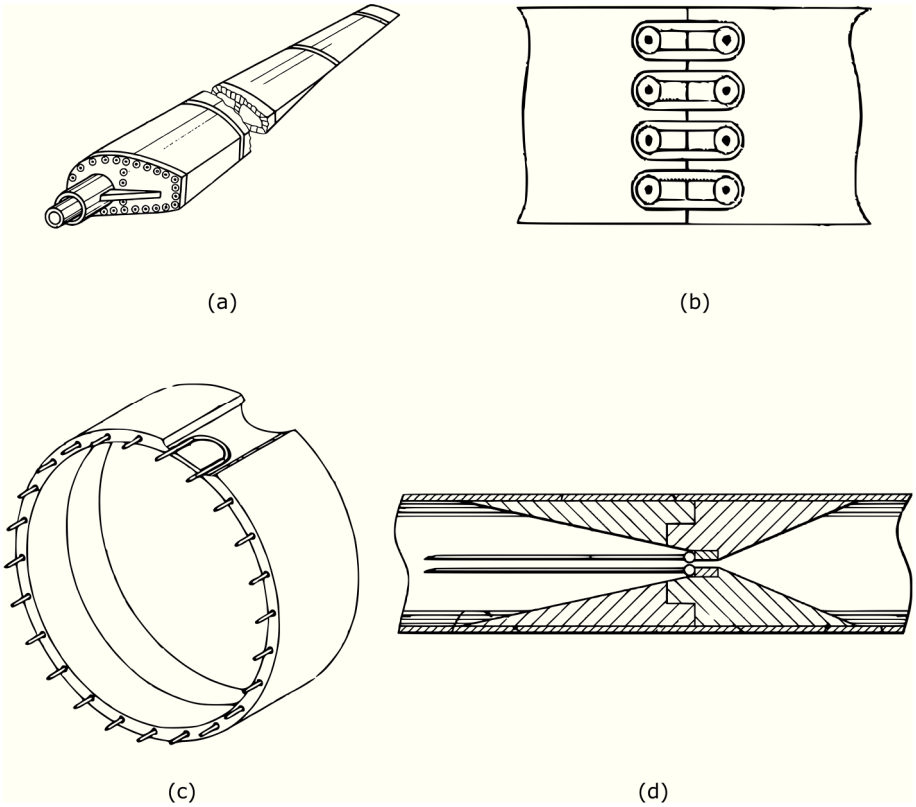

Figure 170: Unique blade connections relying on cables to connect the different segments. (a) Blade using pre-tensioned steel cables to hold together the different segments as an alternative to a spar structure as proposed in Ref. [136]. (b) Joint using pre-tensioned straps around eccentric bolts as proposed in Ref. [134]. (c) U-shaped loops as suggested in Ref. [138]. (d) Segmented blade joint relying on pre-tensioned cables to pull the outer segment towards the hub as proposed in Ref. [135].

A.3.7 Span-wise joint location

While the split location may be determined as to minimize transportation costs, it may also be influenced by structural consequences. The blade loads increase non-linearly towards the root. Meanwhile, modern blade designs use very thick

airfoils near the root, where structural requirements dominate the design and very thin ones toward the tip, where aerodynamic performance dominates. As a consequence, the ratio of section forces to the available cross-section is the highest around the center of the blade [64]. At this location, a very heavy joint would be required. The ratio of section forces to the available cross-section is lower towards the tip portion and towards the root portion, with the tip region experiencing the lowest section forces. However, while this was also true for the 61.5 m blade considered in Ref. [54], a mid-span location was still selected.

Qin et al. [139] investigated splitting a commercial 38 m blade. The study used simple beam theory to investigate the effect of the position of the blade joint. Several factors were considered. First, the curvature of the blade shape was considered. The bolts are assumed to be placed in the axial direction and are therefore less effective and more difficult to introduce in the design at a location where the blade rapidly changes shape. From the perspective of the change in chord length and thickness of the blade this excludes the root and tip regions. It was considered that past the position of maximum chord the derivative of the chord and the derivative of the thickness are limited. As a second factor, the fatigue strength of the joint was considered. This is shown in Figure 171. This was investigated for a commercial 38 m blade by using the equivalent fatigue loads and beam stiffness properties of the blade to obtain a fatigue stress range for various locations along the blade. This shows the lowest stresses towards the tip and a local optimum at the region of maximum chord. This is logical, since the blade stiffness is high near the transition zone. In fact, the fatigue loads could be decreased further by increasing the dimensions and buildup of the material in this region. In addition, a scaling study was performed, where it was concluded that the stresses scale linearly with the blade length, but that the joint strength scales less than linearly with increasing the bond length. This indicates that the chosen joining method is not suited for larger blades. Alternatives such as the use of two rows of bolts were suggested.

Limitations of this study are however the assumption that the blade behaves in a linear fashion and that the loads can be spread equally over the blades. Both these assumptions are not true as has been demonstrated by various authors. Research projects that developed prototype segmented blades used FEM to investigate how the loads were spread over the bolts giving high importance to the load factors. Furthermore, it was demonstrated that non-linear effects result in deformations of the blade cross-section, altering the load distribution in a bolted joint. This is even the case for very stiff components as demonstrated in Ref. [140].

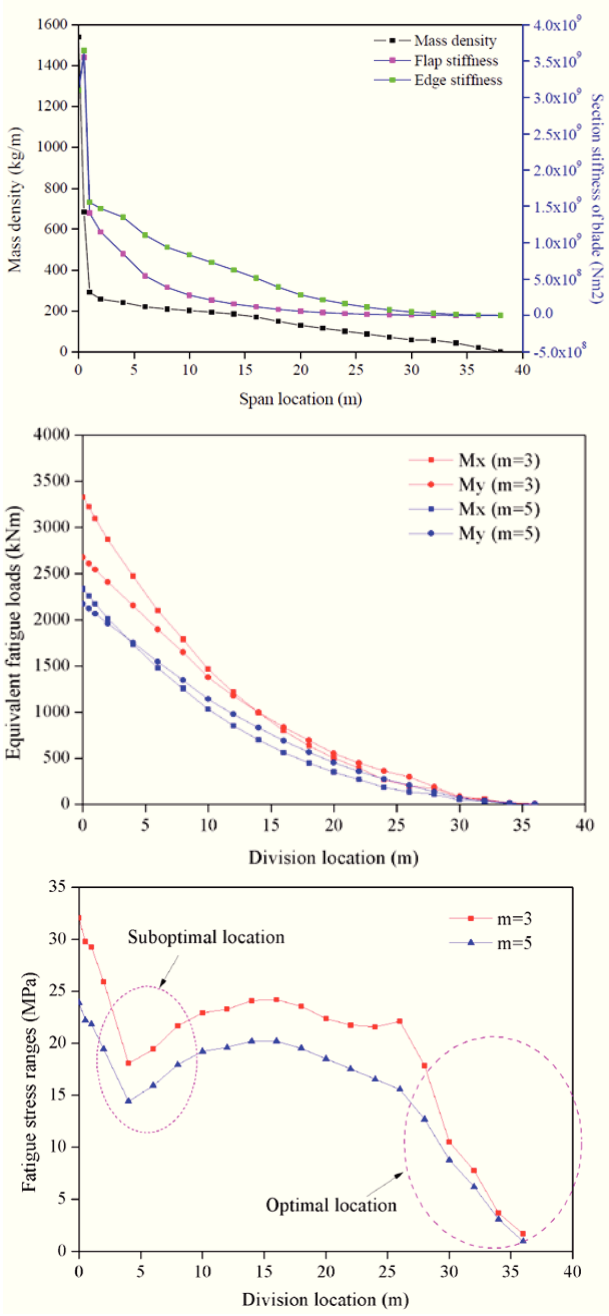

Figure 171: Data presented by Qin et al. [139] for a 38 m blade designed by CTC. (top) Mass and stiffness distribution for the blade. (middle) Equivalent fatigue loads. (bottom) Resulting section loads from fatigue. Two span-wise regions where segmentation may be interesting are identified: near the position of maximum chord and near the tip.

A.4 Conclusion

The feasibility of a segmented blade largely depends on the risk of the chosen concept. In this respect concepts that require only limited changes from existing approaches pose less risk and are more likely to succeed.

For example, concepts that do not require division of the blade's main structural components such as the use of separate leading or trailing edge segments are only small modifications since these require only limited loads to be transmitted across the connections. For this reason, active trailing edge flaps are more likely to succeed than telescopic blades. Similarly, aerodynamically shaped root extenders pose only a small modification from existing root extenders, which are well known in the industry. Furthermore, concepts incorporating a spar-bridge are close to joints used in sail-planes and tip brakes and have been shown to be feasible. Joints using longitudinal bolts have also been successful and are well known from the blade root design. The fact that large modern blades typically prefer the use of inserts to form a lightweight joint indicates that such joints are better suited for segmentation than flanged, hub type and T-bolt joints. On the other hand, breaking up the blade's main structural components poses significant challenges regarding production, maintenance costs and reliability. The failure of the T-bolt prototype blade in Ref. [56] and the unfavorable cost calculation for the T-bolt prototype blade in Ref. [23] indicate the difficulty of making this approach successful. Adhesive joints are also well known in the industry and are sometimes preferred because of their structural and economic efficiency [52]. However, the step from controlled conditions to in-field production of such connections is large. Yet, it may be possible to assemble the blade segments using local, perhaps temporary facilities. Furthermore, to avoid air entrapments, such adhesive joints would most likely be produced using vacuum infusion.

The issues related to the manufacturing of larger blades are already being countered by manufacturing separate blade components. These are mostly assembled in the factory using either adhesive or mechanical joints. While blade segmentation poses serious challenges, the wide variety of possibilities and the potential benefits are bound to lead to further developments in this field.

A.5 Bibliography

[1] T. James and A. Goodrich, "Supply Chain and Blade Manufacturing Considerations in the Global Wind Industry," 12-Dec-2013.

[2] K. Smith, "WindPACT Turbine Design Scaling Studies Technical Area 2: Turbine, Rotor, and Blade Logistics," National Renewable Energy Laboratory, Kirkland, Washington, NREL/SR-500-29439, 2001.

[3] J. Flores, S. Chan, and D. Homola, "A Field Test and Computer Simulation Study on the Wind Blade Trailer," *Transp. Res. Board*, Mar. 2015.

[4] E. García, "Innoblade®:Gamesa's Track Record on Blade Modularity," presented at the Advances in rotor blades for wind turbines, Bremen, 25-Feb-2014.

[5] P. Grabau, "Seaborne Transportation of Wind Turbine Blades," WO2009068031 (A1), 04-Jun-2009.

[6] A. V. Rebsdorf, "Transportation Method for a Wind Turbine Blade," US2012227357 (A1), 13-Sep-2012.

[7] K. Schibsbye and J. T. Sullivan, "Apparatus for Railroad Transportation of Wind Turbine Blades," US8641339 (B2), 04-Feb-2014.

[8] D. A. Griffin, "Blade system design studies volume I: Composite technologies for large wind turbine blades," Sandia National Laboratories, SAND2002-1879, Jul. 2002.

[9] J. Cotrell *et al.*, "Analysis of transportation and logistics challenges affecting the deployment of larger wind turbines: summary of results," National Renewable Energy Laboratory, NREL/TP-5000-61063, Jan. 2014.

[10] H. Stiesdal, P. B. Enevoldsen, K. Johansen, J. J. O. Kristensen, M. Noertem, and M. Winther-Jensen, "Method for manufacturing windmill blades," EP1310351 (A1), 19-Apr-2006.

[11] A. Wobben, "Transport Vehicle for a Rotor Blade of a Wind-Energy Turbine," WO03057528 (A1), 17-Jul-2003.

[12] M. Kawada, "Transporting Method and Transporter of Irregular Shaped Elongated Article," JP2004243805 (A), 02-Sep-2004.

[13] J. Nies, "Transport device for an elongate object such as a rotor blade for a wind turbine or the like," US8226342 (B2), 24-Jul-2012.

[14] G. Pedersen, "A Vehicle for Transporting a Wind Turbine Blade, a Control System and a Method for Transporting a Wind Turbine Blade," WO2007147413 (A1), 27-Dec-2007.

[15] S. C. Landrum and T. C. King, "Wind turbine blade transportation system and method," US7591621 (B1), 22-Sep-2009.

[16] P. Grabau, "Transporting and storing curved wind turbine blades," US7690875 (B2), 06-Apr-2010.

[17] D. Berry, S. Lockard, K. Jackson, M. Zuteck, and T. Ashwill, "Blade Manufacturing Improvements Remote Blade Manufacturing

Demonstration," Sandia national laboratories, Warren, SAND2003-0719, May 2003.
[18] J. Jensen, "A Method for the Transport of a Long Windmill Wing and a Vehicle for the Transport Thereof," WO2006000230 (A1), 05-Jan-2006.
[19] G. K. S. Pedersen, "Vehicle for transporting a wind turbine blade, a control system and a method for transporting a wind turbine blade," US8306695, Nov-2012.
[20] M. Emich, "Transport for difficult-to-get-to developments," *Windpower Engineering & Developement.*, pp. 8–9, 2013.
[21] S. Ashraf, "Large Wind Turbine Blade Transportation Solution: The Aeroscraft," *Wind Systems*, Apr-2013.
[22] F. Miceli, "Carrying blades with a balloon," *Wind farms construction*, 07-May-2012..
[23] A. G. Dutton, C. Kildegaard, C. Kensche, F. Hahn, D. R. V. van Delft, and G. D. de Winkel, "Design, structural testing, and cost effectiveness of sectional wind turbine blades," Aug. 1997.
[24] *Koninklijk besluit betreffende het wegverkeer van uitzonderlijke voertuigen*. 2010.
[25] T. Kellner, "Why A Lattice Tower Wind Turbine Can Be Taller, Stronger - GE," *GE Reports*, 10-Mar-2014. [Online]. Available: https://www.ge.com/reports/post/79185604909/friends-in-high-places/. [Accessed: 16-Mar-2018].
[26] G. Pérez, D. L. R. Arocena, P. Sanz, and C. Savii, "Tower Section for Automatically Raising a Wind Turbine and Automatic Raising Method for Same," WO2017203065 (A1), 30-Nov-2017.
[27] J. M. Adrian, *Modularization in the Wind Turbine Industry: Discontinuity in the Governance of Value Chains and Its Spatial Implications*. Lit Verlag, 2017.
[28] C. Niu and M. C. Y. Niu, *Airframe Structural Design: Practical Design Information and Data on Aircraft Structures*. Conmilit Press Limited, 1999.
[29] D. A. Griffin, "WindPACT Turbine design scaling studies technical area 1ø eComposite blades for 80-to 120-meter rotor," NREL, NREL/SR-500-29492, 2001.
[30] P. J. Schubel, "Technical cost modelling for a generic 45-m wind turbine blade producedby vacuum infusion (VI)," *Renew. Energy*, vol. 35, no. 1, pp. 183–189, Jan. 2010.
[31] R. Rohden, "Rotor Blade for a Wind Energy Installation," WO2007131937 (A1), 22-Nov-2007.
[32] A. Mikhail, "Low Wind Speed Turbine Development Project Report," NREL, NREL/SR-500-43743, 2009.
[33] A. Wobben, "Rotor Blade for a Wind Power Installation," WO02051730 (A3), 07-Nov-2002.
[34] T. Vronsky and M. Hancock, "Segmented Rotor Blade Extension Portion," WO2010013025 (A3), 04-Nov-2010.

[35] P. W. Judge, "Segmented Wind Turbine Blade," US7854594 (B2), 21-Dec-2010.
[36] P. Broome and P. Hayden, "An Aerodynamic Fairing for a Wind Turbine and a Method of Connecting Adjacent Parts of Such a Fairing," WO2011064553 (A3), 05-Jan-2012.
[37] A.. van Wingerde, D. R. V. van Delft, K. Molenveld, H. L. Bos, B. H. Bulder, and H. de Bonte, "BLADECO Eindrapport.pdf," BLDPV1-05, May 2002.
[38] I. A. De La Rua, E. S. Pascual, and S. A. Collado, "Blade insert," US8388316, Mar-2013.
[39] H. Mark, "Modular wind turbine blade with both spar and foil sections forming aerodynamic profile," GB2488099 (A), 22-Aug-2012.
[40] S. Siegfriedsen, "Rotor Blade for Wind Power Installations," WO0146582 (A2), 28-Jun-2001.
[41] T. K. Barlas and G. A. M. van Kuik, "Review of state of the art in smart rotor control research for wind turbines," *Prog. Aerosp. Sci.*, vol. 46, no. 1, pp. 1–27, Jan. 2010.
[42] T. Barlas *et al.*, "SMART ROTOR BLADES AND ROTOR CONTROL FOR WIND TURBINES - State of the Art - Knowledge Base Report for UpWind WP 1B3," 2006.
[43] M. H. Dawson, "Variable Length Wind Turbine Blade," DE-FG36-03GO13171, May 2006.
[44] S. V. Pasupulati, J. Wallace, and M. Dawson, "Variable length blades wind turbine," in *Power Engineering Society General Meeting, 2005. IEEE*, 2005, pp. 2097–2100.
[45] M. Imraan, R. N. Sharma, and R. G. J. Flay, "Wind tunnel testing of a wind turbine with telescopic blades: The influence of blade extension," *Energy*, vol. 53, pp. 22–32, May 2013.
[46] M. Dawson and J. Wallace, "Variable Length Wind Turbine Blade Having Transition Area Elements," WO2010120595 (A1), 21-Oct-2010.
[47] D. Castaignet *et al.*, "Full-scale test of trailing edge flaps on a Vestas V27 wind turbine: active load reduction and system identification: Full-scale test of trailing edge flaps on a Vestas V27 wind turbine," *Wind Energy*, vol. 17, no. 4, pp. 549–564, Apr. 2014.
[48] J. C. Berg, M. F. Barone, and N. C. Yoder, "SMART wind turbine rotor: data analysis and conclusions," *SAND2014-0712 Sandia Natl. Lab. Albuq. NM*, 2014.
[49] J. Berg, B. Resor, J. Paquette, and J. White, "SMART wind turbine rotor: design and field test," *SAND2014-0681 Sandia Natl. Lab. Albuq. NM*, 2014.
[50] L. J. Fingersh, M. M. Hand, and A. S. Laxson, "Wind turbine design cost and scaling model," National Renewable Energy Laboratory, NREL/TP-500-40566, Dec. 2006.
[51] P. Hibbard, "Wind Turbine Blade," US8177515 (B2), 15-May-2012.

[52] K. K. Wetzel, "Modular Blade Design & Manufacturing," presented at the Wind Turbine Blade Workshop 2014, 2014.
[53] J. J. Nies, "Adaptive rotor blade for a wind turbine," US8231351, Jul-2012.
[54] E. Saenz, I. Nuin, R. Montejo, and J. Sanz, "Development and validation of a new joint system for sectional blades: Joint system for sectional blades," *Wind Energy*, vol. 18, no. 3, pp. 419–428, Mar. 2015.
[55] E. M. Moroz, *Multi-piece wind turbine rotor blades and wind turbines incorporating same*. 2008.
[56] P. Vionis *et al.*, "Development of a MW scale wind turbine for high wind complex terrain sites; the MEGAWIND project," in *Proceedings of the EWEC*, 2006, vol. 2006.
[57] A. E. D. Walters, *methods of manufacture*. 2011.
[58] F. Sayer, F. Bürkner, M. Blunk, A. M. van Wingerde, and H. G. Busmann, "Influence of Loads and Environmental Conditions on Material Properties over the Service Life of Rotor Blades," *DEWI MAGAZIN*, Feb-2009.
[59] B. H. Pedersen, I. A. De La Rua, R. R. Sola, E. S. Pascual, and H. R. Savii, "Sensorised blade joint," US20090116962, Aug-2008.
[60] L. Petri and R. Sancho, "Reversible System for Sectioning Wind Generator Blades in Several Parts," WO2008084126 (B1), 12-Sep-2008.
[61] H. Stiesdal, "Method and Connecting Piece for Assembling Windmill Blade Sections," WO2006056584 (A1), 01-Jun-2006.
[62] M. L. Baker and C. P. Arendt, "Lightweight composite truss wind turbine blade," US7517198, Apr-2009.
[63] P. Rudling, "Wind Turbine Blade," US8696317 (B2), 15-Apr-2014.
[64] J. Birkemeyer and L. Beyland, "Segmentation technology for large onshore blades," presented at the IQPC Conference "Advances in Rotor Blades for Wind Turbines," Bremen, 27.02-2014.
[65] G. Sieros, P. Chaviaropoulos, J. D. Sørensen, B. H. Bulder, and P. Jamieson, "Upscaling wind turbines: theoretical and practical aspects and their impact on the cost of energy: Upscaling wind turbines: theoretical and practical aspects," *Wind Energy*, vol. 15, no. 1, pp. 3–17, Jan. 2012.
[66] N. J. Tobergte, "Apparatus and method for transporting and aligning wind turbine rotor blade," US8172493, May-2012.
[67] M. Baker, C. Arendt, B. Madrid, and S. Vilhauer, "Efficient Wind Turbine Blades, Wind Turbine Blade Structures, and Associated Systems and Methods of Manufacture, Assembly and Use," WO2010065928 (A1), 10-Jun-2010.
[68] R. M. Zirin *et al.*, "Multi-Segment Wind Turbine Blade and Method for Assembling the Same," US7740453 (B2), 22-Jun-2010.
[69] J. T. Livingston, "Structure and method for self-aligning rotor blade joints," US8167569, May-2012.

[70] P. L. Baehmann, T. Miebach, E. J. Telfeyan, W. W.-L. Lin, C. S. Yerramalli, and S. C. Quek, "Method for Assembling Jointed Wind Turbine Blade," US2010132884 (A1), 03-Jun-2010.
[71] S. G. Riddell, "Joint design for rotor blade segments of a wind turbine," US7922454 (B1), 12-Apr-2011.
[72] S. A. Kyriakides, S. G. Riddell, and A. M. Walker, "Method for Assembling a Multi-Segment Wind Turbine Rotor Blade with Span-Wise Offset Joints," US2013091705 (A1), 18-Apr-2013.
[73] M. D. Banea and L. F. M. da Silva, "Adhesively bonded joints in composite materials: an overview," *Proc. Inst. Mech. Eng. Part J. Mater. Des. Appl.*, vol. 223, no. 1, pp. 1–18, Jan. 2009.
[74] J. T. Livingston and H. Driver, "Wind blade joint bonding grid," US8221085, Jul-2012.
[75] R. Arelt, "Method for producing a rotor blade, a corresponding rotor blade and a wind power plant," US2006127222 (A1), 15-Jun-2006.
[76] H. D. Driver, W. W. Lin, and J. T. Livingston, "Modular Wind Turbine Blades with Resistance Heated Bonds," US2009148300 (A1), 11-Jun-2009.
[77] D. A. Spera, J. B. Esgar, M. Gougeon, and M. D. Zuteck, "Structural properties of laminated Douglas fir/epoxy composite material," 1990.
[78] M. a Gougeon and J. C. Gougeon, "Wind turbine blade joint assembly and method of making wind turbine blades," US4474536 (A), 02-Oct-1984.
[79] A. Bech, "Wind Turbine Blades Made of Two Separate Sections, and Method of Assembly," US8348622 (B2), 08-Jan-2013.
[80] C. Bhat, D. J. Noronha, and F. A. Saldana, "Structural Performance Evaluation of Segmented Wind Turbine Blade Through Finite Element Simulation," *Int. J. Mech. Aerosp. Ind. Mechatron. Manuf. Eng.*, vol. 9, no. 6, 2015.
[81] Composite Materials Handbook: Polymer Matrix Composites Materials Usage, Design, And Analysis, vol. 3, 5 vols. 2002.
[82] D. A. Whiley and P. T. Hayden, "Wind Turbine Rotor," US8262360 (B2), 11-Sep-2012.
[83] H. Frederiksen, "A method of producing a composite structure via intermediate products and a composite structure obtainable by the method," EP2033769 (A1), 11-Mar-2009.
[84] E. Hau, *Wind Turbines*. Berlin, Heidelberg: Springer Berlin Heidelberg, 2013.
[85] National Research Council, *Assessment of Research Needs for Wind Turbine Rotor Materials Technology*. Washington, D.C.: NATIONAL ACADEMY PRESS, 1991.
[86] U. Hütter, *Tragende Flugzeugteile aus glasfaserverstärkten Kunststoffen.*.
[87] H. Hosseini-Toudeshky, M. Jahanmardi, and M. S. Goodarzi, "Progressive debonding analysis of composite blade root joint of wind turbines under fatigue loading," *Compos. Struct.*, vol. 120, pp. 417–427, Feb. 2015.

[88] T. Ashwill, "Sweep-Twist Adaptive Rotor Blade: Final Project Report," Sandia National Laboratories, SAND2009-8037, Jan. 2010.
[89] V. Martínez, A. Güemes, D. Trias, and N. Blanco, "Numerical and experimental analysis of stresses and failure in T-bolt joints," *Compos. Struct.*, vol. 93, no. 10, pp. 2636–2645, Sep. 2011.
[90] R. D. A. Harismendy, P. Amezqueta, M. Sanz, M. Nuin, M. Lasa, and R. Sanz, "Sistema De Amarre Para La Union De Tramos De Palas De Aerogenerador Partidas," ES2352945 (A1), 16-Feb-2011.
[91] P. Quell, U. Bendel, M. Schubert, and C. Eusterbarkey, "Rotor blade attachment," US8133029, Mar-2012.
[92] F. Doorenspleet, R. Arelt, and E. Eyb, "Rotor Blade for a Wind Turbine," US7517194 (B2), 14-Apr-2009.
[93] A. Wobben, "Connection of a Wind Energy Plant Rotor Blade to a Rotor Hub," WO9906694 (A1), 11-Feb-1999.
[94] P. Hayden, P. Broome, and D. Whiley, "An Insert and Method for Forming an End Connection in a Uni -Axial Composite Material," WO2010041008 (A1), 15-Apr-2010.
[95] T. Vronsky and F. H. Hahn, "Wind turbine rotor blade," US 8105040, Jan-2012.
[96] J. R. Faddoul, "Test evaluation of a laminated wood wind turbine blade concept," DOE/ NASA, DOE/NASA/20320-30, 1981.
[97] A. Raina, T. S. Wullenschneider, R. M. Barnhart, K. K. Wetzel, and C. Yang, "Insert and Method of Attaching Insert to Structure," US2015071701 (A1), 12-Mar-2015.
[98] L. N. McEwen, F. H. Louarn, J. Sellier, and A. J. Chignell, "Wind or tidal turbine blade having an attachment," US20130108464, Aug-2010.
[99] F. Sorensen, R. Schytt-Nielsen, and F. Soerensen, "Method of manufacturing a wind turbine blade root," US7530168 (B2), 12-May-2009.
[100] U. Bendel, M. Werner, and M. Knops, "Method for Establishing A Blade Connection of a Rotor Blade, A Blade Connection and a Securing Element for a Blade Connection," US2011044817 (A1), 24-Feb-2011.
[101] C. Kildegaard, "Embedding element to be embedded in the end part of a windmill blade, a method producing such an embedding element as well as embedding of such embedding elements in a windmill blade," US2005106029 (A1), 19-May-2005.
[102] E. Grove-Nielsen, "A root bushing for a wind turbine rotor blade, a wind turbine rotor blade, a wind turbine and a method for manufacturing a wind turbine rotor blade for a wind turbine," EP2952735 (A1), 09-Dec-2015.
[103] L. Feigl, "Wind Turbine Blade Connector Assembly," WO2013014228 (A1), 31-Jan-2013.

[104] R. Schmidt, C. Weimer, and H. Stadtfeld, "Blade Connection for the Rotor Blades of a Wind-Energy Turbine and a Method for the Production Thereof," WO03082551 (A1), 09-Oct-2003.
[105] J. L. Tangler, "The evolution of rotor and blade design," presented at the WindPower 2000, Palm Springs, California, 2000.
[106] K. J. Jackson, M. D. Zuteck, C. P. van Dam, K. J. Standish, and D. Berry, "Innovative design approaches for large wind turbine blades," *Wind Energy*, vol. 8, no. 2, pp. 141–171, Apr. 2005.
[107] C. Kensche, "Fatigue of composites for wind turbines," *Int. J. Fatigue*, vol. 28, no. 10, pp. 1363–1374, Oct. 2006.
[108] "UpWind: Design limits and solutions for very large wind turbines," Mar. 2011.
[109] ecogreen4us.com, *Wind Turbine Gamesa G10X - 4.5 MW*..
[110] Y. Montejo *et al.*, "System for Joining Component Portions of Wind-Turbine Blades," WO2012156547 (A1), 22-Nov-2012.
[111] P·e·桑斯, "Screwed connection for a modular blade," CN106662069 (A), 10-May-2017.
[112] L. MONREAL, E. CALLÉN, D. L. R. AROCENA, C. SAVII, and P. SANZ, "Device for Joining a Modular Blade," WO2017174828 (A1), 12-Oct-2017.
[113] K. Aarhus, "Blade Root Extender for a Wind Turbine," US8337161 (B2), 25-Dec-2012.
[114] H. Heerkes and R. Scherer, "Wind Turbine Rotor, and Hub and Extender Therefor," WO0142647 (A2), 14-Jun-2001.
[115] A. Wobben, "Wind Turbine Blade Root Spacer for Increasing the Separation of the Blade Tip from the Tower," WO03060319 (A1), 24-Jul-2003.
[116] R. Joassard, P. Bodin, and G. Filippi, "Wind generator for power plant, has offset unit offsetting leading edge such that main axis extended between center of root base of blades and opposite ends of blades does not pass through rotational axis of hub," FR2863318 (A1), 10-Jun-2005.
[117] B. S. Linscott, J. T. Dennett, and L. H. Gordon, "The Mod-2 Wind Turbine Development Project," DOE/NASA, Final report DOE/NASA/20305-5, Jul. 1981.
[118] B. S. Linscott, "DOE large horizontal axis wind turbine development at NASA Lewis Research Center," DOE/NASA, DOE/NASA/20320-47, 1982.
[119] H. Lu, P. Zeng, L. Lei, Y. Yang, Y. Xu, and L. Qian, "A smart segmented blade system for reducing weight of the wind turbine rotor," *Energy Convers. Manag.*, vol. 88, pp. 535–544, Dec. 2014.
[120] G. A. Curtin, "Expansion assembly for a rotor blade of a wind turbine," US20110142636, Oct-2010.
[121] G. Olthoff, "Removable rotor blade tip," US20130236321, Sep-2011.
[122] A. Hoffmann, D. Dulle, and C. Clemens, "Rotor Blade Tip," US2016090963 (A1), 31-Mar-2016.

[123] P. L. Gay and P. L. Gay, "Wind Turbine Blade Tip Brake Apparatus and Method," US8403641 (B2), 26-Mar-2013.
[124] J.-P. Pajard, "Aircraft wing including a plurality of dismountable members," US8128032, Mar-2012.
[125] B. E. Thompson and R. D. Lotz, "Sailplane carry-through structures made with composite materials," *J. Aircr.*, vol. 33, no. 3, pp. 596–600, May 1996.
[126] P. Rudling, "A Root End Joint for a Wind Turbine Blade," WO2009034292 (A2), 19-Mar-2009.
[127] A. Bech and P. Hibbard, "A Sectional Blade," WO2010023299 (A2), 04-Mar-2010.
[128] P. Hibbard and M. Hancock, "Sectional Wind Turbine Blade," US9388789 (B2), 12-Jul-2016.
[129] E. Eyb, "Modular Rotor Blade for a Wind Turbine and Method for Assembling Same," US7654799 (B2), 02-Feb-2010.
[130] W. Wang, B. Jin, Z. Liu, Q. Dang, and S. Wang, "Segmented Wind Rotor Blade for Wind Turbine Generator System and Assemblying Method Thereof," US2012213642 (A1), 23-Aug-2012.
[131] P. M. Finnigan, C. Lanaud, G. Rengarajan, and G. Qian, "System and Method for Joining Turbine Blades," US8123488 (B2), 28-Feb-2012.
[132] M. M. Torres and M. Torres, "Pala De Aerogenerador Dividida En Tramos Y Proceso De Fabricacion De La Misma," ES2343712 (A1), 06-Aug-2010.
[133] G. Llorente and O. Velez, "Wind Turbine Blade," WO2005100781 (A1), 27-Oct-2005.
[134] A. Wobben, "Butt connection for hollow profile members," US7481624, Jan-2009.
[135] D. J. Kootstra, "Wind turbine rotor blade joint," US8172539, May-2012.
[136] R. Doellinger, R. Schindler, and D. Franz, "Rotor blade comprising a plurality of individual sections," US4389162 (A), 21-Jun-1983.
[137] R. R. Cairo and R. R. Cairo, "Modular blades and methods for making same," US7393184 (B2), 01-Jul-2008.
[138] H. Klein, "Rotor blade or rotor blade segment for a wind turbine," US8888462, Nov-2014.
[139] Z. Qin, L. Zhang, K. Yang, J. Wang, C. Liao, and J. Xu, "Determining Division Location for Sectional Wind Turbine Blades," *Energies*, vol. 10, no. 9, p. 1404, Sep. 2017.
[140] H. G. Lee, M. G. Kang, and J. Park, "Fatigue failure of a composite wind turbine blade at its root end," *Compos. Struct.*, vol. 133, pp. 878–885, Dec. 2015.